

**Functional characterization of ORMDL proteins
involved in endoplasmic reticulum stress and
intestinal inflammation**

Dissertation
zur Erlangung des Doktorgrades
der Mathematisch-Naturwissenschaftlichen Fakultät
der Christian-Albrechts-Universität zu Kiel

vorgelegt von
Marlene Jentzsch

Kiel, 2015

Erster Gutachter: Prof. Dr. Philip Rosenstiel

Zweiter Gutachter: Prof. Dr. Thomas Roeder

Tag der mündlichen Prüfung: 10.12.2015

Zum Druck genehmigt: 10.12.2015

gez. Prof. Dr. Wolfgang J. Duschl, Dekan

Table of content

1 Introduction	1
1.1 Inflammatory bowel disease	1
1.1.1 Non-genetic risk factors for IBD	3
1.1.2 Genetic risk factors for IBD	3
1.2 The unfolded protein response (UPR)	4
1.2.1 Activation of the IRE1 signaling pathway	6
1.2.2 Activation of the ATF6 signaling pathway	7
1.2.3 Activation of the PERK signaling pathway	8
1.2.4 Cross-talk events between the three UPR signaling pathways	8
1.3 Role of ER stress in intestinal epithelial cell homeostasis and IBD	9
1.4 The ORMDL protein family	12
1.4.1 <i>ORMDL</i> genes belong to an evolutionary conserved gene family	12
1.4.2 Association of <i>ORMDL3</i> with several diseases	13
1.4.3 <i>ORMDL</i> proteins regulate the ER homeostasis	14
1.4.3.1 <i>ORMDL</i> proteins affect components of the UPR	14
1.4.3.2 Regulation of the Ca ²⁺ homeostasis by <i>ORMDL</i> proteins	15
1.4.3.3 <i>ORMDL</i> proteins regulate sphingolipid synthesis	15
1.5 Objective of the study	17
2 Methods	19
2.1 Cell biological methods	19
2.1.1 Cell lines	19
2.1.2 Transient transfection of plasmid DNA	20
2.1.3 Transfection of siRNA	20
2.1.4 Life cell XBP1 splicing assay using a XBP1-venus reporter construct	21
2.1.5 Promoter-mediated luciferase reporter assay	22
2.1.6 Flow cytometric analysis	23
2.2 Molecular biological methods	23
2.2.1 Isolation of total RNA	23
2.2.2 cDNA synthesis	23
2.2.3 Endpoint polymerase chain reaction (PCR)	24
2.2.4 Agarose gel electrophoresis	25

2.2.5	Quantitative real-time polymerase chain reaction.....	25
2.2.6	Generation of expression constructs.....	26
2.2.7	Plasmid preparation.....	28
2.2.8	Sanger sequencing.....	29
2.3	Protein biochemical methods.....	29
2.3.1	Total protein lysate preparation.....	29
2.3.2	Cell fractionation.....	30
2.3.3	Protein concentration determination.....	30
2.3.4	Gel electrophoresis of proteins.....	30
2.3.5	Immobilization of proteins by immunoblot.....	31
2.3.6	Immunodetection of proteins.....	32
2.3.7	Co-immunoprecipitation.....	32
2.3.8	Enzyme-linked immunosorbent assay (ELISA).....	33
2.3.9	Measurement of cytokine concentrations.....	33
2.4	Generation, handling and treatment of mice.....	34
2.4.1	Generation of <i>Ormdl1</i> constitutive knockout mice (<i>Ormdl1</i> ^{-/-}).....	34
2.4.2	Generation of <i>Ormdl3</i> conditional mice.....	35
2.4.3	Generation of <i>Ormdl3</i> constitutive knockout mice (<i>Ormdl3</i> ^{-/-}).....	36
2.4.4	Generation of <i>Ormdl3</i> conditional knockout mice (<i>Ormdl3</i> ^{ΔIEC}).....	36
2.4.5	Animal housing and animal care.....	36
2.4.6	Genotyping.....	37
2.4.7	Primary cell isolation.....	38
2.4.8	Induction of acute colitis.....	39
2.4.9	Induction of chronic colitis.....	39
2.4.10	Disease activity index (DAI).....	39
2.4.11	Histology.....	40
2.4.12	Tunicamycin injection.....	41
2.5	Statistical analysis.....	41
3	Results.....	42
3.1	Expression analyses of human and murine <i>ORMDL</i> mRNA.....	42
3.2	ER stress-induced tissue-specific expression of <i>ORMDL</i> proteins.....	42
3.3	The effect of <i>ORMDL</i> proteins on the UPR.....	44
3.3.1	<i>ORMDL</i> proteins inhibit the IRE1 pathway.....	44

3.3.2	ORMDL proteins activate the ATF6 α pathway	45
3.3.2.1	ORMDL proteins reduce p36ATF6 α protein levels and induce the ERSE promoter	46
3.3.2.2	ORMDL3 affects the ERSE promoter mainly through ATF6 α cleavage.....	48
3.3.2.3	N-linked glycosylation of ATF6 α is ORMDL3-dependent	49
3.3.2.4	ORMDL3 induces ATF6 α cleavage	51
3.3.2.5	ORMDL3 and ATF6 α are located in close spatial proximity	53
3.3.2.6	ORMDL3 interacts with ATF6 α	54
3.3.3	ORMDL proteins modulate the PERK pathway	55
3.4	Characterization of <i>Ormdl3</i>^{-/-} mice.....	58
3.4.1	Basal phenotype of <i>Ormdl3</i> ^{-/-} mice	58
3.4.1.1	Analyses of ORMDL homologues in <i>Ormdl3</i> ^{-/-} mice.....	58
3.4.1.2	<i>Ormdl3</i> deficiency results in reduced body weight.....	59
3.4.1.3	Histology of the lung, ileum and colon of <i>Ormdl3</i> ^{-/-} mice	61
3.4.1.4	Cytokine concentrations in <i>Ormdl3</i> ^{-/-} mice	63
3.4.2	<i>Ormdl3</i> ^{-/-} mice are more susceptible to acute DSS-induced colitis	66
3.4.3	Tunicamycin injection induces prolonged UPR in <i>Ormdl3</i> ^{-/-} mice.....	71
3.5	Characterization of <i>Ormdl3</i>^{ΔIEC} mice	76
3.5.1	Basal phenotype of <i>Ormdl3</i> ^{ΔIEC} mice	76
3.5.2	<i>Ormdl3</i> ^{ΔIEC} are less susceptible to chronic DSS-induced colitis.....	77
3.6	Characterization of <i>Ormdl1</i>^{-/-} mice.....	81
3.6.1	Basal phenotype of <i>Ormdl1</i> ^{-/-} mice	81
3.6.2	<i>Ormdl1</i> deficiency causes no significant differences in acute DSS-induced colitis.....	83
4	Discussion.....	85
4.1	Tissue-specific expression patterns of ORMDL homologues.....	85
4.2	ER stress induces a tissue-specific expression pattern of ORMDL proteins	86
4.3	ORMDL proteins function as a regulator of the UPR	87
4.3.1	ORMDL proteins activate the ATF6 α pathway	87
4.3.2	ORMDL proteins facilitate the PERK pathway activation.....	89
4.3.3	ORMDL proteins reduce the activity of the IRE1 pathway.....	89
4.3.4	Cross-talk events between the three UPR branches	90
4.3.5	Proposed mechanisms of ORMDL3 on the UPR pathways.....	91

4.4 Embryonic development is unaffected by ablation of either <i>Ormdl1</i> or <i>Ormdl3</i>	92
4.5 ORMDL3 modulates body growth by affecting IGF1 production	93
4.6 <i>Ormdl3</i> deficiency in mice reduces IFN γ levels and its targets	94
4.7 The role of ORMDL1 and ORMDL3 during intestinal inflammation.....	96
4.7.1 Deletion of <i>Ormdl1</i> or <i>Ormdl3</i> leaves intestinal homeostasis unaffected.....	96
4.7.2 Mice lacking <i>Ormdl3</i> are more susceptible to an acute DSS-induced colitis.....	97
4.7.3 Deletion of <i>Ormdl3</i> in IEC has a protective effect during chronic DSS-induced colitis.....	98
4.8 ORMDL3 protects from prolonged ER stress <i>in vivo</i>	99
4.9 Future prospects	102
5 Summary.....	103
6 Zusammenfassung	105
7 Bibliography	107
8 Supplements.....	126
8.1 List of abbreviations	126
8.2 Applied buffers and solutions	129
8.3 Media.....	130
8.4 Chemicals	130
8.5 Enzymes and inhibitors	131
8.6 Kits	132
8.7 Plasmids and oligonucleotides	132
8.8 Antibodies.....	134
8.9 Devices and consumables.....	135
8.10 List of tables.....	138
8.11 List of figures	139
8.12 Curriculum vitae.....	142
8.13 Acknowledgements	144
8.14 Eidesstattliche Erklärung	145

1 Introduction

1.1 Inflammatory bowel disease

Inflammatory bowel disease (IBD), including the most common forms Crohn's disease (CD) and ulcerative colitis (UC), are idiopathic diseases with a dysregulated immune response to the intestinal microbiota, which leads to mucosal inflammation and destruction of the mucosal integrity (1). In the last decades, especially in industrialized nations the prevalence of IBD increased dramatically (2). CD and UC are clinically relevant with a prevalence rate of 322 per 100,000 and 505 per 100,000 persons in Europe, respectively (3). Both subtypes of IBD show specific gender-dependent incidence rates. In the case of CD, female individuals have a higher incidence rate than male individuals (female:male ratio 1.31:1) (4). Conversely, UC is more common in male individuals compared to female individuals (female:male ratio 1:1.5) (5). Moreover, the incidence and prevalence rates of IBD differ depending on the geographic location. For example, in Europe are the highest annual incidences of UC and CD with 24.3 and 19.2 cases per 100,000 persons and year, respectively. In comparison, in Asia and the Middle East the annual incidence rates of UC and CD are lower with 6.3 and 5 cases per 100,000 persons and year, respectively (3). The higher incidence rates in Europe suggest that the lifestyle of Western industrial societies is a relevant factor contributing to an increased pathogenesis of IBD. Moreover, the incidence rates are age-dependent, although IBD can occur at any age. The peak age of IBD manifestation is between the ages of 16 and 24 years (6,7).

The differentiation between the two major forms of IBD, CD and UC, can be made by the distribution and nature of the inflammatory changes. CD may affect segments of the entire gastrointestinal tract from the mouth to the anus, whereas UC is limited to the colon. The discontinuous inflammation in CD is transmural and affects all layers of the intestine (8). UC is characterized by diffuse mucosal inflammation with extensive superficial mucosal and submucosal ulcerations (9). Many clinical symptoms of both IBD subtypes are quite similar, including persistent and chronically relapsing diarrhea, abdominal pain, fever and loss of appetite. Blood in the stool, rectal bleeding and body weight loss may also occur (10,11). Furthermore, IBD patients with severe and long-term active disease have an increased risk for colon cancer (12). About 36 % of patients with IBD are additionally burdened by extra-intestinal manifestations, such as arthritis, fatty liver or growth retardation in children (13). For both diseases currently no cure is available (14,15). Many therapeutic approaches are based on immunosuppressive therapies and aim to alleviate

patient suffering. However, due to the fact that IBD is a lifelong disease and the incidence rates increase worldwide, new therapeutics for better and more effective treatments of UC and CD patients are needed. If the symptoms cannot be controlled by medications anymore, surgeries are performed. Three quarters of CD and one quarter of UC patients require surgery during their life (16). The complication rates of these resectional surgeries are high with 57 % and 31 % for CD and UC, respectively (17). The disease symptoms and the limited medications result in a reduced quality of life.

The human body contains ten-fold more microbial cells than human cells (18). These microorganisms colonize at the boundary surfaces, such as the skin, respiratory or gastrointestinal tract. In the gastrointestinal tract microorganisms reach the highest density (19). For that reason, the intestinal homeostasis highly depends on a complex interaction between gut microbiota, intestinal epithelium and the host immune response (20). The intestinal epithelium participates in the coordination of appropriate immune responses and fulfills the barrier function with a tightly sealed cell layer covered by a mucus biofilm secreted from goblet cells (21). This mucus biofilm is essential for the intestinal homeostasis as suggested by decreased expression levels of the *MUC1* gene in CD patients (22). Paneth cells are highly specialized intestinal epithelial cells (IEC) of the small intestine located in the crypt bottom between the intestinal stem cells. These cells secrete antimicrobial peptides, such as α -defensins, in response to bacterial antigens (23). The secretion of antimicrobial peptides into the crypt lumen protects crypt cells from colonization of pathogens and protects against enteric infections (24). In addition, a variety of different innate immune cells in the epithelium and lamina propria recognize microbe associated patterns such as lipopolysaccharide, peptidoglycan-derived muramyl dipeptide, lipoteichoic acid, single and double stranded RNA and methylated DNA through pattern recognition receptors, including Toll-like receptors (TLR) and nucleotide binding domain (NOD) like receptors (NLR) (1). The essential roles of TLRs and NLRs during intestinal inflammation were demonstrated in several studies (25–27). In IBD patients the tolerance towards the commensal gut microbiota seems to be impaired and the immune response is dysregulated.

Although there have been many studies on this field, the mechanisms of disease manifestation are not fully understood at the moment (28). However, it has been shown that multiple non-genetic and genetic risk factors are involved in the pathogenesis and manifestation of the complex diseases CD and UC (29,30). It is thought that CD and UC arise due to non-genetic factors in genetically predisposed individuals (31). Additionally, epigenetic mechanisms, such as DNA methylation (32) and histone modification (33), can affect the pathogenesis of IBD.

1.1.1 Non-genetic risk factors for IBD

Non-genetic risk factors have an important impact on the manifestation of IBD, as demonstrated by concordance rates among monozygotic twins of only 10-15 % for UC and 30-50 % for CD (34,35). Furthermore, studies with migrants from countries with low incidents rates to countries with high incidents rates revealed increased risk of these individuals to develop IBD (36). Thus, non-genetic, environmental factors contribute to the development and manifestation of IBD in genetically predisposed individuals.

One of the identified environmental risk factor is smoking (37). Smoking can function as a disease-specific environmental risk factor that exacerbate CD while being protective in UC (38). Also high levels of hygiene and the lack of exposure to enteric pathogens in childhood predispose individuals to CD (39). For example, exposure to pets in early life decreases the risk of IBD (40). Additionally, the dietary intake influences the disease risk of IBD (41). High intakes of total fats, total polyunsaturated fatty acids, omega-6 fatty acids and meat increase the risk of IBD, whereas high fiber and fruit intake decrease the risk of CD and high vegetable intake decreases the risk of UC (42). Furthermore, a protective effect of breastfeeding on the risk of IBD was noticed. The risk decreased by 33 % and by 23 % for CD and UC, respectively (43).

1.1.2 Genetic risk factors for IBD

Genetic studies, including linkage mapping and genome-wide association studies (GWAS), identified genetic risk factors that contribute to the pathogenesis of IBD. In 1996, linkage mapping studies discovered the first genetic risk factor for CD at the *IBD1* locus on chromosome 16 (44). This region was later identified to encode the nucleotide-binding oligomerization domain-containing protein 2 (NOD2) (45). Today, *NOD2* is known as one of the strongest susceptibility genes associated with CD (46). However, mutations in a single gene are usually not sufficient to induce IBD, indicating that CD and UC are complex, multi-genetic diseases (47). The search for novel genetic risk factors was revolutionized by high-throughput technologies. GWAS enabled the discovery of a broad range of genetic risk factors associated with IBD. Due to a meta-analysis of GWAS and ImmunoChip data the number of susceptibility loci increased to 163 for IBD (48), which explain approximately 20-25 percent of the disease risk (49). Twenty-eight of the identified risk loci are shared between CD and UC, such as the interleukin 23 receptor (*IL23R*), X-box binding protein 1 (*XBP1*) or orosomucoid 1 (*Saccharomyces cerevisiae*)-like protein 3 (*ORMDL3*) (50,51). Other genetic risk loci are only associated with either CD or UC. For example, genetic variations in *NOD2* or the autophagy-related protein 16-like 1

(*ATG16L1*), are unique for CD (52), whereas genetic variants in tyrosine-protein phosphatase non-receptor type 2 (*PTPN2*), probable E3 ubiquitin-protein ligase (*HERC2*) and signal transducer and activator of transcription 3 (*STAT3*) were linked only to the pathogenesis of UC (53). The identified susceptibility loci for CD and UC reveal that alterations in a variety of pathways are involved in the pathogenesis of IBD, for instance the genetic risk loci *NOD2* elucidated that defects in proper microbial sensing and the innate immune system are associated with the development of CD. Other genetic risk loci, including *XBP1*, *AGR2* (encoding the anterior gradient protein-2) and *ORMDL3*, identified endoplasmic reticulum (ER) stress and alterations in the unfolded protein response (UPR) as a pathogenic mechanism in IBD. Over the last decade, further studies supported the link between dysregulated UPR and the pathogenesis of IBD.

1.2 The unfolded protein response (UPR)

ER can be found in all eukaryotic cells and is composed of a continuous membrane system that forms a dynamic network of tubules and cisternae with a single lumen. The membrane of the ER represent more than half of the total membrane of an average mammalian cell (54). In the cell, the ER plays a crucial role in the biosynthesis, maturation and transport of lipids and proteins. Only properly folded proteins are transported from the ER to the Golgi apparatus for further modifications, while incompletely folded proteins remain in the ER until they are properly folded. However, incompletely folded proteins may also be delivered to the cytosol to undergo ER-associated protein degradation (ERAD) through ubiquitination and degradation by the 26S proteasome (55). Under physiological conditions, the protein load of the ER and the protein folding capacity are well balanced. However, the protein folding and maturation function is highly sensitive to disturbances of the ER homeostasis, including virus infection, inflammation, alteration in ER calcium homeostasis, changes in temperature or pH, oxidative stress, glucose deprivation as well as high-fat diet (56). These disturbances alter the function of the organelle and induce the accumulation of unfolded or misfolded proteins inside the ER. This cellular condition is termed ER stress, which activates the evolutionarily conserved mechanism of the UPR (57). The UPR signal transduction gets induced when unfolded proteins exceed the capacity of the ER chaperones leading to the activation of three transmembrane ER signaling proteins, including activating transcription factor 6 (ATF6), double-stranded RNA-activated protein kinase (PKR)-like endoplasmic reticulum kinase (PERK) and inositol-requiring enzyme-1 (IRE1) (58) (Fig. 1.1). The most common theory about the activation of the UPR signal transduction is that the key chaperone 78-kDa glucose-regulated protein (GRP78) functions as a negative regulator of the three ER

signaling proteins, which prevents the activation of the UPR. When unfolded proteins accumulate in the ER to a larger amount, GRP78 gets released from the three ER signaling proteins in order to support proper protein folding. The release of GRP78 enables unfolded proteins to bind directly to ATF6, PERK and IRE1 resulting in the activation of the three UPR signaling branches (59). The main intent of this signal transduction pathway is to restore the ER homeostasis and its protein-folding function by transcriptional upregulation of ER chaperones and expansion of the ER (60). The UPR is an adaptive mechanism and plays a crucial role especially in secretory highly active cell types, such as pancreatic β cells, plasma cells, hepatocytes, goblet cells and Paneth cells. However, if the load of unfolded proteins in the ER is prolonged or severe, the UPR induces apoptosis (61) and probably also autophagy (62).

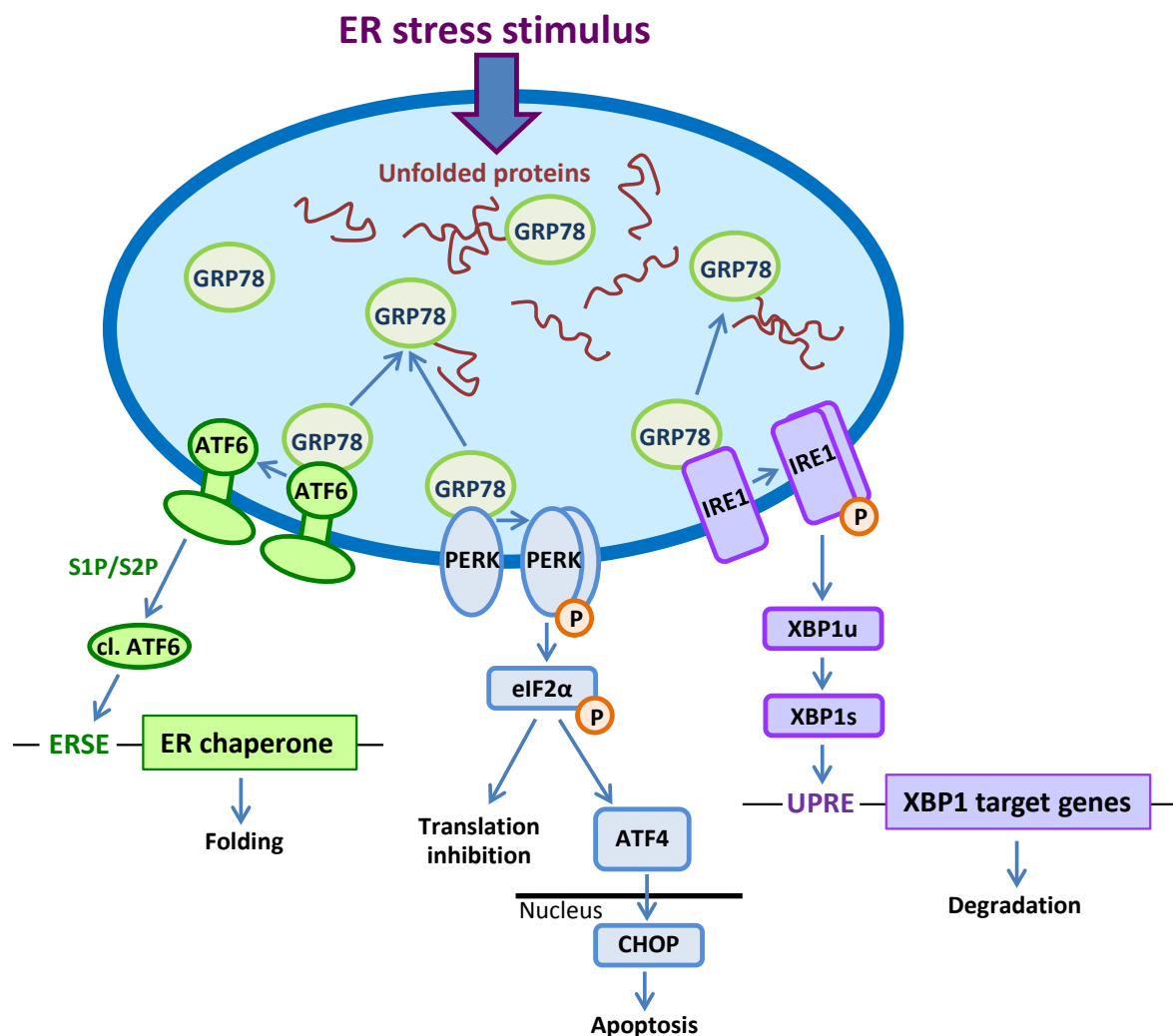


Fig. 1.1: Overview of the UPR with its three signaling pathways.

Cellular stress conditions result in the accumulation of unfolded proteins inside the ER leading to the release of the chaperone 78-kDa glucose-regulated protein (GRP78) from the three transmembrane ER signaling proteins activating transcription factor 6 (ATF6), protein kinase-like ER kinase (PERK) and inositol-requiring enzyme-1 (IRE1). Unfolded proteins bind directly to the ER signaling proteins, which results in the activation of the three UPR pathways to induce chaperone transcription, apoptosis and protein degradation. See text for detailed explanations and definitions of abbreviations (adapted from Hetz, 2012 (63)).

1.2.1 Activation of the IRE1 signaling pathway

The evolutionarily most conserved and best-investigated branch of the mammalian UPR signaling pathway involves IRE1 (64). Already in yeast cells, Ire1p senses ER stress and mediates UPR by upregulation of genes involved in protein folding and secretion (65). Homologous proteins of the other two UPR signaling pathways, ATF6 or PERK, are not present in the yeast genome (66). In mammalian cells, two homologues for IRE1 are found, IRE1 α and IRE1 β , which are expressed in a variety of tissues (67) or only in the intestinal (68) and airway mucous cells (69), respectively. In contrast to IRE1 β , IRE1 α is essential for placental development and embryonic viability (71). During ER stress, mainly IRE1 α mediates the UPR response and the activation of UPR target genes (72). IRE1 is a 100 kDa type I ER transmembrane protein with a serine/threonine kinase (73) and an endoribonuclease (74) activity in its cytosolic region.

Under unchallenged conditions, the N-terminal luminal domain of IRE1 is bound by GRP78. In response to ER stress, GRP78 dissociates from IRE1, causing its oligomerization, *trans*-autophosphorylation and a conformational change that activates its endoribonuclease domain. This activation of IRE1 enables a unique UPR signaling mechanism through the unconventional splicing of the messenger ribonucleic acids (mRNA) encoding XBP1 (Fig. 1.1). This splicing event removes 26 intronic nucleotides from the mRNA of *XBP1* and consequently alters its reading frame (75). The spliced form of XBP1 functions as a potent transcription factor activating the unfolded protein response element (UPRE) (76) and its target genes which control ER protein folding, glycosylation, membrane expansion, phospholipid biosynthesis and ERAD (77).

Additionally to *XBP1* splicing, the RNase activity of IRE1 is also involved in a conserved mechanism termed regulated IRE1-dependent decay of mRNA (RIDD) (78). This rapid degradation mechanism of ER-localized mRNAs supports the folding machinery by stopping the production of new proteins that challenge the ER. The cleavage events occur at consensus sequences similar to the XBP1 splicing sites (74). The resulting mRNA fragments are further degraded by the exosome. The RIDD activity of IRE1 β is stronger compared to IRE1 α (72). Furthermore, IRE1 was identified to form complexes with the tumor necrosis factor receptor-associated factor 2 (TRAF2) and subsequently activates the c-Jun amino-terminal kinase (JNK) and nuclear factor kappa-light-chain-enhancer of activated B cells (NF- κ B) pathway through the recruitment of the I κ B kinase (79,80). These processes enable the IRE1 pathway to also react on inflammatory events.

1.2.2 Activation of the ATF6 signaling pathway

The ATF6 signaling pathway leads mainly to the induction of a pro-survival transcriptional program during ER stress (81). ATF6 is a type II ER transmembrane protein with its C-terminal domain inside the ER lumen and a cytosolic N-terminal domain (82,83). Its N-terminus contains a basic leucine zipper motif responsible for the activation of UPR target genes (84). In *C. elegans* ATF6 is present as a single gene, whereas two closely related isoforms, ATF6 α (90 kDa) and ATF6 β (110 kDa), exist in mammalian cells (85). However, mainly ATF6 α mediates the UPR signaling pathway and the transcription of ER chaperones (86).

Under physiological conditions, the ER chaperone GRP78 binds to the luminal domain of ATF6 α and blocks its two Golgi apparatus localization signals (87). During ER stress, GRP78 releases ATF6 α , which can be transported by COPII-coated vesicles from the ER to the Golgi apparatus, where ATF6 α is cleaved by site 1 and site 2 proteases (S1P and S2P) (88) (Fig. 1.1). The cleavage events proceed as a sequential action of the serine protease S1P at the ER luminal domain of ATF6 α , followed by the metalloprotease S2P-mediated cleavage at the transmembrane region of ATF6 α (89). The resulting cytosolic 50 kDa fragment of ATF6 α (p50ATF6 α) enters the nucleus, binds to the ER stress response element (ERSE) sequence through binding to the nuclear transcription factor Y (NF-Y) and activates gene transcription (90). The consensus sequence of ERSE is CCAAT-N(9)-CCACG and acts in *cis* of many UPR-regulated genes (91). The transcription of UPR target genes, including ER chaperones such as the GRP78, the 94 kDa glucose-regulated protein (GRP94) and the protein kinase inhibitor of 58 kDa (p58^{IPK}), are strongly induced to support protein folding and restore the ER homeostasis (92). The ERSE promoter and its target genes are also inducible by XBP1, however to a much lesser extent (93). Despite this functional overlap, in mammalian cells, ATF6 α is induced and has an essential role during protein folding, modification and secretion, especially during ER stress conditions. Experiments with *ATF6 α ^{-/-}* mouse embryonic fibroblasts (MEFs) revealed attenuated upregulation of the main ER chaperones GRP78 and GRP94 upon ER stress (85). Especially, persistent and recurring ER stress resulted in reduced survival rates of *ATF6 α ^{-/-}* MEFs. This protective role of ATF6 α was also observed *in vivo*, where *ATF6 α ^{-/-}* mice were not able to survive intraperitoneal injections with the ER stress-inducing reagent tunicamycin (TM) (62).

1.2.3 Activation of the PERK signaling pathway

The main function of the PERK signaling pathway is to modulate translational activity within the cell. However, this pathway is also capable of inducing pro-apoptotic signals in case of chronic or severe ER stress conditions. PERK is a type I transmembrane protein with its C-terminal domain inside the ER lumen and its N-terminal domain towards the cytosol (95). The C-terminal domain functions as an ER stress sensor and the N-terminal domain is required for the oligomerization of PERK during ER stress (96).

Similar to ATF6 α , the ER-luminal domain of PERK is bound to GRP78 under physiological conditions. Upon ER stress, GRP78 dissociates from PERK resulting in the activation of the PERK signaling pathway (Fig. 1.1). The release of GRP78 initiates oligomerization and autophosphorylation of PERK, which induces the phosphorylation of the eukaryotic translation initiation factor 2 α (eIF2 α) on serine residue 51 (97). The phosphorylated form of eIF2 α inhibits the translation initiation to alleviate ER stress induced by the influx of new synthesized proteins into the ER, hence reduces the protein folding load (98). Paradoxically, some mRNAs are able to bypass this inhibition and are even upregulated by p-eIF2 α . These mRNAs contain an internal ribosome entry site (IRES) sequence in the 5' untranslated region, such as *ATF4* that encodes the activating transcription factor 4 (99). The transcriptional induction of *ATF4* induces the transcription of CCAAT-enhancer-binding homologous protein (CHOP), a transcription factor that facilitates ER stress-induced apoptosis by repressing Bcl2 expression (100). Additionally, CHOP increases the expression of the growth-arrest DNA damage gene 34 (GADD34), which forms a complex with protein phosphatase 1 (PP1) and functions then as a phosphatase that dephosphorylates the serine residue 51 of p-eIF2 α (101). This mechanism provides a negative feedback to the PERK signaling pathway and controls the duration of the inhibitory effect on the translation initiation.

Furthermore, the PERK signaling pathway is also involved in the phosphorylation and, therefore, activation of the transcription factor NF- κ B (102) and nuclear factor erythroid 2-related factor (NRF2) (103). The pathway member CHOP plays an essential role in regulating IL-23 protein levels (104). Thus, components of the PERK pathway may affect the regulation of redox homeostasis and inflammatory processes.

1.2.4 Cross-talk events between the three UPR signaling pathways

The UPR is an adaptive network that allows cross-talk events between the three major signaling branches to enable a fine-tuned ER stress response dependent on the type and duration of stress as well as on the challenged cell type. The communication between the

three branches coordinates the ER stress response to restore the ER homeostasis or to undergo cell death.

Cross-talk events were identified between all three UPR branches. For example, the activated cleaved form of ATF6 α also induces the transcription of *XBP1* in addition to its typical target genes such as the ER chaperones *GRP78* and *GRP94* (105). This mechanism allows the ATF6 α signaling pathway to influence the IRE1 branch without being able to bind directly to the UPRE sequence (106). In contrast, the spliced form of XBP1 can directly influence the ATF6 α signaling pathway by binding directly to the ERSE sequence, the typical target of ATF6 α (65). This event enhances the transcription of ER chaperones. The connection between the ATF6 α and the IRE1 pathway acts efficiently during ER stress conditions depending on its duration. The ER chaperone induction of ATF6 α functions faster compared to the XBP1 signal transduction, because the activation of ATF6 α depends only on cleavage events, whereas XBP1 needs to be translated from its mRNA to induce the target genes. Furthermore, ATF6 α heterodimerizes with the spliced form of XBP1 to control the expression of genes involved in ERAD through the URPE (85). During late stages of ER stress, the dimerization of the cleaved ATF6 fragments and the unspliced form of XBP1 facilitate the degradation of both proteins to reestablish physiological conditions in the cell (107).

The ATF6 α and IRE1 branches are also linked to the PERK pathway. The PERK pathway member CHOP is strongly induced by ATF4 but can also be stimulated by ATF6 α and XBP1 (108,109). Further support of the communication between the three UPR signaling pathways was provided by PERK-deficient cells, which were still able to induce its downstream target CHOP, however more slowly (110).

1.3 Role of ER stress in intestinal epithelial cell homeostasis and IBD

Unresolved ER stress and a disrupted UPR in IECs have been implicated in the development of intestinal inflammation (51). Especially the intestinal epithelium relies on an intact UPR, because it contains highly secretory cell types that are constantly exposed to environmental antigens and commensal microorganisms. The main cell types in the intestinal epithelium are absorptive enterocytes, goblet cells, Paneth cells and enteroendocrine cells (111). Beside their function as a physical barrier, these cells types secrete hormones, highly glycosylated mucins or defensins to protect the host (21). In particular, goblet and Paneth cells appear particularly sensitive towards unresolved ER stress and disturbances in the UPR signaling pathways (112).

The first indication of a connection between a disrupted UPR and the development of intestinal inflammation was given by GWAS from IBD patients. These studies identified disease susceptibility loci within or in close proximity to several genes including *XBP1*, *AGR2* and *ORMDL3* that encode proteins associated with functions in the ER or in the UPR signaling pathways (113). Additionally, mucosal tissues of patients with active forms of CD or UC revealed increased expression levels of the ER chaperone GRP78 (114) and upregulated phosphorylation of eIF2 α (115). Furthermore, *in vivo* studies were performed to investigate the role of a properly functioning UPR on the IEC homeostasis. One of the first animal studies, which linked ER stress to the development of spontaneous intestinal inflammation, was performed with IEC-specific *Xbp1*-deficient (*Xbp1* ^{Δ IEC}) mice. The absence of XBP1 in IECs resulted in ER stress with increased protein levels of the ER chaperone GRP78 and spontaneous enteritis characterized by crypt abscesses and infiltrations of immune cells. In addition, the small intestine of *Xbp1* ^{Δ IEC} mice revealed strongly reduced numbers of Paneth cells and goblet cells, resulting in impaired mucosal defense against oral *Listeria monocytogenes* infection. *Xbp1* ^{Δ IEC} mice are also more susceptible to the colitis-inducing agent dextran sodium sulfate (DSS). Moreover, *Xbp1* deficiency in IECs induces IRE1 α hyperactivation and increased JNK phosphorylation (51). This hyperactivation of IRE1 α results in the activation of the I κ B kinase, which phosphorylates I κ B proteins and targets them for polyubiquitination (116). The subsequent degradation by the 26S proteasome causes the release of NF- κ B that induces the transcription of pro-inflammatory cytokines and enzymes to modulate inflammatory processes (117). Another genetic risk factor for IBD that impacts the UPR is the protein disulfide isomerase *AGR2* (118). Under physiological conditions *AGR2* regulates developmental processes and functions as a survival factor that stimulates cell proliferation, cell adhesion, cell migration and inhibits apoptosis (119,120). However, increased expression levels of *AGR2* result in several types of metastatic adenocarcinomas (121–123), whereas decreased expression levels were associated with increased risk for CD and UC (118). Another study revealed that the deficiency of *Agr2* in mice affects the intestinal homeostasis characterized by elevated ER stress, decreased *Mucin 2* expression in goblet cells and multiple Paneth cell abnormalities resulting in spontaneous terminal ileitis and colitis (124). Also *ORMDL3* has been associated with IBD and ER stress (125). However, *Ormdl3*-deficient or IEC-specific *Ormdl3*-deficient mice are not yet described in the literature. Therefore, the exact role of this ER transmembrane protein in IBD remains to be elucidated (126).

In addition to the mentioned susceptibility genes that have been associated with human IBD by GWAS, further components of the UPR signaling pathway were studied to identify

the role of unresolved ER stress in the development of intestinal inflammation. These studies revealed that also components of the ATF6 pathway are involved in maintaining the intestinal homeostasis. For example, the deletion of the main regulator of ER chaperone gene expression, *Atf6α*, resulted in an increased disease activity during a DSS-induced colitis in mice. During this treatment, *Atf6α*^{-/-} mice suffered from severe body weight loss, rectal bleeding, mucosal damage and reduced expression of ER chaperones, including GRP78, GRP94 and p58^{IPK}. The same study also showed an increased sensitivity of *p58*^{IPK}^{-/-} mice to DSS, along with increased protein levels of the ER chaperone GRP78 and the pro-apoptotic protein CHOP (127). Furthermore, an inducible deletion of the ATF6α target *Grp94* in mice compromises the intestinal homeostasis, resulting in severe body weight loss, profound loss of intestinal villus structure and death (70). Additional evidence for the importance of the ATF6 branch in regulating the level of susceptibility to DSS-induced colitis was given by a mouse model with a hypomorphic allele of the membrane-bound transcription factor S1P-encoding gene, *Mbtps1*. This missense mutation in mice, which is also termed *woodrat* because of the effect of this mutation on the coat color (128), resulted in increased susceptibility to DSS-induced colitis (129). Due to the indispensable role of S1P during the cleavage and the resulting activation of *Atf6α*, *woodrat* mice exhibited reduced levels of the ER chaperones GRP78 and GRP94 in the colon upon DSS administration (129). All of these studies demonstrate the importance of the ATF6 branch in maintaining the intestinal homeostasis especially during DSS-induced colitis. Also the role of the PERK pathway on the pathogenesis of intestinal inflammation was investigated *in vivo*. The investigation of mice with a non-phosphorylatable Ser51A1a mutant of eIF2α in IECs (*eIF2α*^{AVA/IEC} mice) revealed dysregulated UPR signaling pathways in IECs and disrupted protein secretion functions of Paneth cells in the small intestine under physiological conditions. The loss of p-eIF2α resulted in an increased sensitivity of *eIF2α*^{AVA/IEC} mice to DSS and oral infection of *Salmonella Typhimurium*, demonstrating the important role of epithelial p-eIF2α in mucosal homeostasis (130). In contrast to other evaluated UPR components, the deletion of the pro-apoptotic factor *Chop*, which functions as a downstream target of PERK and p-eIF2α via ATF4, resulted in an improved course of the disease during DSS- and TNBS (trinitrobenzene sulfonic acid)-induced colitis (131). Moreover, mouse studies were performed to investigate the role of the IRE1 pathway in maintaining the intestinal homeostasis. Besides the described *Xbp1*^{ΔIEC} mice, *Ern1* (encodes IRE1α) conditional knockout mice were studied to get a better insight into the impact of this UPR pathway on the development of intestinal inflammation. These conditional knockout mice provide *Ern1*-deficient embryos with functionally normal placentas to circumvent embryonic lethality of *Ern1*^{-/-} mice (71). In colon tissues of these mice that express IRE1α only in their

placenta, *Xbp1* mRNA was not spliced and the protein expression of GRP78 was reduced. In contrast to *Xbp1^{ΔIEC}* mice, goblet cells of *Ern1^{-/-}* mice were inconspicuous (132). Interestingly, NF-κB phosphorylation and enteritis was diminished in mice with deletions of *Xbp1* and *Ern1* in intestinal epithelial cells compared to *Xbp1^{ΔIEC}* mice, indicating that NF-κB activation and ileitis is controlled by IRE1α (133). Additionally, the second isoform of IRE1, IRE1β (encoded by *Ern2*), was investigated *in vivo*. In contrast to the ubiquitously expressed IRE1α, IRE1β is only expressed in intestinal and airway mucous cells (69). Under physiological conditions, colonic mucosa tissues of *Ern2^{-/-}* mice exhibit elevated levels of the ER stress marker GRP78. Upon DSS treatment, GRP78 levels were even further increased in colonic tissues of *Ern2^{-/-}* mice and these mice were more susceptible to DSS-induced colitis than wild-type mice (68). IRE1β was also identified to promote efficient protein folding and secretion of mucin 2 in goblet cells by degrading *Mucin 2* mRNA (132). Thus IRE1β plays an important role in protecting the colonic epithelium, because Mucin 2 is the most prominent protein secreted from goblet cells and contributes to the barrier between the intestinal epithelium and the lumen (134).

For many components of the UPR the mentioned studies identified an important role in maintaining the intestinal homeostasis and regulating inflammatory processes. Beside pattern recognitions receptors (e.g. NOD2), immune signaling molecules (e.g. STAT3) or autophagy (e.g. ATG16L1), failures or disturbances in the UPR of IECs were identified to induce intestinal inflammation and may contribute to the pathogenesis of IBD in humans.

1.4 The ORMDL protein family

1.4.1 *ORMDL* genes belong to an evolutionary conserved gene family

In 2002, the orosomuroid 1 (*Saccharomyces cerevisiae*)-like (*ORMDL*) gene family was described for the first time by Hjelmqvist *et al.* (135). This gene family is highly evolutionarily conserved between yeast, plants and human. In the genome of vertebrates three *ORMDL* genes were identified, termed *ORMDL1*, *ORMDL2* and *ORMDL3*. Each of the three genes is localized on a different chromosome in mammalian cells. In the human genome, *ORMDL1* is located on chromosome 2, *ORMDL2* on chromosome 12 and *ORMDL3* on chromosome 17. The comparison of the encoded proteins revealed high positional identities. 77 % of the amino acid residues were conserved throughout the three human sequences (Fig. 1.2). The pairwise comparison between human and murine *ORMDL* orthologs revealed even 95 % positional identities. Two conserved homologues of the *ORMDL* gene were also identified in the genome of plants (including *Arabidopsis thaliana*) and yeast (*Saccharomyces cerevisiae*), termed *ORM1* and *ORM2*. Only one

ORMDL gene is present in the genome of microsporidias (*Encephalitozoon cuniculi*), invertebrates (including *Drosophila melanogaster*) and urochordates (*Ciona intestinalis*). However, in the genome of the nematode *Caenorhabditis elegans* no homologous sequence was found (135).

```

human_ORMDL1  MNVGV AHSEVNP NTRVMNSRGMWLT YALGVGL LHIVLLS IPFFSVPV AWTLTNII HNLGM 60
human_ORMDL3  MNVGVTAHSEVNP NTRVMNSRGIWLSYVLA IGLLHIVLLS IPFVSVPVV WTLTNLIH NMGM 60
human_ORMDL2  MNVGV AHSEVNP NTRVMNSRGIW LAYIILVGL LHMVLLS IPFFSIPV VWTLTNVI HNLAT 60
      ****.*****:***:* : :****:*****.*:*.*****:***:.

human_ORMDL1  YVFLHAVKGT PPFETPDQG KARLLTHWE QLDYGVQ FTSSRKFFT ISPIILYFL ASFYTKYD 120
human_ORMDL3  YIFLHTVKGT PPFETPDQG KARLLTHWE QMDYGVQ FTASRKFLT ITPIVLYFL TSFYTKYD 120
human_ORMDL2  YVFLHTVKGT PPFETPDQG KARLLTHWE QMDYGLQ FTSSRKFLS ISPIVLYLL ASFYTKYD 120
      *:***:*****:***:***:****: :*:**:*:*.*****

human_ORMDL1  PTHFILNTAS LLSVLI PKMPQLHG VRIFGINKY 153
human_ORMDL3  QIH FVLNTV SLSVLI PKLPQLHG VRIFGINKY 153
human_ORMDL2  AAHFLINTAS LLSVLLP KLPQFHG VRVFGINKY 153
      **:*.**.*:***:***:***:****:*****

```

Fig. 1.2: Alignment of the human *ORMDL* amino acid sequences using the CLUSTALW2 program.

1.4.2 Association of *ORMDL3* with several diseases

Single nucleotide polymorphisms (SNPs) in close proximity to the *ORMDL3* gene were identified by association studies as risk variants for a variety of diseases, including bronchial asthma (136), CD (137), UC (138), type 1 diabetes (139), glioma (140), primary biliary cirrhosis (141), rheumatoid arthritis (142) and ankylosing spondylitis (143). In both bronchial asthma and CD genetic variants were shown to elevate *ORMDL3* expression levels (125,137). In the case of CD, the most significant disease associated expression quantitative trait locus (eQTL) affects *ORMDL3* (137). The association of *ORMDL3* with bronchial asthma and IBD are interesting as lung and intestine are composed of partially similar surface cell types, such as epithelial cells and goblet cells. Additionally, both tissues are exposed to potential harmful antigens and highly depend on an intact immune system that controls the balance between antigen responsiveness and non-responsiveness (144). These associations of *ORMDL3* with diseases involved in dysregulated immune response provide evidence of the participation of *ORMDL3* in inflammatory processes. In contrast to *ORMDL3*, *ORMDL1* and *ORMDL2* were not associated with IBD by GWAS. However, analysis of gene expression associated SNPs identified *ORMDL1* as a promising eQTL influencing hypertension (145), whereas *ORMDL2* is not linked to any disease so far.

1.4.3 ORMDL proteins regulate the ER homeostasis

ORMDL proteins are ER-resident transmembrane proteins with a molecular mass of 17.4 kDa. These proteins contain two transmembrane domains, with a loop into the ER lumen and the N- and C-terminus facing the cytoplasm (146). ORMDL proteins are ubiquitously expressed in fetal as well as adult tissues (135). Although ORMDL proteins lack characteristic functional domains, these proteins were identified to influence several cellular pathways and processes in the cell, including UPR, Ca^{2+} signaling, sphingolipid and ceramide synthesis, which are thought to affect the ER homeostasis or to be induced by elevated or dysregulated ER stress.

1.4.3.1 ORMDL proteins affect components of the UPR

The first study of ORMDL proteins by Hjelmqvist *et al.* implied a role of ORMDL proteins in the UPR (135). The absence of both Orm proteins in yeast activated the UPR constitutively (147,148). Additionally, deletions of the *ORM* genes in yeast affected their cell growth and ability to respond to chemically induced ER stress using dithiothreitol (DTT), a strong reducing agent, or tunicamycin (TM), a glycosylation inhibitor. Mutants with only one functional *ORM* gene were able to respond comparable to the wild-type strain to DTT or tunicamycin, suggesting partial functional redundancies of the two yeast homologues. Interestingly, the phenotype of the double knockout mutants could also be rescued by functional complementation with the human *ORMDL3*, indicating functional and structural evolutionary conservations of this gene family (135).

For ORMDL proteins further *in vitro* studies indicated a role in regulating components of the UPR also in mammalian cells, however these data are inconsistent. Cantero-Recasens *et al.* demonstrated an influence of ORMDL3 on the PERK pathway (146). Their study revealed that overexpression of ORMDL3 in HEK-293 cells resulted in elevated p-eIF2 α protein levels without affecting *XBP1* splicing. In contrast, overexpression of ORMDL3 in fibroblast-like cells (Cos-7) reduced the UPRE promoter activity, indicating less *XBP1* splicing (138). However, Miller *et al.* reported increased ERSE promoter activities in ORMDL3 overexpressing lung epithelial cells (A549), whereas the IRE1 and the PERK signaling branch were left unchanged (149). An additional study observed no differences in UPR activation in SV40-transformed normal human airway epithelial cells (1HAE) treated with *ORMDL3* siRNA (small interfering RNA) (125). Whether these discrepancies are a result of the strength of the ER stress, the investigated cell type or depending on the nature of the ER stress inducer, is not known.

In summary, there is no common understanding of the functional principle of ORMDL3 on the three UPR signaling branches so far.

1.4.3.2 Regulation of the Ca²⁺ homeostasis by ORMDL proteins

Alterations in the Ca²⁺ homeostasis of the ER result in ER stress and activate the UPR signaling pathway (150). ORMDL3 was identified to regulate ER-mediated Ca²⁺ homeostasis, which is crucial during protein folding (146). Appropriate Ca²⁺ levels in the ER are essential for proper protein assembly and folding, whereas abnormal Ca²⁺ levels can induce the pathophysiology of many diseases (151). The homeostasis in the ER is maintained by Ca²⁺ release channels and pumps that enable the exit of Ca²⁺ from the ER to the cytoplasm or return Ca²⁺ to the ER, respectively (152). In this process ORMDL3 was shown to interact and affect the sarco-endoplasmic reticulum Ca²⁺ ATPase (SERCA). Overexpression of ORMDL3 revealed elevated cytosolic Ca²⁺ levels and reduced ER-mediated Ca²⁺ signaling in HEK-293 cells. Knockdown of endogenous ORMDL3 reinforced the release of ER Ca²⁺ (146). Thus, ORMDL3 was found to function as a negative regulator of SERCA. Controversial results were demonstrated by Miller *et al.*, whereby overexpression of ORMDL3 induced *SERCA2b* mRNA expression in lung epithelial cells (A549) (149). A recent study from Miller *et al.* in 2014 supported their previous *in vitro* results by showing increased mRNA expression level of *Serca2b* in transgenic mice overexpressing human ORMDL3 (153). Furthermore, the effect of ORMDL3 on the Ca²⁺ homeostasis was also shown to modify lymphocyte activation *in vitro*, which provides an additional indication for the connection of ORMDL3 and inflammatory processes (154). Thus, ORMDL3 regulates the ER Ca²⁺ levels and maintains the ER homeostasis.

1.4.3.3 ORMDL proteins regulate sphingolipid synthesis

In response to ER stress, the sphingolipid synthesis is thought to be modulated by ORMDL proteins (155). Studies in yeast, plants and human cells identified a fundamental role of ORMDL proteins in the sphingolipid synthesis and homeostasis. In yeast, increased expression levels of *ORM1* or *ORM2* reduced levels of the long-chain base 1 (*LCB1*) and *LCB2*, whereas cells with deletions of *ORM1* or *ORM2* showed highly elevated levels of *LCB1* and *LCB2* (156). *LCB1* and *LCB2* encode the serine palmitoyltransferase (*LCB1/2* in yeast and *SPTLC1/2/3* in mammals), an essential enzyme in the first and rate-limiting step in sphingolipid synthesis (157). Sphingolipids are important components of eukaryotic cell membranes and play vital roles in cell signaling crucial for cell growth and survival (158). In this process, Orm proteins were proposed to

form a complex with the serine palmitoyltransferase. Additionally, Orm proteins act directly on Lcb1 and Lcb2, suggesting that Orm1 and Orm2 negatively regulate sphingolipid synthesis. Loss of *Orm1* and *Orm2* increased the activity of the serine palmitoyltransferase, resulting in toxic accumulations of sphingolipids (156). As a potential regulatory mechanism of Orm proteins on the serine palmitoyltransferase activity the phosphorylation status of this protein was identified in yeast (159). However, ORMDL proteins in mammalian cells lack the sequence, which is phosphorylated in yeast (160). Similar results were also obtained in plants. *ORMDL* genes were identified to control sphingolipid homeostasis in plants, as shown for the example of rice plants (161). Main metabolites of complex sphingolipids are ceramides, which are also *de novo* synthesized by serine palmitoyltransferase (162). Similar to sphingolipid levels, ceramide levels were also elevated upon siRNA-mediated knockdown of all three *ORMDL* genes in mammalian cells (156,160,163). Based on these findings, ORMDL proteins are thought to be negative regulators of the ceramide and sphingolipid synthesis and this function is even more pronounced during the ER stress response.

1.5 Objective of the study

IBD with its major subtypes, CD and UC, are complex multigenic disorders with several identified risk loci, including an eQTL affecting *ORMDL3*. The role and the function of *ORMDL3* *in vitro* and *in vivo* with regard to the pathogenesis of chronic intestinal inflammation are incompletely understood and investigated. Thus, the general objective of this study is to analyze the effect of ORMDL proteins on the three UPR signaling branches during ER stress and its impact on the intestinal homeostasis and regeneration under baseline and challenging conditions.

Major questions:

1. Effect of ER stress on ORMDL proteins: Determination of ORMDL protein expression levels during chemically-induced ER stress in several cell lines and primary murine cells in order to investigate whether ORMDL protein levels are influenced by ER stress.
2. Regulatory capacity of ORMDL proteins on the UPR: At the moment there is no common understanding of the functional mechanism of *ORMDL3* on the three UPR signaling branches. Previous investigations have shown controversial roles of *ORMDL3* on the UPR, ranging from no effect to affecting one or another signaling branch only (as referred in chapter 1.4.3). Detailed *in vitro* investigation of the impact of human ORMDL proteins on the UPR signaling branches should clarify several questions:
 - a. Do ORMDL proteins modify the UPR?
 - b. In case that ORMDL proteins affect the UPR, which components and UPR signaling branches are regulated?
 - c. How could ORMDL proteins be able to regulate the UPR signaling branches?
3. Role of ORMDL proteins *in vivo*: For a detailed *in vivo* analysis of the association of *ORMDL3* as genetic risk loci for human IBD, there is a high demand for the generation and investigation of *Ormdl3*-deficient mice. Since the high amino acid identity of 84 % between *ORMDL1* and *ORMDL3* points to functional redundancies of these proteins, a comparable phenotype analysis of *Ormdl1*-deficient mice is of fundamental interest too. The deficient mice provide an opportunity to examine the role of *ORMDL1* and/or *ORMDL3* in a living multicellular organism:

- a. Does the depletion of *Ormdl1* or *Ormdl3* affect the basal phenotype and in particular the intestinal homeostasis?
- b. How does the deficiency of *Ormdl1* or *Ormdl3* in mice affect the susceptibility to DSS-induced colitis?
- c. Are *Ormdl1*- and *Ormdl3*-deficient mice more susceptible to intraperitoneal injections of the ER stress-inducing reagent tunicamycin?

2 Methods

2.1 Cell biological methods

2.1.1 Cell lines

Cell lines used for *in vitro* investigation were purchased from the Leibniz-Institute DSMZ-German Collection of Microorganisms and Cell Cultures or from the American Type Culture Collection (ATCC) (Table 2.1). All applied cell lines were cultured at 37 °C and 5 % (v/v) carbon dioxide in their appropriate nutrition media (Gibco/Life Technologies, Darmstadt, Germany).

Table 2.1: Overview of applied cell lines

Cell line	Company	Product nr.	Species	Cell type	Nutrition medium
HeLa	DSMZ	ACC-57	human	cervix carcinoma	RPMI, 10 % (v/v) FCS
HEK-293	DSMZ	ACC-305	human	embryonal kidney	DMEM, 10 % (v/v) FCS
HT-29	DSMZ	ACC-299	human	colon adenocarcinoma	DMEM, 10 % (v/v) FCS
RAW 264.7	ATCC	TIB-71	murine	macrophage-like	DMEM, 10 % (v/v) FCS

The cell lines were passaged twice per week for maintenance. Cells were washed with PBS and treated with a trypsin/EDTA solution (Life Technologies, Darmstadt, Germany) for 5 min at 37 °C. The resulting cell suspension was centrifuged at 300 g for 5 min. The cell pellet was resuspended in 5 ml fresh nutrition medium. A dilution of cells was transferred into new culture flasks for maintaining cultured cells or sowed with a defined cell number for experiments (Table 2.2). All steps were performed under sterile conditions using a laminar flow workbench (Thermo Scientific, Bremen, Germany).

Table 2.2: Overview of applied cell culture dishes for experiments with cell lines

Experiment	Cell culture dish	Cell number/well	Medium volume [ml]
Cell fractionation	10 cm dish	5×10^6	10
Co-immunoprecipitation	10 cm dish	5×10^6	10
Protein lysates	6-well plate	2×10^5	2
RNA isolation	6-well plate	2×10^5	2
FACS measurement	6-well plate	2×10^5	2
Fluorescence microscopy	6-well plate	2×10^5	2
Reporter gene assay	96-well plate	2×10^5	0.1

2.1.2 Transient transfection of plasmid DNA

Plasmid DNA was transiently transfected into cultured eukaryotic cells by lipofection using FuGENE® 6 transfection reagent (Promega, Mannheim, Germany). The cationic liposome formulation FuGENE® 6 forms complexes with negatively charged plasmid DNA. This complex can fuse with the cell membrane which allows plasmid DNA to enter the cell.

The appropriate amount of FuGENE® 6 was diluted in Opti-MEM® (Life Technologies, Darmstadt, Germany) and incubated for 5 min at room temperature (Table 2.3). Plasmid DNA was added to the transfection mix and incubated for additional 15 min. After incubation, the transfection mix was added dropwise to the cells. The transfection mix was distributed by gently shaking the cell culture dish horizontally. The cells were placed back into the incubator for 24 h. All steps were performed under sterile conditions.

Table 2.3: Overview of formats and volumes of plasmid DNA transfections

Cell culture dish	Opti-MEM® volume [μ l]	DNA [μ g]	FuGENE® [μ l]
10 cm dish	500	5	15
6-well plate	100	1	3
96-well plate	5	0.05	0.15

2.1.3 Transfection of siRNA

Transfection of small interfering RNA (siRNA) into cultured eukaryotic cells was performed using siPORT™ *Amine* transfection reagent (Life Technologies, Darmstadt, Germany). The positively charged lipid-based formulation of siPORT™ *Amine* forms complexes with negatively charged siRNA which can fuse with the cell membrane and enables the siRNA to enter the cell.

For the transfection of siRNA the appropriate volume of siPORT™ *amine* was diluted in a 1.5 ml reaction tube with Opti-MEM® (Table 2.4). Target-specific siRNA was mixed with Opti-MEM® in a second 1.5 ml reaction tube. Both tubes were incubated separately for 10 min at room temperature. The solutions of both tubes were combined and incubated for additional 10 min. After incubation, the solution was added dropwise to the cells and distributed in the well by gently shaking the plate horizontally. Cells were placed back into the incubator for 24 h. All steps were performed under sterile conditions.

Table 2.4: Overview of formats and volumes of siRNA transfections

Cell culture dish	Opti-MEM® volume [μ l]	siPORT™ [μ l]	siRNA [μ M]
6-well plate	100	5	7.5
96-well plate	5	0.25	0.375

2.1.4 Life cell XBP1 splicing assay using a XBP1-venus reporter construct

ER stress induces the UPR which consists of three distinct signal pathways including ATF6 α , IRE1 and PERK. Activation of IRE1 causes mRNA splicing of the transcription factor XBP1. This splicing event can be monitored in life cells using a XBP1-venus construct (164). A green fluorescent protein variant, called venus, was fused to the C-terminus of the human XBP1 sequence (Fig. 2.1). Under baseline conditions, XBP1 splicing does not occur. The translation of *XBP1* ends at its stop codon which is localized upstream of the venus fusion. Hence, the venus construct is not in the open reading frame of *XBP1*, thus not translated. Under ER stress conditions, 26 nucleotides are spliced out of the *XBP1* mRNA introducing a frame shift. Due to this frame shift, the translation of the spliced *XBP1* mRNA ends only at the stop codon of the venus protein fused in frame. To prevent induction of UPR target genes by overexpression of XBP1-venus, a pCAX-XBP1 Δ DBD-venus plasmid was used. In this construct the DNA-binding domain (DBD) of XBP1 is deleted and therefore this construct cannot induce UPR target genes. The expressed green fluorescent XBP1-venus fusion protein can be detected by fluorescence microscopy or fluorescence-activated cell sorting (FACS) technique.

For detection of XBP1 splicing HEK-293 cells were co-transfected with pCAX-XBP1 Δ DBD-venus and either pCMV-HA, pCMV-HA-ORMDL1 or pCMV-HA-hORMDL3 as described in chapter 2.1.2. In an additional approach, HEK-293 cells were treated with a mix of siRNA for hORMDL1, hORMDL2 and hORMDL3 or control scrambled siRNA (allStars negative control siRNA, Qiagen, Hilden, Germany) and transfected with pCAX-XBP1 Δ DBD-venus to detect XBP1 splicing as described. 24 h after transfection, cells were treated with DMSO as a control or 20 μ g/ml tunicamycin diluted in DMSO for 24 h. Fluorescence intensity was investigated by fluorescence microscopy and quantified by FACSCalibur cell analysis system (BD Biosciences, Heidelberg, Germany) detecting spliced XBP1-venus fluorescence. The results are displayed as geometric mean fluorescent intensity.

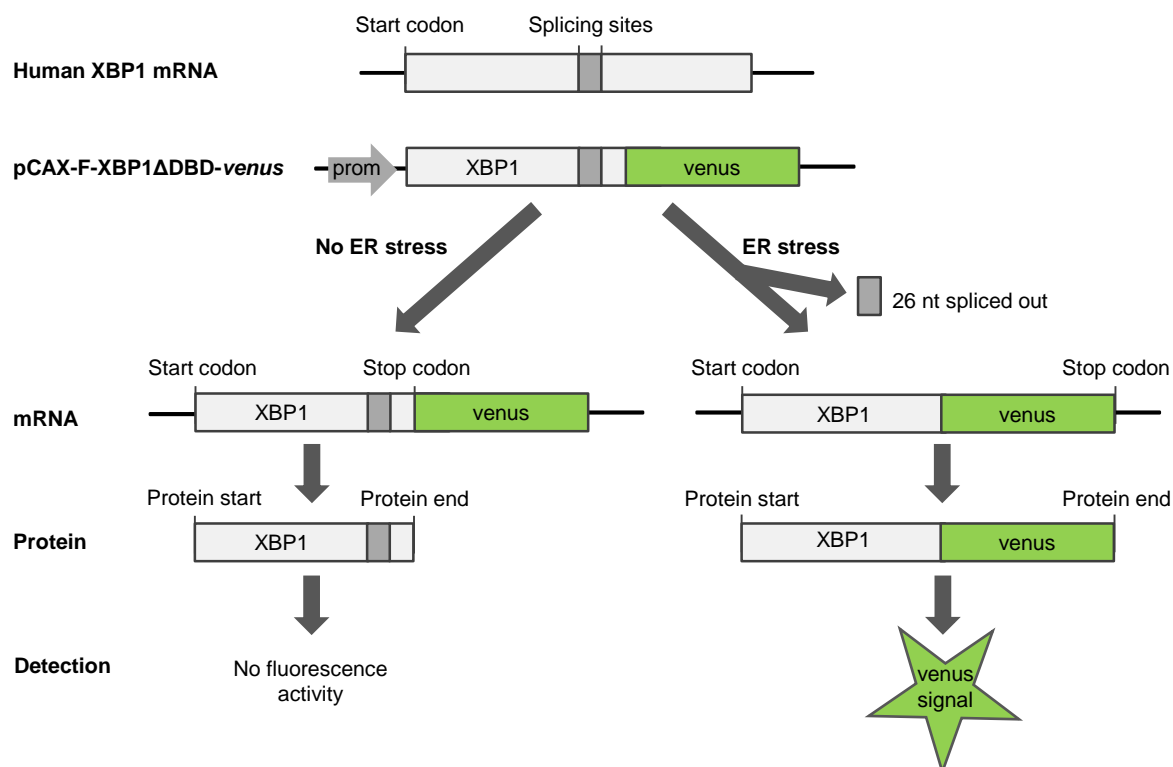


Fig. 2.1: Functional principle of the life cell XBP1 splicing assay using a XBP1-venus reporter construct.

Fusion of XBP1 and venus, a variant of green fluorescence protein, enables life cell monitoring of XBP1 splicing. Under normal conditions, splicing of *XBP1* mRNA does not occur, leading to the translation into the XBP1 protein without venus fusion. During ER stress 26 nucleotides are spliced out of the *XBP1* mRNA resulting in a frame shift expressing fluorescent XBP1-venus fusion protein. Figure was adapted from (164).

2.1.5 Promoter-mediated luciferase reporter assay

Each of the three UPR branches can activate specific intracellular response elements, which was analyzed using the dual-luciferase reporter assay system (Promega, Mannheim, Germany). Each promoter region of the response elements was cloned upstream of the luciferase from firefly (*Photinus pyralis*). The luciferase from *Renilla* (*Renilla reniformis*) was used as an internal transfection and cell viability control. The activation of the response elements was quantified by normalizing the firefly bioluminescence to the *Renilla* bioluminescence.

HEK-293 cells were sowed on 96-well plates at a density of 2×10^4 cells per well. After 24 h, cells were transfected with 12 ng of one of the ER stress firefly luciferase reporter constructs and 3 ng of the *Renilla* luciferase plasmid pRL-TK. For the measurement of the luciferase activity, cells were lysed using 25 μ l of 1X passive lysis buffer and subjected to a freeze-thaw cycle for complete cell lysis. Substrate addition and luminescence measurement was automatized by Tecan Infinite F200 pro plate reader using the i-control software (Tecan, Männedorf, Switzerland). The quotient of response element dependent firefly luminescence and *Renilla* luminescence resulted in relative light units (RLU).

2.1.6 Flow cytometric analysis

Cell surface expression of interferon gamma (IFN γ) target genes, including the major histocompatibility complex (MHC) class I (MHC I) and class II (MHC II), were investigated by flow cytometry. 1×10^5 cell from the lamina propria fraction of *Ormdl3*^{-/-} and wild-type mice were preincubated with anti-CD16/32 to block Fc receptors and prevent unspecific antibody binding, washed with FACS wash buffer and incubated with the indicated antibody conjugates for 30 min at 4°C in a final volume of 10 μ l FACS wash buffer. After the staining, cells were washed three times with FACS wash buffer and fixed using 1 % paraformaldehyde solution. The appropriate isotype-matched control antibodies were included in the experiment to determine the level of background staining. Flow cytometric analyses were performed on a FACSCalibur cell analysis system (BD Biosciences, Heidelberg, Germany) using BD CellQuest ProTM software (BD Biosciences, Heidelberg, Germany). All applied antibodies are listed in the supplementary information (Table 8.12).

2.2 Molecular biological methods

2.2.1 Isolation of total RNA

Murine tissue samples were ground using mortar and pestle in liquid nitrogen to prevent RNA degradation. The grounded samples were lysed in 700 μ l RLT buffer (Qiagen, Hilden, Germany) containing 1% 2-mercaptoethanol. Resulting sample lysates were applied to QIAshredder columns for homogenization. The RNA extraction was performed using the RNeasy Mini Kit (Qiagen, Hilden, Germany) according to the manufacturer's protocol. An incorporated on-column DNase step was carried out to avoid contaminations by genomic DNA. The purified RNA was eluted in 50 μ l RNase-free water and the RNA concentration was determined using the NanoDrop ND-1000 spectrophotometer (PeqLab Biotechnologie GmbH, Erlangen, Germany). RNA samples were stored at -80 °C.

2.2.2 cDNA synthesis

For reverse transcriptase the Maxima H Minus First Strand cDNA Synthesis Kit (Thermo Scientific, Bremen, Germany) was selected to generate complementary DNA (cDNA) from an RNA template. According to the manufacturer's protocol, 500 ng to 1 μ g total RNA was used as template for the generation of cDNA. In a first step, the RNA was incubated with Oligo(dt)18 oligonucleotide, dNTP mix and water at 65 °C for 5 min (Table 2.5). Subsequently, 5X RT buffer and Maxima H Minus reverse transcriptase (RT) was added to the mixture and incubated as indicated. The synthesized cDNA was diluted 1:10 with nuclease-free water and stored at -20 °C until further usage.

Table 2.5: Components and incubation conditions of a reverse transcription reaction mixture

Step	Component	Quantity	Incubation
1.	RNA	500 ng	5 min at 65 °C
	Oligo(dt) ₁₈ oligonucleotide	0.125 µl	
	dNTP mix (10 mM each)	0.5 µl	
	nuclease-free water	to 7.5 µl	
2.	5X RT buffer	2 µl	10 min at 25 °C
	Maxima H Minus RT	0.5 µl	15 min at 50 °C 5 min at 85 °C

2.2.3 Endpoint polymerase chain reaction (PCR)

Endpoint polymerase chain reactions (PCRs) were performed for semi-quantitative mRNA analyses of transcripts of interests. cDNA samples were used as starting material for endpoint PCRs. Levels of mRNA expression were determined by target-specific oligonucleotides, which amplified exon spanning PCR products with sizes between 150 and 500 bp. All applied oligonucleotides were designed with annealing temperatures of 60 °C and were synthesized by Microsynth AG (Balgach, Switzerland). The full list of used oligonucleotides is given in the supplementary material (Table 8.8). The amplification was carried out by PCR using GoTaq™ polymerase (Promega, Mannheim, Germany) in a 96-well thermocycler (Applied Biosystems, Carlsbad, USA). PCR components and the cycling protocol are given in Table 2.6. The amplification of target genes were conducted with low cycle numbers to ensure amplifications in the unsaturated PCR phase.

Table 2.6: Components and cycling protocol for endpoint PCRs

PCR component	Volume [µl]	Temperature [°C]	Time	Cycles
cDNA	2	95	3 min	1
dNTPs mix (10 mM each)	1	95	30 sec	28-33
Oligonucleotide mix (10 µM each)	1	T _{anneal}	30 sec	
5X GoTaq™ buffer	5	72	30 sec	
GoTaq™ polymerase	0.4	72	7 min	1
Nuclease-free water	ad 20	4	hold	1

For the semi-quantitative analyses, PCR products were separated by agarose gel electrophoresis (2.2.4). The intensity of the PCR products was visualized upon exposure to UV light in the Molecular Imager ChemiDoc XRS Imaging System (Bio-Rad, Munich, Germany). The housekeeper gene *GAPDH* was used as an internal control for gene expression normalization.

2.2.4 Agarose gel electrophoresis

DNA fragments and PCR product sizes were verified by agarose gel electrophoresis. This method separates negatively charged DNA fragments according to their size in an electric field. Agarose gel electrophoresis was performed with a gel concentration of 1 % LE agarose and 0.5 % TAE buffer. A constant voltage of 120 V and a maximum current of 300 mA were applied using Bio-Rad Power Pac 300 power supply (Bio-Rad, Munich, Germany). Due to the addition of 2 μ l SYBR Safe DNA gel stain, a DNA-intercalating agent, the size of DNA fragments can be visualized upon exposure to UV light in the Molecular Imager ChemiDoc XRS Imaging System (Bio-Rad, Munich, Germany). The SmartLadder MW-1700-10 (Eurogentec, Cologne, Germany) was used as a DNA fragment size marker.

2.2.5 Quantitative real-time polymerase chain reaction

Quantitative real-time PCRs (qPCRs) enabled the quantification of mRNA levels using target-specific oligonucleotides. The qPCR method is based on the PCR technique with an additional DNA quantification step at the end of each amplification cycle. SYBR Green, a DNA intercalating fluorescent dye, was used for quantification.

For qPCR, oligonucleotides were designed based on the coding region of the gene of interest with annealing temperatures of 60 °C and amplicon lengths of 150 to 350 bp. The oligonucleotides were synthesized by Microsynth AG (Balgach, Switzerland). All employed oligonucleotides are listed in the supplementary information (Table 8.8). The SYBR[®] Select Master Mix (Life Technologies, Darmstadt, Germany) was used for qPCR according to the manufacturer's protocol. 5 μ l of sample cDNA was mixed with 5 μ M of each oligonucleotide and 4.5 μ l SYBR[®] Select Master Mix. The reaction was carried out on 384-well plates using the 7900 HT Fast Real-Time PCR System (Applied Biosystems, Carlsbad, USA). All results were normalized to their respective *GAPDH* housekeeper mRNA level and shown as foldchange relative to a reference.

In some experiments predesigned TaqMan probes were applied, which were obtained from Applied Biosystems (Carlsbad, USA). The employed TaqMan probes and their order numbers are listed in the supplementary information (Table 8.9).

2.2.6 Generation of expression constructs

An overview of all employed plasmids is located in the supplementary material (Table 8.7). Plasmids were either generated by Gateway® cloning or by traditional restriction enzyme-based cloning.

Gateway® cloning

Plasmids, such as pCMV-HA-EGFP, pCMV-HA-hORMDL1 or pCMV-HA-hORMDL3, were constructed using the Gateway® cloning system (Life Technologies, Darmstadt, Germany). In a first step, the target sequence was generated by a hot start PCR (Table 2.7) using specific oligonucleotides with overhangs containing *attB*-recombination sites. The hot start PCR technique was applied to avoid the generation of non-specific PCR amplicons due to the inhibition of the Phusion Hot Start II polymerase activity at low temperatures. The resulting PCR product was analyzed by gel electrophoresis and isolated from the gel using the QIAquick Gel Extraction Kit (Qiagen, Hilden, Germany) according to the manufacturer's protocol.

Table 2.7: Reaction mixture and cycling protocol for a cloning hot start PCR

PCR component	Quantity/ Volume	Temperature [°C]	Time	Number of cycles
DNA template	200 ng	98	30 sec	1
10 mM dNTPs	0.5 µl	98	10 sec	30
Oligonucleotide mix (10 µM each)	1 µl	T _{anneal}	20 sec	
5X Phusion HF buffer	5 µl	72	30 sec/kb	
Phusion Hot Start II polymerase	0.25 µl	72	7 min	1
Nuclease-free water	ad 25 µl	4	hold	1

The purified PCR product was inserted into the donor vector (pDONR221) by a BP Clonase II reaction (Table 2.8) (Life Technologies, Darmstadt, Germany), which replaced the negative selection marker *ccdB* with the PCR product. The reaction was incubated at 25 °C for 1 h, followed by digestion of phage enzymes using Proteinase K treatment at 37 °C for 15 min.

For the transformation, one shot TOP10 *Escherichia coli* cells (Life Technologies, Darmstadt, Germany) were thawed and 2 µl of the Proteinase K-treated BP Clonase II reaction were added. The mixture was incubated on ice for 30 min, applied to a 42 °C water bath for 30 sec and placed back on ice for 3 min. After the treatment, cells were supplied with 250 µl of S.O.C. medium (Life Technologies, Darmstadt, Germany) and incubated on a shaker at 37 °C for 1 h. 100 µl of the suspension were plated on

kanamycin containing agar plates. Due to the negative selection marker *ccdB*, which codes for a growth inhibiting protein (165), only positively recombined clones grew overnight at 37 °C. Single clones were picked using sterile pipette tips, purified (as described in chapter 2.2.7) and verified by Sanger sequencing (as described in chapter 2.2.8) employing M13 oligonucleotides. Plasmids containing the target sequence were called entry plasmid.

The second cloning step using the LR Clonase II (Life Technologies, Darmstadt, Germany) was performed to obtain plasmids, which contain N-terminal GFP or HA sequences upstream of the target sequence. The plasmids pDEST53 or pCMV-HA-GW were used as destination plasmids. The LR Clonase II reaction (Table 2.8) was incubated on ice for 30 min and transformed into one shot TOP10 *Escherichia coli* cells. Plasmids were prepared as described in chapter 2.2.7.

Table 2.8: Gateway cloning: Components for BP and LR Clonase II reactions

BP Clonase II reaction Component	Quantity/ Volume	LR Clonase II reaction Component	Quantity/ Volume
PCR product	150 ng	Entry plasmid	150 ng
pDONR221	150 ng	Destination plasmid	150 ng
TE buffer	ad 10 µl	TE buffer	ad 10 µl
BP Clonase II	2 µl	LR Clonase II	2 µl

Restriction enzyme-based cloning

Restriction enzyme-based cloning was performed to generate plasmids such as pGL3-ATF4 and pGL3-ERSE. The cloning method was performed as described exemplary for the pGL3-ERSE construct.

The target sequence was amplified by PCR with target-specific oligonucleotides, which contained overhangs with sequences for selected restriction enzymes. The 5' oligonucleotide carried the sequence for the restriction enzyme *KpnI* and the 3' oligonucleotide for *BglI*. A hot start PCR was performed on cDNA from HeLa cells applying the protocol shown in Table 2.7. To validate the correct PCR product by size, 5 µl of the PCR reaction were loaded on an agarose gel and visualized by UV light using the Molecular Imager ChemiDoc XRS Imaging System (Bio-Rad, Munich, Germany). The remaining PCR reaction was cleaned up by the QIAquick PCR Purification Kit (Qiagen, Hilden, Germany) according to the manufacturer's protocol.

The purified PCR product served as the insert for the target-vector pGL3-Basic. For the cloning, the purified PCR product and the target-vector were incubated separately with a

KpnI and *BglII* containing restriction enzyme mix (Table 2.9) at 37 °C for 1 h. The digestion resulted in an insert and a target-vector with sticky ends. The digested sequences were separated on an agarose gel and purified using the QIAquick Gel Extraction Kit (Qiagen, Hilden, Germany) according to the manufacturer's protocol.

Table 2.9: Exemplary components of double digest reactions

Component	Insert	Target-vector
DNA	0.3 µg	1 µg
10X NEB buffer	2 µl	2 µl
<i>KpnI</i> (10 U/µL)	1 µl	1 µl
<i>BglII</i> (10 U/µL)	1 µl	1 µl
Aqua bidest.	ad 20 µl	ad 20 µl

To increase the number of positive clones, the backbone of the target-vector was treated with FastAP thermosensitive alkaline phosphatase (Thermo Scientific, Bremen, Germany). The enzyme removes 5'- and 3'-phosphate groups from DNA. Due to this treatment, the backbone of the target-vector was not able to religate. The digested and purified vector was incubated with 1 µl of FastAP thermosensitive alkaline phosphatase and 1X of 10X Fast AP buffer for 10 min at 37 °C. The enzyme was inactivated at 75 °C for 5 min.

Due to a ligation reaction the insert was incorporated into the backbone of the target-vector. DNA ligases join DNA fragments by forming phosphodiester bonds between a free 5'-phosphate group and 3'-hydroxyl group. The ligation was performed using the Rapid DNA Ligation Kit (Roche, Basel, Switzerland). In detail, the insert was added to the vector backbone in a molar ratio of 3:1 with a maximum total DNA amount of 200 ng and filled up to 10 µl of DNA dilution buffer. 10 µl of T4 DNA ligation buffer and 1 µl of T4 DNA ligase were added and incubated for 10 min at room temperature. For the transformation of one shot TOP10 *Escherichia coli* cells 5 µl of the ligation reaction were used. The transformation was performed as described above for the gateway cloning system.

2.2.7 Plasmid preparation

Plasmid mini preparations were performed to identify positive clones after generation of expression constructs. Four clones per transformation were picked using sterile pipette tips and cultured overnight in 3 ml LB medium at 37 °C in a shaker. The medium was supplemented with either 3 µl of 100 mg/ml ampicillin or 3 µl of 50 mg/ml kanamycin depending on the selection marker of the cloned plasmid. Plasmid DNA was isolated using the GeneJET Plasmid Miniprep Kit (Thermo Scientific, Bremen, Germany)

according to the manufacturer's protocol. The sequence of the isolated plasmid DNA was identified using Sanger sequencing (chapter 2.2.8). For larger DNA quantity, 100 ml LB medium was inoculated and cultured overnight in a shaker at 37 °C. Plasmid DNA was isolated using the PureLink[®] HiPure Plasmid Filter Midiprep Kit (Life Technologies, Darmstadt, Germany) according to the manufacturer's protocol. The DNA concentration was determined using the NanoDrop ND-1000 spectrophotometer (PeqLab Biotechnologie GmbH, Erlangen, Germany). Plasmid DNA was stored at -20 °C for further usage.

2.2.8 Sanger sequencing

The precise order of nucleotides in all generated plasmids was determined by Sanger sequencing (166) using the BigDye Terminator v1.1 cycle sequencing Kit (Life Technologies, Darmstadt, Germany). 300 ng of plasmid DNA was mixed with 3.3 µM of a template-specific oligonucleotide, 1.5 µl of BigDye, 1 µl of 5X sequencing buffer and 4 µl PCR-grade water. During the following PCR, the fluorescent labeled ddNTPs were incorporated into the PCR products. The PCR program contained an initial denaturation step at 96 °C for 1 min, followed by cycling 30 times through a denaturation step at 96 °C for 10 sec, annealing phase at 50 °C for 5 sec and an elongation phase at 60 °C for 4 min. A laser of the 3730xl DNA Analyzer (Applied Biosystems, Carlsbad, USA) detected the fluorescence of the incorporated ddNTPs while passing through thin capillaries filled with a gel matrix for separation. DNA sequences were analyzed using the Sequencher 5.0 software (Gene Codes Corporation, Ann Arbor, USA).

2.3 Protein biochemical methods

2.3.1 Total protein lysate preparation

Total protein lysates were extracted to analyze the protein content of cells by applying the gel electrophoresis technique. Adhered cells in a 6-well plate were washed twice with ice-cold PBS and lysed using 100 µl cold RIPA buffer, containing 1X Halt[™] combined protease and phosphatase inhibitor (Thermo Scientific, Bremen, Germany). Lysates were stored on ice for 30 min to ensure complete cell lysis. Afterwards, lysates were centrifuged at 16000 g for 15 min at 4 °C to remove cell debris and genomic DNA. Supernatant was transferred to new 1.5 ml reaction tubes. Protein lysates were stored short-term at -20 °C or at -80 °C for several months.

2.3.2 Cell fractionation

Cell fractionations were performed to isolate cytosolic, membrane and nuclear proteins. To this end, cells were washed with ice-cold PBS and incubated on ice for 10 min with cell fractionation buffer 1. Cells were scraped from their culture dish, lysed by pushing them 15 times through a 26G needle on a syringe and centrifuged at 1000 g for 10 min at 4 °C. The resulting cell pellet was resuspended using cell fractionation buffer 2 and incubated overnight on an end-over-end rotator at 4 °C. The suspension was centrifuged at 16000 g for 15 min at 4 °C to obtain the nuclear fraction. The supernatant from the first centrifugation step was further separated by centrifugation at 16000 g for 45 min at 4 °C. The resulting supernatant contained cytosolic proteins. The membrane containing pellet was resuspended in RIPA buffer. All buffers were supplemented with 1X Halt™ combined protease and phosphatase inhibitors.

2.3.3 Protein concentration determination

Protein concentration was determined using the Bio-Rad DC (detergent compatible) protein assay (Bio-Rad, Munich, Germany). The colorimetric assay is based on the Lowry method (167) where copper ions react with peptide bonds under alkaline conditions, leading to subsequent reduction of the folin reagent by the copper-treated proteins. This results in the development of a characteristic blue color with a maximum absorbance at 750 nm. 5 µl of protein lysate were diluted with 5 µl of aqua bidest. and mixed with the assay reagents. After 15 min, absorbance of protein samples were determined and correlated with protein concentrations using a bovine serum albumin (BSA) standard curve.

2.3.4 Gel electrophoresis of proteins

The separation of proteins by their molecular weight was performed using either sodium dodecyl sulfate polyacrylamide gel electrophoresis (SDS-PAGE) or pre-cast NuPAGE® Bis-Tris gel electrophoresis (Life Technologies, Darmstadt, Germany).

According to the Laemmli standard protocol (168) for SDS-PAGE, proteins were treated with the reducing agent dithiothreitol (DTT) to dissociate disulfide bonds. Additionally, the anionic detergent SDS denaturizes proteins and masked their intrinsic charges by negatively charged sulfate groups. Applying an electric field to the polyacrylamide gel matrix causes the separation of proteins by their molecular weight. The discontinuous gel for SDS-PAGE was composed of a stacking and a separating gel (Table 2.10). Ammonium persulfate (APS) and tetramethylethylenediamine (TEMED) were added for

the polymerization of the polyacrylamide matrix in the gels. Electrophoresis was performed in two steps using Tris-glycine-SDS (TGS) buffer. During the first step, proteins concentrate at the interface of stacking and separation gel by applying a constant current of 15 mA and a maximum voltage of 300 V per gel for 30 min. In the second step, proteins were fractionated by their molecular weight in the separating gel at a constant current of 30 mA and a maximum voltage of 300 V per gel.

Table 2.10: Gel components for SDS-PAGE

Gel component	Stacking gel [μ l]	Separating gel [μ l]
Aqua bidest.	1950	2500
4X Stacking buffer	750	-
4X Separation buffer	-	2500
Polyacrylamide	300	5000
10 % (w/v) APS	30	100
TEMED	3	10

The separation of a broad molecular weight range from 14 to 260 kDa was obtained by employing pre-cast gradient NuPAGE[®] 4-12% Bis-Tris protein gel electrophoresis (Life Technologies, Darmstadt, Germany). Pre-cast NuPAGE[®] Bis-Tris gels are made with Bis-Tris/HCL buffer and do not contain SDS. These gels operate at a neutral pH during separation (169). 4-Morpholinepropanesulfonic acid (MOPS) running buffer enables chloride ion tailing towards the anode as the electric field is applied. The neutral pH of the pre-cast gel diminishes the reactivity of disulfide bonds. Pre-cast NuPAGE[®] gels were run in the XCell SureLock Mini Cell system (Life Technologies, Darmstadt, Germany). Separation of the proteins was achieved by applying a constant voltage of 160 V and a maximum current of 300 mA for 1 h.

In both cases, protein lysates were mixed with 5X sample buffer and heated at 95 °C for 5 min. An equal protein amount was loaded into the wells of the gels. The molecular weight of the proteins was estimated by the prestained PageRuler plus protein ladder 10-250K (Thermo Scientific, Bremen, Germany).

2.3.5 Immobilization of proteins by immunoblot

The immunoblot technique allows electrophoretic transfer of separated proteins from polyacrylamide gels to polyvinylidene difluoride (PVDF) membranes (170). This method enables immunodetection of proteins by specific antibodies.

PVDF membranes (Bio-Rad, Munich, Germany) were activated with methanol for 10 sec, washed in aqua bidest. and incubated in anode buffer 1 for 5 min. One blot paper (Bio-

Rad, Munich, Germany) each was equilibrated in either anode buffer 1, anode buffer 2 or cathode buffer. After protein separation by gel electrophoresis, the blotting sandwich was assembled in the following way: thick blot paper soaked with cathode buffer, gel, PVDF membrane, thick blot paper soaked with anode buffer 1 and thin blot paper soaked with anode buffer 2. The electrophoretic transfer of the proteins was carried out using the Trans-Blot® Turbo™ Transfer System (Bio-Rad, Munich, Germany) at a constant current of 0.1 A and a maximum voltage of 25 V for 30 min.

2.3.6 Immunodetection of proteins

The visualization of transferred proteins of interest was achieved by immunodetection with specific primary antibodies and horseradish peroxidase (HRP)-conjugated secondary antibodies. The HRP enzyme activity is detectable by incubating the membrane with an enhanced chemiluminescent (ECL) substrate (GE Healthcare, Freiburg, Germany).

To prevent unspecific interactions of the PVDF membrane and the antibody, the PVDF membrane was blocked with either 5 % (w/v) non-fat dry milk or 5 % (w/v) BSA for 1 h. The membrane was incubated with a specific primary antibody at room temperature for one hour. Subsequently, the membrane was washed with TTBS three times for 10 min. The secondary antibody was incubated with the membrane for 30 min at room temperature. The secondary antibody was removed and the membrane was washed with TTBS three times for 15 min at room temperature. For detection, the membrane was treated with ECL substrate for 1 min, exposed to chemiluminescence hyperfilm and developed using an automated developer machine (Agfa, Mortsel, Belgium).

For analyzing different proteins on one membrane, primary and secondary antibodies were removed by stripping. Therefore, membranes were incubated with stripping buffer at 55 °C for 20 min and washed with TTBS three times for 10 min. Membranes were incubated with new primary antibodies after blocking with either 5 % (w/v) non-fat dry milk or 5 % (w/v) BSA for 1 h.

2.3.7 Co-immunoprecipitation

Co-immunoprecipitations (CO-IP) are widely used to identify physiologically relevant protein-protein interactions. Target-specific antibodies, which are mostly coupled to beads, capture intact protein complexes and allow to co-immunoprecipitate unknown members of the complex. For the identification of new interaction partners, co-precipitated proteins are resolved by SDS-PAGE and detected by immunoblotting.

In this study, CO-IPs were used to elucidate a potential interaction of ORMDL3 and ATF6 α . ORMDL3 and ATF6 α were co-transfected into 10 ml of HEK-293 cells (as described in chapter 2.1.2). After 24 h, the cells were lysed using 500 μ l RIPA buffer containing 1X Halt™ combined protease and phosphatase inhibitor and vortexed three times for 45 sec to achieve complete cell lysis. Cell debris were removed by centrifugation of the lysis suspension at 16000 g for 15 min at 4 °C. In the meantime 25 μ l of magnetic dynabeads® coupled with protein G (Life Technologies, Darmstadt, Germany) were incubated for one hour with 1 μ g of the target-specific antibody, which either detected HA- or FLAG-tagged proteins. Dynabeads coupled with a specific antibody were added to the cell lysate and incubated at 4 °C overnight for dynabead-antigen complex formation. This complex was washed three times using CO-IP binding and washing buffer to remove nonspecifically bound proteins. The complex was eluted from dynabeads by incubating the beads with 22 μ l CO-IP elution buffer for 5 min at room temperature. Dynabeads were removed from the suspension by applying the samples to a magnetic field. The pH of the suspension was adjusted to 7.5 using 10 μ l Tris buffer. After adding 7 μ l 5X SDS-loading buffer and boiling the samples for 5 min at 95 °C, samples were resolved on a SDS-PAGE and used for immunoblotting to detect the presence of co-precipitated proteins.

2.3.8 Enzyme-linked immunosorbent assay (ELISA)

Enzyme-linked immunosorbent assays (ELISA) were applied for quantification of the growth hormone (GH) or insulin-like growth factor 1 (IGF1) in the serum of *Ormdl3*-deficient mice. The ELISA method involves antigen-specific capture antibodies immobilized to a plate. After adding the serum sample to the plate, antigens bind to the capture antibody. Enzyme-labeled antibodies are applied for detection.

Quantification of GH was performed using the Rat/Mouse Growth hormone ELISA kit (EMD Millipore, Schwalbach, Germany). Serum concentrations of IGF1 were determined using the Mouse/Rat IGF1 quantikine ELISA kit (R&D systems, Minneapolis, USA). Both kits were performed according to the manufacturer's protocol.

2.3.9 Measurement of cytokine concentrations

For the determination of cytokines levels from murine serum, the Bio-Plex Pro™ Mouse Cytokine 23-plex immunoassay (Bio-Rad, Munich, Germany) was used. The multiplex magnetic bead-based assay enables the detection of 23 cytokines from 12.5 μ l of serum. Blood was collected in lithium-heparin tubes, centrifuged at 10000 g for 5 min and the resulting serum was stored at -80 °C until further usage. The immunoassay measurement has been performed in cooperation with Bioglobe Service in Hamburg, Germany.

2.4 Generation, handling and treatment of mice

2.4.1 Generation of *Ormdl1* constitutive knockout mice (*Ormdl1*^{-/-})

The role of *Ormdl1* was studied *in vivo* using *Ormdl1*-deficient mice (*Ormdl1*^{-/-}). The murine *Ormdl1* gene is located on chromosome 1 and consists of 4 exons separated by 3 introns. The knockout was achieved by deleting exon 2 with the translation initiation codon (NM_145517) in collaboration with genOway SA (Lyon, France). The targeting vector contained the cDNA of exon 2 flanked by bacteriophage P1-derived *loxP* sites and a neomycin resistance gene cassette flanked by flippase recognition target (FRT) sites in intronic sequences (Fig. 2.2). The targeting vector was electroporated into 129Sv embryonic stem cells and incorporation into the genome by homologous recombination. Positive recombined embryonic stem cells were microinjected into C57BL/6J blastocysts. Blastocysts were transferred into pseudo-pregnant mice and allowed to develop. The resulting male chimeras were bred to C57BL/6 Flp deleter mice (C57BL/6-Tg(CAG-Flpe)2) for germline transmission and *in vivo* removal of selection markers by Cre recombinase. *Ormdl1*^{-/-} mice were generated by breeding the mice to Cre deleter mice (C57BL/6-Gt(ROSA)26Sor^{tm9(Cre/ESR1)}) resulting in the deletion of exon 2 by recombination of the two *loxP* site. The obtained mice were backcrossed for nine generations to a C57BL/6J background at the Central Animal Facility of the Schleswig-Holstein University Hospital Kiel, Germany.

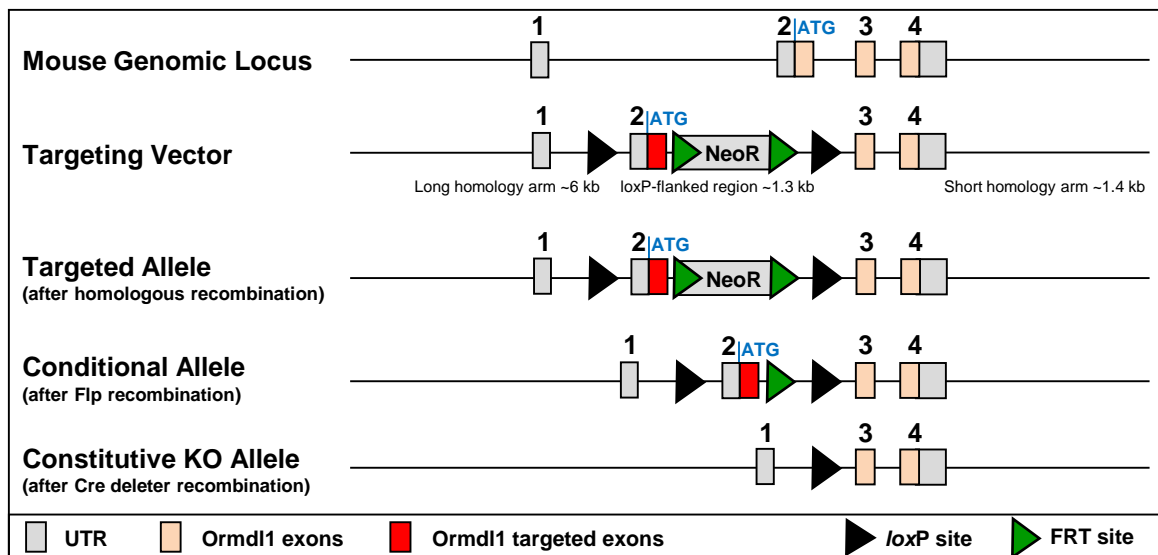


Fig. 2.2: Targeting strategy for the generation of conditional and constitutive *Ormdl1* knockout alleles. For *Ormdl1* deletion a targeting vector was designed to flank exon 2 by *loxP* sites and a neomycin resistance cassette for positive selection. The neomycin resistance gene was excised *in vivo* by breeding with Flp deleter mice. Mating of these mice with Cre deleter mice resulted in *Ormdl1*^{-/-} mice.

2.4.2 Generation of *Ormdl3* conditional mice

In this study, *Ormdl3* conditional and constitutive knockout mice were used to investigate the mode of function of *Ormdl3* *in vivo*. In cooperation with TaconicArtemis GmbH (Cologne, Germany), the murine *Ormdl3* gene (ensemble gene ID: ENSMUSG00000038150) was isolated to create the targeting vector (Fig. 2.3). Due to the fact, that exon 2 of *Ormdl3* contains the translation initiation codon, exon 2 to 4 were flanked by *loxP* sites in intronic sequences. The sequence between the two *loxP* sites was deleted by Cre recombinase. Additionally, the targeting vector contained positive selection markers such as puromycin and neomycin resistances. The targeting vector was electroporated into C57BL/6N Tac embryonic stem cells. The sequence of the targeting vector was incorporated into the genome replacing the original sequence by homologous recombination. Embryonic stem cells with the incorporated modified sequence were isolated using double positive selection with puromycin and neomycin. Positive cells were microinjected into mouse blastocysts and transferred into pseudopregnant female mice. The resulting chimeras were bred with Flp deleter mice (C57BL/6-Tg(CAG-Flp)2Arte) for germline transmission and removal of selection markers. The resulting *Ormdl3* conditional mice allow the generation of conditional and constitutive knockout mice.

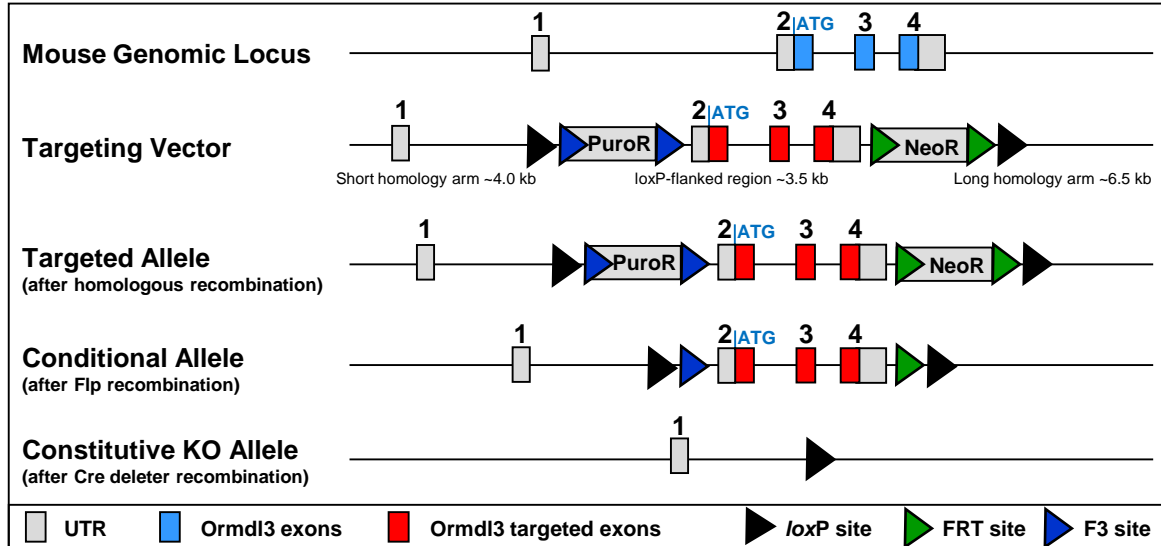


Fig. 2.3: Overview of the targeting strategy for the generation of conditional and constitutive *Ormdl3* knockout alleles.

The translation initiation codon of *Ormdl3* is located on exon 2 and the coding region is from exon 2 to exon 4. The coding region was flanked by *loxP* sites and selection markers were flanked by either F3 sites (PuroR, puromycin resistance) or by FRT sites (NeoR, neomycin resistance). The targeting strategy enables the generation of conditional and constitutive *Ormdl3* knockout mice, which is explained in detail in the chapters 2.4.3 and 2.4.4.

2.4.3 Generation of *Ormdl3* constitutive knockout mice (*Ormdl3*^{-/-})

To study the effect of *Ormdl3* on the entire organism, *Ormdl3*-deficient mice were generated by breeding *Ormdl3* conditional mice to Cre deleter mice (C57BL/6-*Gt(ROSA)26Sor*^{tm9(Cre/ESR1)Arte}). The loss of function of *Ormdl3* was achieved by deleting the entire protein coding sequence from exon 2 to 4 after Cre-mediated recombinase, which is ubiquitously expressed under the control of the *Gt(ROSA)26Sor* gene on chromosome 6. The obtained mice with a constitutive knockout allele were bred with C57BL/6N wild-type mice to remove the Cre recombinase, which could cause unspecific side effects. Additional backcrossing was not needed, due to the generation of these mice in C57BL/6N Tac embryonic stem cells. For all experiments in this study, mice were bred heterozygously to generate *Ormdl3*^{-/-} and their wild-type littermates.

2.4.4 Generation of *Ormdl3* conditional knockout mice (*Ormdl3*^{ΔIEC})

Since *ORMDL3* had been identified as a susceptibility gene for CD and UC, *Ormdl3* conditional knockout mice were generated, where the lack of *Ormdl3* is restricted to intestinal epithelial cells (IECs) of the villi and crypt cells of the small and large intestine (*Ormdl3*^{ΔIEC}). For the generation of *Ormdl3*^{ΔIEC} mice, *Ormdl3* conditional mice were crossed with B6.SJL-Tg(Vil-cre)997Gum/J (villin-cre) mice. Villin-cre mice express the Cre recombinase under the control of the *villin 1* promoter, which leads to Cre-mediated recombination of *loxP* sites resulting in a tissue-specific deletion of *Ormdl3*. Beside the mainly described expression of *villin 1* in intestinal epithelial cells, *villin 1* can also be found in cells of the kidney proximal tubulus and in the duct of pancreas and biliary system (171). In this study, mice were bred heterozygously for *villin 1* in order to generate *Ormdl3*^{ΔIEC} and their wild-type littermates.

2.4.5 Animal housing and animal care

Mice were housed under specific pathogen-free conditions in individually ventilated cages at the Central Animal Facility of the Schleswig-Holstein University Hospital Kiel, Germany. Animals were maintained in a 12 h light-dark cycle under barrier conditions at 21°C ± 2°C and 60% ± 5% humidity and were provided with food and tap water *ad libitum*. All experiments were performed according to the German guidelines for animal care and protection. The animal research in this study was approved by the institutional review boards (Table 2.11).

Table 2.11: License numbers for approved animal research

License number	Designated use
V 312-7224.121-33	killing for tissue harvesting
V 312-72241.121-33 (26-3/10)	acute and chronic DSS-induced colitis
V 312-7224.121-33 (77-6/13)	tunicamycin treatment

2.4.6 Genotyping

Genotyping was performed to distinguish between heterozygous mice and homozygous wild-type or knockout mice by performing PCR analyses of genomic DNA. The genomic DNA was extracted from tail biopsies of three to four weeks old mice by boiling with 100 μ l of 50 mM sodium hydroxide (NaOH) for 1 h. After centrifugation the genomic DNA-containing supernatant was collected and submitted to two independent touch-down PCRs per mouse line. Therefore, GoTaq DNA polymerase (Promega, Mannheim, Germany) was applied. Components for the PCR reaction and profile are shown in (Table 2.12). Applied oligonucleotides are listed in the supplementary information (Table 8.8).

Table 2.12: PCR components and profile for genotyping

Component	Volume	Number of cycles	Temp [°C]	Time
DNA	1 μ l	1	95	2 min
5X GoTaq Green Buffer	4 μ l	10	95	30 sec
dNTPs (10 mM each)	0.5 μ l		65 to 55 (-1 °C/cycle)	5 sec
Oligonucleotide for (10 μ M)	0.25 μ l		72	4 min
Oligonucleotide rev (10 μ M)	0.25 μ l	33	95	10 sec
GoTaq Polymerase	0.5 μ l		55	5 sec
Nuclease-free water	13.5 μ l		72	4 min
		1	72	7 min
		1	4	∞

The resulting amplicon lengths were determined by gel electrophoresis (as described in chapter 2.2.4) followed by exposure to UV light for visualization. The genotype of a mouse was determined by combining the received amplicon lengths of the two PCR analyses (Table 2.13).

Table 2.13: Overview of expected amplicon lengths after genotyping PCR.

Genotype	<i>Ormdl1</i>		<i>Ormdl3</i>		Genotype	PCR cond	PCR cre
	PCR WT	PCR KO	PCR WT	PCR KO			
+/+	1632 bp	no band	194 bp	no band	<i>Ormdl3</i> ^{fl/fl}	388 bp	no band
+/-	1632 bp	2015 bp	194 bp	277 bp	<i>Ormdl3</i> ^{ΔIEC}	388 bp	1000 bp
-/-	no band	2015 bp	no band	277 bp			

Generic PCR product profiles of genotyping PCRs for *Ormdl1*^{-/-}, *Ormdl3*^{-/-} and *Ormdl3*^{ΔIEC} mice are shown in Fig. 2.4. Sizes of the PCR amplicons were estimated using the SmartLadder MW-1700-10 (Eurogentec, Cologne, Germany).

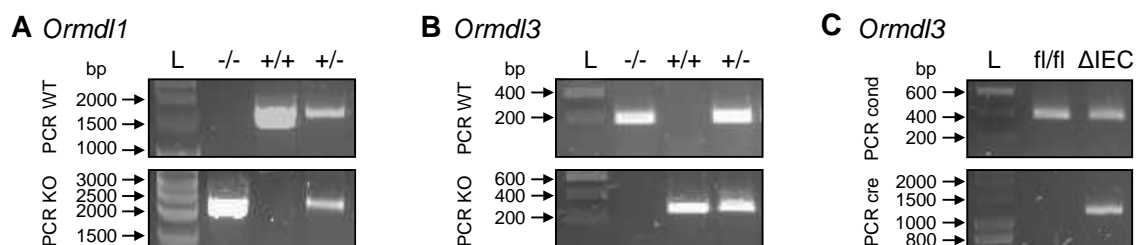


Fig. 2.4: Representative example of genotyping results obtained from *Ormdl1*^{-/-} (A), *Ormdl3*^{-/-} (B) and *Ormdl3*^{ΔIEC} (C) mice.

Genomic DNA was isolated from mouse tails to perform genotyping PCRs. PCR products were separated by agarose gel electrophoresis and the genotype was determined by interpreting the resulting amplicon sizes. L represents the molecular weight marker of the DNA SmartLadder MW-1700-10.

2.4.7 Primary cell isolation

Primary murine cells were isolated to investigate proteins at basal level or upon stimulation *ex vivo*.

Bone marrow-derived macrophages (BMDMs) were obtained from femoral bone marrow. These cells were used for controlled studies of macrophages *ex vivo*. Cells were isolated from femur and tibia bones by flushing with 30 ml BMDM medium and plated for differentiation in a 150 mm dish at 37 °C and 5 % (v/v) CO₂. The depleted medium was replaced with fresh warm BMDM medium after three days. After seven days of culturing, BMDMs were harvested, counted using the Cellometer Auto T4 Plus (PeqLab Biotechnologie GmbH, Erlangen, Germany) and seeded into culture dishes with a defined cell number for experiments according to Table 2.14.

Primary murine splenocytes were isolated to study primary immune cells, such as T cells and B cells, *ex vivo*. The spleen was mashed through a 0.4 μm cell strainer into a 50 ml tube. Mixed splenocytes were isolated from the mashed spleen using mouse Biocoll (Biochrom, Berlin, Germany) by centrifugation without breaks at 1250 g for 20 min at room temperature. The resulting interphase was collected and washed 3 times with splenocyte medium by centrifugation at 300 g for 10 min. Cells were counted and seeded into culture dishes with the appropriate cell numbers (Table 2.14).

Murine intestinal epithelial cells were isolated from PBS-flushed small intestine. Slices of the small intestine were incubated with 1.5 mM EDTA in HBSS for 20 min at 37 °C followed by vortexing for 30 sec. Supernatant was centrifuged at 300 g for 10 min. The resulting pellet was washed with 5 ml PBS. Cells were counted using the Cellometer Auto

T4 Plus and seeded into culture dishes with the appropriate cell number in MEM supplemented with 20 % (v/v) FCS and 1 % (v/v) penicillin and streptomycin (Table 2.14).

Table 2.14: Overview of cell culture formats for experiments with primary murine cells.

cell culture dish	cell number/well	media volume [ml]
6-well plate	1×10^6	2
12-well plate	5×10^5	1
96-well plate	5×10^4	0.1

IECs and cells from the lamina propria were isolated from small intestine and colon tissues using the Lamina Propria Dissociation Kit (Miltenyi Biotec, Bergisch Gladbach, Germany). 10 weeks old mice were sacrificed and the intestine removed, flushed with PBS and cut longitudinally into pieces of approximately 0.5 cm length. Isolation and purification of intraepithelial lymphocytes and lamina propria cells was performed according to the manufacturer's protocol. The fraction of intraepithelial lymphocytes also contained IECs. Due to this reason, this fraction was named IEC fraction in this study.

2.4.8 Induction of acute colitis

Experimental acute colitis was induced in 10 weeks old male mice by administration of 2.5% (w/v) dextran sodium sulfate (DSS) in autoclaved drinking water for 6 days, followed by one day of regular drinking water. Mice were exposed to drinking water with or without DSS *ad libitum*. As recommended by Wirtz *et al.* (172), DSS-containing water was replaced on day three to prevent bacterial growth. Mice were monitored and weighted every day. Mice were sacrificed on day 8.

2.4.9 Induction of chronic colitis

Chronic colitis in 10 weeks old male mice was induced by three cycles of 1.5% (w/v) DSS in autoclaved drinking water for five days, followed by regular drinking water for five days. Mice were exposed to water with or without DSS *ad libitum*. DSS-containing water was replaced on day three to prevent bacterial growth. In every cycle, the mice were monitored and weighed at least every other day. Mice were sacrificed on day 30.

2.4.10 Disease activity index (DAI)

During DSS-induced colitis experiments, the course of the disease was monitored and scored using the disease activity index (DAI), a combined score of stool blood, stool consistency and body weight loss. Scores were determined as indicated in Table 2.15.

Table 2.15: Scoring criteria for the determination of the disease activity index.

Score	Stool blood	Stool consistency	Body weight loss [%]
0	Hemoccult negative	formed	0
1			1-4.99
2	Hemoccult positive	unformed	5-9.99
3			10-19.99
4	visible bleeding	liquid	> 20

2.4.11 Histology

Hematoxylin and Eosin staining (HE staining)

HE staining enables blue coloring of the nucleus by hemalaun, a complex formed of aluminium ions and oxidized hematoxylin, as well as red coloring of eosinophilic structures by Eosin.

For histological studies, tissues were fixed in 10 % (v/v) PBS buffered formalin for 24 h followed by dehydration and embedding in paraffin wax. Tissues were cut into 3.5 µm sections using the Leica RM 2255 microtome (Leica Microsystems, Wetzlar, Germany) and mounted on microscope slides. Before staining, histological sections were deparaffined by applying a decreasing alcoholic dilution series using the xylol replacing reagent Roti[®]-Histol (Carl Roth, Karlsruhe, Germany) for 10 min, 3 times 100 % ethanol for 10 min, 2 times 96 % ethanol for 2 min, 70 % ethanol for 2 min and water for 5 min. Slides were stained with hemalaun for 5 min and exposed to tap water for blueing. After staining with Eosin G for 2 min, slides were shortly washed using aqua bidest. and dried by an increasing alcoholic series. Slides were coverslipped using Roti Histokit (Carl Roth, Karlsruhe, Germany).

Histological scoring of colonic sections after DSS treatment

Histological scoring of HE stained colonic sections were applied for the assessment of the severity of colitis. As described by Laroui *et al.* (173), images were scored blinded based on three parameters including infiltration of immune cells, crypt damage and ulceration (Table 2.16). Scores from each parameter were summed up to result in a maximum histological score of 11.

Table 2.16: Overview of the three histological scoring components

Score	Severity of inflammation	Crypt damage	Ulceration
0	rare inflammatory cells in the lamina propria	intact crypts	absence of ulcer
1	increased number of granulocytes in the lamina propria	crypt loss of the basal one-third	1 or 2 foci of ulcerations
2	confluence of inflammatory cells extending into the submucosa	crypt loss of the basal two-third	3 or 4 foci of ulcerations
3	transmural extension of the inflammatory infiltrate	entire crypt loss	confluent or extensive ulceration
4		change of epithelial surface with erosion	
5		confluent erosion	

2.4.12 Tunicamycin injection

For *in vivo* ER stress induction, a single intraperitoneal injection of 1 mg tunicamycin per kg body weight (BW) was applied for 8 h, 24 h, 48 h or 7 d. During the experiment, body weight and overall appearance of the mice was monitored daily. At the end of the treatment, mice were anaesthetized using 100 mg/kg BW Ketamin (Ketanest, Pfizer, New York, USA) plus 16 mg/kg BW Xylazin (Rompun, Bayer, Leverkusen, Germany) for final blood collection by cardiac puncture. Kidney and liver tissues were obtained and either fixed in 10 % (v/v) PBS buffered formalin for HE staining or snap-frozen in liquid nitrogen and stored at -80 °C for RNA and protein analyses.

2.5 Statistical analysis

The Student's unpaired *t*-test was performed for all statistical analyses using the GraphPad Software (GraphPad Software Inc., La Jolla, USA). Data were plotted in GraphPad Prism 5 with mean and standard error of the mean (SEM). Significance levels were depicted as (*) for statistically significant with $p \leq 0.05$, (**) strongly significant with $p \leq 0.01$ and (***) for highly significant with $p \leq 0.001$. Statistical analysis was performed when applicable.

3 Results

3.1 Expression analyses of human and murine *ORMDL* mRNA

SNPs in close proximity to the human *ORMDL3* gene were associated with a variety of diseases, including asthma and IBD. However, so far the impact of *ORMDL* proteins on the pathogenesis of these diseases is not fully elucidated. Moreover, molecular functions of *ORMDL* proteins, in this regard, are largely unknown (163).

To get a first insight into the specific *in vivo* function of *ORMDL* proteins and to investigate whether these proteins have potential tissue-specific functions, mRNA expression analyses were performed. Human and murine mRNA levels of *ORMDL1*, *ORMDL2* and *ORMDL3* were studied on a variety of tissues by semi-quantitative endpoint PCR (Fig. 3.1). Transcripts of the three genes showed ubiquitous expression patterns in the examined tissues. Interestingly, the largest variation in tissue-specific transcript levels was observed for *ORMDL3*. The highest mRNA level of the human *ORMDL3* was detected in liver, spleen and pancreas (Fig. 3.1A). The murine *Ormdl3* gene was additionally highly expressed in skeletal muscle (Fig. 3.1B).

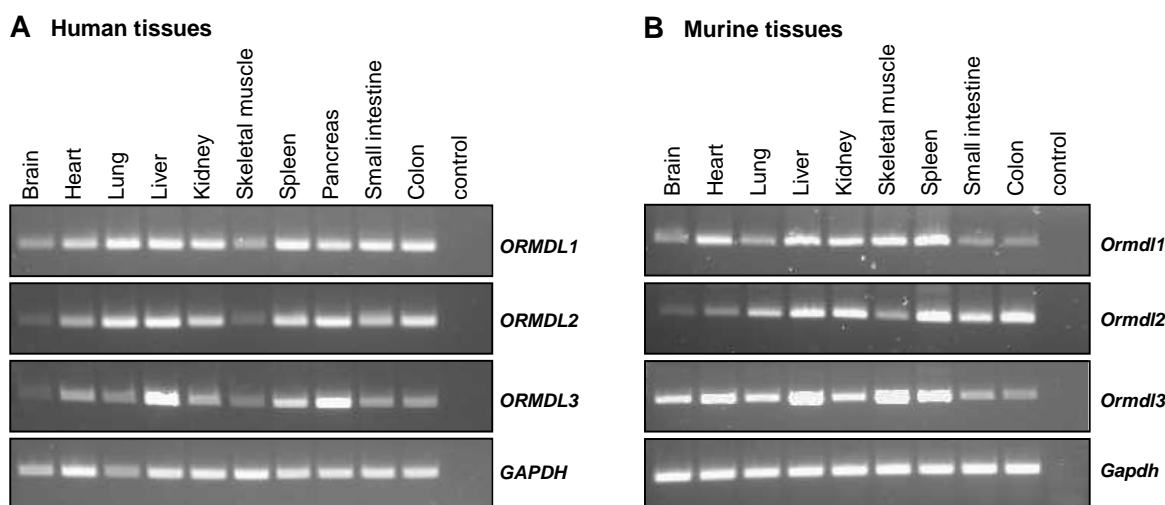


Fig. 3.1: Analyses of human and murine *ORMDL* transcripts investigated by endpoint PCR.

Transcript levels of *ORMDL1*, *ORMDL2* and *ORMDL3* in various (A) human and (B) murine tissues were assessed by endpoint PCR. Water was used as no template control. *GAPDH* mRNA expression served as internal control for the applied cDNA amount.

3.2 ER stress-induced tissue-specific expression of *ORMDL* proteins

ORMDL proteins have been reported to be involved in the UPR (135). Typically, proteins involved in the UPR, such as ATF6 α , XBP1, CHOP and their target genes, show

increased protein levels upon ER stress induction (86,174). For the investigation of ORMDL protein levels during ER stress, immortalized cell lines and primary cells were treated with the ER stress-inducing agents tunicamycin (TM) or thapsigargin (TG) and evaluated using immunoblotting analyses. Due to the close resemblance of the three ORMDL proteins with around 80 percent amino acid identity (135), antibodies cannot distinguish between ORMDL1, ORMDL2 and ORMDL3. Thus it has to be noted that immunoblotting analyses enables only the visualization of total ORMDL protein levels with all three members of the ORMDL family.

Efficiency of ER stress induction was confirmed by increased GRP78 protein levels (Fig. 3.2). 24 h of tunicamycin or thapsigargin treatment revealed increased protein levels for ORMDL in the murine RAW 264.7 macrophage cell line (Fig. 3.2A), primary murine macrophages (Fig. 3.2D) and primary murine mixed splenocytes (Fig. 3.2E). In contrast, ER stress in intestinal epithelial cells, such as cells from the human colon adenocarcinoma cell line HT-29 (Fig. 3.2B) or primary murine small intestinal cells (Fig. 3.2F), resulted in reduced ORMDL protein levels. Interestingly, ORMDL protein levels were not altered in cells of the human embryonic kidney cell line HEK-293 after 24 h of tunicamycin or thapsigargin treatment (Fig. 3.2C). These findings indicate a diverse induction pattern of ORMDL proteins in various cell lines.

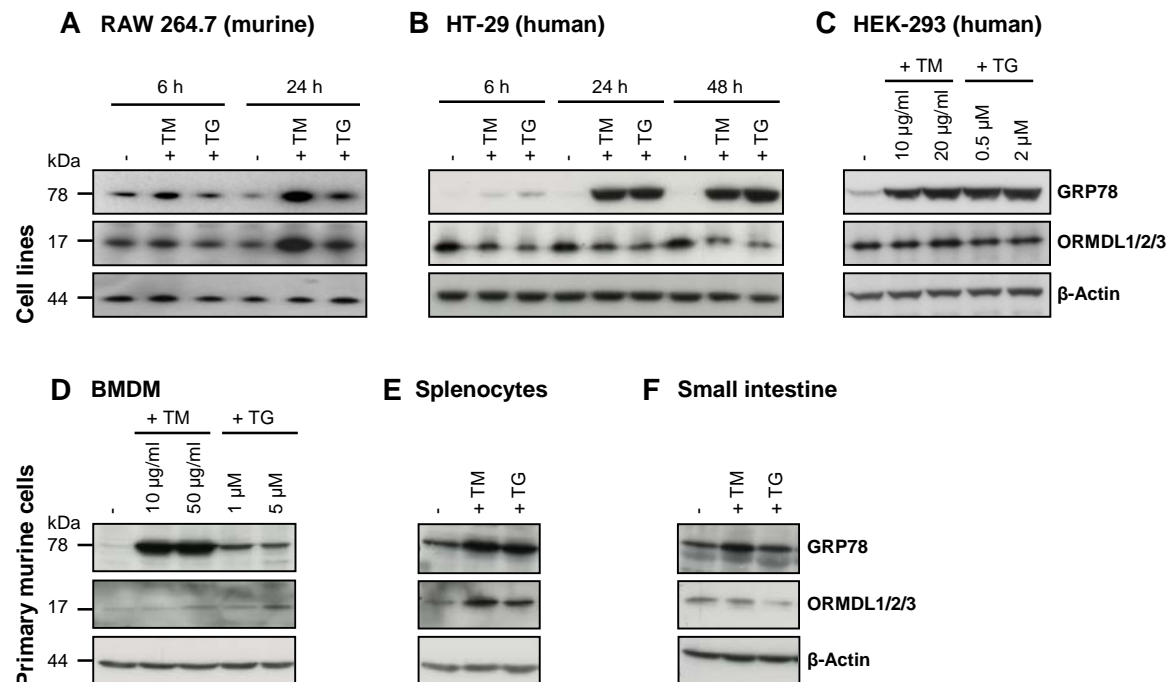


Fig. 3.2: ER stress-inducing reagents alter ORMDL protein levels *in vitro*.

Mouse macrophage cell line RAW 264.7 (A), human colon adenocarcinoma cell line HT-29 (B), human embryonic kidney cell line HEK-293 (C), primary murine bone marrow-derived macrophages (BMDMs) from wild-type (C57BL/6) mice (C), primary murine splenocytes from wild-type mice (D) and primary murine small intestine cells from wild-type mice were treated with 20 µg/ml tunicamycin (TM) or 2 µM thapsigargin (TG) for 24 h, unless otherwise indicated. Cell lysates were resolved on a SDS-PAGE and analyzed by immunoblotting with antibodies recognizing GRP78, ORMDL1/2/3 or β-Actin, used as a loading control.

3.3 The effect of ORMDL proteins on the UPR

The observed regulation of ORMDL protein levels during ER stress (Fig. 3.2) suggested that ORMDL proteins are involved in the UPR pathways. Promoter-mediated luciferase reporter assays, immunoblotting and FACS analysis were performed to investigate the effect of ORMDL proteins on the three major arms of the UPR including IRE1, ATF6 and PERK. Due to the association of ORMDL1 and ORMDL3 with a variety of diseases, the main focus of this study lies on these two members of the ORMDL protein family.

3.3.1 ORMDL proteins inhibit the IRE1 pathway

During ER stress, IRE1 gets autophosphorylated and induces mRNA splicing of the transcription factor *XBP1*. The spliced form of *XBP1* functions as the main inducer of the UPRE promoter (86). To investigate the impact of ORMDL on the IRE1 pathway, mRNA splicing of *XBP1* was monitored by FACS analyses using the *XBP1* Δ DBD-venus construct. In ORMDL3 overexpressing cells the fluorescence intensity was decreased, thus *XBP1* splicing was significantly reduced already under normal conditions and even stronger after 24 h of tunicamycin treatment (Fig. 3.3A). A similar, but not significant, tendency was observed in HEK-293 cells overexpressing ORMDL1. In order to exclude transfection or overexpression artifacts of ER membrane proteins such as ORMDL proteins, HEK-293 cells were treated with a mix of siRNAs against *ORMDL1*, *ORMDL2* and *ORMDL3* or a scrambled siRNA as a control (Fig. 3.3B). Confirming the findings from the overexpression experiments, siRNA knockdown of *ORMDL1*, *ORMDL2* and *ORMDL3* resulted in increased fluorescence intensities in untreated as well as in tunicamycin- or thapsigargin-treated cells.

As a consequence of *XBP1* mRNA splicing, the UPRE promoter gets activated. Promoter-mediated luciferase reporter assays in ORMDL1 and ORMDL3 overexpressing HEK-293 cells revealed reduced UPRE promoter activities after tunicamycin-treatment (Fig. 3.3C). This result was confirmed by siRNA treatment (Fig. 3.3D), where the knockdown of ORMDL proteins significantly induced the UPRE promoter activity. Upon tunicamycin and thapsigargin treatment, this effect was even reinforced. Taken together, the results of the UPRE promoter-mediated luciferase reporter assays were consistent with those from the *XBP1*-venus splicing analyses, indicating ORMDL proteins as repressors of the IRE1 pathway.

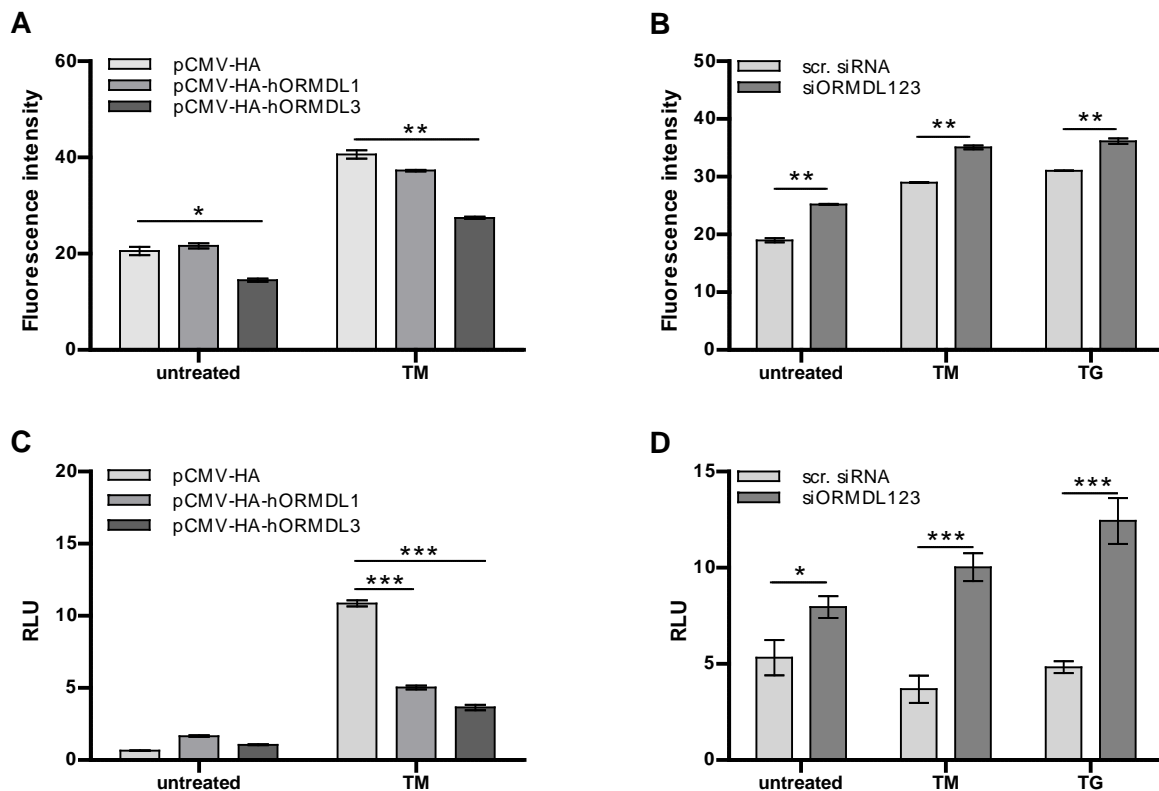


Fig. 3.3: ORMDL proteins reduce *XBP1* mRNA splicing and UPRE promoter activation.

The effect of ORMDL1 or ORMDL3 overexpression (A) as well as siRNA-based *ORMDL* knockdown (B) on *XBP1* mRNA splicing was evaluated using the life-cell *XBP1* monitoring assay. HEK-293 cells were transfected as indicated and additionally transfected with pCAX-*XBP1* Δ DBD-venus. After 24 h, the cells were stimulated with 4 μ l DMSO as a control, 20 μ g/ml tunicamycin (TM) or 2 μ M thapsigargin (TG) for additional 24 h. The appearance of fluorescent *XBP1*-venus protein in the cells was monitored by flow cytometry and displayed as geometric mean fluorescence intensity. UPRE promoter activity was measured by promoter-mediated luciferase reporter assays after ORMDL1 and ORMDL3 overexpression (C) or *ORMDL* knockdown using siRNA (D). HEK-293 cells were additionally co-transfected with a firefly luciferase reporter pGL3B-UPRE and *Renilla* luciferase as a transfection control. The cells were treated with 20 μ g/ml of tunicamycin (TM) or 2 μ M thapsigargin (TG) for 24 h. Luciferase activities were determined by flow cytometry and relative luciferase units (RLU) were calculated. Assays were performed in quintuples. Error bars represent means \pm SEM. Statistical analyses was performed by two-way ANOVA followed by Student's *t*-test for unpaired samples.

3.3.2 ORMDL proteins activate the ATF6 α pathway

ER stress induces the translocation of ATF6 α from the ER to the Golgi apparatus, where it is cleaved by Site-1 protease (S1P) and Site-2 protease (S2P). The cleaved N-terminal fragment of ATF6 α (ATF6 α (N)) activates the ERSE promoter and, subsequently, the transcription of chaperones such as GRP78 and GRP94 (175). Besides the mainly described 50 kDa cleavage product of ATF6 α (176), also 36 kDa and 60 kDa fragments of ATF6 α have been identified and are discussed to induce the ERSE promoter during ER stress (177).

3.3.2.1 ORMDL proteins reduce p36ATF6 α protein levels and induce the ERSE promoter

The impact of ORMDL3 on the cleavage of endogenous ATF6 α was determined by immunoblotting analyses. Commercially available antibodies against ATF6 α solely detected protein bands with a size around 36 kDa. This 36 kDa fragment of ATF6 α (p36ATF6 α) was reduced in ORMDL3 overexpressing HEK-293 cells after 30 min, 1 h and 3 h of tunicamycin treatment (Fig. 3.4A). Consistent with the overexpression data, the opposite effect was observed in cells treated with *ORMDL1*, *ORMDL2* and *ORMDL3* siRNA (Fig. 3.4B). For siRNA-mediated knockdown, HT-29 cells were chosen, because of their high basal ORMDL protein levels compared to HEK-293 cells.

In detail, knockdown of the three *ORMDL* homologues in HT-29 revealed increased p36ATF6 α protein levels after 10 min, 30 min, 1 h and 3 h of tunicamycin treatment compared to cells treated with scrambled siRNA.

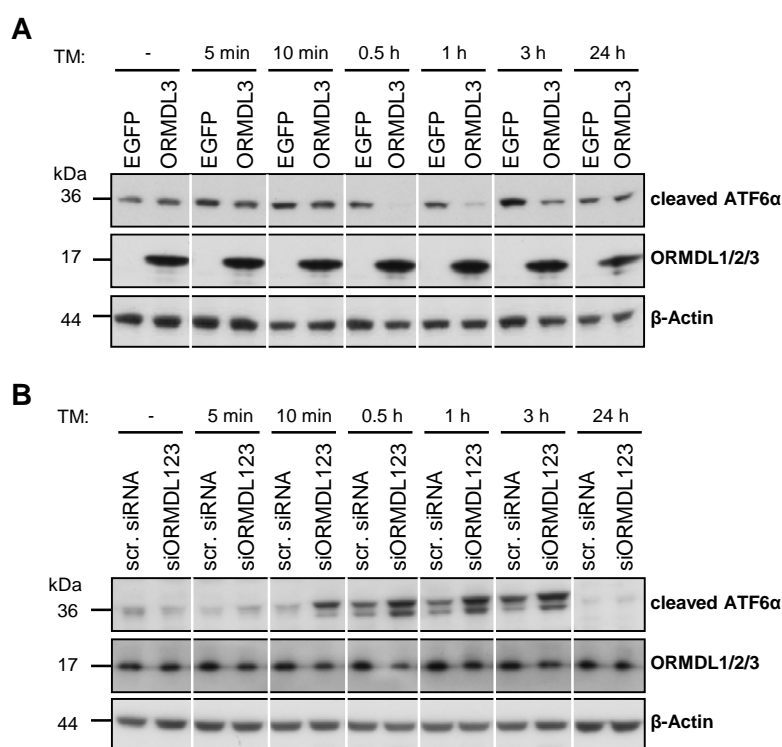


Fig. 3.4: ORMDL proteins regulate the p36ATF6 α fragment.

HEK-293 cells were transfected with an ORMDL3 expression plasmid (pCMV-HA-hORMDL3) (A) and HT-29 cells were treated with siRNA against *ORMDL1*, *ORMDL2* and *ORMDL3* (B). After 24 h, cells were left untreated or treated using 5 μ g/ml tunicamycin (TM) for indicated durations. Total cell lysates were resolved on a SDS-PAGE and analyzed by immunoblotting using antibodies against ATF6 α , ORMDL1/2/3 or β -Actin as a loading control.

Cleavage of ATF6 α enables the resulting N-terminal fragment to enter the nucleus, where it induces the ERSE promoter and regulates the expression of ER chaperones (175,178). Cell fractionations were performed to investigate the effect of ORMDL3 on the translocation of p36ATF6 α (Fig. 3.5A). ORMDL3 overexpressing cells showed increased p36ATF6 α protein levels in the nuclear fraction upon ER stress. In addition, p36ATF6 α disappeared from the cytosolic fraction only in ORMDL3 overexpressing cells after 10 h of tunicamycin treatment. The downstream effect of the increased nuclear transcriptionally

active ATF6 α fragment was examined by ERSE luciferase reporter assay (Fig. 3.5B). In this experiment, HEK-293 cells overexpressing ORMDL1 and ORMDL3 revealed increased basal and ER stress-induced ERSE promoter activities.

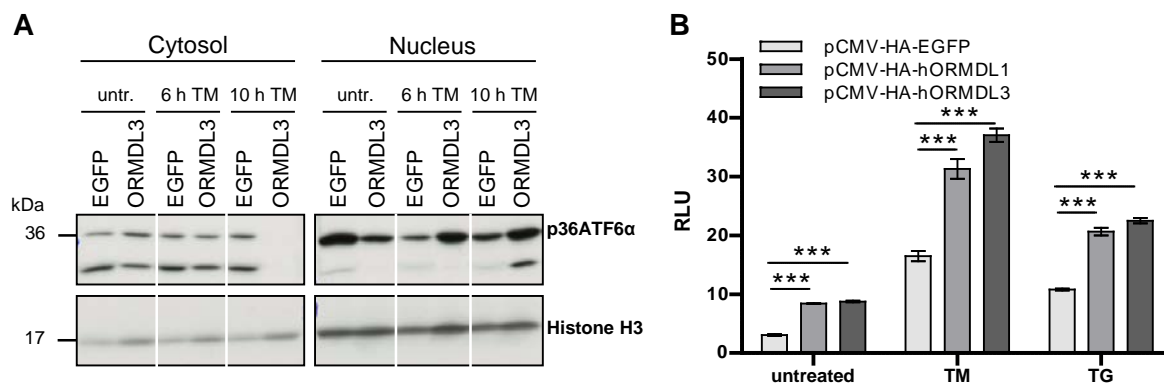


Fig. 3.5: ORMDL proteins induce translocation of p36ATF6 α to the nucleus and activate the ERSE promoter.

(A) Cell fractionations were performed using HEK-293 cells transfected with an ORMDL3 (pCMV-HA-hORMDL3) or an EGFP (pCMV-HA-EGFP) expression plasmid. Cells were left untreated or treated using 5 μ g/ml tunicamycin (TM) for the indicated durations. Cytosolic and nuclear fractions were resolved on a SDS-PAGE and analyzed by immunoblotting using antibodies against ATF6 α , or Histone H3, used as a loading control. (B) Effects of ORMDL1 and ORMDL3 overexpression on the ERSE promoter were measured by luciferase reporter assays. HEK-293 cells were co-transfected with a firefly luciferase reporter pGL3B-ERSE, *Renilla* luciferase for normalization and pCMV-HA-EGFP, pCMV-HA-hORMDL1, or pCMV-HA-hORMDL3. After 24 h, cells were left untreated or treated with 20 μ g/ml tunicamycin (TM) or 2 μ M thapsigargin (TG) for additional 24 h. Error bars represent means \pm SEM. Statistical analyses was performed by two-way ANOVA followed by Student's *t*-test for unpaired samples.

To investigate whether the effect of ORMDL proteins on p36ATF6 α and ERSE promoter activity is S1P-dependent, cells were treated with the well established serine protease inhibitor 4-(2-Aminoethyl) benzenesulfonyl fluoride hydrochloride (AEBSF) (179). AEBSF treatment resulted in reduced p36ATF6 α protein levels in all observed cells independent of ORMDL proteins (Fig. 3.6A). This finding supports the hypothesis raised by Liu *et al.* (180) that p36ATF6 α is a S1P-dependent ATF6 α cleavage fragment. AEBSF stimulation equalized the p36ATF6 α protein levels in HEK-293 cells transfected with ORMDL3 and EGFP. In line with this result, also the ERSE promoter activity remained unchanged after tunicamycin treatment in ORMDL1 and ORMDL3 overexpressing HEK-293 cells, which were co-stimulated with AEBSF for 24 h (Fig. 3.6B).

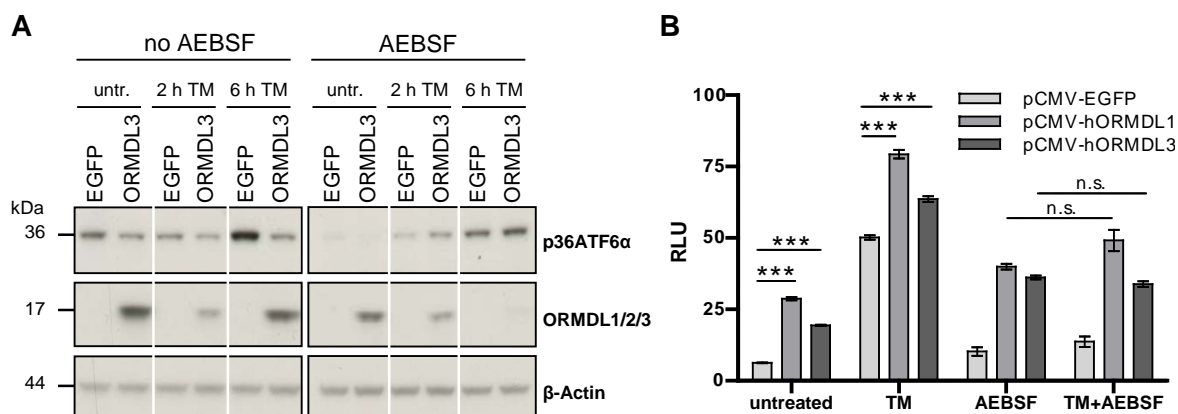


Fig. 3.6: The effect of ORMDL proteins on the p36ATF6 α fragment is modulated by S1P.

(A) HEK-293 cells were transfected with an ORMDL3 (pCMV-HA-hORMDL3) or an EGFP (pCMV-HA-EGFP) expression plasmid. Cells were left untreated or were pretreated for 1 h using 300 μ M AEBSF prior to stimulation with 5 μ g/ml tunicamycin (TM). Total cell lysates were resolved on a SDS-PAGE and analyzed by immunoblotting using antibodies against ATF6 α , ORMDL1/2/3 or β -Actin as a loading control. (B) Effects of AEBSF and ORMDL1 or ORMDL3 overexpression on the ERSE promoter were measured by luciferase reporter assays. HEK-293 cells were co-transfected with a firefly luciferase reporter pGL3B-ERSE, *Renilla* luciferase for normalization and pCMV-HA-EGFP, pCMV-HA-hORMDL1, or pCMV-HA-hORMDL3. After 24 h, cells were left untreated or treated with 20 μ g/ml tunicamycin (TM) for additional 24 h in the presence or absence of 300 μ M AEBSF. Error bars represent means \pm SEM. Statistical analyses was performed by two-way ANOVA followed by Student's *t*-test for unpaired samples. n.s. indicates not significant differences.

3.3.2.2 ORMDL3 affects the ERSE promoter mainly through ATF6 α cleavage

To determine whether the effect of ORMDL3 on the ATF6 α branch was influenced only by ATF6 α cleavage events or also by cross-talk events with other UPR mediators, an ERSE luciferase reporter assay was performed in presence or absence of UPR mediator-specific siRNAs. The ERSE promoter activity has been reported to be mainly activated by ATF6 α cleavage products (90). However, other UPR mediators, such as XBP1 (93) and ATF4 (181), are capable to bind the ERSE and function as transcription factors, but to a lesser extent.

Knockdown of *ATF6 α* in EGFP overexpressing HEK-293 cells validated the specificity of the ERSE luciferase reporter assay (Fig. 3.7A). In those cells, only a minor increase in ERSE promoter activity was detected after 24 h of tunicamycin treatment. As expected, cells treated with siRNA against ATF4, PERK, IRE1 or control siRNA revealed elevated ERSE promoter activations upon tunicamycin stimulations. A similar tendency for ERSE promoter activity was observed in ORMDL3 overexpressing HEK-293 (Fig. 3.7B). However, upon ER stress induction by tunicamycin, the ERSE promoter was more induced in cells treated with siRNA against *ATF6 α* , indicating a weak cross-talk effect. Thus, the effect of ORMDL3 on the ERSE promoter activity is mainly, but not exclusively, mediated by the ATF6 α pathway.

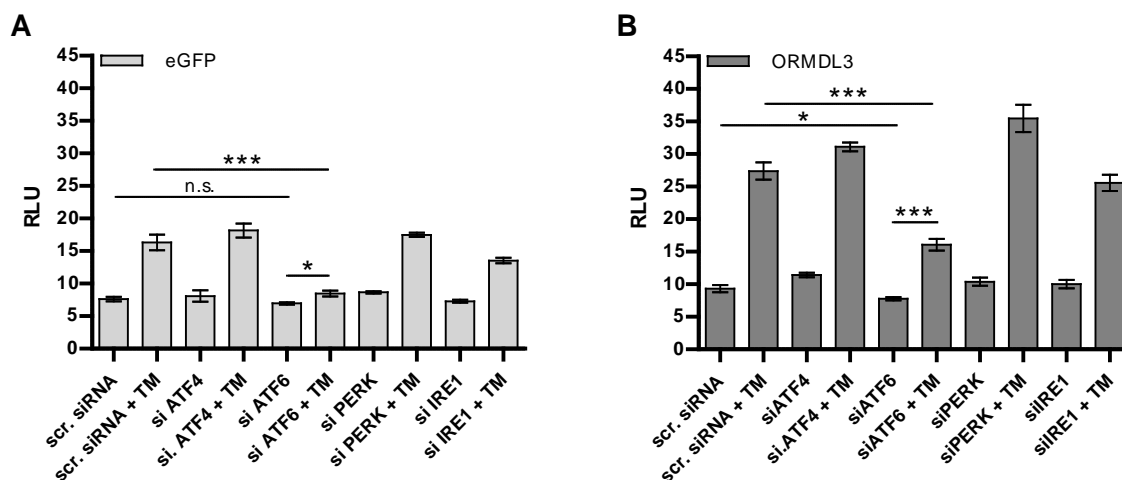


Fig. 3.7: Effects of all UPR pathway mediators on the ERSE promoter activity.

ERSE promoter activity was quantified by promoter-mediated luciferase reporter assays. HEK-293 cells were treated with siRNA as indicated and co-transfected with a firefly luciferase reporter pGL3B-ERSE, *Renilla* luciferase for normalization and a plasmid containing EGFP (A) or ORMDL3 (B). 24 h after transfection, cells were left untreated or treated with 5 μ g/ml tunicamycin (TM) for additional 24 h and thereafter assayed using a luminometer. Assays were performed in quintuples. Error bars represent means \pm SEM. Statistical analyses was performed by two-way ANOVA followed by Student's *t*-test for unpaired samples. n.s. indicates not significant differences.

3.3.2.3 N-linked glycosylation of ATF6 α is ORMDL3-dependent

Since commercially available antibodies did not recognize the full-length form of ATF6 α (ATF6 α FL), but overexpression of ORMDL3 revealed a distinct impact on the endogenous 36 kDa cleavage fragment of ATF6 α (Fig. 3.4), ATF6 α FL was investigated using a FLAG-tagged ATF6 α expression construct. Immunoblotting analyses indicated an ORMDL3-dependent alteration of ATF6 α FL (Fig. 3.8A). Untreated HEK-293 cells transfected with an ORMDL3 expression construct showed reduced protein levels for ATF6 α FL and an emerging slightly smaller band of ATF6 α . This smaller band has been described as the unglycosylated form of ATF6 α (ATF6 α UG), which exhibits a faster rate of constitutive transport to the Golgi apparatus and results in higher levels of transcriptionally active ATF6 α in the nucleus (182). Tunicamycin treatment for 1, 3 and 6 h further enhanced the effect of ORMDL3 leading to reduced levels of ATF6 α FL and increased levels of ATF6 α UG. Most prominent, after 8 h of treatment, ATF6 α FL even disappeared and in addition, as sign of an increased ATF6 α activation, ATF6 α UG was mitigated in ORMDL3 overexpressing cells compared to control cells.

In order to investigate whether the effect of ORMDL3 on ATF6 α FL especially depends on stimulations with a glycosylation inhibiting agent such as tunicamycin, cells were treated with thapsigargin (Fig. 3.8B). In contrast to tunicamycin, thapsigargin induces ER stress by blocking the ER calcium ATPase pump without affecting the glycosylation machinery. As expected, thapsigargin treatment did not affect the level of ATF6 α UG. However after

3 h of thapsigargin treatment, ORMDL3 overexpressing cells showed reduced ATF6 α FL protein levels indicating an increased cleavage rate of ATF6 α . Efficiency of ER stress induction by thapsigargin was confirmed by increased ATF4 protein levels. The effect of ORMDL3 on ATF6 α FL was further validated by siRNA-mediated knockdown of *ORMDL1*, *ORMDL2* and *ORMDL3* (Fig. 3.8C). Down-regulation of ORMDL proteins revealed increased ATF6 α FL protein levels compared to control siRNA-treated cells.

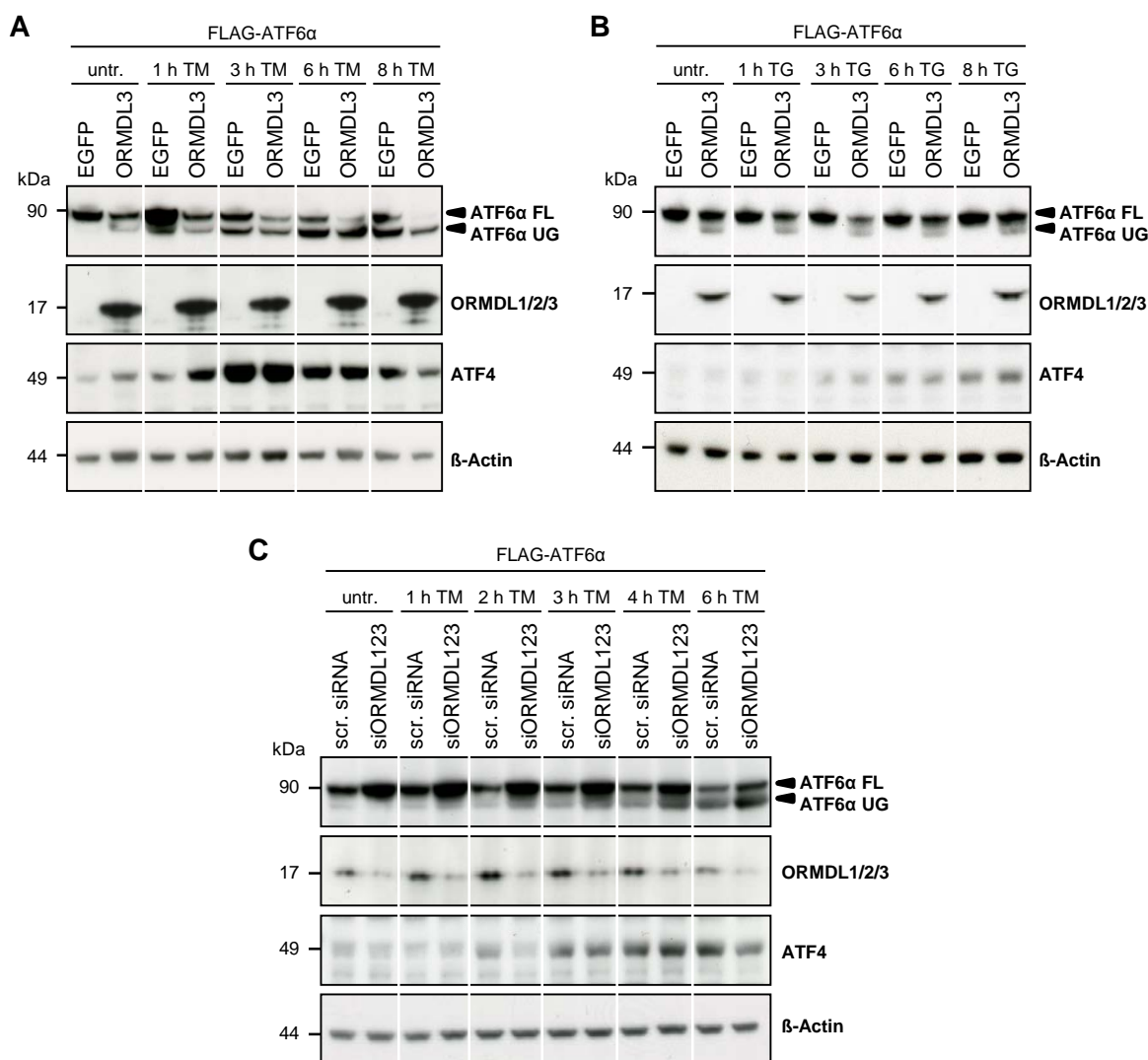


Fig. 3.8: The full length form of ATF6 α is affected by ORMDL3.

Effects of pCMV-HA-hORMDL3 overexpression (A, B) and siRNA-based down-regulation of *ORMDL1*, *ORMDL2* and *ORMDL3* (siORMDL1/2/3) (C) on ATF6 α FL were examined by immunoblotting analyses HEK-293 cells co-transfected with FLAG-ATF6 α . After 24 h, cells were left untreated or treated using 5 μ g/ml tunicamycin (TM) (A, C) or 0.5 μ M thapsigargin (TG) (B) for indicated durations. Cell lysates were resolved on a SDS-PAGE and analyzed by immunoblotting using antibodies specific to FLAG, ORMDL1/2/3, ATF4 or β -Actin as a loading control. Anti-FLAG antibody was used to detect FLAG-tagged ATF6 α .

To ensure that the ATF6 α UG fragment is the unglycosylated form of ATF6 α FL, HEK-293 cell lysates were treated with endoglycosidase H (Endo H) to reduce the *N*-glycans to a single residue (183). As for 6 h treatment with tunicamycin, incubation with Endo H

resulted in a protein band with a similar size as the band for ATF6 α UG (Fig. 3.9). Interestingly, another N-linked glycoprotein, translocon-associated protein alpha (TRAP α), did not show increased unglycosylated bands in ORMDL3 overexpressing cells indicating a unique effect of ORMDL3 on ATF6 α N-linked glycosylation

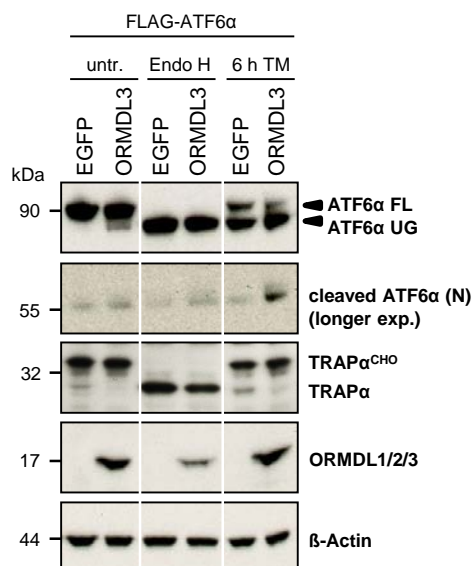


Fig. 3.9: Effect of ORMDL3 on ATF6 α functions independently of glycosylation processes.

HEK-293 cells were co-transfected with FLAG-ATF6 α and ORMDL3 or EGFP expression constructs. After 24 h, cells were left untreated or treated with 5 μ g/ml tunicamycin (TM) for 6 h. Indicated cell lysates were incubated with endoglycosidase H (Endo H) and resolved on a SDS-Page. Immunodetection was performed using antibodies against FLAG, TRAP α , ORMDL1/2/3 or β -Actin as a loading control. Anti-FLAG antibody was used to detect FLAG-tagged ATF6 α .

3.3.2.4 ORMDL3 induces ATF6 α cleavage

To clarify the impact of ORMDL3 on ATF6 α cleavage, FLAG-ATF6 α was overexpressed in HEK-293 cells and ATF6 α FL and its cleavage fragments were visualized with an anti-FLAG antibody. First, a dose-dependency was investigated, where increasing amounts of ORMDL3 were co-transfected with a constant concentration of an FLAG-ATF6 α expression construct (Fig. 3.10A). This experiment revealed increasing levels of ATF6 α UG and a cleavage fragment ATF6 α (N) with a molecular mass of 55 kDa in cells with rising concentrations of ORMDL3. Upregulation of the ATF6 α (N) level after 3 h of tunicamycin treatment confirmed this fragment as a specific cleavage product of ATF6 α FL. As expected from the above mentioned results, the effect of ORMDL3 on ATF6 α cleavage was observed in untreated as well as tunicamycin-treated cells. Thus, ORMDL3 overexpression is sufficient to induce ATF6 α cleavage also in the absence of tunicamycin.

Cleaved ATF6 α (N) has been reported to enter the nucleus, where it functions as a transcriptional regulator of ER chaperones (175). Cell fractionations were performed to investigate the influence of ORMDL3 on the translocation of the ATF6 α (N) fragment into the nucleus (Fig. 3.10B). Nuclear fractions show higher ATF6 α (N) protein levels in ORMDL3 overexpressing cells, which was further increased after ER stress induction using tunicamycin.

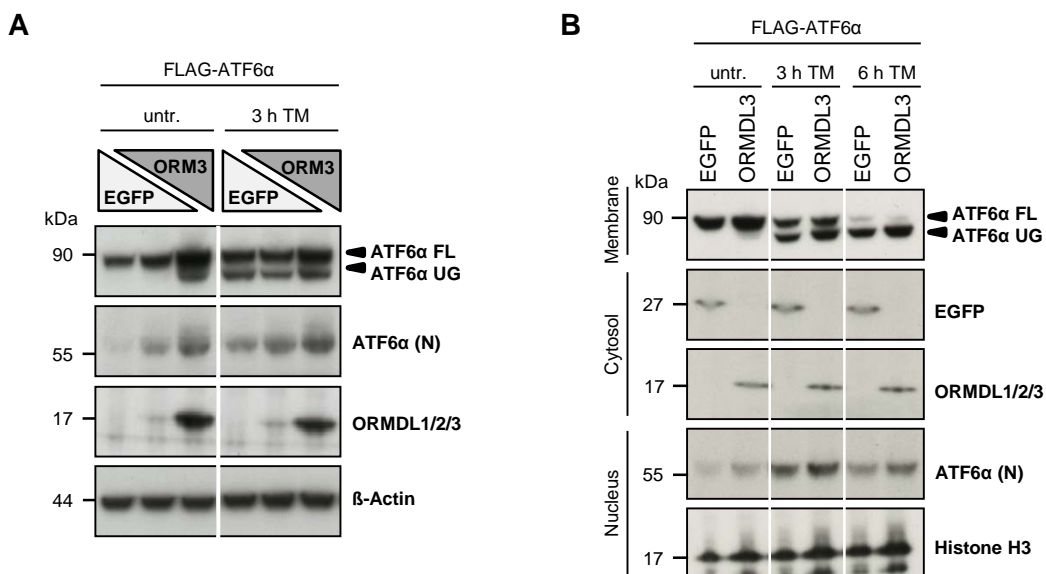


Fig. 3.10: Dose-dependent effect of ORMDL3 on ATF6α UG and ATF6α (N).

(A) HEK-293 cells were co-transfected with FLAG-ATF6α and ORMDL3 (ORM3) or EGFP expression constructs, in increasing or decreasing amounts, respectively. (B) For cell fractionations HEK-293 cells were co-transfected with FLAG-ATF6α and ORMDL3 or EGFP expression constructs in equal amounts. After 24 h, cells were left untreated or treated with 5 μg/ml tunicamycin (TM) for indicated durations. Total cell lysates (A) or cell fractions (B) were resolved on a SDS-PAGE and analyzed by immunoblotting using antibodies specific to FLAG, ORMDL1/2/3, EGFP and β-Actin or Histone H3 as a loading control. Anti-FLAG antibody was used to detect FLAG-tagged ATF6α.

ATF6α is constitutively synthesized and restores ATF6α FL after cleavage (105). For the investigation of the degradation rate of ATF6α FL, HEK-293 cells were treated with cycloheximide (CHX) to inhibit protein synthesis (Fig. 3.11). ATF6α FL protein levels were more rapidly decreased in ORMDL3 overexpressing cells compared to EGFP overexpressing cells.

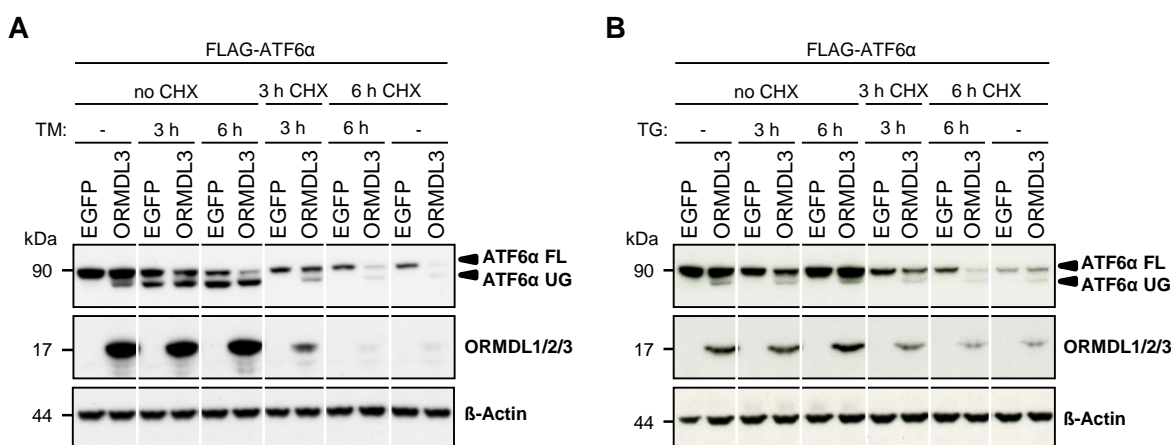


Fig. 3.11: CHX-treated ORMDL3 overexpressing cells display increased cleavage of ATF6α FL.

HEK-293 cells were co-transfected with a FLAG-ATF6α and an ORMDL3 or an EGFP expression plasmid. After 24h, cells were treated with or without 50 μl/ml cycloheximide (CHX) in presence or absence of 5 μg/ml tunicamycin (TM) (A) or 0.5 μM thapsigargin (TG) (B) for indicated durations. Cell lysates were resolved on a SDS-Page and analyzed by immunoblotting using antibodies against FLAG, ORMDL1/2/3 or β-Actin as a loading control. Anti-FLAG antibody was used to detect FLAG-tagged ATF6α.

3.3.2.5 ORMDL3 and ATF6 α are located in close spatial proximity

Due to the distinct effects of ORMDL3 on ATF6 α cleavage and N-linked glycosylation, co-localization studies were performed. HeLa cells were co-transfected with EGFP-ATF6 α and either RFP-ORMDL3 or RFP as a control. RFP-ORMDL3, in contrast to RFP (Fig. 3.12A), was distributed in an ER-like structure similar to the structure of EGFP-ATF6 α (Fig. 3.12B). Especially the enlargement of the images identified similar clustering of both proteins around the nucleus (Fig. 3.12C). By overlaying the images for EGFP-ATF6 α and RFP-ORMDL3 a close spatial proximity of both proteins was demonstrated, suggesting a possible interaction of ORMDL3 and ATF6.

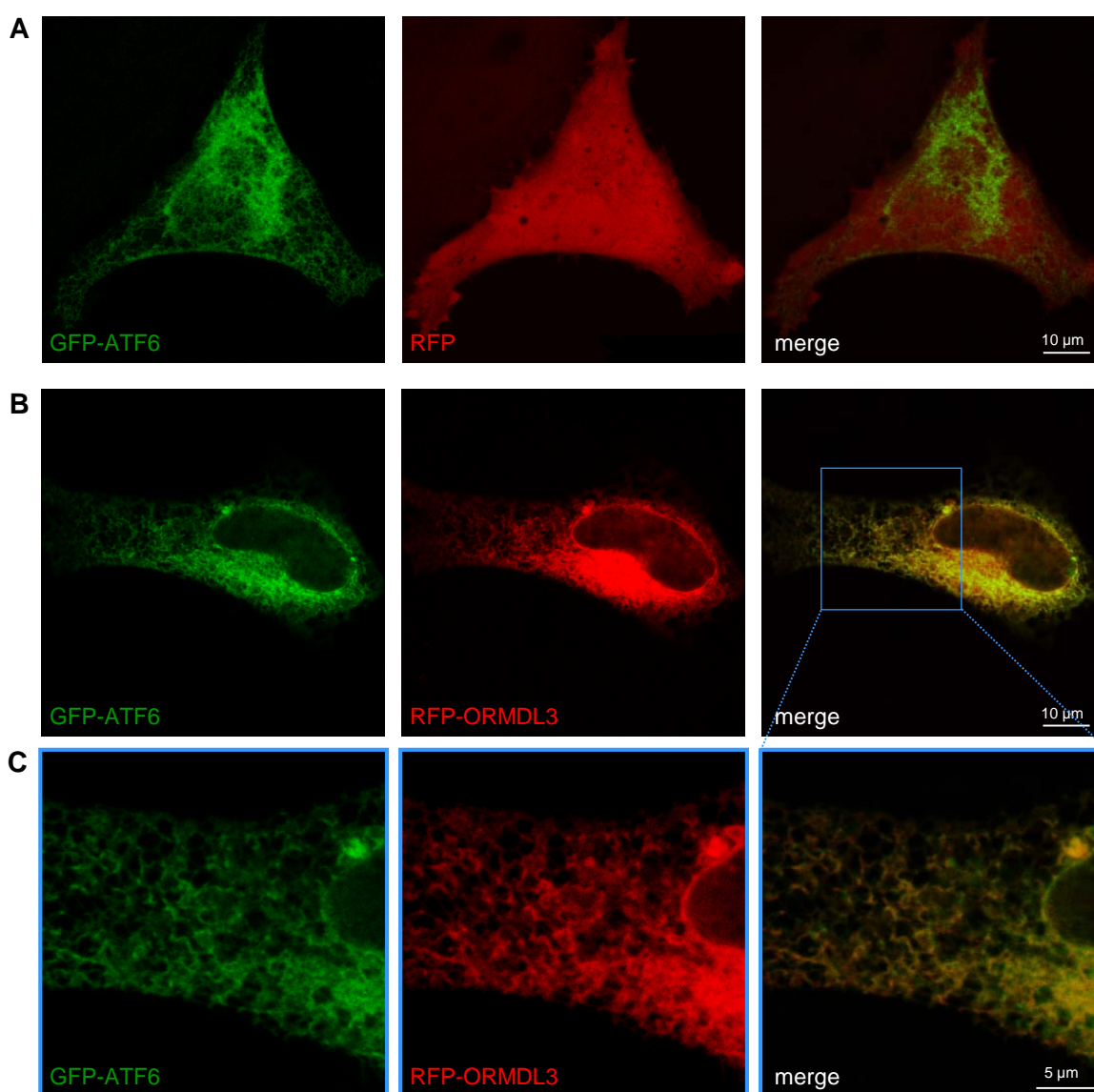


Fig. 3.12: ORMDL3 co-localizes with ATF6 α .

HeLa cells were co-transfected with plasmids for GFP-ATF6 α and (A) RFP or (B) RFP-ORMDL3. 24 h after transfection, images were taken from viable cells. Bottom images (C) show an enlargement of the outlined area in the image of (B). Merged images are displayed on the right.

3.3.2.6 ORMDL3 interacts with ATF6 α

Co-immunoprecipitation (CO-IP) studies were performed using cells co-transfected with FLAG-ATF6 α and HA-ORMDL3 or HA-EGFP. The first CO-IP approach used an anti-HA antibody, which recognizes HA-tagged ORMDL3 or EGFP as a control. In immunoblotting experiments, ATF6 α was only detected in ORMDL3 overexpressing cells using an anti-FLAG antibody (Fig. 3.13A). The interaction remained intact also after tunicamycin stimulation. The specificity of the interaction was confirmed by CO-IP using the opposite approach, where an anti-FLAG antibody was used (Fig. 3.13B). In this setting, FLAG-ATF6 α precipitated only ORMDL3 and not EGFP. Both approaches revealed protein-protein-interaction of the ER-resident proteins ORMDL3 and ATF6 α FL.

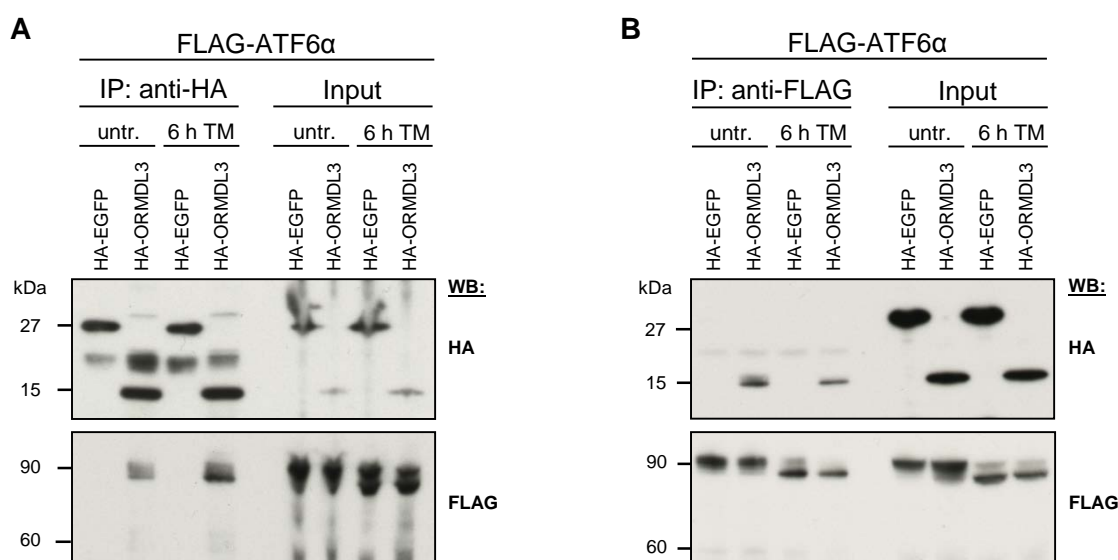


Fig. 3.13: Interaction of ORMDL3 and ATF6 α shown by co-immunoprecipitation.

HEK-293 cells were co-transfected with plasmids for HA-ORMDL3, HA-EGFP and FLAG-ATF6 α . After 24 h, cells were left untreated or treated with 5 μ g/ml tunicamycin (TM) for 6 h. CO-IPs were performed using antibodies against either HA (A) or FLAG (B). Immunoprecipitates (IP) and cell lysates (3 % input) were resolved on a SDS-PAGE and analyzed by immunoblotting using antibodies to FLAG or HA. The anti-HA antibody detected EGFP at approximately 27 kDa and ORMDL3 at 17 kDa.

3.3.3 ORMDL proteins modulate the PERK pathway

Activation of PERK by ER stress leads to phosphorylation of eIF2 α (p-eIF2 α), which mediates global repression of protein translation as well as activation of the transcription factor ATF4 and the pro-apoptotic factor CHOP (184). To investigate the effect of ORMDL1 and ORMDL3 on the promoter activity of ATF4, a promoter mediated luciferase reporter assay was used (Fig. 3.14A). For that reason, ORMDL1 and ORMDL3 were overexpressed in HEK-293 cells, which resulted in significantly increased ATF4 promoter activities already under unchallenged conditions. This effect of ORMDL1 and ORMDL3 was even reinforced during ER stress induced by tunicamycin or thapsigargin treatment for 24 h. Interestingly, the ATF4 promoter activity was slightly more increased in HEK-293 cells transfected with ORMDL3 compared to ORMDL1 overexpressing cells. Due to that finding, ORMDL3 overexpressing HEK-293 cells were chosen to investigate the PERK pathway on protein levels. Similar to the increased ATF4 promoter activities in these cells, the upstream regulator of ATF4 p-eIF2 α was also affected. ORMDL3 overexpressing HEK-293 cells disclosed faster phosphorylation of eIF2 α , especially after 1 and 3 h of tunicamycin treatment (Fig. 3.14B). After 6 h of treatment, ORMDL3 overexpressing cells elucidated lower amounts of p-eIF2 α compared to EGFP overexpressing cells. Additionally, the pro-apoptotic factor CHOP, which is a downstream target of ATF4, was stronger upregulated in ORMDL3 overexpressing HEK-293 cells after 6 h of tunicamycin administration. After 24 h of tunicamycin treatment, protein levels of CHOP and p-eIF2 α were reduced in ORMDL3 overexpressing HEK-293 cells, indicating a faster ER stress response followed by a more quickly removal of increased ER stress mediators during the recovery phases.

The opposite approach using siRNA against *ORMDL3* or against all *ORMDL* homologues disclosed confirming data. The ATF4 promoter activity was decreased in HEK-293 cells transfected with siRNA against all *ORMDL* homologues (Fig. 3.14C). This effect was reinforced after 24 h of tunicamycin- and thapsigargin-induced ER stress. Investigations of the protein levels confirmed the data obtained from the promoter mediated luciferase reporter assay (Fig. 3.14D). Knockdown of all *ORMDL* homologues led to reduced CHOP protein levels after 6 h of tunicamycin treatment. Taken together, these results suggest that *ORMDL* proteins accelerate activation of the PERK pathway. This in turn might enhance effective ER stress response in order to control cell fate or cope with ER stress.

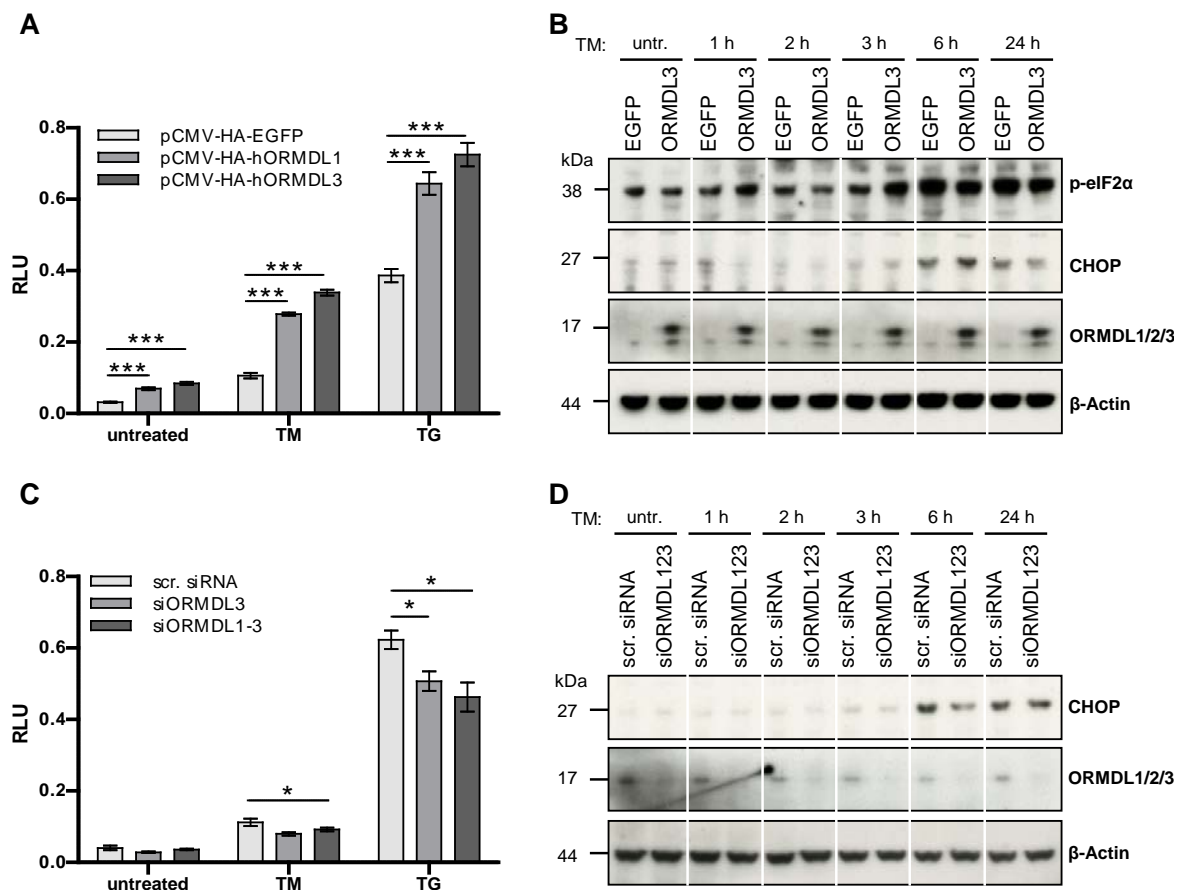


Fig. 3.14: ORMDL proteins modulate the PERK pathway.

The effect of ORMDL1 (pCMV-HA-hORMDL1) or ORMDL3 (pCMV-HA-hORMDL3) overexpression (A) as well as siRNA-based *ORMDL* knockdown (C) on the ATF4 promoter activity was quantified by promoter-mediated luciferase reporter assay. HEK-293 cells were additionally co-transfected with a firefly luciferase reporter pGL3B-ATF4 and *Renilla* luciferase for normalization. 24 h after transfection, cells were left untreated or treated with either 20 μ g/ml tunicamycin (TM) or 2 μ M thapsigargin (TG) for additional 24 h and assayed using a luminometer. Assays were performed in quintuples. Error bars represent means \pm SEM. Statistical analyses was performed by two-way ANOVA followed by Student's *t*-test for unpaired samples. Protein levels were analyzed by immunoblotting of HEK-293 cells transfected with either an EGFP or ORMDL3 containing plasmid (B) or with siRNA against all three *ORMDL* homologues. Cells were left untreated or treated with 20 μ g/ml tunicamycin (TM) for indicated durations. Cell lysates were resolved on a SDS-PAGE and probed by immunoblotting with antibodies against CHOP, p-eIF2 α , ORMDL1/2/3 or β -Actin, used as a loading control.

Due to the distinct impact of ORMDL proteins on ATF6 α and its signaling pathway, an ORMDL3-dependent cross-talk effect of ATF6 α on the PERK pathway was investigated (Fig. 3.15). HEK-293 cells treated with siRNA against *ATF6 α* revealed no induction of the ATF6 α target GRP78, indicating a sufficient down-regulation of this UPR branch. Interestingly, phosphorylation of eIF2 α was more pronounced in EGFP and ORMDL3 overexpressing cells treated with siRNA against *ATF6 α* . However, in these cells CHOP protein levels were reduced, indicating a distinct cross-talk effect of ATF6 α on CHOP. Also the impact of ORMDL3 on CHOP protein levels in cells treated with control siRNA was annulled in cells with siRNA-mediated knockdown of *ATF6 α* .

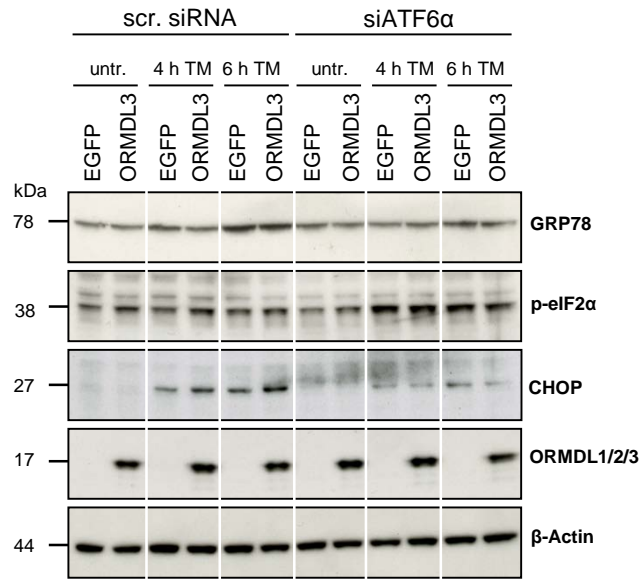


Fig. 3.15: ORMDL3 promotes ATF6 α -dependent CHOP induction.

HEK-293 cells were treated with control siRNA (scr. siRNA) or ATF6 α -specific siRNA. After 24 h, cells were transfected with a FLAG-ATF6 α and an ORMDL3 or an EGFP expression plasmid. Cells were left untreated or treated with 5 μ g/ml tunicamycin (TM) for indicated durations. Cell lysates were resolved on a SDS-Page and analyzed by immunoblotting using antibodies against GRP78, p-eIF2 α , CHOP, ORMDL1/2/3 or β -Actin as a loading control.

3.4 Characterization of *Ormdl3*^{-/-} mice

Due to the association of ORMDL3 with a variety of diseases, further investigation focused on the impact of ORMDL3 on the entire organism. Already the *in vitro* studies mentioned above revealed ORMDL3 as a regulator of the UPR pathways. However, the validity of *in vitro* studies is limited due to a great simplification of the system by using immortalized cell lines in an artificial environment. For that reason, *Ormdl3*-deficient (*Ormdl3*^{-/-}) mice were generated to identify the role of ORMDL3 in a complex organism at baseline conditions as well as during challenging conditions such as DSS-induced colitis and tunicamycin treatment. Due to the association of ORMDL3 with IBD, DSS-induced colitis experiments were performed to elucidate the role and the mechanism of ORMDL3 in the development of these diseases. Additionally, systemic administration of tunicamycin to *Ormdl3*^{-/-} mice was used in order to gain insights into the effect of ORMDL3 on the ER stress homeostasis *in vivo*.

3.4.1 Basal phenotype of *Ormdl3*^{-/-} mice

3.4.1.1 Analyses of ORMDL homologues in *Ormdl3*^{-/-} mice

Ormdl3 deficiency in mice was identified by genotyping (as described in chapter 2.4.6) and validated by mRNA expression analyses of liver and colon tissues (Fig. 3.16). In the investigated tissues of *Ormdl3*^{-/-} mice no *Ormdl3* transcripts were observed confirming the deletion of *Ormdl3* in the whole organism.

Due to the high amino acids homology of the three ORMDL proteins, the question arises, if the loss of ORMDL3 can be compensated by upregulation of the two other ORMDL proteins. To address this question, mRNA expression patterns of all three murine *Ormdl* genes in liver and colon tissues of *Ormdl3*^{-/-} mice were analyzed by semi-quantitative endpoint PCR (Fig. 3.16A). The mRNA expression levels of *Ormdl1* and *Ormdl2* in the observed tissues of *Ormdl3*^{-/-} mice revealed no obvious alterations compared to the mRNA expression levels in wild-type (*Ormdl3*^{+/+}) mice.

Additionally, protein levels of all three ORMDL homologues in liver and colon tissues were investigated by immunoblotting with a pan-specific ORMDL1/2/3 antibody (Fig. 3.16B). Similar to the investigated transcript levels, ORMDL protein levels were markedly reduced but not compensated by upregulation of ORMDL1 or ORMDL2 in the observed tissues of *Ormdl3*^{-/-} mice.

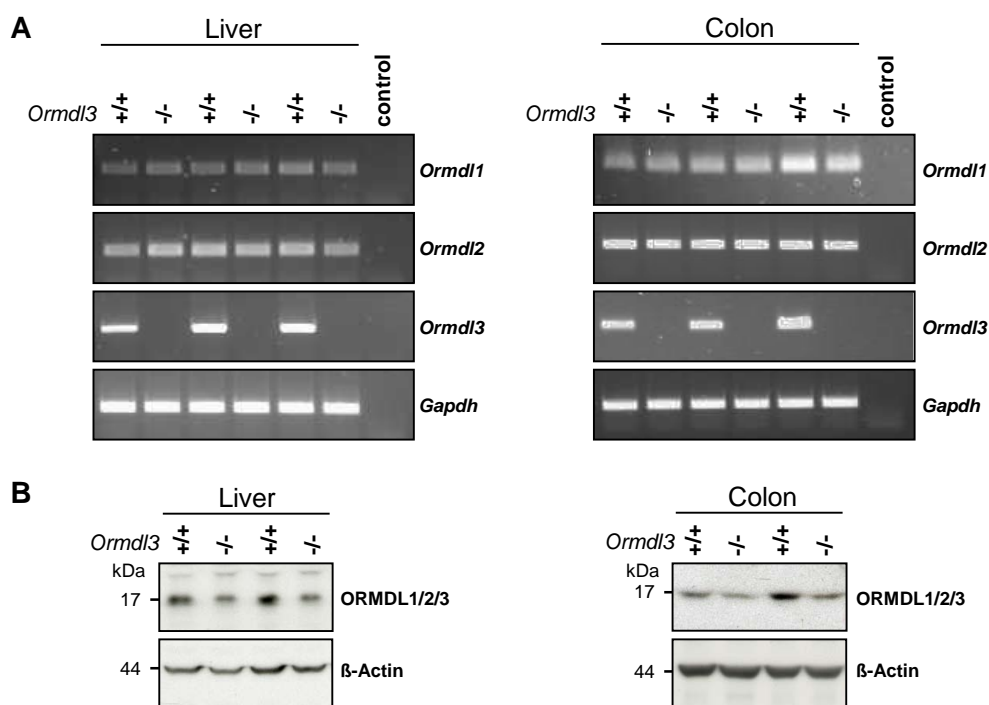


Fig. 3.16: mRNA expression and protein levels of ORMDL homologues in *Ormdl3*^{-/-} mice.

(A) Expression pattern of *Ormdl1*, *Ormdl2* and *Ormdl3* mRNA in liver (left) and colon (right) tissues from three *Ormdl3*^{+/+} and *Ormdl3*^{-/-} littermate pairs were assessed by endpoint PCR. Water was used as control. *Gapdh* mRNA expression served as an internal control for the applied cDNA amount. (B) Total cell lysates of liver (left) and colon (right) tissues from two *Ormdl3*^{+/+} and *Ormdl3*^{-/-} littermate pairs were resolved on a SDS-PAGE and analyzed by immunoblotting using antibodies against ORMDL1/2/3 or β -Actin as a loading control.

3.4.1.2 *Ormdl3* deficiency results in reduced body weight

Homozygous *Ormdl3*^{-/-} mice were viable, fertile and were born from heterozygous breeding pairs at the expected Mendelian ratio (22.7 %; n = 455 pups), indicating no embryonic lethality of this genotype. The overall behavior and coat were inconspicuous. However, the most obvious phenotype of these mice was their significantly reduced body weight (Fig. 3.17A). Analyses of body weights revealed that *Ormdl3*^{-/-} mice were approximately 10 % lighter in weight than their wild-type littermates at an age of 10 weeks (Fig. 3.17B). This phenomenon was gender-independent.

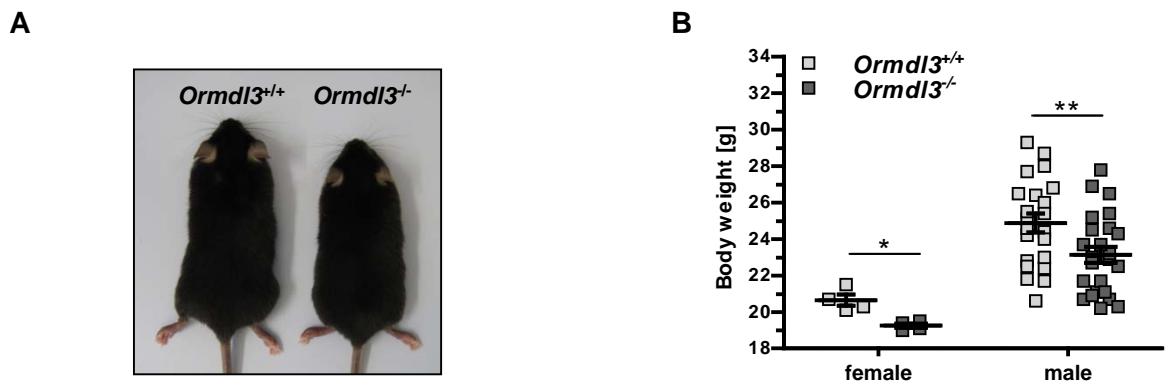


Fig. 3.17: *Ormdl3^{-/-}* mice exhibit reduced body weight.

(A) Representative example of a male *Ormdl3^{+/+}* (left) and *Ormdl3^{-/-}* (right) littermate pair at 10 weeks of age. (B) Body weights of 10 weeks old mice based on 4 female *Ormdl3^{+/+}* and 4 female *Ormdl3^{-/-}* mice (left) as well as 22 male *Ormdl3^{+/+}* and 24 male *Ormdl3^{-/-}* mice (right). Two-tailed paired Student's *t*-test was performed for statistical analysis. Data represents means \pm SEM.

Reduced body weights of *Ormdl3^{-/-}* mice were investigated by analyzing the concentration of a major postnatal growth regulator, the growth hormone (GH). In the serum of *Ormdl3^{-/-}* mice levels of GH tend to be lower than in the serum of their wild-type littermates (Fig. 3.18). The investigated trend was observed in female as well as in male mice at the age of 4 weeks. Additionally, also 10 weeks old male *Ormdl3^{-/-}* mice showed the same trend in the serum level of GH compared to their wild-type littermates.

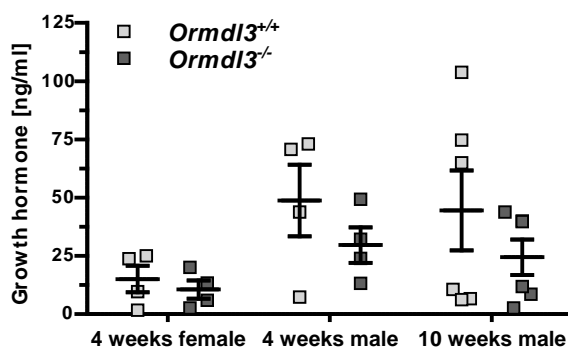


Fig. 3.18: Level of growth hormone in the serum of 4 and 10 weeks old wild-type and *Ormdl3^{-/-}* mice.

Levels of growth hormone in the serum of 4 and 10 weeks old mice were determined by ELISA. Cohorts consisted of four to five mice per group. Two-tailed paired Student's *t*-test was performed for statistical analysis. Data represents means \pm SEM.

Another key component of the growth control pathway, the insulin-like growth factor 1 (IGF1), is known to be reduced in the serum accompanied by diminished GH levels (185). In agreement with the tendency of reduced GH, also IGF1 was slightly reduced in the serum of *Ormdl3^{-/-}* mice, which was most prominent in 4 weeks old female mice (Fig. 3.19A). Due to the fact, that IGF1 is mainly produced in the liver in response to GH stimulation, liver IGF1 levels were investigated. In liver tissues of female and male *Ormdl3^{-/-}* mice significantly reduced *Igf1* mRNA expression levels were detected (Fig. 3.19B).

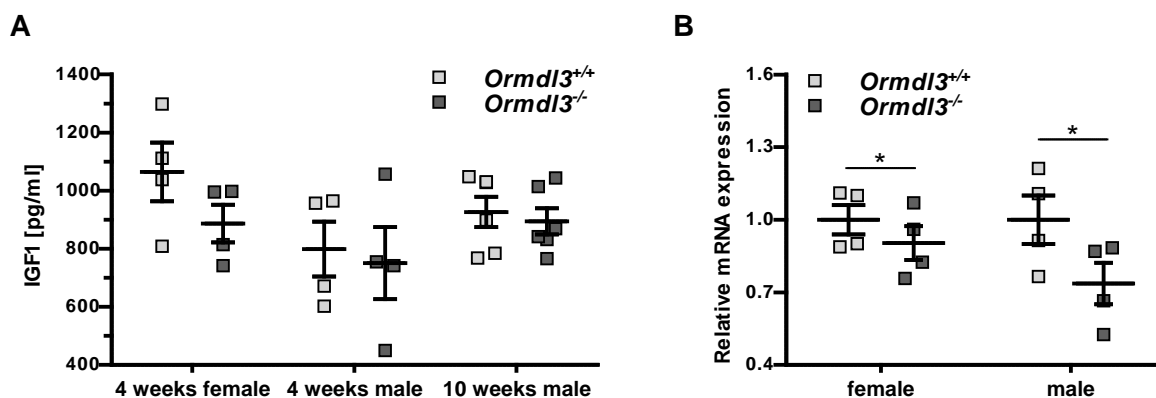


Fig. 3.19: Effect of *Ormdl3* deletion on serum IGF1 levels and liver *Igf1* mRNA expression.

(A) Serum insulin-like growth factor 1 (IGF1) concentrations of 4 and 10 weeks old mice were determined by ELISA. (B) The liver mRNA levels of *Igf1* were quantified by qPCR and normalized against *Gapdh* mRNA expression. The cohorts consisted of four to five mice per group. Two-tailed paired Student's *t*-test was performed for statistical analysis. Data represents means \pm SEM.

3.4.1.3 Histology of the lung, ileum and colon of *Ormdl3*^{-/-} mice

For further investigation, lung, ileum and colon tissues (Fig. 3.20A and Fig. 3.21A,B) were chosen due to the association of ORMDL3 with asthma (149), CD (137) and UC (138), respectively. Additionally, histological analyses were performed from liver tissues of *Ormdl3*^{-/-} and wild-type mice (Fig. 3.20B), because the liver as vital organ for protein synthesis and detoxification is especially susceptible to ER stress (186).

For this histological analysis, tissues of untreated 10 weeks old male mice were stained with hematoxylin and eosin. No obvious differences in histological appearance of all observed tissues were found between *Ormdl3*^{-/-} mice and their wild-type littermates. In detail, lung tissues were composed of alveoli with similar structures in both genotypes (Fig. 3.20A). Similar structures were also obtained from liver tissues of *Ormdl3*^{-/-} and wild-type mice (Fig. 3.20B).

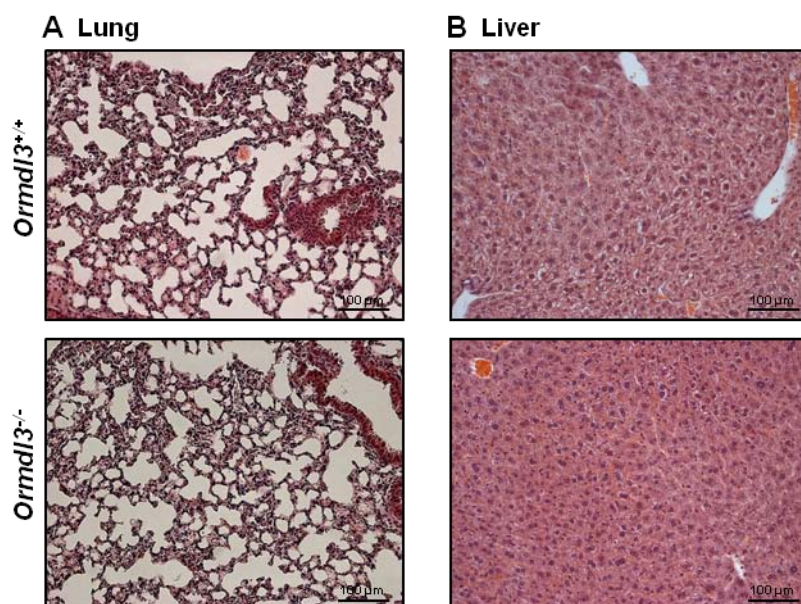


Fig. 3.20: Hematoxylin and eosin staining of lung and liver tissues from wild-type and *Ormdl3*^{-/-} mice. Paraffin-embedded sections (3.5 μm) of formalin-fixed lung (A) and liver (B) tissues were stained with hematoxylin and eosin and visualized at 200x magnification. Scale bars represent 100 μm.

Ileum tissues of *Ormdl3*^{-/-} and wild-type mice showed comparable structures (Fig. 3.21A). Additionally, the thickness of the submucosa and the muscularis externa were not affected by the deletion of *Ormdl3*. Also colon tissues revealed unaltered crypt architectures in *Ormdl3*^{-/-} mice (Fig. 3.21B). The investigated intestinal tissues were composed of similar numbers and appearances of Paneth cells and goblet cells in both genotypes. The appearance of the muscularis mucosae and the submucosa of colon tissues showed no genotype-mediated abnormalities.

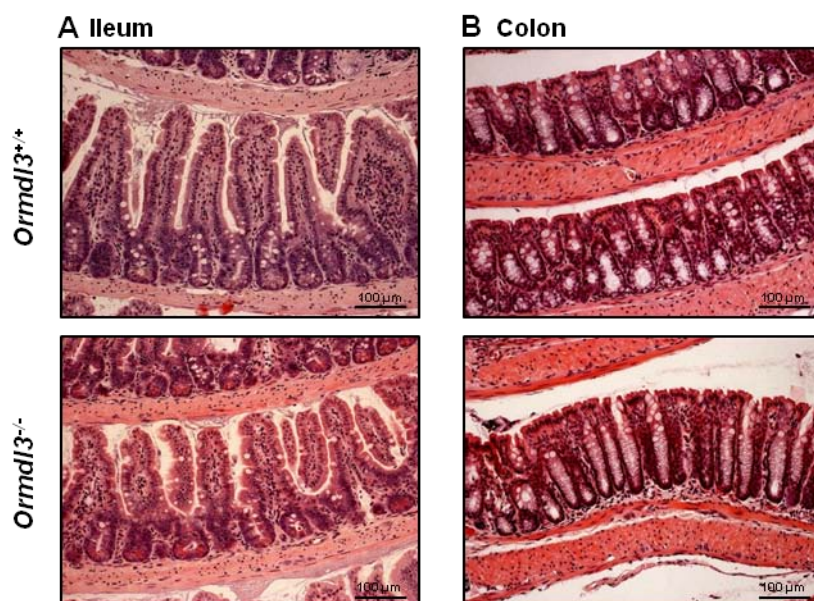


Fig. 3.21: Hematoxylin and eosin staining of ileum and colon tissues from wild-type and *Ormdl3*^{-/-} mice.

Paraffin-embedded sections (3.5 μm) of formalin-fixed ileum (A) and colon (B) tissues were stained with hematoxylin and eosin and visualized at 200x magnification. Scale bars represent 100 μm.

As a proxy for cell composition of the small intestine and the colon from *Ormdl3*^{-/-} mice, mRNA expression analyses of indicator transcripts were examined (Fig. 3.22A-B). The mRNA expression levels of well established cell type markers such as villin (*Vil*), mucin 2 (*Muc2*), leucine-rich repeat-containing G-protein coupled receptor 5 (*Lgr5*) and lysozyme 1 (*Lyz1*) were analyzed by qPCR to measure the content of epithelial cells, goblet cells, intestinal stem cells and Paneth cells, respectively. Deletion of *Ormdl3* did not alter mRNA expression levels of all mentioned genes, indicating that the cell composition in the small intestine as well as in the colon seems to be unaffected.

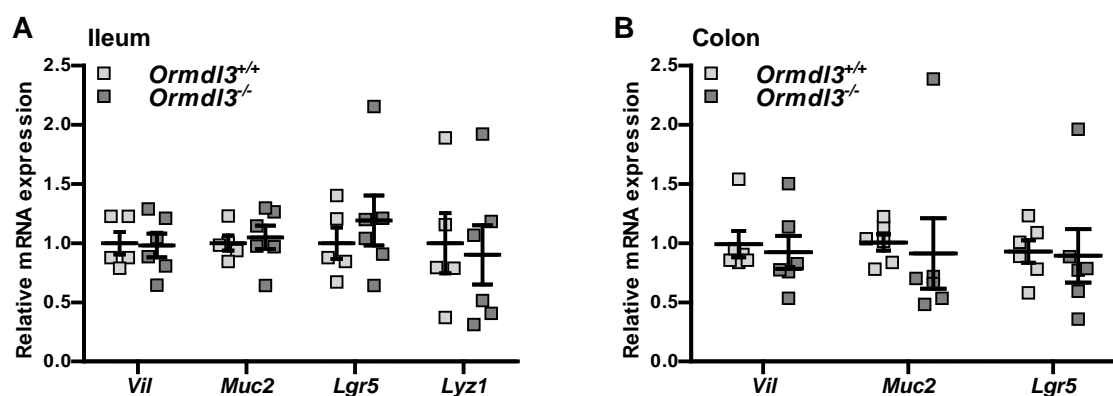


Fig. 3.22: *Ormdl3* deficiency does not affect marker transcripts in ileum and colon tissues.

Total RNA was isolated from small intestine (A) and colon (B) of 10 weeks old *Ormdl3*^{-/-} mice and their wild-type littermates. The mRNA levels of Villin (*Vil*), Mucin 2 (*Muc2*), Leucine-rich repeat-containing G-protein coupled receptor 5 (*Lgr5*) and Lysozyme 1 (*Lyz1*) were quantified by qPCR and normalized against *Gapdh* mRNA expression. The qPCRs were performed using TaqMan probes. Cohorts consisted of six male mice per genotype. Data represents means \pm SEM.

3.4.1.4 Cytokine concentrations in *Ormdl3*^{-/-} mice

Due to the fact that cytokines play a vital role in the development of chronic diseases, such as asthma or IBD (187), cytokine levels were determined in the serum of *Ormdl3*^{-/-} mice. The investigated cytokine concentrations of IL-1 β , IL-10 and IL-12 p40 in the serum of *Ormdl3*^{-/-} mice were comparable to those of their wild-type littermates (Fig. 3.23). Additionally, other determined cytokines such as IL-1 α , IL-2, IL-6 and IL-13 were also not altered in the observed mice (data not shown). However, TNF α , IFN γ and IL-12 p70 concentrations in the serum of *Ormdl3*^{-/-} mice tend to be lower than in the serum of *Ormdl3*^{+/+} mice.

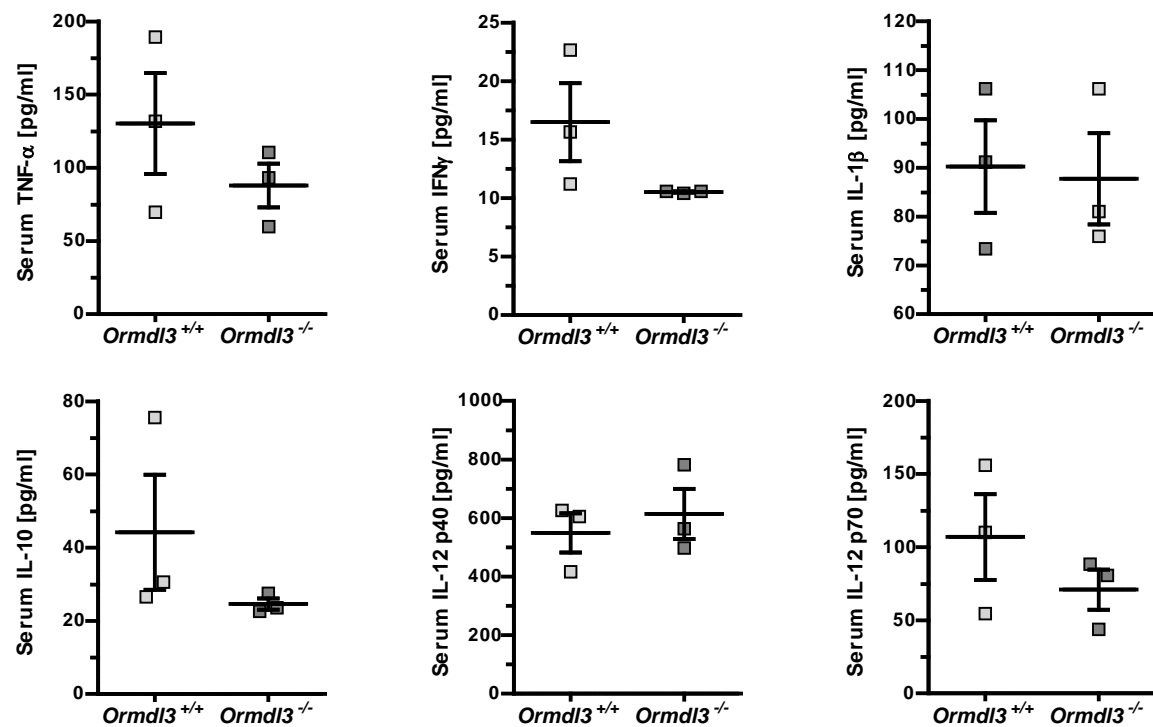


Fig. 3.23: Representative examples of serum cytokines of *Ormdl3*^{-/-} and wild-type mice.

Serum cytokine concentrations of 10 weeks old *Ormdl3*^{-/-} mice and their wild-type littermates were determined by Bio-Plex Pro™ Mouse Cytokine 23-plex immunoassay. The cohorts consisted of three male mice per genotype. Data represents means ± SEM.

IFN γ levels were further explored, because IFN γ was described to induce proteolytic processing of ATF6 α (189) and ORMDL3 was shown in the present study to modulate ATF6 α cleavage. In addition, IFN γ is essential for regulation of the intestinal epithelial homeostasis (190). The tendency of reduced IFN γ concentration in the serum of *Ormdl3*-deficient mice was additionally investigated by qPCR of liver, colon and spleen tissues. Interestingly, the mRNA levels of *Ifn γ* were significantly reduced in proximal colon tissues and slightly diminished in liver tissues of *Ormdl3*^{-/-} mice (Fig. 3.24A-B). In spleen tissues no genotype-dependent *Ifn γ* alterations were observed (Fig. 3.24C). This indicates a tissue-specific *Ifn γ* mRNA expression in *Ormdl3*^{-/-} mice with even significantly altered expression levels in the colon.

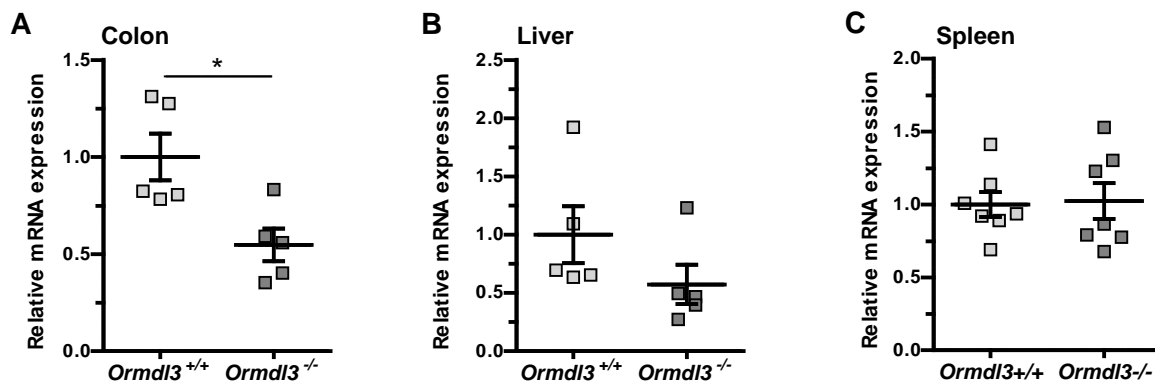


Fig. 3.24: Tissue-specific effect of *Ormdl3* on *Ifny* mRNA levels.

Total RNA was isolated from proximal colon (A), liver (B) and spleen (C) of 10 weeks old *Ormdl3*^{-/-} mice and their wild-type littermates. The mRNA levels of *Ifny* were quantified by qPCR and normalized against *Gapdh* mRNA expression. The cohorts consisted of five male mice per genotype. Two-tailed unpaired Student's *t*-test was performed for statistical analysis. Data represents means \pm SEM.

The effect of *Ormdl3* deficiency on *Ifny* mRNA expression levels was further investigated in colon tissues. Lamina propria fractions were isolated from colon tissues using the lamina propria dissociation kit. Isolated cells were stained and measured using the FACScalibur to analyze IFN γ -specific cell surface targets such as MHC (major histocompatibility complex) class I (MHCI) and MHC class II (MHCII) molecules on CD11b⁺ cells (Fig. 3.25).

Cell debris with low granularity (side scatter, SSC) and size (forward scatter, FSC) were excluded from further evaluation (Fig. 3.25A+C). To this end, only cells from the gated region 1 (R1) were investigated for cell-surface expression of CD11b and MHCI or MHCII. CD11b/MHCI double-positive cells were gated (R3) and examined for two mice per genotype. The percentage of CD11b/MHCI double-positive cells isolated from the lamina propria of *Ormdl3*^{-/-} mice was lower compared to their wild-type littermates (Fig. 3.25B). A similar tendency was observed for the percentage of CD11b/MHCII double-positive cells (Fig. 3.25D). Thereby, the amount of CD11b⁺ cells was comparable between *Ormdl3*^{-/-} and wild-type mice. These findings suggest *Ormdl3*-dependent alterations in IFN γ levels influencing MHCI and MHCII cell-surface expression on CD11b⁺ myeloid cells of the lamina propria fraction in the colon.

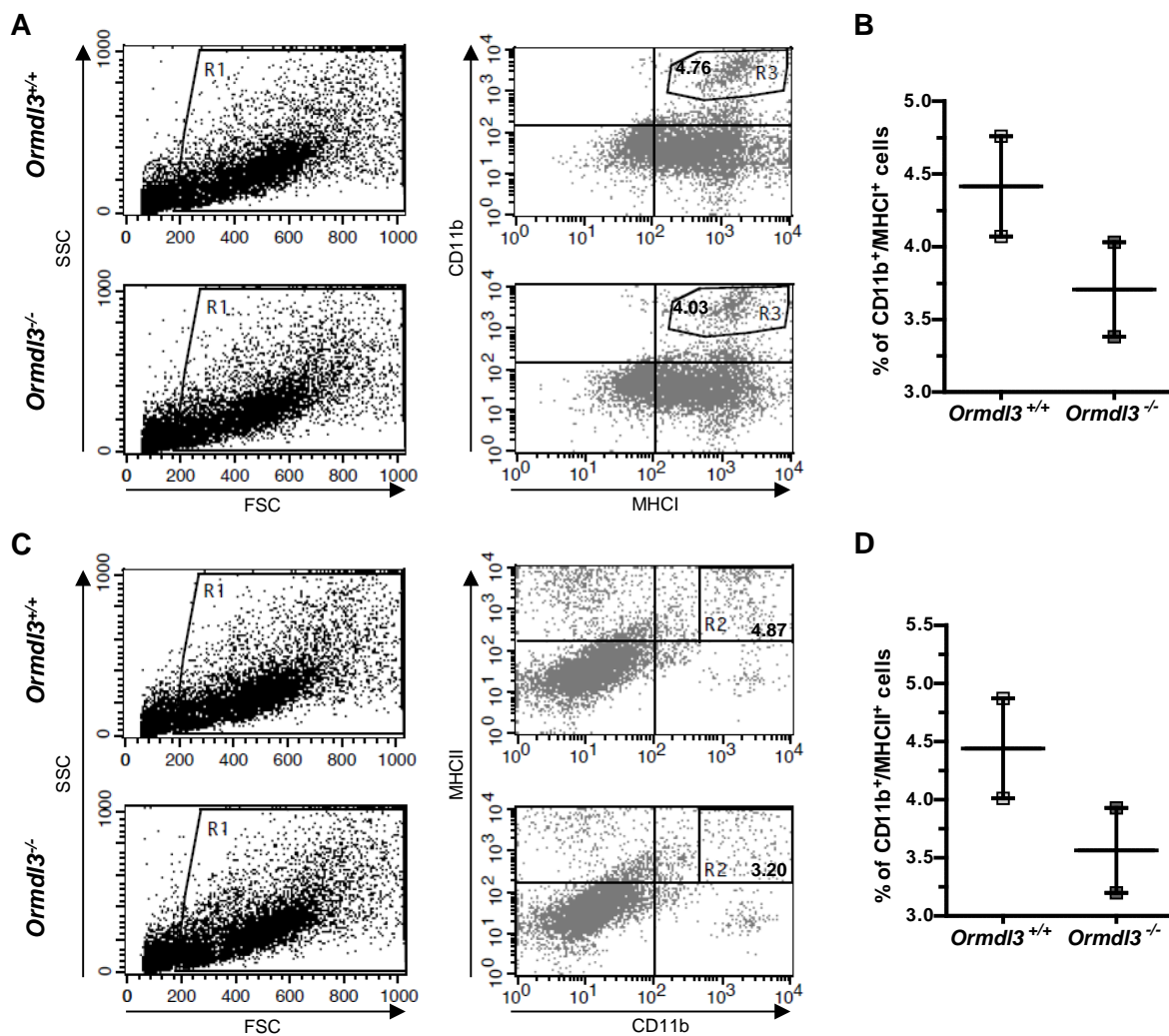


Fig. 3.25: *Ormdl3*^{-/-} mice express less MHCI and MHCII on CD11b⁺ lamina propria cells.

Lamina propria fractions were isolated from colon tissues of 10 weeks old *Ormdl3*^{-/-} mice and their wild-type littermates. Cells were stained using specific antibodies for CD11b and MHCI (A+B) or MHCII (C+D). Representative SSC/FSC scatter dot plots and FACS profiles of CD11b and MHCI (A) or MHCII (C) cell-surface expression pattern are given. The percentage of MHCI CD11b double positive cells (B) and CD11b/MHCII double positive cells (C) were determined in R3 and R2, respectively. Data show the mean \pm SEM from two animals per group.

3.4.2 *Ormdl3*^{-/-} mice are more susceptible to acute DSS-induced colitis

ORMDL3 had been identified by GWAS as a susceptibility loci for CD (137) and UC (138). However, under baseline conditions *Ormdl3*^{-/-} mice do not show any signs of inflammation (Fig. 3.20 and Fig. 3.23). To investigate the role of ORMDL3 during intestinal inflammation, mice were challenged with 2.5 % DSS in their drinking water to induce an acute colitis. The severity of DSS-induced colitis was monitored daily by measuring body weight (Fig. 3.26A). Already on day one *Ormdl3*^{-/-} mice lost weight but recovered again until day four, whereas wild-type littermates maintained their body weights until day four. After day four, body weights decreased faster in *Ormdl3*-deficient mice than compared to their wild-type littermates. Additionally, the course of the disease was monitored and

scored using the disease activity index (DAI), a combined score of stool blood, stool consistency and body weight loss. On day one and six of DSS treatment, the course of the disease was significantly worse in *Ormdl3*^{-/-} mice than in their wild-type littermates. In summary, the progression of the DAI showed a similar trend as the body weight loss.

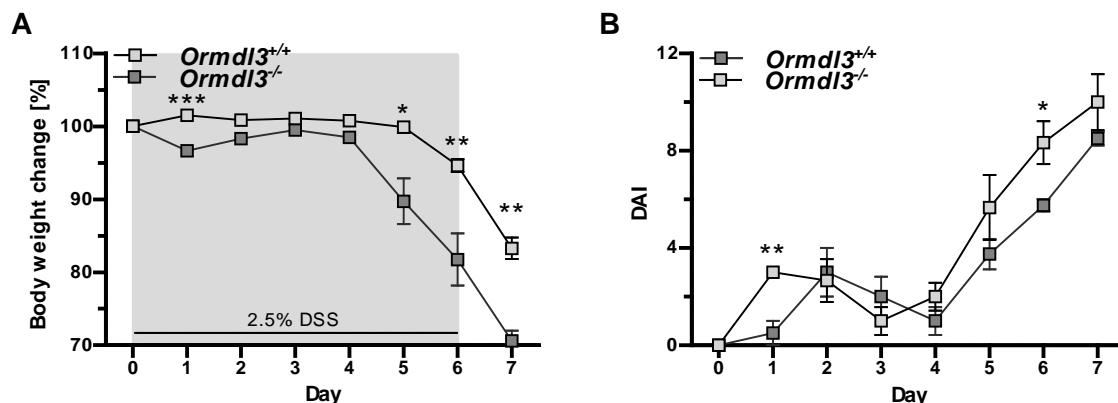


Fig. 3.26: *Ormdl3* deficiency increases susceptibility to DSS-induced colitis.

2.5 % DSS was administered in drinking water for six days and thereafter replaced by regular drinking water. (A) Body weight changes of treated littermates ($n=4$ for *Ormdl3*^{+/+}; $n=3$ for *Ormdl3*^{-/-}) are shown in percent of initial weights. (B) Clinical severity was assessed daily using the disease activity score (DAI). Two-tailed unpaired Student's *t*-test was performed for statistical analysis. Data represents means \pm SEM.

Another indication for the severity of a DSS-induced colitis is the degree of colon shortening (191). DSS administration induced colon shortening in all treated mice, however, colon length of untreated and DSS-treated *Ormdl3*^{-/-} mice were comparable to their wild-type littermates (Fig. 3.27A). In addition, reduced liver weight has been reported to correlate with the degree of colitis in DSS-treated hamsters (192). *Ormdl3*^{-/-} mice showed significantly less liver weight than *Ormdl3*^{+/+} mice after DSS treatment, although the liver weight were comparable in untreated mice (Fig. 3.27A), indicating a more severe course of the disease in *Ormdl3* deficient mice.

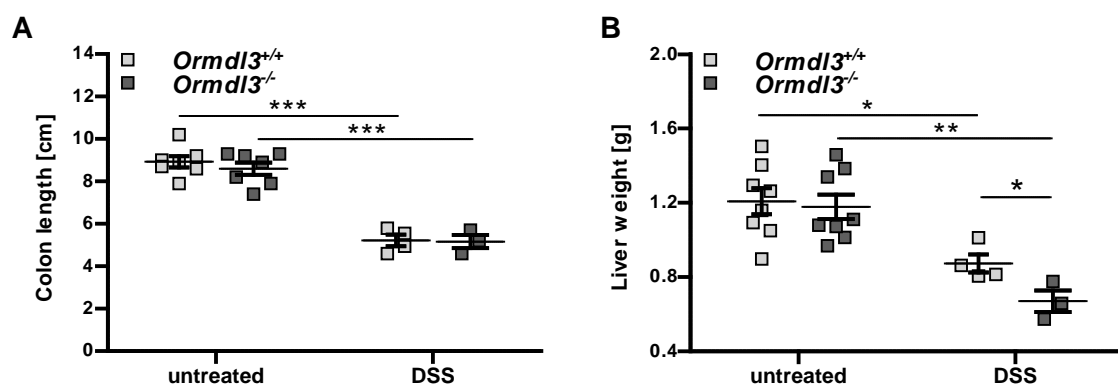


Fig. 3.27: DSS-induced colitis affects colon length and liver weight of *Ormdl3*^{-/-} and wild-type mice.

Colon length (A) and the liver weight (B) of untreated ($n=7-8$) and DSS-treated littermates ($n=4$ for *Ormdl3*^{+/+}; $n=3$ for *Ormdl3*^{-/-}) were determined. Two-tailed unpaired Student's *t*-test was performed for statistical analysis. Data represents means \pm SEM.

Distal colon tissues, which are most affected during DSS administration (191), were investigated by histological analysis of hematoxylin and eosin stained tissues. Colon tissues of both genotypes revealed strong effects of DSS administration. However, histological score analysis, which combines values for crypt damage, severity of inflammation and ulceration, showed slightly higher DSS injury scores for *Ormdl3*^{-/-} mice than for wild-type mice (Fig. 3.28A). A higher score represented a more severe DSS-induced colitis. Comparison of histological sections of an exemplary littermate pair showed more intense infiltrations of immune cells, crypt damage, crypt abscesses and crypt loss in *Ormdl3*^{-/-} mice (Fig. 3.28B).

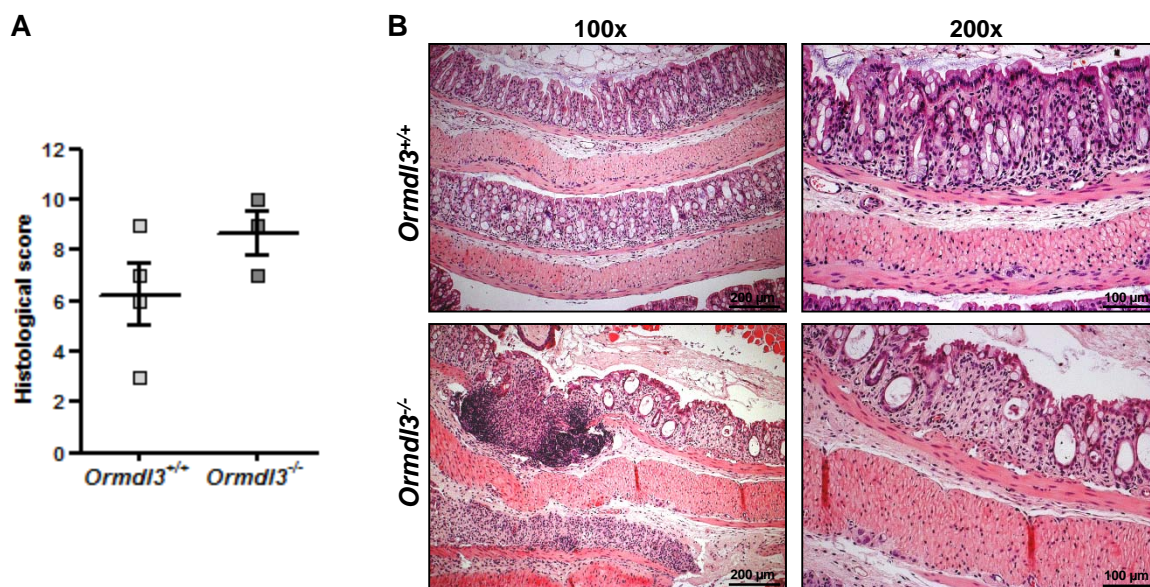


Fig. 3.28: Histological scores and HE stainings of *Ormdl3*^{-/-} and wild-type mice after DSS treatment.

Paraffin-embedded sections (3.5 μ m) of fixed colon tissues were stained with hematoxylin and eosin and visualized at 100x and 200x magnification. (A) The histological score, a combined score of crypt damage, severity of inflammation and ulceration, was evaluated in a blinded manner. Data represents means \pm SEM. (B) Distal colon tissues from the distal part of a littermate pair are exemplary shown. The scale bars represent 200 μ m and 100 μ m in the 100x and 200x magnifications, respectively.

It has been shown, that the level of the pro-inflammatory cytokine IL-1 β correlate with the severity of intestinal inflammation (193). Interestingly, DSS-treated *Ormdl3*^{-/-} mice revealed significantly elevated IL-1 β serum levels compared to wild-type mice (Fig. 3.29A). Additionally, secretion of the pro-inflammatory cytokines IL-6 and TNF α was also slightly higher in the serum of *Ormdl3*^{-/-} mice than in wild-type mice (Fig. 3.29B, C). However, serum concentration of the pro-inflammatory cytokine chemokine (C-X-C motif) ligand 1 (CXCL1) was not altered between the investigated genotypes (Fig. 3.29D). As for untreated *Ormdl3*^{-/-} mice (Fig. 3.23), serum levels of the pro-inflammatory cytokine IFN γ was slightly reduced in *Ormdl3*-deficient mice after DSS administration (Fig. 3.29E).

Secretion of the anti-inflammatory cytokine IL-10 showed an increased tendency in DSS-treated *Ormdl3*^{-/-} mice compared to the wild-type mice (Fig. 3.29F).

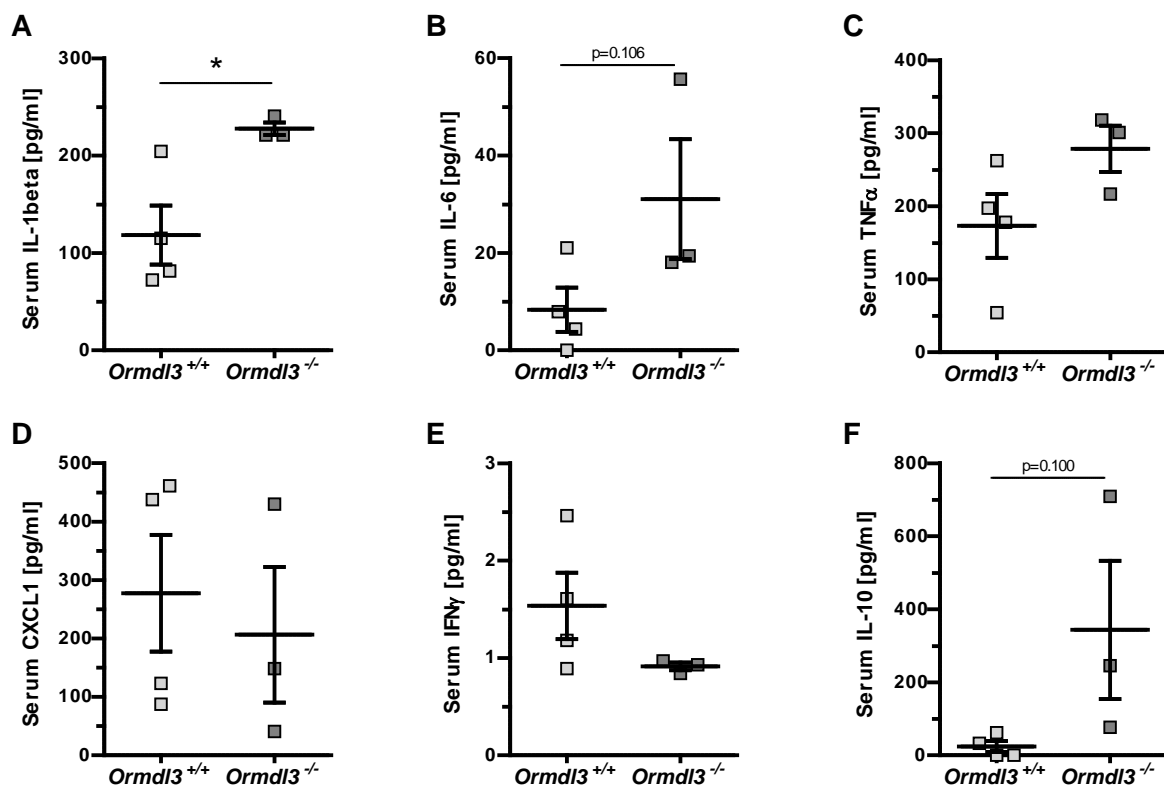


Fig. 3.29: DSS-induced cytokine secretion in *Ormdl3*^{-/-} and wild-type mice.

Ormdl3^{-/-} and wild-type mice were treated for six days with 2.5% DSS in drinking water and an additional day with normal drinking water. Serum cytokine concentrations were determined by Bio-Plex Pro™ Mouse Cytokine immunoassay (Bio-Rad). Cohorts consisted of 4 *Ormdl3*^{+/+} mice and 3 *Ormdl3*^{-/-} mice. Two-tailed unpaired Student's *t*-test was performed for statistical analysis. Data represents means ± SEM.

Due to the fact, that ORMDL proteins are involved in the cellular UPR (135) and unresolved ER stress induces intestinal inflammation (51), mRNA expression pattern of components of the UPR were investigated by qPCR (Fig. 3.30). After DSS treatment, mRNA expression levels of *Atf6α*, *Grp94*, *Atf4* and *Chop* in *Ormdl3*^{-/-} mice were similar to those in wild-type mice. Although mRNA expression levels of *Atf4* and *Chop* were comparable in both genotypes, mRNA levels of its target gene *Gadd34* tend to be higher expressed in *Ormdl3*-deficient mice after DSS administration. In addition, spliced *Xbp1* was less expressed in colon tissues of *Ormdl3*^{-/-} mice.

Furthermore, mRNA expression levels of UPR mediators were also analyzed in liver and spleen tissues (not shown), which were comparable to those from colon tissues.

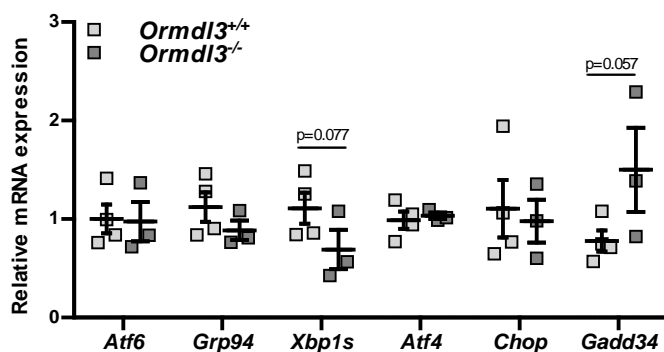


Fig. 3.30: DSS-induced colonic mRNA expression of genes involved in the UPR in *Ormdl3*^{-/-} and wild-type mice.

Ormdl3^{-/-} and wild-type mice were treated for six days with 2.5% DSS in drinking water and an additional day with normal drinking water. The mRNA expression in colon tissues were investigated by qPCR and normalized against *Gapdh*. Cohorts consisted of 4 *Ormdl3*^{+/+} mice and 3 *Ormdl3*^{-/-} mice. Two-tailed unpaired Student's *t*-test was performed for statistical analysis. Data represents means \pm SEM.

At the end of the acute colitis experiment, both genotypes were affected by DSS, which might be the reason for molecular markers of the UPR not being significantly altered between the genotypes (Fig. 3.30). To further assess the UPR during the development of colitis, protein levels of colon tissues were investigated after short-term DSS-treatments ranging from two to four days. Immunoblotting analysis revealed prolonged phosphorylation of eIF2 α (p-eIF2 α) in colon tissues of DSS-treated *Ormdl3*^{-/-} mice, although basal level of p-eIF2 α was lower in these mice compared to its littermates (Fig. 3.31A). However, the downstream target of p-eIF2 α , ATF4, was not significantly altered between both genotypes. In liver tissues, which are affected by DSS already after one day of treatment (194), p-eIF2 α was also prolonged upregulated in *Ormdl3*^{-/-} mice after DSS treatment (Fig. 3.31B). This observation was supported by elevated levels of CHOP, a downstream target of p-eIF2 α . Additionally, levels of ORMDL proteins increased during the DSS treatment in the investigated tissues of *Ormdl3*^{-/-} mice, indicating a protective role during colitis.

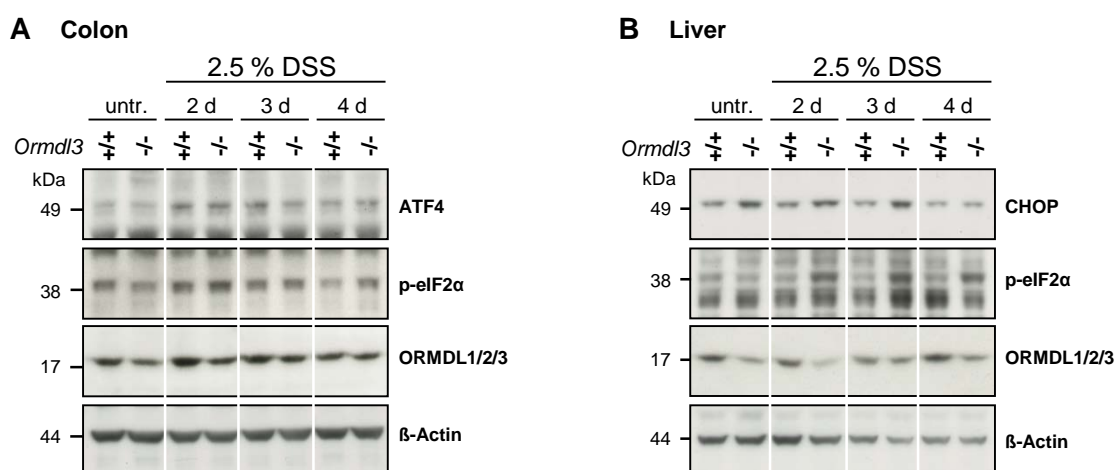


Fig. 3.31: Short-term DSS treatment induces prolonged upregulation of p-eIF2 α in *Ormdl3*^{-/-} mice.

Mice were left untreated or treated with 2.5 % DSS in drinking water for indicated durations. Total cell lysates of colon (A) and liver (B) tissues from *Ormdl3*^{+/+} and *Ormdl3*^{-/-} littermate pairs were resolved on a SDS-PAGE and analyzed by immunoblotting using antibodies to ORMDL1/2/3 or β -Actin as loading control.

3.4.3 Tunicamycin injection induces prolonged UPR in *Ormdl3*^{-/-} mice

Several investigations pointed to an influence of ORMDL3 on ER stress pathways and brought the liver into focus. First, the earlier described *in vitro* results in HEK-293 cells led to the conclusion that ORMDL3 is involved in mechanisms which protect cells against ongoing stress. Second, challenging *Ormdl3*^{-/-} mice with 2.5 % DSS for short durations revealed prolonged upregulation of p-eIF2 α , indicating unresolved ER stress (Fig. 3.31). Third, a systemic ER stress effect of DSS-treated animals in the liver became prominent (Fig. 3.31). For these reasons and to investigate whether deficiency in *Ormdl3* influences the susceptibility to chemically induced ER stress, *Ormdl3*^{-/-} mice were challenged with a sublethal dose of tunicamycin (1 mg/g body weight). During the first five days, all mice lost weight continuously (Fig. 3.32). After day five, mice gained weight again, however *Ormdl3*^{-/-} mice recovered slightly slower than their wild-type littermates. All treated mice survived the tunicamycin challenge.

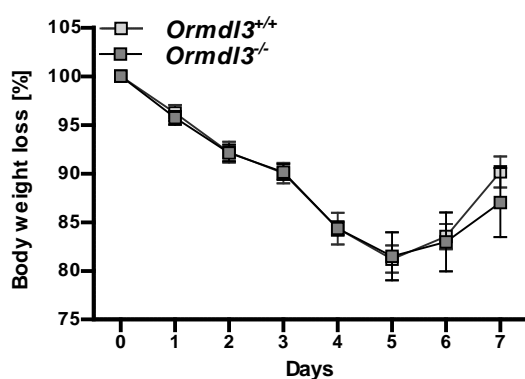


Fig. 3.32: Effect of tunicamycin injection on body weight of *Ormdl3*^{-/-} mice.

Ormdl3^{-/-} and *Ormdl3*^{+/+} mice were injected intraperitoneally with tunicamycin (TM; 1 mg/kg body weight) or vehicle. Body weight was determined daily and is represented after normalization to their initial body weights on day 0. The cohorts consisted of seven male mice per genotype. Two-tailed unpaired Student's *t*-test was performed for statistical analysis. Data represents means \pm SEM.

Intraperitoneally injection of tunicamycin primary affects liver and kidney (195). To gain a more detailed insight into tunicamycin-mediated molecular alterations, groups of mice were sacrificed after 8, 24, 48 h or 7 d of treatment. Dissections after 48 h of treatment disclosed obvious lighter liver colors in *Ormdl3*^{-/-} mice compared to their wild-type littermates (Fig. 3.32A). To address the reason for the pale liver color, lipid accumulations were investigated using the cytosolic lipid protein marker adipose differentiation related protein (ADRP) (196). Immunoblotting analysis revealed a postponed kinetic of ADRP protein expression in *Ormdl3*^{-/-} mice (Fig. 3.33B). In detail, protein levels of ADRP were increased in wild-type mice already after 8 h, whereas *Ormdl3*^{-/-} mice showed no alterations of ADRP protein levels at that time point. After 24 h of tunicamycin administration, both genotypes expressed ADRP in approximately same amounts. However, after 48 h of tunicamycin treatment, ADRP protein levels decreased again in wild-type mice, whereas *Ormdl3*^{-/-} mice still exhibited high ADRP protein levels. To validate this finding, liver protein lysates of all littermate pairs treated with tunicamycin for

48 h were investigated by immunoblotting (Fig. 3.33C). Assessment of these liver tissues showed increased ADRP protein levels in three out of four *Ormdl3*^{-/-} mice.

Additionally, UPR signaling in tunicamycin-treated mice was investigated by monitoring ER stress mediators and chaperones. The ATF4 pathway was examined by immunoblotting using antibodies to p-eIF2 α and its target CHOP (Fig. 3.33B). In line with the ADRP protein expression pattern, the kinetic of eIF2 α phosphorylation was postponed in *Ormdl3*^{-/-} mice. These mice showed lower levels of p-eIF2 α after 24 h of tunicamycin treatment compared to wild-type mice. However, after 48 h until the end of the experiment *Ormdl3*^{-/-} mice exhibited prolonged eIF2 α phosphorylation, whereas in wild-type mice p-eIF2 α reached the baseline level. Interestingly, deletion of *Ormdl3* resulted in an increased protein expression of the pro-apoptotic factor CHOP after 8 and 24 h of tunicamycin administration.

ATF6 α FL was also affected by intraperitoneally injection of tunicamycin. After 24 h of tunicamycin treatment, only wild-type mice showed reduced protein levels of ATF6 α FL, indicating ER stress-induced ATF6 α FL cleavage. At the same time point, *Ormdl3*^{-/-} mice exhibited ATF6 α FL protein levels comparable to those of untreated mice. Similar to the *in vitro* results (Fig. 3.8C), a protein band with a slightly lower kDa size of ATF6 α appeared in wild-type mice after 24 h of tunicamycin treatment. This slightly lower protein band indicates the potentially unglycosylated form of ATF6 α FL. Similar observations were made for the translocon-associated protein subunit alpha (TRAP α). TRAP α was initially investigated to confirm the efficacy of tunicamycin injection, which results in inhibition of glycosylation. Similar to *ATF6 α* ^{-/-} mice (94), the protein levels of unglycosylated TRAP α (TRAP α ^{UG}) were lesser in *Ormdl3*^{-/-} mice early after tunicamycin injection (24 h) but were augmented at later time points (48 h). After 7 days of treatment, liver tissues of *Ormdl3*^{-/-} mice still showed a weak protein band of TRAP α ^{UG}, whereas wild-type mice revealed only the full length form of TRAP α and a not described protein band. The ATF6 α targets, GRP78 and GRP94, were induced in all tunicamycin-treated mice over time. Alterations in GRP78 and GRP94 protein levels were observed only after 24 h of tunicamycin administration, where *Ormdl3*^{-/-} mice showed a delayed onset of protein expression. However, expression of GRP78 and GRP94 proteins are not only induced by ATF6 α but also by the spliced form of XBP1 (86). Therefore, *Xbp1* mRNA splicing was monitored over time using semi-quantitative endpoint PCRs. In the early phase after only 8 h of treatment, both genotypes responded to tunicamycin by *Xbp1* splicing (Fig. 3.33D). After this time point, wild-type mice restored the unspliced form of *Xbp1*, whereas *Ormdl3*^{-/-} mice revealed persistent splicing of *Xbp1* until the end of the experiment. In accordance with a potential protective role of ORMDL proteins, their protein levels were upregulated in response to tunicamycin, especially in wild-type (Fig. 3.33B).

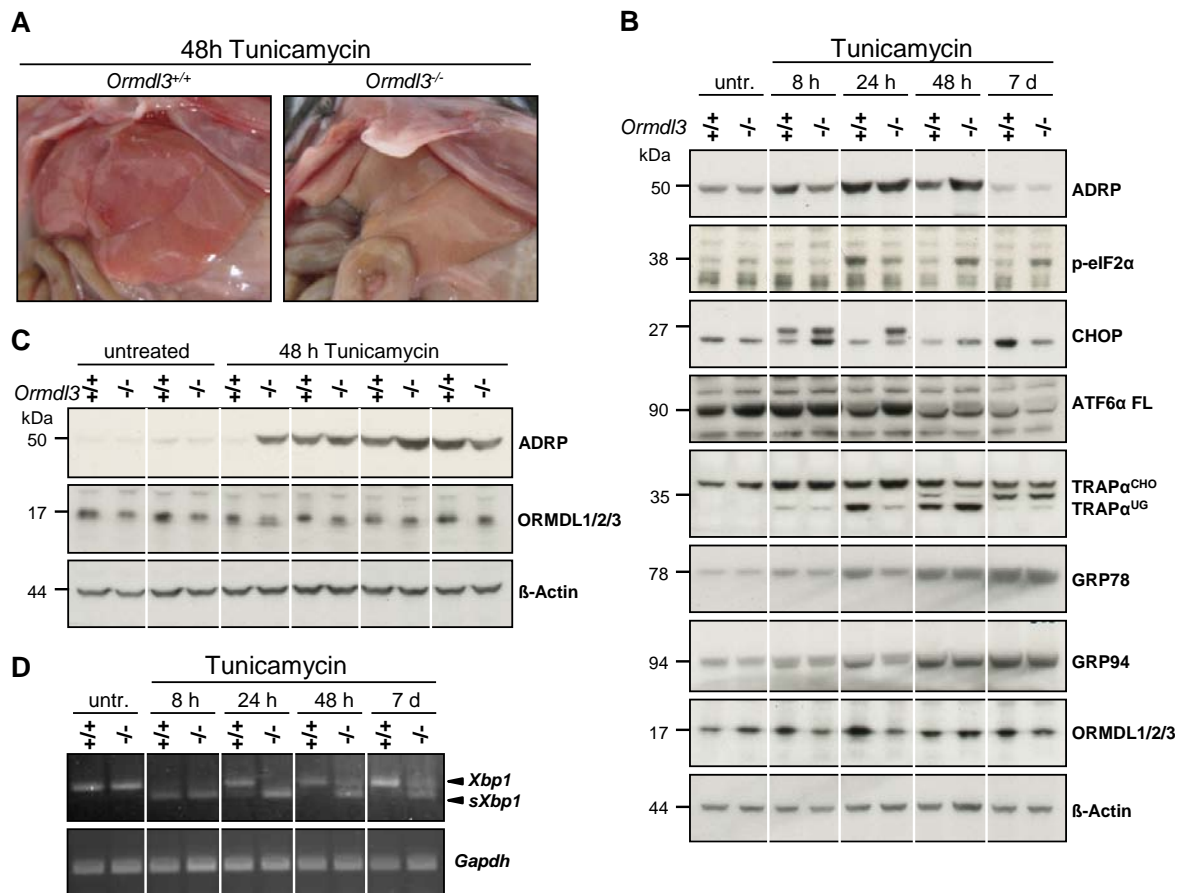


Fig. 3.33: ORMDL3 regulates ER stress-dependent chaperone expression in the liver upon tunicamycin injection.

Ormdl3^{-/-} and *Ormdl3*^{+/+} littermate mice were intraperitoneally injected with tunicamycin (1 mg/kg body weight) and sacrificed after 8, 24, 48 h or 7 d. (A) Livers of treated mice were dissected and photographed after 48 h. (B+C) Protein lysates from liver tissues were probed by immunoblot as indicated. (D) RNA was isolated from the same samples and analyzed for unspliced *Xbp1* (*Xbp1*) and spliced *Xbp1* (*sXbp1*) mRNA by semi-quantitative endpoint PCR. *Gapdh* mRNA expression served as an internal control for the applied cDNA amount.

Besides liver tissues, also kidney tissues were affected after intraperitoneal injections of tunicamycin. ADRP protein levels were prolonged upregulated in both organs of *Ormdl3*^{-/-} mice after 48 h of tunicamycin treatment (Fig. 3.34A). Additionally, as already seen in liver tissues, the pro-apoptotic factor CHOP was prolonged upregulated in kidney tissues of *Ormdl3*^{-/-} mice compared to their wild-type littermates. As expected from the literature, the high protein level of CHOP in kidney tissues was postponed for 24 h compared to liver tissues, indicating that kidneys were secondary affected organs by tunicamycin injection. Protein levels of the ER stress marker GRP78 increased during the experiment, but there were no significant alterations between the observed genotypes. Also mRNA splicing of *Xbp1* did not show significant alterations between *Ormdl3*^{-/-} and their wild-type littermates (Fig. 3.34B).

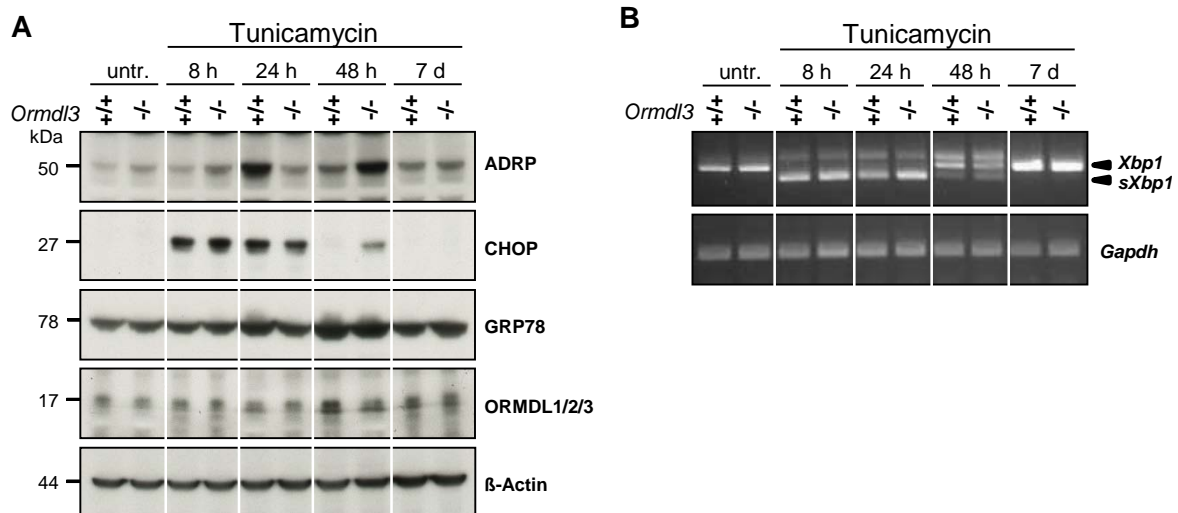


Fig. 3.34: *Ormdl3* deficiency prolongs upregulation of ADRP and CHOP in kidney tissues.

Ormdl3^{-/-} and *Ormdl3*^{+/+} littermate mice were intraperitoneally injected with tunicamycin (1 mg/kg body weight) and sacrificed after 8, 24, 48 h or 7 d. (A) Protein lysates of kidney tissues were probed by immunoblot as indicated. (B) RNA was isolated from the same samples and analyzed for unspliced *Xbp1* (*Xbp1*) and spliced *Xbp1* (*sXbp1*) mRNA by endpoint PCR. *Gapdh* mRNA expression served as an internal control for the applied cDNA amount.

To investigate the pale liver (Fig. 3.33A) and prolonged upregulation of ADRP (Fig. 3.33B) in *Ormdl3*^{-/-} mice in more detail, lipid contents in serum and liver of tunicamycin-treated mice were investigated. Upon tunicamycin injection mice exhibited increased hepatic triglycerides and decreased plasma lipids, including plasma triglycerides, cholesterol and high-density lipoprotein (HDL) cholesterol (197). Liver concentrations of triglycerides increased during the tunicamycin treatment as expected, however without any significant differences between the observed genotypes (Fig. 3.35A). Also concentrations of serum triglycerides showed no markedly differences between *Ormdl3*^{-/-} and wild-type mice in response to tunicamycin administration (Fig. 3.35B). Interestingly, after 8 h of tunicamycin treatment, serum cholesterol concentrations decreased slightly faster in *Ormdl3*^{-/-} mice than in wild-type mice (Fig. 3.35C). This tendency might be a result of the significantly decreased serum HDL cholesterol concentrations in *Ormdl3*^{-/-} mice after 8 h of tunicamycin administration (Fig. 3.35D), as ER stress in metabolic disorders has been identified to reduce HDL biogenesis (198). These findings demonstrate that *Ormdl3*^{-/-} mice show a stronger response to tunicamycin treatment with a potentially more pronounced metabolic disorder.

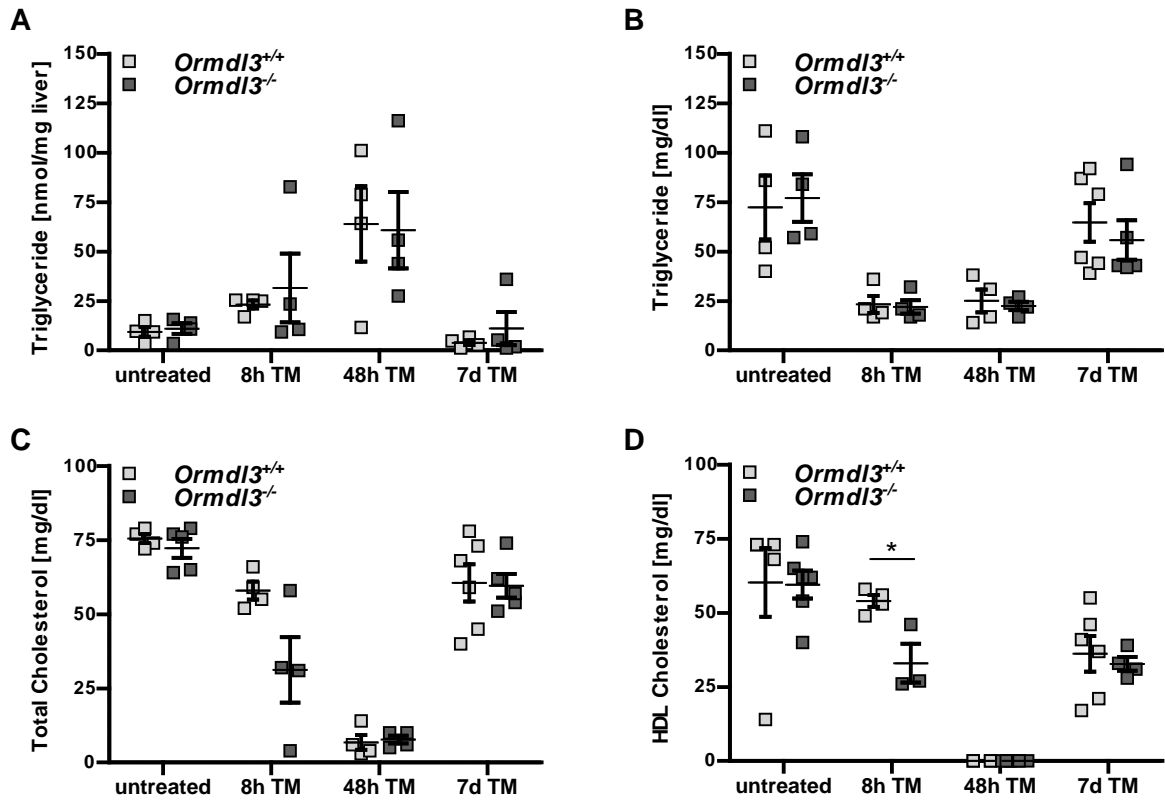


Fig. 3.35: Tunicamycin administration affects lipid contents in $Ormdl3^{-/-}$ and wild-type mice.

$Ormdl3^{-/-}$ and $Ormdl3^{+/+}$ littermate mice were intraperitoneally injected with tunicamycin (TM; 1 mg/kg body weight) and sacrificed after 8, 24, 48 h or 7 d. Concentrations of hepatic triglycerides (A) and serum lipids, including plasma triglycerides (B), cholesterol (C) and high-density lipoprotein (HDL) cholesterol (D) were determined. Two-tailed unpaired Student's *t*-test was performed for statistical analysis. Data represents means \pm SEM.

3.5 Characterization of *Ormdl3*^{ΔIEC} mice

Due to the association of *ORMDL3* as a potential risk variant for IBD, further investigation focused on the effect of *Ormdl3* deficiency particularly in intestinal epithelia cells (IEC). For this reason, mice with an IEC-specific deficiency of *Ormdl3* (*Ormdl3*^{ΔIEC} mice) were investigated.

3.5.1 Basal phenotype of *Ormdl3*^{ΔIEC} mice

Ormdl3^{ΔIEC} mice were generated by applying the Cre-mediated homologous recombination technology as described in chapter 2.4.4. For the validation of the IEC-specific deletion of *Ormdl3*, mRNA expression levels of the three *Ormdl* homologues were investigated in IECs and lamina propria cells by semi-quantitative endpoint PCR. As expected, *Ormdl3* mRNA was not expressed in IECs of small intestinal and colon tissues isolated from *Ormdl3*^{ΔIEC} mice whereas their wild-type (*Ormdl3*^{fl/fl}) littermates exhibited normal mRNA expression levels of *Ormdl3* (Fig. 3.36A-B). Similar to *Ormdl3*^{-/-} mice, mRNA expression levels of the other two *Ormdl* homologues in IECs were comparable between the observed genotypes and did not compensate the loss of *Ormdl3* by upregulation of *Ormdl1* or *Ormdl2*. In addition, mRNA expression of *Ormdl3* remained unaffected in lamina propria cells of *Ormdl3*^{ΔIEC} mice. Interestingly, small intestine and colon tissue of the wild-type mouse revealed a higher *Ormdl3* mRNA expression level in lamina propria cells than in IECs.

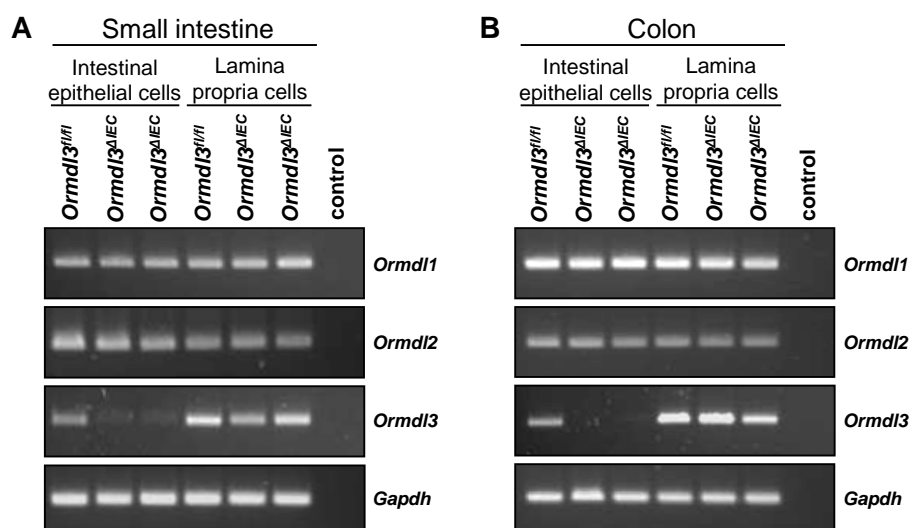


Fig. 3.36: mRNA expression levels of *Ormdl* homologues in *Ormdl3*^{ΔIEC} and wild-type mice.

Intestinal epithelial and lamina propria cells were isolated from small intestine (A) and colon (B) tissues of one *Ormdl3*^{fl/fl} mouse and two *Ormdl3*^{ΔIEC} littermate mice. Total mRNA was isolated and expression patterns of *Ormdl1*, *Ormdl2* and *Ormdl3* were assessed by semi-quantitative endpoint PCR. Water was used as control. *Gapdh* mRNA expression served as an internal control for the applied cDNA amount.

Characterization of *Ormdl3*^{ΔIEC} mice also comprised the breeding behavior and physical appearance. These mice showed normal longevity and fertility. No overt behavioral or physical abnormalities were observed. Body weights (*Ormdl3*^{fl/fl} 25.44 ± 0.42 g; *Ormdl3*^{ΔIEC} 25.21 ± 0.51 g; *n* = 15 each) were inconspicuous.

Histological analysis of kidney and colon tissues was performed for further assessment of *Ormdl3*^{ΔIEC} mice. Kidney tissues were additionally investigated, because beside the mainly describes expression of *villin 1* in intestinal epithelial cells, *villin 1* was also found in cells of the renal proximal tubulus (171). Tissues of 10 weeks old male mice were stained with hematoxylin and eosin. No obvious differences in histological appearance of all observed tissues were found between *Ormdl3*^{ΔIEC} mice and their wild-type littermates (Fig. 3.37).

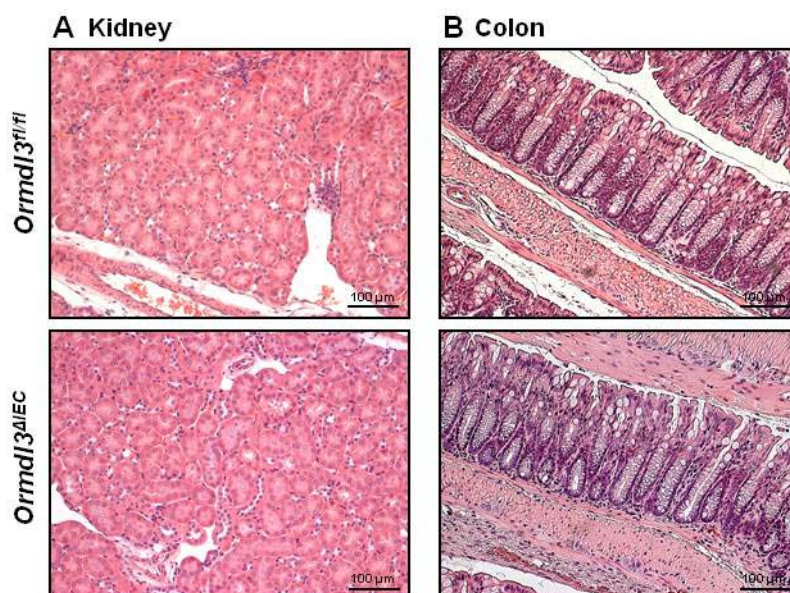


Fig. 3.37: HE stainings of kidney and colon tissues of wild-type and *Ormdl3*^{ΔIEC} mice.

Paraffin-embedded sections (3.5 μm) of formalin-fixed kidney (A) and colon (C) tissues were stained with hematoxylin and eosin and visualized at 200x magnification. Scale bars represent 100 μm.

3.5.2 *Ormdl3*^{ΔIEC} are less susceptible to chronic DSS-induced colitis

Ormdl3^{ΔIEC} mice were challenged with three cycles of DSS in their drinking water to assess the effect of *Ormdl3* deletion in IECs during chronic colitis. In each cycle mice were treated with 1.5 % DSS in their drinking water for five days, followed by five days consumption of normal drinking water. After the first cycle of DSS treatment, body weight of wild-type and *Ormdl3*^{ΔIEC} mice reduced similarly (Fig. 3.38). However, *Ormdl3*^{ΔIEC} mice gained faster weight than their wild-type littermates during the first regeneration phase. This difference in body weight remained during the second cycle of DSS administration. The second regeneration phase revealed again a faster increase in body weight of

Ormdl3^{ΔIEC} mice compared to their wild-type littermates. The faster recovery of *Ormdl3^{ΔIEC}* mice led to a significantly higher body weight during the third cycle of DSS treatment. Surprisingly though, the third DSS administration was less effective with just little body weight loss for both genotypes. At the end of the experiment, *Ormdl3^{ΔIEC}* mice showed slightly higher body weight than wild-type mice, indicating that *Ormdl3^{ΔIEC}* mice tend to be less susceptible to a DSS-induced chronic colitis.

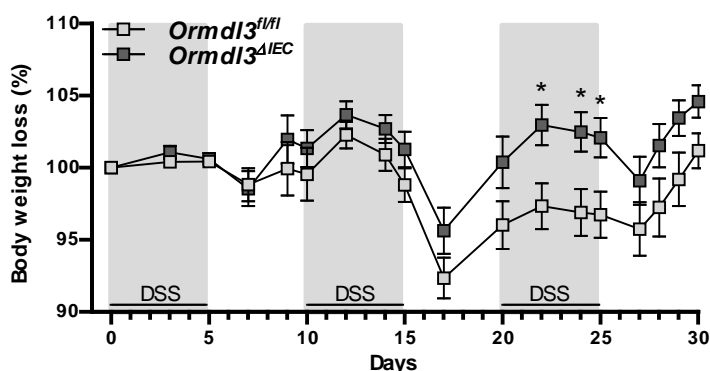


Fig. 3.38: Body weight assessment of *Ormdl3^{ΔIEC}* mice during chronic DSS-induced colitis.

Chronic colitis was induced by three cycles of 1.5 % DSS treatment for five days, followed by administration of normal drinking water for five days. Body weight changes were calculated for each mouse as percentage of initial body weight on day zero. Cohorts consisted of 15 male mice per genotype. Two-tailed unpaired Student's *t*-test was performed daily for statistical analysis. Data represents means \pm SEM.

Colon length and spleen weight were determined to evaluate the disease severity at the end of the chronic colitis (Fig. 3.39A). Shortening of the colon, which has been identified as an indicator of colitis (199), were observed in a similar manner for both DSS-treated genotypes. Additionally, DSS-induced chronic colitis is characterized by increased spleen weights (199). This extraintestinal manifestation was equally pronounced in *Ormdl3^{ΔIEC}* mice and wild-type mice (Fig. 3.39B).

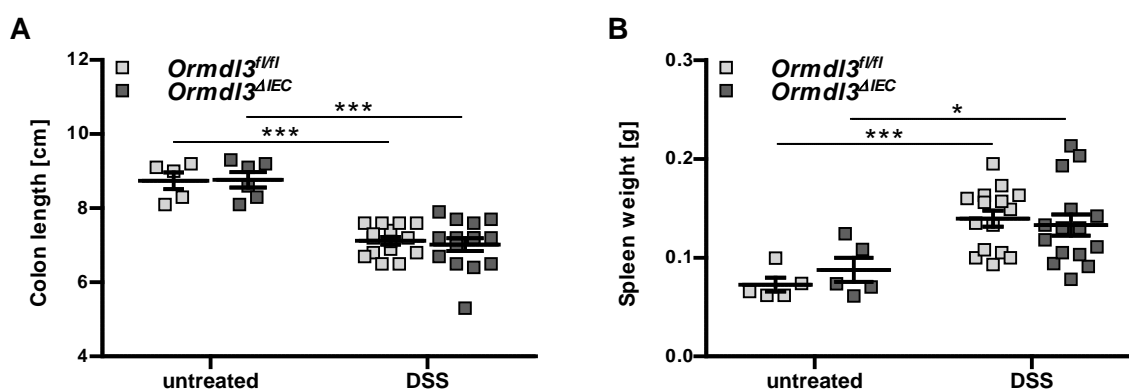


Fig. 3.39: Colon length and spleen weight in *Ormdl3^{ΔIEC}* and wild-type mice during chronic colitis.

Colon length (A) and spleen weight (B) of untreated ($n=5$ of each genotype) and DSS-treated mice ($n=15$ of each genotype) were determined. Two-tailed unpaired Student's *t*-test was performed for statistical analysis. Data represents means \pm SEM.

DSS-induced colitis affects mostly the distal colon (191). For this reason, a more detailed investigation of distal colon tissues was performed by histological analysis using hematoxylin and eosin staining. Histological score analysis was performed fully blinded based on the severity of inflammation, ulceration and crypt damage (as explained in chapter 2.4.11). DSS-treated colon tissues of *Ormdl3*^{ΔIEC} mice revealed significantly lower histological scores than *Ormdl3*^{fl/fl} mice (Fig. 3.40A), indicating less affected colon tissues during DSS-induced colitis. Histological sections of an exemplary littermate pair demonstrates a more intense infiltrations of immune cells and crypt disorder in the colon of *Ormdl3*^{fl/fl} mice compared to *Ormdl3*^{ΔIEC} mice (Fig. 3.40B).

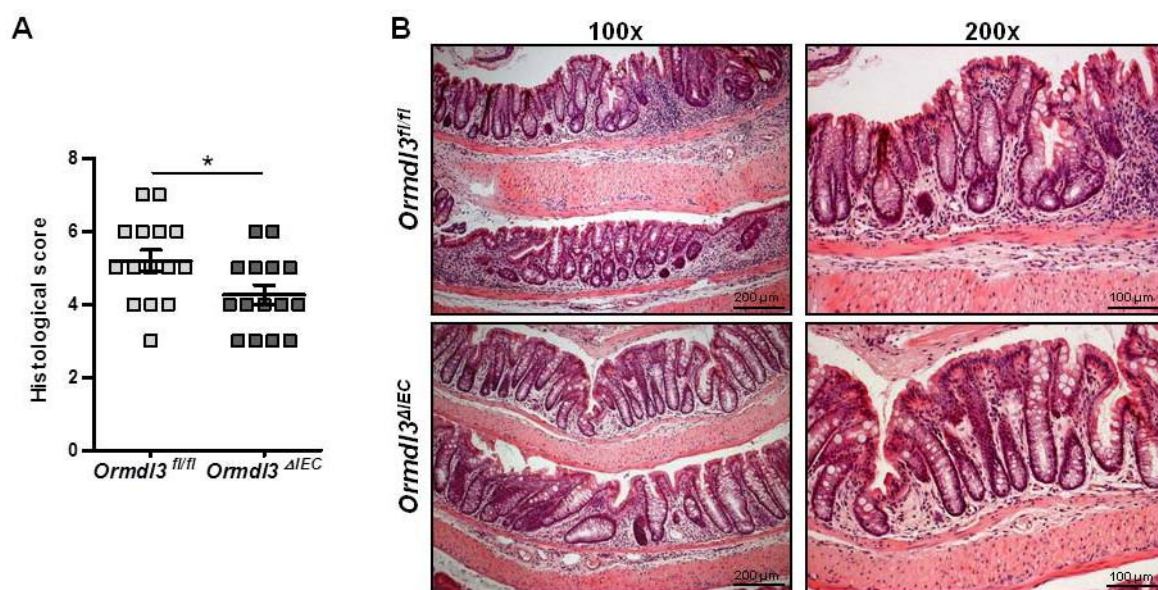


Fig. 3.40: Histological scores and HE stainings of *Ormdl3*^{ΔIEC} and *Ormdl3*^{fl/fl} mice after DSS treatment. Paraffin-embedded sections (3.5 μm) of formalin-fixed colon tissues were stained with hematoxylin and eosin and visualized at 100x and 200x magnification. (A) The histological score, a combined score of crypt damage, severity of inflammation and ulceration, was evaluated in a blinded manner. Cohorts consisted of 15 male mice per genotype. Two-tailed unpaired Student's *t*-test was performed for statistical analysis. Data represents means ± SEM. (B) Distal colon tissues of a littermate pair are exemplary shown. Scale bars represent 200 μm and 100 μm in the 100x and 200x magnifications, respectively.

Due to significant differences in histological analysis between *Ormdl3*^{ΔIEC} and their *Ormdl3*^{fl/fl} littermates, further investigation was performed. Therefore, serum cytokine concentrations were determined by Bio-Plex Pro™ Mouse Cytokine immunoassay. Typically, during chronic DSS-induced colitis the disease severity correlates positively with increased serum concentrations of IL-1β, IL-6, TNFα, CXCL1, IFNγ and IL-10 (200). IL-6 tends to be less secreted into the serum of *Ormdl3*^{ΔIEC} mice compared to their wild-type littermates (Fig. 3.41B). All other investigated serum cytokine concentrations were comparable between *Ormdl3*^{ΔIEC} and *Ormdl3*^{fl/fl} mice (Fig. 3.41).

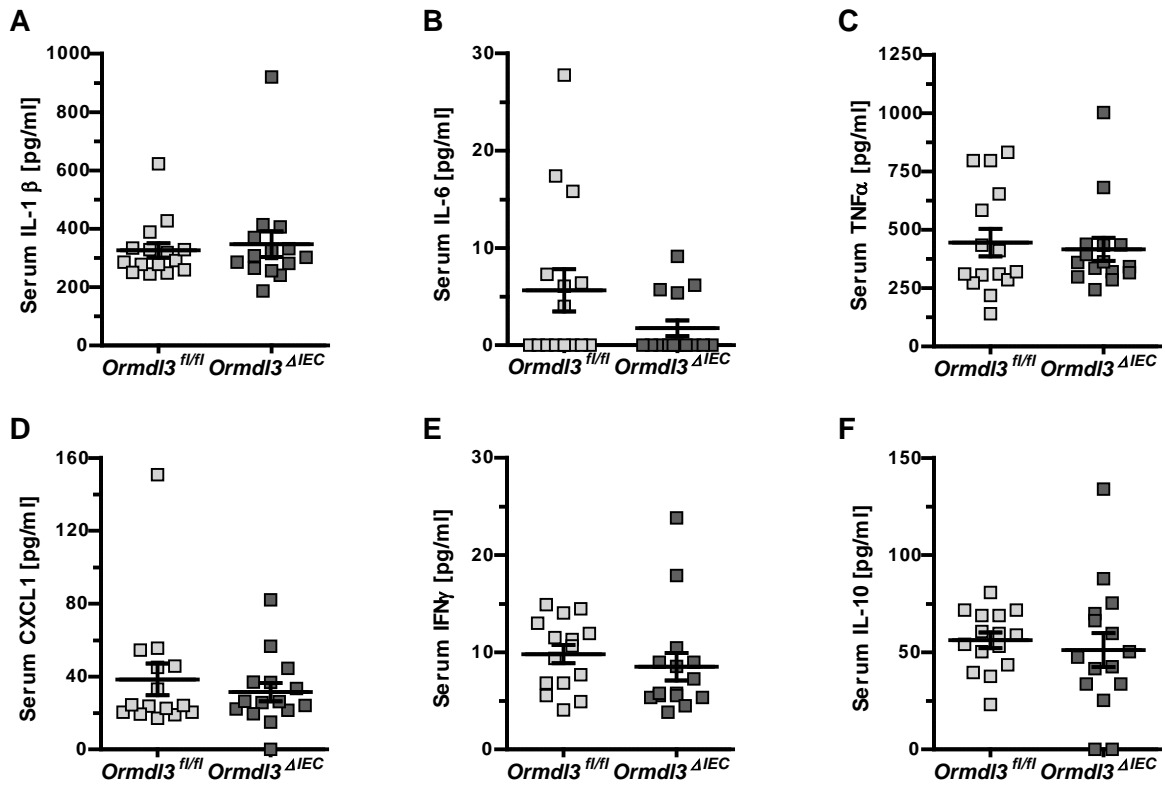


Fig. 3.41: DSS-induced cytokine secretion in *Ormdl3^{ΔIEC}* and *Ormdl3^{fl/fl}* mice.

Cytokine concentrations in the sera of *Ormdl3^{ΔIEC}* and *Ormdl3^{fl/fl}* mice were determined by Bio-Plex Pro™ Mouse Cytokine immunoassay after three cycles of DSS administration, where each cycle composed five days consumption of drinking water containing 1.5 % DSS followed by five days consumption of normal drinking water. Cohorts consisted of fifteen male mice per genotype. Two-tailed unpaired Student's *t*-test was performed for statistical analysis. Data represents means \pm SEM.

3.6 Characterization of *Ormdl1*^{-/-} mice

Besides ORMDL3, also ORMDL1 showed significant *in vitro* effects on the three pathways of the UPR. Due to these observed effects and the high homology to *Ormdl3*, *Ormdl1*-deficient mice were assessed under basal conditions as well as upon induction of DSS-induced colitis.

3.6.1 Basal phenotype of *Ormdl1*^{-/-} mice

Deletion of *Ormdl1* was validated by genotyping (as described in chapter 2.4.6). Levels of mRNA of all three *Ormdl* homologues were investigated by semi-quantitative endpoint PCR. Liver as well as colon samples of *Ormdl1*^{-/-} and their wild-type littermates were subjected to mRNA expression analysis. In contrast to *Ormdl3*^{-/-} mice, *Ormdl1*^{-/-} mice were generated by deleting only exon two on which the start codon is located. For that reason, the deletion of the first two and the last two exons were investigated by semi-quantitative endpoint PCR. Investigations of exon one and two revealed no transcript levels, confirming the deletion of the start codon (Fig. 3.42). However, mRNA of exon three and four was still expressed. The deletion of exon two of *Ormdl1* was not compensated by an upregulation of *Ormdl2* or *Ormdl3* mRNA expression levels.

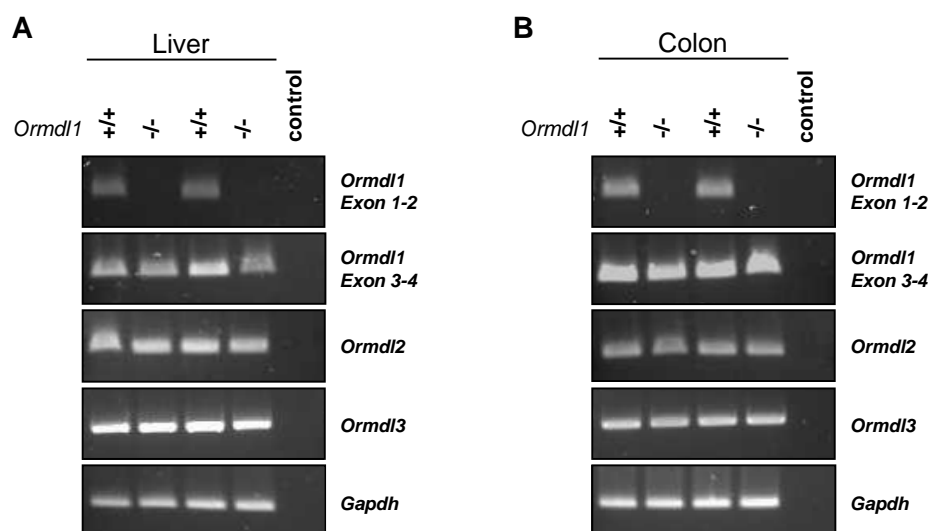


Fig. 3.42: mRNA expression levels of *Ormdl* homologues in *Ormdl1*^{-/-} mice.

The mRNA expression patterns of *Ormdl1*, *Ormdl2* and *Ormdl3* mRNA in liver (A) and colon (B) tissues from two *Ormdl1*^{+/+} and *Ormdl1*^{-/-} littermate pairs were assessed by endpoint PCR. Water was used as control. *Gapdh* mRNA expression served as an internal control for the applied cDNA amount.

Additionally, levels of all three ORMDL proteins in liver and colon tissues were investigated by immunoblotting (Fig. 3.43). Total protein levels of ORMDL1, ORMDL2 and ORMDL3 showed no markedly differences in the examined tissues of *Ormdl1*^{-/-} mice.

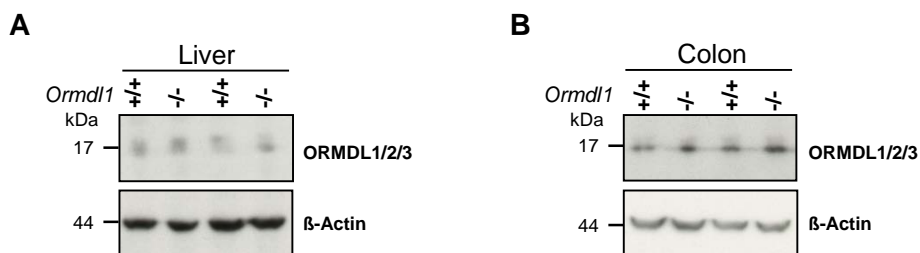


Fig. 3.43: Protein levels of ORMDL1, ORMDL2 and ORMDL3 in *Ormdl1*^{-/-} and wild-type mice.

Total cell lysates of liver (A) and colon (B) tissues from two *Ormdl1*^{+/+} and *Ormdl1*^{-/-} littermate pairs were resolved on a SDS-PAGE and analyzed by immunoblotting using antibodies against ORMDL1/2/3 or β -Actin as a loading control.

Basal phenotyping revealed that *Ormdl1* deficiency in mice did not affect lifespan or fertility. Physical appearance and body weight of ten weeks old mice (*Ormdl1*^{+/+} 25.92 \pm 0.50 g; *Ormdl1*^{-/-} 26.16 \pm 0.23 g; $n = 9$ each) were inconspicuous. Behavioral abnormalities were not detected.

Due to the high amino acid identity of ORMDL1 and ORMDL3 and the association of ORMDL3 with IBD, ileum and colon tissues of *Ormdl1*^{-/-} mice were examined by histological analysis (Fig. 3.44). The probed tissues of *Ormdl1*^{-/-} and wild-type mice showed similar morphological appearances and no genotype-specific differences.

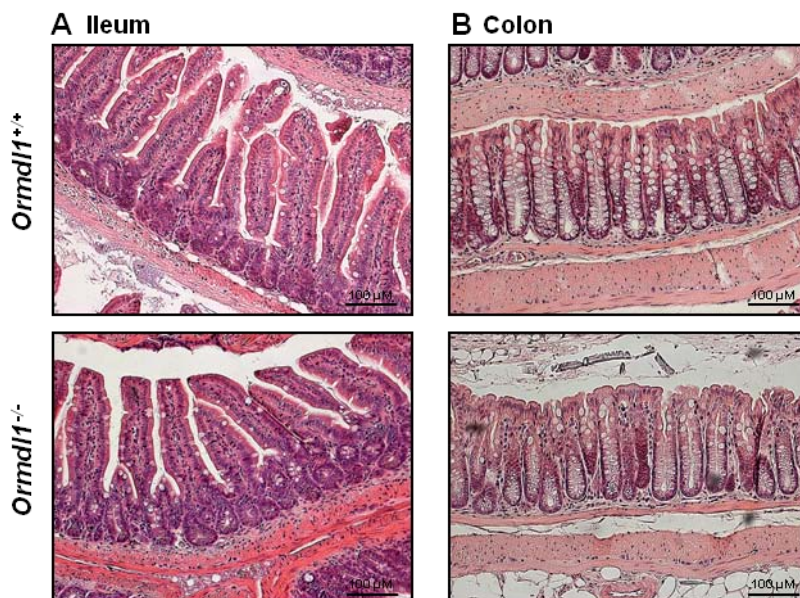


Fig. 3.44: HE staining of ileum and colon tissues of wild-type and *Ormdl1*^{-/-} mice.

Paraffin-embedded sections (3.5 μ m) of formalin-fixed ileum (A) and colon (B) tissues were stained with hematoxylin and eosin and visualized at 200x magnification. Scale bars represent 100 μ m.

3.6.2 *Ormdl1* deficiency causes no significant differences in acute DSS-induced colitis

Ormdl1-deficient mice were subjected to an acute DSS-induced colitis to investigate the effect of *Ormdl1* deficiency during intestinal inflammation. The acute colitis was induced by providing mice with drinking water containing 2.5 % DSS. During this phase, no significant difference in body weight change occurred between *Ormdl1*^{-/-} mice and their wild-type mice (Fig. 3.45). After five days of DSS administration, the DSS containing water was replaced by normal drinking water to facilitate the regeneration phase. During this second phase, *Ormdl1*^{-/-} mice started to recover on day eight, whereas the body weight of their wild-type littermates further decreased. However, the observed differences in body weight changes were not significant. This experiment had to be terminated on day nine, because three wild-type mice reached the critical body weight.

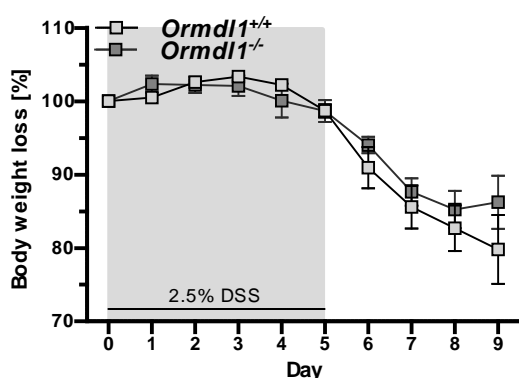


Fig. 3.45: Comparable body weight loss in *Ormdl1*^{-/-} and wild-type mice during DSS-induced colitis.

Acute DSS-colitis in *Ormdl1*^{-/-} and wild-type littermate mice was induced by 2.5 % DSS in drinking water for five days, followed by normal drinking water for four additional days. Body weights were monitored daily and the changes were calculated for each mouse as a percentage of initial body weight on day zero. Cohorts contained three *Ormdl1*^{-/-} or four wild-type mice. Two-tailed unpaired Student's *t*-test was performed for statistical analysis. Data represents means \pm SEM.

In order to assess the severity of the acute colitis, typically affected organs such as colon, liver and spleen were investigated in more detail. Shortening of colon length is widely used as a parameter to reflect DSS-induced colitis in mice, which was observed in DSS-treated *Ormdl1*^{-/-} as well as wild-type mice (Fig. 3.46A). However, wild-type mice revealed larger reductions in colon length than *Ormdl1*^{-/-} mice, indicating less intestinal inflammation in the knockout mice. By contrast, oral DSS administration induced a greater increase in spleen weight of *Ormdl1*^{-/-} mice compared to wild-type mice (Fig. 3.46B). This phenomenon of enlarged spleens is known to correlate with the progress of inflammation (199). Liver weights remained similar in both genotypes treated with DSS (*Ormdl1*^{+/+} 1.008 \pm 0.057 g; *Ormdl1*^{-/-} 1.081 \pm 0.120 g).

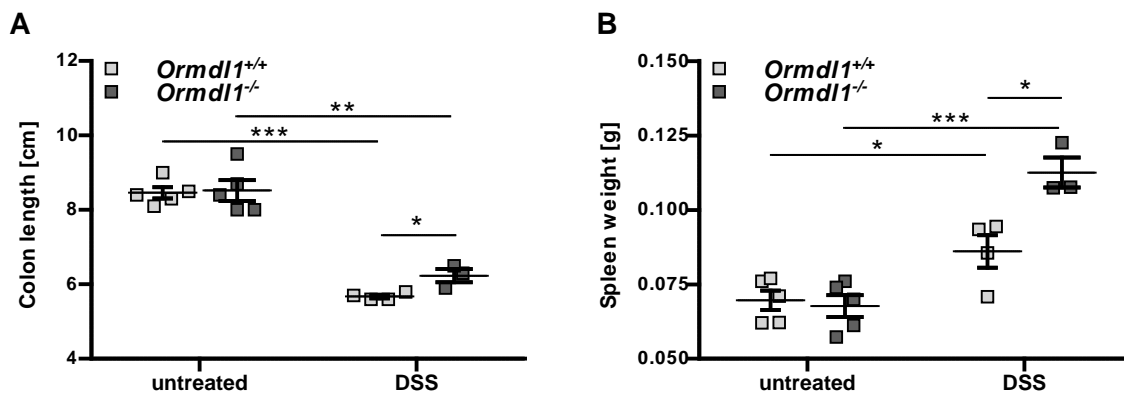


Fig. 3.46: Colon length and spleen weight of *Ormdl1*^{-/-} mice after acute DSS-induced colitis.

Acute colitis was induced by oral administration of 2.5 % DSS for five days followed by four days of normal drinking water. Colon length (A) and the spleen weight (B) of untreated ($n=5$ of each genotype) and DSS-treated mice (*Ormdl1*^{+/+} $n=4$; *Ormdl1*^{-/-} $n=3$) were determined. Two-tailed unpaired Student's *t*-test was performed for statistical analysis. Data represents means \pm SEM.

Histological analysis of DSS-treated colon tissues of *Ormdl1*^{-/-} and their wild-type littermates revealed similar tissue damages with comparable histological scores (Fig. 3.47). Colon tissues of both genotypes showed similar manifestations of immune cells infiltration, partial epithelial loss and ulceration of crypts.

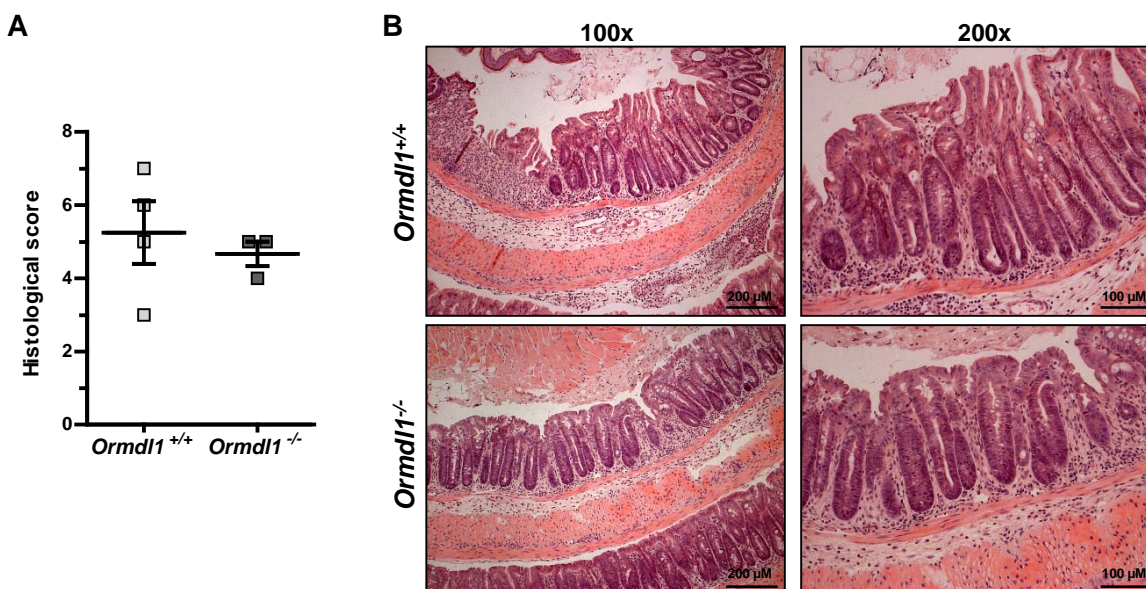


Fig. 3.47: Histological scores and HE stainings of *Ormdl1*^{-/-} and *Ormdl1*^{+/+} mice after DSS treatment.

Ormdl1^{-/-} and *Ormdl1*^{+/+} mice were treated with 2.5 % DSS in drinking water for five days followed by normal drinking water for additional four days. Paraffin-embedded sections (3.5 μ m) of formalin-fixed colon tissues were stained with hematoxylin and eosin and visualized at 100x and 200x magnification. (A) The histological score was evaluated in a blinded manner. Cohorts consisted of four wild-type and three *Ormdl1*^{-/-} mice. Two-tailed unpaired Student's *t*-test was performed for statistical analysis. Data represents means \pm SEM. (B) Distal colon tissues of a littermate pair are exemplary shown. The scale bars represent 200 μ m and 100 μ m in the 100x and 200x magnifications, respectively.

4 Discussion

IBD, with its two most common forms CD and UC, is characterized by chronic or recurring immune activation and inflammation of the gastrointestinal tract. Although recent approaches increased the knowledge on genetic background and, thus, etiology of IBD, the exact functional effects of most genetic risk loci are yet unknown. Among those risk loci is *ORMDL3* (50,51). Even though *ORMDL3* was identified as one of the strongest known eQTL for CD (137), the causative role and mechanism of *ORMDL3* in the pathogenesis of IBD is unclear. Nevertheless, recent publications found *ORMDL* proteins to be involved in the regulation of ER stress response (146,149) and since *Xbp1^{ΔIEC}* mice suffer from ER stress and display spontaneous enteritis (51), the hypothesis at the begin of this study was that *ORMDL* proteins may also regulate ER stress-associated intestinal inflammation. This study investigates for the first time effects of *ORMDL* proteins on all three UPR branches. Additionally, this study comprises the first mouse models to analyze the *in vivo* function of *ORMDL* proteins during chemical-induced ER stress and colitis.

4.1 Tissue-specific expression patterns of *ORMDL* homologues

Approximately a decade after the first description of the three human *ORMDL* proteins (135), their function remains still largely unknown (163). Investigation of the expression pattern is often used to suggest functional differences of a gene in individual tissues (201). This study reveals that human and murine *ORMDL* homologues are expressed in all examined tissues under baseline conditions (Fig. 3.1), suggesting that *ORMDL* proteins exert their function in various tissues. However, mRNA expression levels of the three *ORMDL* homologues point out some tissue-specific differences. In contrast to unaltered *ORMDL1* mRNA levels, *ORMDL2* and *ORMDL3* mRNA levels varied throughout the investigated tissues, suggesting a more pronounced tissue-specific function of *ORMDL2* and *ORMDL3* than *ORMDL1*. Interestingly, the highest level of the human *ORMDL3* mRNA was detected in liver, spleen and pancreas, which may indicate an important role of *ORMDL3* in highly secretory and immune relevant cells. Similar to *ORMDL* proteins, also other UPR members had been described to be differently expressed in various tissues, indicating tissue and cell type specialization of the UPR, which is poorly understood so far (64).

4.2 ER stress induces a tissue-specific expression pattern of ORMDL proteins

Typically, proteins involved in the UPR, such as CHOP and GRP94, are upregulated during ER stress conditions (202). Also ORMDL protein levels are elevated in RAW 264.7 macrophage cells, primary macrophages and primary murine splenocytes upon ER stress induction (Fig. 3.2). In accordance with these findings, Miller *et al.* showed ER stress-induced upregulation of *ORMDL3* mRNA expression levels in RAW 246.7 macrophage cells and A549 lung epithelial cells (149). This upregulation supports the hypothesis that ORMDL proteins play a vital role in the UPR of immune relevant cells and are elevated in order to cope with ER stress. In contrast to macrophages and splenocytes, ER stress suppresses ORMDL protein levels in intestinal epithelial cells (Fig. 3.2). Although reduced ORMDL protein levels had not been described so far, unchanged *ORMDL* mRNA expression levels were observed in peripheral blood neutrophils treated with *Alternaria* allergen (149), which is known to induce ER stress (203). Taken together, ORMDL proteins seem to function in an up to now unknown cell type-specific manner during ER stress conditions.

It can be hypothesized, that tissue-specific alterations of ORMDL protein levels upon ER stress induction could be caused by different susceptibility rates of various cell types. Due to their natural environment intestinal epithelial cells are continuously challenged by many foreign stimuli, whereas bone marrow derived macrophages are not directly in contact with challenging or ER stress inducing agents. This could be a reason for the different types of replies of various cell types to ER stress-inducing reagents. However, ER stress-induced tissue-specific expression pattern of ORMDL proteins may point to functional differences of ORMDL proteins between several cell types under challenging conditions. Recent investigations identified cell type-specific expression patterns also for some novel UPR components, including the old astrocyte specifically induced substance (OASIS) (204) and the cAMP responsive element-binding protein (CREBH) (205). For example, *OASIS* transcript levels are upregulated in C6 glioma cells upon thapsigargin treatment, whereas in mouse embryonic fibroblasts *OASIS* transcript levels are reduced after this treatment (204). This indicates that UPR components, such as OASIS and ORMDL proteins, can be differently regulated during ER stress. Even though there is no detailed explanation for the ER stress-induced cell type-specific expression patterns, these regulations may enable specialized cells a proper ER stress response according to their needs. Altered expression levels of ORMDL proteins may also have different functions in individual tissues during pathophysiological conditions and affect the disease outcome. Importantly, this thesis demonstrates tissue-specific differences *in vivo* in *Ormdl3*-deficient

mice treated with tunicamycin or DSS to determine the impact of ER stress on liver tissue or the intestine, respectively. These experiments are discussed in chapter 4.7 and 4.8.

Interestingly, the identified risk variant of *ORMDL3* is thought to regulate its expression level as illustrated by *in vitro* experiments (136). However, in ileal and colonic biopsies of CD and UC patients no influence on *ORMDL3* expression level was observed (143). A possible explanation of unaffected mRNA expression level in IBD patients might be that *ORMDL3* is differently expressed in distinct cell types as observed in this study. For that reason, future studies are needed to investigate *ORMDL3* expression levels of IBD patients in separated cell types.

4.3 *ORMDL* proteins function as a regulator of the UPR

The UPR, with its three signaling branches, is a cellular stress response to maintain and restore the ER homeostasis after being in contact with ER stress-inducing agents or conditions. To cope with ER stress cells activate several cytoprotective pathways, which are fundamental for cell survival. However, during prolonged ER stress the aim of the UPR changes to induce apoptotic cell death. The role of *ORMDL* proteins on the three UPR branches are examined in this study. A major finding of the present work is that *ORMDL* proteins regulate all three branches of the UPR differently. Thereby, as discussed in the following chapters, *ORMDL* proteins facilitate activation of the ATF6 α and PERK pathways, but repress the IRE1 pathway.

4.3.1 *ORMDL* proteins activate the ATF6 α pathway

Under ER stress conditions the ATF6 α pathway gets activated and ATF6 α undergoes S1P- and S2P-dependent cleavage resulting in cleavage fragments with sizes of 50 to 70 and 36 kDa (206). The present study elucidates for the first time a direct effect of *ORMDL* proteins on the ATF6 α pathway and the involved cleavage events. Despite surprisingly reduced levels of p36ATF6 α in whole cell lysates (Fig. 3.4A), increased ERSE promoter activity and nuclear localization of p36ATF6 α were detected in *ORMDL3* overexpressing HEK-293 cells (Fig. 3.5). The elevated ERSE promoter activities are confirmed by a study of Miller *et al.* using A549 lung epithelial cells (149), indicating a general mechanism of *ORMDL3* activating the ERSE promoter in different cell types.

In line with an increased ERSE promoter activity, *ORMDL3* overexpression induces ATF6 α cleavage and results in elevated p50ATF6 α fragments (Fig. 3.9). In addition, *ORMDL3* affects the glycosylation status of ATF6 α FL. The glycosylation status of ATF6 α is thought to function as a sensor during ER stress conditions, such as virus infection or

starvation (207). Not properly glycosylated proteins accumulate in the ER, which induces the ERSE promoter and synthesis of ER chaperones. Interestingly, overexpression of ORMDL3 reveals unglycosylated bands for ATF6 α (Fig. 3.8A,B), which has not been described so far. However, other studies support these results of the present work by demonstrating faster transport rates of the unglycosylated form of ATF6 α to the Golgi apparatus, increased nuclear translocations of its cleavage products and elevated ERSE promoter activities (182,208). Comparable to ORMDL3 also other proteins, such as the ribosome-associated membrane protein 4 (RAMP4), were identified to control the glycosylation status of various proteins through specific interaction sequences and, as a consequence, regulate the activity of its targets (209,210). Thus, the investigated impact of ORMDL proteins on the N-linked glycosylation status of ATF6 α may function as an initial regulatory response mechanism for ATF6 α activation, which is especially important during challenging conditions in order to rapidly respond to changing environmental conditions. Future investigation should determine how ORMDL3 affects the glycosylation status of ATF6 α and whether the effect of ORMDL3 is specific for ATF6 α or whether ORMDL3 also influences the glycosylation status of other proteins with similar structures.

The impact of ORMDL3 on ATF6 α suggests that both proteins are in close spatial proximity to each other. Indeed, ATF6 α and ORMDL3 are localized in the ER (87,135) and show overlapping expression sites (Fig. 3.12). Furthermore, co-immunoprecipitation studies suggest a relevant physical interaction between ORMDL3 and ATF6 α (Fig. 3.13). This interaction may stimulate the activity and translocation of ATF6 α , comparable to the enhanced activation of ATF6 α through its interaction with Ying Yang 1 (YY1) (175). Mingqing *et al.* speculates about the co-activating function of YY1 on ATF6 α during ER stress, which could be caused by anchoring the protein complex to the ERSE or by inducing other proteins to activate ATF6 α (175). However, the interaction of ORMDL3 with ATF6 α could also cover the glycosylation sites of ATF6 α , which may impede the glycosylation. Interestingly, some protein interactions were shown to be sensitive to altered levels of glycosylation as observed for GRP94 and lectin osteosarcoma amplified 9 (OS-9) (211), which was not the case for ORMDL3 and ATF6 α , indicating a relevant physical interaction during normal as well as ER stress conditions.

In conclusion, ORMDL3 affects the ATF6 α pathway by regulating the glycosylation status of ATF6 α and thus its cleavage. This impact is most likely caused through the interaction of ORMDL3 with ATF6 α . In context of IBD, these findings suggest a supporting effect of ORMDL3 on the ATF6 α activity and its target genes, which is potentially involved in the pathogenesis of UC and CD since alterations in the ATF6 α pathway were demonstrated in the colon of IBD patients (212).

4.3.2 ORMDL proteins facilitate the PERK pathway activation

Elevated ORMDL3 protein levels also facilitate PERK pathway activation, indicated by increased ATF4 promoter activity and elevated CHOP protein level in ORMDL3 overexpressing HEK-293 cells (Fig. 3.14A,B). In line with these findings, eIF2 α phosphorylation is induced by ORMDL3, which was confirmed by a study of Cantero-Recasens *et al.* using HEK-293 cells (146). The effect of ORMDL proteins on the PERK pathway is additionally supported by siRNA-mediated *ORMDL1/2/3* knockdown approaches in the present work (Fig. 3.14C,D). In contrast to this study and the work of Cantero-Recasens *et al.* (146), Hsu *et al.* observed no alterations of p-eIF2 α levels or *CHOP* transcript levels in SV40-transformed normal airway epithelial cells treated with siRNA against *ORMDL3* (125). These inconsistent findings might be due to different investigated cell types.

The obtained results of the PERK pathway investigation suggest an *in vivo* impact of ORMDL proteins during ER stress conditions, which may influence the pathogenesis of IBD. Interestingly, also intestinal epithelial cells of IBD patients revealed elevated p-eIF2 α and CHOP levels (212,213). Taken these observations into account, increased expression levels of *ORMDL3*, as they are described for IBD patients (137), and the subsequent increase in p-eIF2 α might negatively affect the intestinal homeostasis and promote the development of intestinal inflammation.

4.3.3 ORMDL proteins reduce the activity of the IRE1 pathway

In contrast to the induction of ATF6 α and PERK, ORMDL proteins repress the IRE1 pathway, indicated by reduced *XBP1* mRNA splicing and UPRE promoter activation under baseline as well as ER stress conditions (Fig. 3.3A,B). These results are supported by studies of McGovern *et al.* using HEK-293 cells (138). However, Miller *et al.* found no obvious alterations of *XBP1* splicing in the lung epithelial cell line A549 transfected with ORMDL3 (149). These divergent results again indicate cell type-specific differences similar to those observed for the PERK pathway. Possibly endogenous ORMDL protein levels are uniquely regulated in the investigated cell types and therefore affect all three UPR pathways differently. Interestingly, differently regulated IRE1 and ATF6 α pathways were identified also during hepatitis C virus infection, which is known to induce ER stress (214). Hepatitis C virus infections suppress the IRE1 pathway to reduce ERAD, whereas the ATF6 α pathway is upregulated to stimulate protein folding (215). This example illustrates the possibility of differentially regulated UPR signaling pathways during ER stress, which was observed in this study in response to elevated ORMDL3 protein levels.

In the context of IBD, the impact of ORMDL3 on the IRE1 pathway might directly affect the intestinal homeostasis. In humans, several genetic variants within *XBP1* were identified as potential genetic risk factors for IBD and colonic tissue of IBD patients show increased levels of spliced *XBP1*, suggesting that altered *XBP1* splicing is involved in chronic intestinal inflammation (212). Thus, altered ORMDL3 levels influencing *XBP1* splicing may negatively affect the intestinal homeostasis.

4.3.4 Cross-talk events between the three UPR branches

ER stress is generally thought to induce all three branches of the UPR in parallel. However, the timing of these signaling pathways and their cross-talk events are highly dynamic mechanisms depending on the ER stress duration as well as on the type and concentration of the stimulus (63). In addition, many target genes are not exclusively induced by only one UPR branch. For example, activation of ATF6 α is not only crucial for ERSE-induced transcription of ER chaperones but also facilitates transcription of *XBP1* and *CHOP* (105). Furthermore, *in vivo* studies showed that alterations or depletions of several UPR components in murine IECs induce components of other UPR branches possibly by cross-talk events (51,130). To this end, cross-talk events enable cells to compensate the loss of a UPR component by up-regulating other pathway members. However, the complex mechanisms of cross-talk events between the UPR branches are not fully understood.

Due to the variety of molecular cross-talk events, it is difficult to determine the impact of ORMDL proteins on only one of the three UPR branches. In this study, cross-talk effects influencing ATF6 α activation are determined using ERSE promoter-mediated luciferase reporter assays in combination with siRNA-mediated knockdowns of several UPR components (Fig. 3.7). Only siRNA-mediated knockdown of *ATF6 α* results in strongly reduced ERSE promoter activities during ER stress, demonstrating a high specificity of the ERSE promoter assay. However, the ERSE activity in ORMDL3 overexpressing cells is still higher than in EGFP overexpressing cells after tunicamycin treatment, which might be due to the activation of the other two UPR branches mediated by ORMDL3. In this context, components of the PERK pathway are known to facilitate ATF6 α cleavage and thus activate the ERSE promoter (181). For example, diminished ATF6 α activation in response to ER stress was identified in murine liver tissue lacking *Perk*, which indicates that the PERK pathway also facilitates activation of the ATF6 α pathway and the ERSE promoter (181). In line with this, ORMDL3 might additionally trigger the ERSE promoter due to its inducing impact on the PERK pathway.

However, an substantial role of ATF6 α in the UPR was suggested by Wu *et al.*, showing that genes containing either ERSE or UPRE sequences in their promoters require ATF6 α binding for their full activation (94). In addition, ATF6 α was demonstrated to co-regulate the PERK pathway member CHOP (109,216), which may be the primary effect responsible for the induction of the PERK pathway by ORMDL proteins. Thus, the results of this study indicate that the regulation of the three UPR branches by ORMDL3 is a complex mechanism, which allows a flexible ER stress response with cross-talk events depending on the type, duration and strength of the stimulus. For further investigation it would be of great interest to clearly identify the mode of action of these cross-talk events between the three UPR branches mediated by ORMDL proteins. This would help to explore the functional mechanism of ORMDL proteins in a complex multicellular system like the human body.

4.3.5 Proposed mechanisms of ORMDL3 on the UPR pathways

Summarizing the *in vitro* results of this study, ORMDL proteins regulate the three UPR branches differently (Fig. 1.1). Elevated levels of ORMDL3 facilitate the activation of the ATF6 α and the PERK pathways, but repress the IRE1 pathway.

The most distinct impact of ORMDL3 was observed on the ATF6 α pathway. ORMDL3 interacts with ATF6 α and suppresses the glycosylation of the full length form of ATF6 α . This unglycosylated form of ATF6 α exhibits faster transport rates to the Golgi apparatus, increased cleavage rates and, as a consequence, triggers the ERSE promoter activity. The induced ATF6 α cleavage by ORMDL3 influences also directly CHOP protein levels with no need of affecting the phosphorylation of eIF2 α . Independently of its impact on ATF6 α , ORMDL3 is capable to facilitate the phosphorylation of eIF2 α and the activation of the ATF4 promoter. In contrast to that, ORMDL3 suppresses the IRE1 pathway, which is demonstrated by reduced mRNA splicing rates of *XBP1* and diminished UPRE promoter activities as a result of elevated ORMDL3 levels.

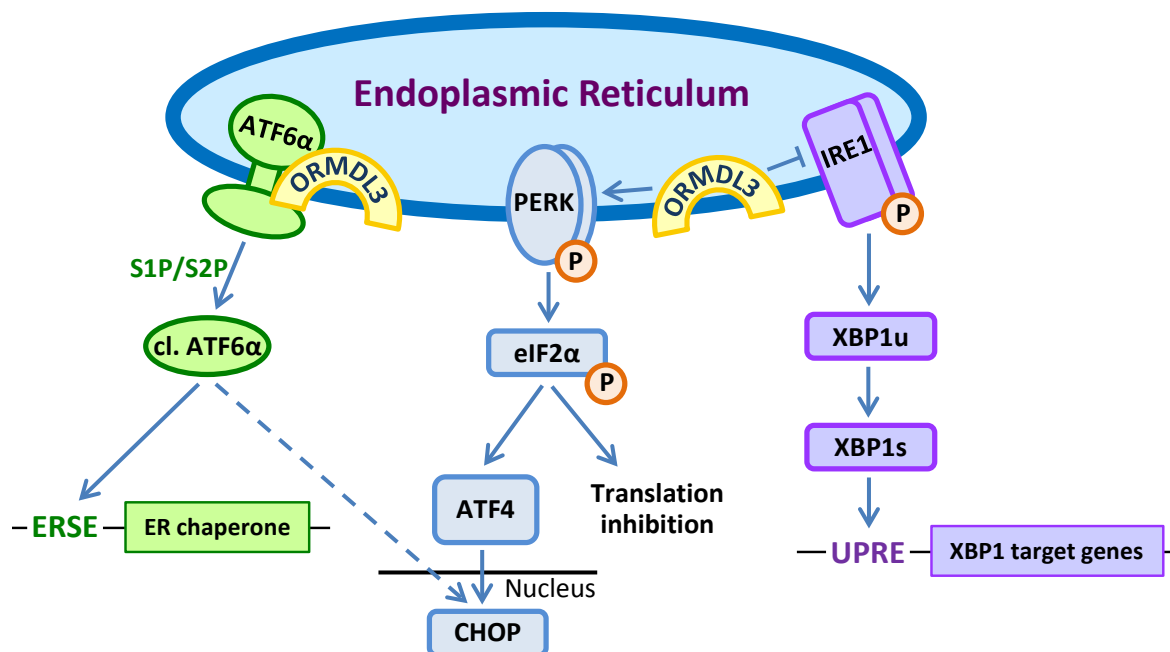


Fig. 4.1: Proposed mechanisms of ORMDL3 on the UPR pathways.
See text for detailed explanations.

4.4 Embryonic development is unaffected by ablation of either *Ormdl1* or *Ormdl3*

The UPR plays a crucial role during embryonic and postnatal development. Especially during embryonic development many UPR mediators are indispensable. Complete deletion of either the UPR sensor IRE1 α (encoded by *Ern1*) or its target gene *Xbp1* results in embryonic lethality in mice at day 12.5 (217) or day 14.5 of gestation (218), respectively. Also the knockout of the major ER chaperone *Grp78* in mice leads to lethality prior embryonic day 7.5 (219). Furthermore, genomic excision of *Grp94*, which is an important target gene of ATF6 α (65), induces embryonic lethality in mice as early as on day 7 of gestation (220). Although GRP94 is mainly induced by ATF6 α (85), *Atf6 α* -deficient mice develop normally. Mice with a deletion of the other closely related ATF6 isoform, *Atf6 β* , disclosed no abnormalities (94). Even though the transcriptional activity of ATF6 α is substantially higher than that of ATF6 β , both isoforms are required for proper adjustment of ER chaperones (221). For that reason, genetic depletion of both, *Atf6 α* and *Atf6 β* , causes embryonic lethality in mice, indicating essential overlapping functions during early stages of development (85). Interestingly, some members of the PERK pathway, such as PERK itself (222), CHOP (223) and GADD34 (224), are expendable during embryonic development. However, mice with a deletion of *Atf4*, another member of the PERK pathway, are partial lethal during embryonic development (225,226). These different outcomes in the embryonic development of components of the PERK branch suggest complex cross-talk events. Although there is a clear correlation between the UPR

and ORMDL proteins, the development of any *Ormdl* knockout in mice has never been elucidated. Interestingly, similar to *Atf6 α* ^{-/-} mice and to mouse models with a deletion of genes involved in the PERK pathway, *Ormdl1*^{-/-} and *Ormdl3*^{-/-} mice are born at the expected Mendelian ratio. This indicates that neither ORMDL1 nor ORMDL3 alone is required for organogenesis and embryonic development, at least if the remaining ORMDL homologues are intact. The double or triple knockout of *Ormdl* genes could affect synergistically embryonic development, as reported for the double knockout of the *Atf6* homologues, *Atf6 α* and *Atf6 β* (85). Nevertheless, it is hard to speculate about the phenotype of double or triple knockout *Ormdl* mice, because at least partial functional redundancies of the ORMDL homologues are conceivable due to the shown phenotype rescue using the human ORMDL3 in *ORM1/2* double knockout yeast (135). Thus, the effect of a double or triple knockout of *Ormdl* genes in regard to embryonic development and organogenesis in mammals remains to be elucidated, and is subject of ongoing investigation.

4.5 ORMDL3 modulates body growth by affecting IGF1 production

The present study identifies for the first time that genetic deletion of *Ormdl3* causes postnatal growth retardation in mice (Fig. 3.17) without affecting organ development (Fig. 3.20, Fig. 3.21). Postnatal growth in mammals is mainly regulated by the coordinated action of GH and IGF1 (227). IGF1 expression levels are significantly reduced in muscle tissues of 4 weeks old *Ormdl3*^{-/-} mice (Fig. 3.19B), whereas circulating GH levels are just slightly diminished (Fig. 3.18). This may indicate that the main regulatory effect of ORMDL3 on growth is mediated through IGF1 and takes place in the first weeks after birth, because at that early time point IGF1 is almost exclusively responsible for postnatal growth (228). The early growth deficit of *Ormdl3*^{-/-} mice continues throughout their ageing (Fig. 3.17). The hypothesis of reduced growth due to altered IGF1 production in *Ormdl3*^{-/-} mice is supported by studies showing that *Igf1*^{-/-} mice are born 35 % smaller than their wild-type littermates (229) and continue to grow with retarded rates reaching only 30 % of normal body weights (230), whereas mice deficient for GH or GH receptor grow normally during the first two weeks after birth before reaching growth retardation (228,231).

Interestingly, genetic deletions of several other UPR components also result in growth abnormalities. Especially members of the ATF6 and PERK branches, which are down-regulated in cells lacking ORMDL proteins, are fundamental for postnatal growth. For example, the ATF6 α target GRP94 is essential for local IGF1 production, which was identified by the genetic deletion of muscle GRP94 resulting in retarded postnatal body

growth caused by inhibited local IGF1 production (232,233). In addition, *Perk*^{-/-} mice exhibit neonatal growth retardation with a 50 % reduction in body weight at the age of 3 weeks, which is attributed to low IGF1 levels derived from liver tissue (234,235). Thus, these findings demonstrate a link between UPR components, body growth and altered IGF1 levels, which is also shown for ORMDL3 in the present study.

Although *Ormdl1* and *Ormdl3* have high sequence homologies, *Ormdl1*^{-/-} mice develop and grow without any abnormalities (Fig. 3.44). For that reason, ORMDL1 is thought to be expendable during developmental and growth processes. This exchangeable role of ORMDL1 may result in only slight effects of *Ormdl1* deficiency on total ORMDL protein level, whereas ablation of *Ormdl3* in mice results in a significant reduction (Fig. 3.43; Fig. 3.16). This clear impact on total ORMDL protein level may cause a more pronounced phenotype of *Ormdl3*^{-/-} mice. On the other hand, it can be speculated that the three ORMDL proteins may function differently or in a cell type-specific manner with ORMDL3 depicting a profound role in cells producing hormones responsible for body growth, such as IGF1-producing liver cells.

In contrast to the observed growth retardation in mice with an ablation of *Ormdl3*, a single knockout of one of the two ORMDL homologues *ORM1/2* in yeast is not sufficient to induce growth abnormalities (135). However, *ORM1/2*-deficient yeast are retarded in cell growth, clearly demonstrating that each of the two yeast homologues is capable to compensate the loss of the other *ORM* gene. Interestingly, IGF1 signaling exists also in yeast and may be responsible for growth abnormalities caused by *ORM1/2* deficiency. Together with the findings of the present study this may indicate that through evolutionary processes the regulation of growth processes are incorporated into the *ORMDL3* gene in particular. In summary, this study provides evidence that ORMDL3, but not ORMDL1, is required for normal postnatal growth by regulating local IGF1 production.

4.6 *Ormdl3* deficiency in mice reduces IFN γ levels and its targets

Inflammatory cytokines are of crucial importance for the intestine because they regulate the gut homeostasis during unchallenged conditions as well as during intestinal inflammation (236). Out of 23 investigated cytokines only IFN γ , TNF α and IL-12 p70 display reduced levels in the serum of unchallenged *Ormdl3*^{-/-} mice (Fig. 3.23). In addition, *Ifny* is significantly lower expressed in colon tissue of *Ormdl3*^{-/-} mice. However, spleen tissue reveal unaffected *Ifny* expression levels (Fig. 3.24), suggesting organ-specific effects of ORMDL3 on *Ifny* expression. Interestingly, ORMDL3 protein levels are also differently expressed in intestinal epithelial cells and splenocytes, giving an additionally

indication that ORMDL3 fulfills distinct functions in the colon and the spleen (Fig. 3.2). Thus, the gained results support the hypothesis of cell type-specific functions of ORMDL3, which affects *Ifny* expression.

It may be speculated that in IBD patients perturbed ORMDL3 expression could lead to changes in IFN γ levels, which in turn may facilitate inflammation or interfere with epithelial function. Especially CD is mainly driven by a chronic T helper 1 (Th1)-driven immune response leading to increased production of proinflammatory cytokines, such as IFN γ and IL-12 (237–239). Nevertheless, the functional link between ORMDL3 and IFN γ has not been investigated yet. In the murine system a substantial role of IFN γ in colitis is highlighted by the phenotype of *Ifny*^{-/-} mice, which are less susceptible to DSS-induced colitis (240). In CD patients IFN γ is abundantly produced by intestinal lamina propria cells (241). Together with the results of the present study, it can be proposed that altered *ORMDL3* expression levels in specialized immune cells may result in variations of IFN γ expression levels, which then promotes the pathogenesis of IBD.

In accordance with down-regulated *Ifny* mRNA expression in colon tissue of *Ormdl3*^{-/-} mice, also cell-surface expression levels of IFN γ targets, such as MHCI and MHCII molecules, are significantly reduced in myeloid cells isolated from the lamina propria (Fig. 3.25). MHC molecules are highly important for immune response by binding peptide fragments from extra- and intracellular pathogens and displaying them for the recognition by CD4⁺ and CD8⁺ T cells, respectively (242). Especially epithelial MHCII cell-surface expression levels are highly upregulated in CD patients (243,244). This may indicate that ablation of *Ormdl3* and the resulting reduced cell-surface expression of MHC molecules on CD11b⁺ lamina propria cells function as a protective mechanism for the intestinal homeostasis. Future investigations should explore whether the impact ORMDL3 on MHC molecules is a primary effect or a secondary effect through the regulation of IFN γ expression levels.

Interestingly, ORMDL3 is associated with both IBD and asthma (136,245). Asthma and UC are described to be mainly driven by Th2 cells, which are present during acute exacerbations of the disease and induce the expression of Th2-type cytokines, such as IL-4, IL-5 and IL-13 (246,247). The presence of the same risk factor in Th1 (CD) and Th2 driven disorders is puzzling from classical immunology textbook knowledge. Th1 cells secrete IFN γ , which is crucial for the resolution of allergy-related immunopathologies (248). However, UC patients respond to anti-TNF treatment, which blocks a hallmark Th1 cytokine. In addition, IFN γ -producing Th1 cells were identified in airways of asthmatics (248) and similar to CD patients also acute asthma patients possess increased serum

level of IFN γ (249). Furthermore, lung-targeted overexpression of IFN γ in the airway enhances airway hyperresponsiveness and non-eosinophilic inflammation, while *Ifn γ ^{-/-}* mice are protected from allergen-induced asthma (250). The findings demonstrate effects of IFN γ in both IBD and asthma patients, which may be mediated by ORMDL3.

4.7 The role of ORMDL1 and ORMDL3 during intestinal inflammation

4.7.1 Deletion of *Ormdl1* or *Ormdl3* leaves intestinal homeostasis unaffected

Under physiological conditions, *Ormdl1^{-/-}* and *Ormdl3^{-/-}* mice reveal no signs of spontaneous enteritis or colitis, indicated by inconspicuous histological scores (Fig. 3.21, Fig. 3.44) and unchanged serum cytokine concentrations (Fig. 3.23). The normal phenotype of these mice indicate that either *Ormdl1* or *Ormdl3* are expendable for the homeostasis of the intestine, which might be due to compensatory effects of the other two remaining ORMDL homologues. In line with this hypothesis, the total ORMDL protein level is unchanged in the liver and colon of *Ormdl1*-deficient mice compared to their wild-type littermates (Fig. 3.43). In contrast, the overall ORMDL protein level is reduced in *Ormdl3^{-/-}* mice (Fig. 3.16). However, upon DSS treatment the ORMDL protein level increases in the colon of *Ormdl3^{-/-}* mice suggesting a compensatory regulation of the remaining two ORMDL homologues under pathological conditions (Fig. 3.31). Similar compensatory effects occur in yeast, where *ORM1* or *ORM2* single knockout strains are equally affected by toxic compounds as the wild-type strain, while double knockout mutants are highly sensitive to these agents (135,147). Interestingly, the human ORMDL3 is able to rescue the phenotype of *ORM1/2*-deficient yeast (135), indicating a conserved function even throughout different species. This compensatory effect was also demonstrated *in vitro* using mammalian cell culture, showing that the single knockdown of *ORMDL3* is not sufficient to regulate serine palmitoyltransferase (SPT) activity, whereas the knockdown of all three *ORMDL* homologues affects the SPT activity (251,252). These findings clearly illustrate that the altered function of one *ORMDL* gene can usually be overcome by the presence of the two remaining ORMDL homologues, which may protect *Ormdl1^{-/-}* and *Ormdl3^{-/-}* mice from spontaneous intestinal inflammation. In addition, also genetic deletion of other UPR components, such as *Atf6 α* or *Chop*, did not result in intestinal inflammation (127,131), indicating that a deletion of one of those UPR components is expendable and the remaining UPR components are sufficient to maintain the intestinal homeostasis under physiological conditions, which may also be the case for *Ormdl1^{-/-}* and *Ormdl3^{-/-}* mice.

4.7.2 Mice lacking *Ormdl3* are more susceptible to an acute DSS-induced colitis

An intact UPR is important for the intestinal homeostasis, especially under challenging conditions (127). Due to the ascertained impact of ORMDL proteins on the UPR, the function of ORMDL1 and ORMDL3 during intestinal inflammation was investigated by challenging *Ormdl1*^{-/-} and *Ormdl3*^{-/-} mice with DSS to induce an acute colitis. DSS treatment initiates inflammatory response in the gut, which in part resembles human IBD and is a broadly applied model (253). The common opinion of the mode of action of DSS is that oral administration of this agent is toxic to colonic epithelial cells and causes defects in the barrier integrity (194). In addition, DSS was identified to induce ER stress in IECs (127). During DSS treatment, mice with a genetic deletion of *Ormdl1* reveal a similar course of disease as their wild-type littermates, as suggested by comparable amounts of body weight loss and similar histological scores (Fig. 3.45, Fig. 3.47). Thus, the outcome of this treatment indicates that ORMDL1 has no marked impact on the intestinal homeostasis during DSS-induced intestinal inflammation.

In contrast to the results obtained in *Ormdl1*^{-/-} mice, *Ormdl3*^{-/-} mice are more susceptible to acute DSS-induced colitis, as demonstrated by more pronounced body weight loss and increased DAI (Fig. 3.26). Additionally, DSS-treated *Ormdl3*^{-/-} mice disclose significantly elevated serum levels of IL-1 β (Fig. 3.29), which is one of the main drivers of inflammation in IBD (254,255). Further signs indicate increased sensitivity of *Ormdl3*^{-/-} mice to DSS-induced colitis, including increased histological scores in the colon and significantly reduced liver weight (Fig. 3.28, Fig. 3.27B). Reduced liver weight was also identified in hamsters as a result of DSS treatments (192), which in the case of *Ormdl3*^{-/-} mice suggested a more severe disease progression of the entire organism upon DSS administration. Interestingly, also IBD patients show disorders of the hepatobiliary system, which is a relatively common extra-intestinal manifestation and is probably caused by a shared pathogenesis with IBD or due to the effect of chronic inflammation (256). In summary, the results of this study suggest that ORMDL3 is more important for the intestinal homeostasis and immune responses than ORMDL1.

For investigation of the mechanistic effect of ORMDL3 during the development of colitis, *Ormdl3*^{-/-} mice were treated with DSS for short durations of two to four days. During this treatment, colonic tissues of *Ormdl3*^{-/-} reveal higher and prolonged levels of p-eIF2 α , indicating ongoing ER stress over several days in *Ormdl3*^{-/-} mice, whereas wild-type mice are able to restore the UPR homeostasis (Fig. 3.31). Prolonged ER stress has been identified to cause cellular damage followed by barrier defects, as demonstrated in *Xbp1* ^{Δ IEC} mice (51). *Xbp1* ^{Δ IEC} mice develop spontaneous small intestine inflammation and

are more susceptible to DSS-induced colitis, which is accompanied by increased p-eIF2 α in IECs (133). Additionally, elevated p-eIF2 α was also observed in colonic tissue of IBD patients (212), which supports the hypothesis of an increased sensitivity of *Ormdl3*^{-/-} mice to DSS-induced colitis based on their upregulated colonic p-eIF2 α levels. Interestingly, increased p-eIF2 α occurs also in liver tissue of DSS-treated *Ormdl3*^{-/-} mice, whereas the hepatic p-eIF2 α level was not altered in wild-type mice (Fig. 3.31B), demonstrating that more tissues than just the colon are affected by the intestinal barrier defect. In addition, the protein level of the p-eIF2 α target CHOP is upregulated in the liver of *Ormdl3*^{-/-} mice (Fig. 3.31B). The results of the present study indicate that increased levels of p-eIF2 α and of the pro-apoptotic factor CHOP might be the reason for significantly reduced liver weight in *Ormdl3*^{-/-} mice at the end of the acute DSS colitis experiment. Interestingly, the outcome of various genetic deletions of UPR components indicate that dysregulation of the UPR deteriorates the ability to cope with intestinal inflammation upon DSS treatment (51,130,131), which may also be the case for ORMDL3. Summing up the results of the acute DSS-induced colitis experiment, molecular-biological changes in *Ormdl3*^{-/-} mice support the assumption that ORMDL3 is needed for fine-tuning of the ER stress response.

4.7.3 Deletion of *Ormdl3* in IEC has a protective effect during chronic DSS-induced colitis

ER stress in IECs functions as an originator and perpetrator of intestinal inflammation (257). *Ormdl3* ^{Δ IEC} mice with a genetic deletion of *Ormdl3* particularly in IECs were investigated due to the central role of IECs in not only providing a physical barrier against invasive intestinal pathogens, but also in maintaining the intestinal homeostasis through secretion and regulation of commensal microorganisms and the host immune response (21). The importance of IECs is underlined by studies reporting that intestinal inflammation causes ER stress especially in epithelial cells and that functional impairment of IECs might contribute to IBD (68,258). Similar to *Ormdl3*^{-/-} mice, *Ormdl3* ^{Δ IEC} mice show no apparent abnormalities under physiological conditions (Fig. 3.37). Interestingly, *Ormdl3* ^{Δ IEC} mice are less susceptible to the DSS-induced chronic colitis, indicated by less body weight loss and a faster regeneration rate, especially during the end of the second cycle and the beginning of the third cycle of DSS treatment (Fig. 3.38). However, at the end of the experiment, body weight, spleen weight and serum concentration of various cytokines are not significantly altered between the two groups (Fig. 3.39, Fig. 3.41). This is most probably owing to the low DSS concentration that resulted in only weak effects on body weight during the treatment. Nevertheless, DSS-treated *Ormdl3* ^{Δ IEC} mice disclose significantly lower histological scores than their wild-type littermates at the end of the experiment (Fig. 3.40). These findings suggest that genetic deletion of *Ormdl3* in IECs has

a protective effect during chronic intestinal inflammation, whereas genetic deletion of *Ormdl3* in all cell types revealed contrary findings during acute DSS-induced colitis (Fig. 3.26). These opposite findings may be explained by the tissue-specific function of ORMDL proteins. It will be of great interest to determine, whether mice with a knockout in cells that respond with an ORMDL induction during tunicamycin treatment (e.g. monocytes; Fig. 3.2) display a more severe phenotype during DSS treatment. Thus, further investigation with a monocyte/macrophage-specific knockout of *Ormdl3* may elucidate the function of ORMDL3 in immune relevant cells, because especially macrophages actively produce inflammatory cytokines in response to invading bacteria. However, the different responses of *Ormdl3^{ΔIEC}* and *Ormdl3^{-/-}* mice to DSS treatment may also arise from the duration, concentration and frequency of DSS administration. Interestingly, the activation of some UPR mediators, such as ATF6 α , are differently regulated during acute and chronic stress conditions (94). This suggests that the function of ORMDL3 and the disease outcome may depend also on the duration of ER stress conditions.

4.8 ORMDL3 protects from prolonged ER stress *in vivo*

The dysregulated UPR homeostasis in *Ormdl3^{-/-}* mice during intestinal inflammation indicates that ORMDL3 plays a crucial role in regulating cellular stress conditions. To further investigate the function and the mechanism of ORMDL3 during ER stress *in vivo*, *Ormdl3^{-/-}* mice were intraperitoneally injected with a single sublethal dose of the chemical ER stress inducer tunicamycin, which primarily affects the liver. All mice survived the tunicamycin challenge, demonstrating that ORMDL3 is expendable during persistent ER stress conditions at least for survival at the given tunicamycin concentration (Fig. 3.32). In contrast, deletion of *Atf6 α* , which encoded protein was found to be modulated by ORMDL3, results in high mortality rates during a comparable treatment regime (259). Although the effect of *Ormdl3* deletion is less pronounced compared to the genetic deletion of *Atf6 α* , *Ormdl3^{-/-}* mice showed similar, but attenuated, molecular-biological changes during tunicamycin treatment. Tunicamycin-treated *Ormdl3^{-/-}* mice display a mild form of acute fatty liver degeneration, which is notable by a pale liver color and an increased level of the cytosolic lipid protein marker ADRP after 48 h of treatment (Fig. 3.33). The kidney is as a secondary time-displaced affected organ and shows likewise prolonged upregulation of ADRP level (Fig. 3.34). In addition, serum level of the protective HDL cholesterol decreases significantly faster in *Ormdl3^{-/-}* mice than in wild-type mice (Fig. 3.35), which has been shown as a sign of hepatic steatosis (197). This indicates that *Ormdl3^{-/-}* mice are more susceptible to tunicamycin treatment. However, it is unclear, whether in tunicamycin-treated *Ormdl3*-deficient mice dysregulated lipid metabolism

causes UPR signaling or the other way around. Since ORMDL3 was found to interact with ATF6 α and to influence its cleavage, the resulting assumption is that the phenotype of *Ormdl3*^{-/-} mice during tunicamycin treatment is primarily caused by a dysregulated UPR, which in turn influences the cholesterol metabolism. Interestingly, genetic deletion of other UPR mediators, such as *Atf6 α* , *p58^{IPK}* or a liver-specific excision of *Ire1 α* , result in phenotypes comparable to the one seen in *Ormdl3*^{-/-} mice (260,261), demonstrating that defects in the UPR can lead to hepatic steatosis upon tunicamycin administration. In case of tunicamycin-treated *Ormdl3*^{-/-} mice, the often postulated link between ER stress and lipid metabolism could be confirmed with the present work (262).

During tunicamycin treatment, *Ormdl3*^{-/-} mice disclose dysregulated UPR signaling as expected from the *in vitro* results obtained in this study. Similar to prolonged upregulation of ADRP, also some UPR mediators, such as the pro-apoptotic factor CHOP, p-eIF2 α or spliced *Xbp1*, are prolonged upregulated in liver and kidney of tunicamycin-treated *Ormdl3*^{-/-} mice (Fig. 3.33, Fig. 3.34), reflecting ongoing ER stress and defects in the UPR signaling pathway. Comparable results of permanently elevated CHOP levels and prolonged *Xbp1* splicing were observed also in tunicamycin-treated *Atf6 α* ^{-/-} mice (94), supporting the connection of ORMDL3 and ATF6 α . In addition, also during short-term DSS treatment prolonged upregulated p-eIF2 α protein levels in liver and colon of *Ormdl3*^{-/-} mice appears (Fig. 3.34), indicating similar systemic effects during locally administrated DSS and artificial, systemic ER stress induction by tunicamycin injection. Taking this into account, the results of the present study suggest that alterations in the UPR signaling caused by *Ormdl3* deletion may modulate either liver steatosis or intestinal inflammation depending on the type and the site of action of the ER stress stimulus.

Furthermore, genetic deletion of *Ormdl3* in mice affects the glycosylation status of ATF6 α during ER stress indicated by a delayed appearance of the unglycosylated band of ATF6 α upon tunicamycin injection (Fig. 3.8, Fig. 3.33). A similar mode of action of ORMDL proteins on ATF6 α glycosylation was observed in HEK-293 cells treated with siRNA against the three *ORMDL* homologues (discussed in chapter 4.3.1). These consistent *in vitro* and *in vivo* results clearly demonstrate the impact of ORMDL3 on ATF6 α and reinforce the identified interaction of ORMDL3 and ATF6 α . Additionally, the unglycosylated band of the ATF6 α target GRP94 and the glycosylation status marker TRAP α are prolonged detectable in the liver of *Ormdl3*^{-/-} mice, indicating a general effect of ORMDL3 on the glycosylation machinery during ER stress conditions. Improper glycosylation affects not only the activity of ATF6 α , but also of GRP94 (211). Thus, the ORMDL3-dependend mechanism affecting ATF6 α glycosylation may enable fine-tuning of the ER stress response. Genetic deletion of *Ormdl3* and the resulting loss of the impact

on ATF6 α glycosylation and activation might negatively affect the rapidity of the UPR signaling, which results in an increased sensitivity of *Ormdl3*^{-/-} mice to chemically induced ER stress. Interestingly, the unglycosylated form of ATF6 α has been identified as an inducer of diseases, such as cystic fibrosis (263), indicating the importance of the impact of ORMDL3 on the glycosylation status of ATF6 α . With regard to the development of diseases, tissues of liver steatosis and IBD patients should be investigated with respect to their glycosylation status of ATF6 α and analyzed for a correlation between glycosylation and ORMDL3 levels.

In summary, the results of the present study indicate that ORMDL3 influence the UPR signaling during ER stress mainly by interacting with ATF6 α and affecting its glycosylation status, which induces the activation of this pathway by increased ATF6 α cleavage. Furthermore, ORMDL3 facilitates the PERK pathway activation and represses the IRE1 α pathway. In addition, cross-talk events between the ATF6 α and the PERK pathways are identified. Thus, from this study it can be suggested that loss of *Ormdl3* primary dysregulates UPR signaling, which secondarily might cause defective lipid homeostasis, as illustrated by e.g. altered ADRP and HDL levels. These findings lead to the speculation that the detected molecular link between ORMDL, the UPR and lipid homeostasis is of strong importance for the development and progression of several ER stress-coupled diseases, such as colitis and liver steatosis.

4.9 Future prospects

The results of the present study provide insights into the complex role of ORMDL proteins in the regulation of the UPR and their importance for the intestinal and liver homeostasis, especially during challenging conditions. Based on these findings, new open questions arise.

Deletion of genes involved in the UPR signaling pathways revealed their implication during embryonic and postnatal development. This study disclosed a negative effect of *Ormdl3* deficiency on murine body growth. However, the embryonic development is not affected by *Ormdl3* deletion, which might be due to a compensatory effect of the other remaining ORMDL homologues. To elucidate possible overlapping functions between all three ORMDL proteins, the generation of *Ormdl1/2/3*^(-/-) triple-knockout mice appears reasonable. In the case that triple-knockout mice are viable, further investigation should examine whether their organs are structurally and functionally intact. Additionally, spontaneous intestinal inflammation might occur, as seen in mice with a tamoxifen-induced deletion of the ATF6 α target gene *Grp94*. Furthermore, investigation of the phenotype of *Ormdl1/2/3*^(-/-) triple-knockout mice during challenging conditions, such as DSS-induced colitis or intraperitoneal injection of tunicamycin, could elucidate whether the ORMDL proteins have compensatory functions. In addition, these mice would also enable to examine the impact of *Ormdl1/2/3* deficiency on the ATF6 α pathway in more detail. *Ormdl1/2/3*^(-/-) triple-knockout mice may reveal whether the genetic deletion of *Atf6 α* and the lack of all ORMDL proteins result in a similar phenotype during ER stress condition, which would support the hypothesized connection of these proteins. Thus, the triple-knockout of *Ormdl1/2/3* in mice may gain the understanding of ORMDL proteins in the whole organism. However, the present study already identified the impact of ORMDL3 on the intestinal and liver homeostasis during challenging conditions, which may be transferred into humans to improve the treatment of IBD and its extra-intestinal manifestations.

Apart from this, prospective research may address the cellular and molecular mechanism of ORMDL3 during the pathogenesis of asthma, since ORMDL3 has been associated with both IBD and asthma. The question arises whether the identified effect of ORMDL3 on the intestinal homeostasis also influences lung homeostasis in mice during challenging conditions. In particular, the shown impact on the UPR gives additional insights into the function of ORMDL3, which may also improve research in the field of asthma. Thus, the present study increases the knowledge of ORMDL3 and may serve as a starting point for the development of new approaches to the treatment of chronic inflammatory diseases.

5 Summary

Unresolved and prolonged endoplasmic reticulum (ER) stress has been shown to be involved in the pathogenesis of inflammatory bowel disease (IBD). ER stress describes the condition of an excessive accumulation of unfolded or misfolded proteins in the ER that invokes an essential pathway to restore the function of the ER, termed the unfolded protein response (UPR). Especially hepatocytes and intestinal epithelial cells, including Paneth and goblet cells, strongly depend on a well-functioning UPR due to their high demand on secretory proteins. Unresolved ER stress has been found in inflamed intestinal epithelial cells and genome wide association studies identified UPR-associated genes, such as ORM1-like protein 3 (*ORMDL3*), as potential risk factors for IBD. However, the role and the functional mechanism of *ORMDL3* *in vitro* and *in vivo* with regard to the pathogenesis of chronic intestinal inflammation as well as extra-intestinal manifestations have not been investigated so far. The aim of this study was to explore the effect of *ORMDL* proteins on the three UPR signaling branches and its impact on the intestinal and systemic homeostasis under physiological and challenging conditions.

The present work provides the first evidence of a cell type-specific protein expression pattern of *ORMDL* proteins upon ER stress, which may point to functional differences of *ORMDL* proteins between various cell types under challenging conditions. Additionally, this study demonstrates for the first time, a distinct impact of *ORMDL3* on each of the three UPR signaling branches, where *ORMDL3* activates the ATF6 α and the PERK pathways, but represses the IRE1 pathway. A strong effect of *ORMDL3* on the ATF6 α pathway was demonstrated, whereby overexpression of *ORMDL3* suppresses the glycosylation of the full length form of ATF6 α . The unglycosylated form of ATF6 α has been described to facilitate ATF6 α cleavage and to activate ATF6 α target genes. In line with this, *ORMDL3* promotes the cleavage of ATF6 α and, as a consequence, increases the promoter activity of the ER stress response element (ERSE). In addition, co-immunoprecipitation studies in the present work suggest a physical relevant interaction between *ORMDL3* and ATF6 α . An inducing effect of *ORMDL* proteins also occurs on the PERK pathway, which is mainly caused by crosstalk effects between the ATF6 α and PERK signaling branches. In addition, overexpression of *ORMDL3* results in increased ATF4 promoter activities and elevated protein levels of the pro-apoptotic transcription factor CHOP. In contrast to the inducing effect of *ORMDL3* on the ATF6 α and the PERK pathways, splicing of XBP1 and the activity of the UPRE promoter is diminished as a consequence of *ORMDL3* overexpression. These regulatory mechanisms of *ORMDL3* may enable a proper ER stress response through precisely coordinated activations of several UPR components.

In addition to the mentioned *in vitro* findings, this study investigated for the first time the *in vivo* impact of ORMDL by examining *Ormdl1*- and *Ormdl3*-deficient mice. Interestingly, the depletion of *Ormdl3*, but not *Ormdl1*, leads to reduced body weight as a result of decreased local insulin-like growth factor 1 production in muscle tissue. Although genetic variants in close proximity of the human *ORMDL3* gene have been identified as a potential risk factor for Crohn's disease (CD) and ulcerative colitis (UC), genetic deletion of *Ormdl1* or *Ormdl3* reveal no signs of spontaneous inflammation in mice. Indeed, *Ormdl3*-deficient mice, but not *Ormdl1*-deficient mice, are more susceptible to DSS-induced colitis, as demonstrated by a severe body weight loss, more pronounced crypt damage and significantly increased serum level of the pro-inflammatory cytokine IL-1 β . In addition, short-term DSS-treatment causes prolonged unresolved ER stress in colon and liver of *Ormdl3*-deficient mice. Prolonged unresolved ER stress also appears in the liver of *Ormdl3*-deficient mice upon injection of a sublethal dose of the chemical ER stress inducer tunicamycin. Both experiments indicate that ORMDL3 is crucial to protect against prolonged unresolved ER stress.

In summary, this study provides evidence that ORMDL proteins are crucial regulators of the UPR, with a particular impact on the ATF6 α branch. Especially, ORMDL3 is relevant for maintaining the homeostasis in the ER and the intestinal epithelium. The findings of this study indicate a beneficial regulatory function of ORMDL3 during ER stress conditions and intestinal inflammation.

6 Zusammenfassung

Kontinuierlicher Stress im Endoplasmatischen Retikulum (ER-Stress) ist mit der Pathogenese von chronisch entzündlichen Darmerkrankungen (CED) assoziiert. ER-Stress wird durch die übermäßige Akkumulation von falsch- oder ungefalteten Proteinen im ER hervorgerufen und induziert dadurch einen für die Wiederherstellung der ER-Homöostase essenziellen Signalweg, die sogenannte ungefaltete Proteinantwort (UPR; engl. *unfolded protein response*). Insbesondere intestinale Epithelzellen, wie zum Beispiel Paneth- und Becherzellen, sind aufgrund ihres hohen Bedarfs an sekretorischen Proteinen auf eine intakte UPR angewiesen. Diesbezüglich konnten Studien sowohl im murinen als auch humanen System bereits zeigen, dass während einer Entzündung ER-Stress in intestinalen Epithelzellen vermehrt auftritt. Zusätzlich identifizierten genomweite Assoziationsstudien Gene, die in der UPR involviert sind, als potentielle Risikofaktoren für CED. Eines dieser Gene ist *ORMDL3*, dessen Funktion in Bezug auf die Pathogenese von CED und extraintestinalen Manifestationen jedoch bisher nicht untersucht ist. Aus diesem Grund hatte die vorliegende Arbeit das Ziel, den Effekt von ORMDL Proteinen auf die drei UPR-Signalwege und dessen Auswirkung auf die intestinale und systemische Homöostase zu untersuchen.

Diese Studie liefert erstmals Hinweise auf zelltypspezifische Expressionsprofile von ORMDL Proteinen als Reaktion auf ER-Stress und weist somit auf funktionelle Unterschiede in verschiedenen Zelltypen unter belastenden Bedingungen hin. Zusätzlich verdeutlicht diese Studie zum ersten Mal die verschiedenen Auswirkungen von ORMDL3 auf jeden der drei UPR-Signalwege. Dabei aktiviert ORMDL3 den ATF6 α - und den PERK-Signalweg, wohingegen der IRE1-Signalweg inhibiert wird. Den stärksten Effekt zeigt ORMDL3 auf den ATF6 α -Signalweg, wobei die Überexpression von ORMDL3 die glykosylierte Form von ATF6 α reduziert. In der Literatur finden sich bereits Hinweise, dass die unglykosylierte Form von ATF6 α zunächst zu dessen Spaltung und Aktivierung sowie die sich anschließende Expression von ATF6 α Zielgenen führt. Die in dieser Studie untersuchte Überexpression von ORMDL3 und die damit einhergehende verstärkte Spaltung von ATF6 α sowie die erhöhte Induktion des ERSE-Promotors unterstützen dies. Zusätzlich konnte in dieser Arbeit erstmals die Interaktion von ORMDL3 und ATF6 α mittels Co-Immunopräzipitationsstudien nachgewiesen werden. Eine induzierende Funktion von ORMDL Proteinen konnte auch für den PERK-Signalweg beobachtet werden, welche primär auf eine Verknüpfung der beiden genannten Signalwege zurückzuführen ist. Dies konnte anhand der vermehrten ATF4-Promotoraktivität sowie der Hochregulation des pro-apoptotischen Transkriptionsfaktors CHOP nach ORMDL3

Überexpression verdeutlicht werden. Im Gegensatz zu der induzierenden Wirkung von ORMDL3 auf den ATF6 α - und PERK-Signalweg, konnte in der vorliegenden Arbeit in Folge einer Überexpression von ORMDL3 eine reduzierte Spaltung von XBP1 und eine verminderte Aktivierung des UPR-Promotors beobachtet werden. Diese vielfältigen regulatorischen Mechanismen von ORMDL3 ermöglichen spezialisierten Zellen eine geeignete ER-Stressantwort entsprechend ihrer Anforderungen.

Darüber hinaus wurde in dieser Arbeit erstmals die Auswirkung einer Deletion von jeweils einem *ORMDL* Gen mittels *Ormdl1*- und *Ormdl3*-defizienter Mäuse untersucht. Durch die Deletion von *Ormdl3* kommt es zu einer Reduktion des Körpergewichts infolge einer verringerten lokalen Produktion des insulinähnlichen Wachstumsfaktors 1 (engl. *Insulin-like growth factor 1*) in den Muskeln dieser Tiere. Obwohl genetische Veränderungen von *ORMDL3* im Menschen als potentieller Risikofaktor für Morbus Crohn und Colitis Ulcerosa identifiziert wurden, hat die Deletion von *Ormdl1* oder *Ormdl3* keine spontane intestinale Entzündung im murinen Organismus zur Folge. Hingegen zeigen *Ormdl3*-defiziente, nicht aber *Ormdl1*-defiziente, Mäuse eine erhöhte Anfälligkeit für eine DSS-induzierte Kolitis, welches sich in einer stärkeren Gewichtsreduktion, einer vermehrten Bildung von Kryptabzessen sowie einer erhöhten Serumkonzentrationen des pro-inflammatorischen Zytokins IL-1 β äußert. Die Verabreichung von DSS über einen kürzeren Zeitraum führt ebenfalls zu vermehrtem ER-Stress im Kolon und in der Leber von *Ormdl3*-defizienten Mäusen. Zudem konnten erhöhte ER-Stress-Level im Lebergewebe von *Ormdl3*-defizienten Mäusen nach einer subletalen Dosis des chemischen ER-Stressinduktors Tunicamycin festgestellt werden. Beide *in vivo* Versuche weisen auf einen positiven Effekt von ORMDL3 auf die Rekonstitution der Homöostase im ER hin.

Zusammenfassend verdeutlicht die vorliegende Arbeit, dass ORMDL Proteine als bedeutende Regulatoren der UPR einen starken Einfluss insbesondere auf den ATF6 α -Signalweg ausüben. Zudem konnte gezeigt werden, dass ORMDL3 relevant für die Aufrechterhaltung der Homöostase im ER und im intestinalen Epithel ist. Die Ergebnisse dieser Arbeit weisen erstmals auf eine regulatorische Wirkung von ORMDL3 unter ER-Stressbedingungen sowie bei intestinalen Entzündungen hin.

7 Bibliography

1. Baumgart DC, Carding SR. Inflammatory bowel disease: cause and immunobiology. *The Lancet*. 2007 May 18;369(9573):1627–40.
2. Loftus Jr EV. Clinical epidemiology of inflammatory bowel disease: incidence, prevalence, and environmental influences. *Gastroenterology*. 2004 May;126(6):1504–17.
3. Molodecky NA, Soon IS, Rabi DM, Ghali WA, Ferris M, Chernoff G, et al. Increasing Incidence and Prevalence of the Inflammatory Bowel Diseases With Time, Based on Systematic Review. *Gastroenterology*. 2012 Jan;142(1):46–54.e42.
4. Bernstein CN, Wajda A, Svenson LW, MacKenzie A, Koehoorn M, Jackson M, et al. The epidemiology of inflammatory bowel disease in Canada: a population-based study. *Am J Gastroenterol*. 2006 Jul;101(7):1559–68.
5. Stonnington CM, Phillips SF, Melton LJ, Zinsmeister AR. Chronic ulcerative colitis: incidence and prevalence in a community. *Gut*. 1987 Apr;28(4):402–9.
6. Ott C, Obermeier F, Thielier S, Kemptner D, Bauer A, Schölmerich J, et al. The incidence of inflammatory bowel disease in a rural region of Southern Germany: a prospective population-based study. *Eur J Gastroenterol Hepatol*. 2008 Sep;20(9):917–23.
7. Calkins BM, Lilienfeld AM, Garland CF, Mendeloff AI. Trends in incidence rates of ulcerative colitis and Crohn's disease. *Dig Dis Sci*. 1984 Oct;29(10):913–20.
8. Colombel J-F, Watson AJM, Neurath MF. The 10 remaining mysteries of inflammatory bowel disease. *Gut*. 2008 Jan 4;57(4):429–33.
9. Xavier RJ, Podolsky DK. Unravelling the pathogenesis of inflammatory bowel disease. *Nature*. 2007 Jul 26;448(7152):427–34.
10. Wilkins T, Jarvis K, Patel J. Diagnosis and management of Crohn's disease. *Am Fam Physician*. 2011 Dec 15;84(12):1365–75.
11. Isgar B, Harman M, Kaye MD, Whorwell PJ. Symptoms of irritable bowel syndrome in ulcerative colitis in remission. *Gut*. 1983 Mar;24(3):190–2.
12. Andersen NN, Jess T. Has the risk of colorectal cancer in inflammatory bowel disease decreased? *World J Gastroenterol WJG*. 2013 Nov 21;19(43):7561–8.
13. Ardizzone S, Puttini PS, Cassinotti A, Porro GB. Extraintestinal manifestations of inflammatory bowel disease. *Dig Liver Dis*. 2008 Jul;40, Supplement 2:S253–9.
14. Bandzar S, Gupta S, Platt MO. Crohn's disease: a review of treatment options and current research. *Cell Immunol*. 2013 Dec;286(1-2):45–52.
15. Peyrin-Biroulet L. Advances in the Treatment of Ulcerative Colitis. *Gastroenterol Hepatol*. 2013 Dec;9(12):827–9.
16. Roses RE, Rombeau JL. Recent trends in the surgical management of inflammatory bowel disease. *World J Gastroenterol WJG*. 2008 Jan 21;14(3):408–12.

17. Ba'ath ME, Mahmalat MW, Kapur P, Smith NP, Dalzell AM, Casson DH, et al. Surgical management of inflammatory bowel disease. *Arch Dis Child*. 2007 Apr;92(4):312–6.
18. Savage DC. Microbial ecology of the gastrointestinal tract. *Annu Rev Microbiol*. 1977;31:107–33.
19. Gerritsen J, Smidt H, Rijkers GT, de Vos WM. Intestinal microbiota in human health and disease: the impact of probiotics. *Genes Nutr*. 2011 Aug;6(3):209–40.
20. Rautava S, Walker WA. Commensal Bacteria and Epithelial Cross Talk in the Developing Intestine. *Curr Gastroenterol Rep*. 2007 Oct;9(5):385–92.
21. Peterson LW, Artis D. Intestinal epithelial cells: regulators of barrier function and immune homeostasis. *Nat Rev Immunol*. 2014 Mar;14(3):141–53.
22. Buisine MP, Desreumaux P, Debailleul V, Gambiez L, Geboes K, Ectors N, et al. Abnormalities in mucin gene expression in Crohn's disease. *Inflamm Bowel Dis*. 1999 Feb;5(1):24–32.
23. Salzman NH, Underwood MA, Bevins CL. Paneth cells, defensins, and the commensal microbiota: A hypothesis on intimate interplay at the intestinal mucosa. *Semin Immunol*. 2007 Apr;19(2):70–83.
24. Ouellette AJ. Defensin-mediated innate immunity in the small intestine. *Best Pract Res Clin Gastroenterol*. 2004 Apr;18(2):405–19.
25. Rakoff-Nahoum S, Paglino J, Eslami-Varzaneh F, Edberg S, Medzhitov R. Recognition of commensal microflora by toll-like receptors is required for intestinal homeostasis. *Cell*. 2004 Jul 23;118(2):229–41.
26. Vijay-Kumar M, Sanders CJ, Taylor RT, Kumar A, Aitken JD, Sitaraman SV, et al. Deletion of TLR5 results in spontaneous colitis in mice. *J Clin Invest*. 2007 Dec;117(12):3909–21.
27. Iliev ID, Spadoni I, Mileti E, Matteoli G, Sonzogni A, Sampietro GM, et al. Human intestinal epithelial cells promote the differentiation of tolerogenic dendritic cells. *Gut*. 2009 Nov;58(11):1481–9.
28. Sartor RB. Mechanisms of Disease: pathogenesis of Crohn's disease and ulcerative colitis. *Nat Clin Pract Gastroenterol Hepatol*. 2006;3(7):390–407.
29. Okazaki T, Wang M-H, Rawsthorne P, Sargent M, Datta LW, Shugart YY, et al. Contributions of IBD5, IL23R, ATG16L1, and NOD2 to Crohn's Disease Risk in a Population-Based Case-Control Study: Evidence of Gene-Gene Interactions. *Inflamm Bowel Dis*. 2008 Nov;14(11):1528–41.
30. Molodecky NA, Kaplan GG. Environmental Risk Factors for Inflammatory Bowel Disease. *Gastroenterol Hepatol*. 2010 May;6(5):339–46.
31. El-Tawil A, El-Tawil AM. Genetic Predisposition and Inflammatory Bowel Disease. *Gastroenterol Res*. 2013 Mar 8;6(1):1–3.
32. Harris RA, Nagy-Szakal D, Pedersen N, Opekun A, Bronsky J, Munkholm P, et al. Genome-wide peripheral blood leukocyte DNA methylation microarrays identified a

- single association with inflammatory bowel diseases. *Inflamm Bowel Dis*. 2012 Dec;18(12):2334–41.
33. Tsaprouni LG, Ito K, Powell JJ, Adcock IM, Pouchard N. Differential patterns of histone acetylation in inflammatory bowel diseases. *J Inflamm*. 2011 Jan 27;8(1):1.
 34. Khor B, Gardet A, Xavier RJ. Genetics and pathogenesis of inflammatory bowel disease. *Nature*. 2011 Jun 15;474(7351):307–17.
 35. Halfvarson J, Bodin L, Tysk C, Lindberg E, Järnerot G. Inflammatory bowel disease in a Swedish twin cohort: a long-term follow-up of concordance and clinical characteristics. *Gastroenterology*. 2003 Jun;124(7):1767–73.
 36. Barreiro-de Acosta M, Alvarez Castro A, Souto R, Iglesias M, Lorenzo A, Dominguez-Muñoz JE. Emigration to western industrialized countries: A risk factor for developing inflammatory bowel disease. *J Crohns Colitis*. 2011 Dec;5(6):566–9.
 37. Harries AD, Baird A, Rhodes J. Non-smoking: a feature of ulcerative colitis. *Br Med J Clin Res Ed*. 1982 Mar 6;284(6317):706.
 38. Thomas GAO, Rhodes J, Green JT, Richardson C. Role of smoking in inflammatory bowel disease: implications for therapy. *Postgrad Med J*. 2000 Jan 5;76(895):273–9.
 39. Bernstein CN, Shanahan F. Disorders of a modern lifestyle: reconciling the epidemiology of inflammatory bowel diseases. *Gut*. 2008 Jan 9;57(9):1185–91.
 40. Ng SC, Tang W, Leong RW, Chen M, Ko Y, Studd C, et al. Environmental risk factors in inflammatory bowel disease: a population-based case-control study in Asia-Pacific. *Gut*. 2014 Sep 12;gutjnl – 2014–307410.
 41. Hou JK, Lee D, Lewis J. Diet and inflammatory bowel disease: review of patient-targeted recommendations. *Clin Gastroenterol Hepatol Off Clin Pract J Am Gastroenterol Assoc*. 2014 Oct;12(10):1592–600.
 42. Hou JK, Abraham B, El-Serag H. Dietary Intake and Risk of Developing Inflammatory Bowel Disease: A Systematic Review of the Literature. *Am J Gastroenterol*. 2011 Apr;106(4):563–73.
 43. Jantchou P, Turck D, Baldé M, Gower-Rousseau C. Breastfeeding and risk of inflammatory bowel disease: results of a pediatric, population-based, case-control study. *Am J Clin Nutr*. 2005 Jan 8;82(2):485–6.
 44. Hugot JP, Laurent-Puig P, Gower-Rousseau C, Olson JM, Lee JC, Beaugerie L, et al. Mapping of a susceptibility locus for Crohn's disease on chromosome 16. *Nature*. 1996 Feb 29;379(6568):821–3.
 45. Hugot J-P, Chamaillard M, Zouali H, Lesage S, Cézard J-P, Belaiche J, et al. Association of NOD2 leucine-rich repeat variants with susceptibility to Crohn's disease. *Nature*. 2001 May 31;411(6837):599–603.
 46. Aguilar C, Lenoir C, Lambert N, Bègue B, Brousse N, Canioni D, et al. Characterization of Crohn disease in X-linked inhibitor of apoptosis-deficient male patients and female symptomatic carriers. *J Allergy Clin Immunol [Internet]*. [cited 2014 Oct 23]; Available from: <http://www.sciencedirect.com/science/article/pii/S009167491400606X>

47. Pastorelli L, De Salvo C, Mercado JR, Vecchi M, Pizarro TT. Central Role of the Gut Epithelial Barrier in the Pathogenesis of Chronic Intestinal Inflammation: Lessons Learned from Animal Models and Human Genetics. *Front Immunol* [Internet]. 2013 Sep 17 [cited 2015 Jan 19];4. Available from: <http://www.ncbi.nlm.nih.gov/pmc/articles/PMC3775315/>
48. Jostins L, Ripke S, Weersma RK, Duerr RH, McGovern DP, Hui KY, et al. Host-microbe interactions have shaped the genetic architecture of inflammatory bowel disease. *Nature*. 2012 Nov 1;491(7422):119–24.
49. Lee JC, Parkes M. Genome-wide association studies and Crohn's disease. *Brief Funct Genomics*. 2011 Jan 3;10(2):71–6.
50. Anderson CA, Boucher G, Lees CW, Franke A, D'Amato M, Taylor KD, et al. Meta-analysis identifies 29 additional ulcerative colitis risk loci, increasing the number of confirmed associations to 47. *Nat Genet*. 2011 Mar;43(3):246–52.
51. Kaser A, Lee A-H, Franke A, Glickman JN, Zeissig S, Tilg H, et al. XBP1 Links ER Stress to Intestinal Inflammation and Confers Genetic Risk for Human Inflammatory Bowel Disease. *Cell*. 2008 Sep;134(5):743–56.
52. Cho JH. The genetics and immunopathogenesis of inflammatory bowel disease. *Nat Rev Immunol*. 2008 Jun;8(6):458–66.
53. Franke A, Balschun T, Karlsen TH, Hedderich J, May S, Lu T, et al. Replication of signals from recent studies of Crohn's disease identifies previously unknown disease loci for ulcerative colitis. *Nat Genet*. 2008 Jun;40(6):713–5.
54. Cooper GM. The Endoplasmic Reticulum [Internet]. 2000 [cited 2014 Jul 21]. Available from: <http://www.ncbi.nlm.nih.gov/books/NBK9889/>
55. Meusser B, Hirsch C, Jarosch E, Sommer T. ERAD: the long road to destruction. *Nat Cell Biol*. 2005 Aug;7(8):766–72.
56. Kim I, Xu W, Reed JC. Cell death and endoplasmic reticulum stress: disease relevance and therapeutic opportunities. *Nat Rev Drug Discov*. 2008 Dec;7(12):1013–30.
57. Hetz C, Chevet E, Harding HP. Targeting the unfolded protein response in disease. *Nat Rev Drug Discov*. 2013 Sep;12(9):703–19.
58. Wu J, Kaufman RJ. From acute ER stress to physiological roles of the Unfolded Protein Response. *Cell Death Differ*. 2006;13(3):374–84.
59. Todd DJ, Lee A-H, Glimcher LH. The endoplasmic reticulum stress response in immunity and autoimmunity. *Nat Rev Immunol*. 2008 Sep;8(9):663–74.
60. Chen G, Fan Z, Wang X, Ma C, Bower KA, Shi X, et al. Brain-Derived Neurotrophic Factor Suppresses Tunicamycin-Induced Upregulation of CHOP in Neurons. *J Neurosci Res*. 2007 Jun;85(8):1674–84.
61. Tabas I, Ron D. Integrating the mechanisms of apoptosis induced by endoplasmic reticulum stress. *Nat Cell Biol*. 2011 Mar;13(3):184–90.

62. Ogata M, Hino S, Saito A, Morikawa K, Kondo S, Kanemoto S, et al. Autophagy Is Activated for Cell Survival after Endoplasmic Reticulum Stress. *Mol Cell Biol*. 2006 Dec 15;26(24):9220–31.
63. Hetz C. The unfolded protein response: controlling cell fate decisions under ER stress and beyond. *Nat Rev Mol Cell Biol*. 2012 Feb;13(2):89–102.
64. Walter P, Ron D. The Unfolded Protein Response: From Stress Pathway to Homeostatic Regulation. *Science*. 2011 Nov 25;334(6059):1081–6.
65. Yoshida H, Matsui T, Yamamoto A, Okada T, Mori K. XBP1 mRNA Is Induced by ATF6 and Spliced by IRE1 in Response to ER Stress to Produce a Highly Active Transcription Factor. *Cell*. 2001 Dec;107(7):881–91.
66. Liu CY, Kaufman RJ. The unfolded protein response. *J Cell Sci*. 2003 May 15;116(10):1861–2.
67. Miyoshi K, Katayama T, Imaizumi K, Taniguchi M, Mori Y, Hitomi J, et al. Characterization of mouse Ire1 α : cloning, mRNA localization in the brain and functional analysis in a neural cell line. *Mol Brain Res*. 2000 Dec 28;85(1–2):68–76.
68. Bertolotti A, Wang X, Novoa I, Jungreis R, Schlessinger K, Cho JH, et al. Increased sensitivity to dextran sodium sulfate colitis in IRE1 β -deficient mice. *J Clin Invest*. 2001 Mar 1;107(5):585–93.
69. Martino MB, Jones L, Brighton B, Ehre C, Abdulah L, Davis CW, et al. The ER stress transducer IRE1 β is required for airway epithelial mucin production. *Mucosal Immunol*. 2013 May;6(3):639–54.
70. Liu B, Staron M, Hong F, Wu BX, Sun S, Morales C, et al. Essential roles of grp94 in gut homeostasis via chaperoning canonical Wnt pathway. *Proc Natl Acad Sci U S A*. 2013 Apr 23;110(17):6877–82.
71. Iwawaki T, Akai R, Yamanaka S, Kohno K. Function of IRE1 alpha in the placenta is essential for placental development and embryonic viability. *Proc Natl Acad Sci U S A*. 2009 Sep 29;106(39):16657–62.
72. Imagawa Y, Hosoda A, Sasaka S, Tsuru A, Kohno K. RNase domains determine the functional difference between IRE1 α and IRE1 β . *FEBS Lett*. 2008 Mar 5;582(5):656–60.
73. Cox JS, Shamu CE, Walter P. Transcriptional induction of genes encoding endoplasmic reticulum resident proteins requires a transmembrane protein kinase. *Cell*. 1993 Jun 18;73(6):1197–206.
74. Tirasophon W, Lee K, Callaghan B, Welihinda A, Kaufman RJ. The endoribonuclease activity of mammalian IRE1 autoregulates its mRNA and is required for the unfolded protein response. *Genes Dev*. 2000 Nov 1;14(21):2725–36.
75. Lee K, Tirasophon W, Shen X, Michalak M, Prywes R, Okada T, et al. IRE1-mediated unconventional mRNA splicing and S2P-mediated ATF6 cleavage merge to regulate XBP1 in signaling the unfolded protein response. *Genes Dev*. 2002 Feb 15;16(4):452–66.

76. Hayakawa K, Nakajima S, Hiramatsu N, Okamura M, Huang T, Saito Y, et al. ER Stress Depresses NF- κ B Activation in Mesangial Cells through Preferential Induction of C/EBP β . *J Am Soc Nephrol*. 2010 Jan 1;21(1):73–81.
77. Hotamisligil GS. Endoplasmic reticulum stress and the inflammatory basis of metabolic disease. *Cell*. 2010 Mar 19;140(6):900–17.
78. Hollien J, Weissman JS. Decay of Endoplasmic Reticulum-Localized mRNAs During the Unfolded Protein Response. *Science*. 2006 Jul 7;313(5783):104–7.
79. Yoneda T, Imaizumi K, Oono K, Yui D, Gomi F, Katayama T, et al. Activation of Caspase-12, an endoplasmic reticulum (ER) resident caspase, through tumor necrosis factor receptor-associated factor 2 (TRAF2) dependent mechanism in response to the ER stress. *J Biol Chem* [Internet]. 2001 Jan 29 [cited 2014 Dec 19]; Available from: <http://www.jbc.org/content/early/2001/01/29/jbc.M010677200>
80. Kaneko M, Niinuma Y, Nomura Y. Activation Signal of Nuclear Factor- κ B in Response to Endoplasmic Reticulum Stress is Transduced *via* IRE1 and Tumor Necrosis Factor Receptor-Associated Factor 2. *Biol Pharm Bull*. 2003;26(7):931–5.
81. Chakrabarti A, Chen AW, Varner JD. A Review of the Mammalian Unfolded Protein Response. *Biotechnol Bioeng*. 2011 Dec;108(12):2777–93.
82. Haze K, Yoshida H, Yanagi H, Yura T, Mori K. Mammalian transcription factor ATF6 is synthesized as a transmembrane protein and activated by proteolysis in response to endoplasmic reticulum stress. *Mol Biol Cell*. 1999 Nov;10(11):3787–99.
83. Shen J, Prywes R. ER stress signaling by regulated proteolysis of ATF6. *Methods San Diego Calif*. 2005 Apr;35(4):382–9.
84. Yoshida H, Haze K, Yanagi H, Yura T, Mori K. Identification of the cis-acting endoplasmic reticulum stress response element responsible for transcriptional induction of mammalian glucose-regulated proteins. Involvement of basic leucine zipper transcription factors. *J Biol Chem*. 1998 Dec 11;273(50):33741–9.
85. Yamamoto K, Sato T, Matsui T, Sato M, Okada T, Yoshida H, et al. Transcriptional Induction of Mammalian ER Quality Control Proteins Is Mediated by Single or Combined Action of ATF6 α and XBP1. *Dev Cell*. 2007 Sep 4;13(3):365–76.
86. Lee A-H, Iwakoshi NN, Glimcher LH. XBP-1 Regulates a Subset of Endoplasmic Reticulum Resident Chaperone Genes in the Unfolded Protein Response. *Mol Cell Biol*. 2003 Nov;23(21):7448–59.
87. Shen J, Chen X, Hendershot L, Prywes R. ER Stress Regulation of ATF6 Localization by Dissociation of BiP/GRP78 Binding and Unmasking of Golgi Localization Signals. *Dev Cell*. 2002 Jul;3(1):99–111.
88. Nadanaka S, Yoshida H, Kano F, Murata M, Mori K. Activation of Mammalian Unfolded Protein Response Is Compatible with the Quality Control System Operating in the Endoplasmic Reticulum. *Mol Biol Cell*. 2004 Jan 6;15(6):2537–48.
89. Shen J, Prywes R. Dependence of Site-2 Protease Cleavage of ATF6 on Prior Site-1 Protease Digestion Is Determined by the Size of the Luminal Domain of ATF6. *J Biol Chem*. 2004 Aug 10;279(41):43046–51.

90. Baumeister P, Luo S, Skarnes WC, Sui G, Seto E, Shi Y, et al. Endoplasmic Reticulum Stress Induction of the Grp78/BiP Promoter: Activating Mechanisms Mediated by YY1 and Its Interactive Chromatin Modifiers. *Mol Cell Biol*. 2005 Jan 6;25(11):4529–40.
91. Kokame K, Kato H, Miyata T. Identification of ERSE-II, a new cis-acting element responsible for the ATF6-dependent mammalian unfolded protein response. *J Biol Chem*. 2001 Mar 23;276(12):9199–205.
92. Martindale JJ, Fernandez R, Thuerauf D, Whittaker R, Gude N, Sussman MA, et al. Endoplasmic reticulum stress gene induction and protection from ischemia/reperfusion injury in the hearts of transgenic mice with a tamoxifen-regulated form of ATF6. *Circ Res*. 2006 May 12;98(9):1186–93.
93. Yamamoto K. Differential Contributions of ATF6 and XBP1 to the Activation of Endoplasmic Reticulum Stress-Responsive cis-Acting Elements ERSE, UPRE and ERSE-II. *J Biochem (Tokyo)*. 2004 Sep 1;136(3):343–50.
94. Wu J, Rutkowski DT, Dubois M, Swathirajan J, Saunders T, Wang J, et al. ATF6alpha optimizes long-term endoplasmic reticulum function to protect cells from chronic stress. *Dev Cell*. 2007 Sep;13(3):351–64.
95. Cui W, Li J, Ron D, Sha B. The structure of the PERK kinase domain suggests the mechanism for its activation. *Acta Crystallogr D Biol Crystallogr*. 2011 May 1;67(Pt 5):423–8.
96. Pomar N, Berlanga JJ, Campuzano S, Hernández G, Elías M, de Haro C. Functional characterization of *Drosophila melanogaster* PERK eukaryotic initiation factor 2 α (eIF2 α) kinase. *Eur J Biochem*. 2003;270(2):293–306.
97. Bertolotti A, Zhang Y, Hendershot LM, Harding HP, Ron D. Dynamic interaction of BiP and ER stress transducers in the unfolded-protein response. *Nat Cell Biol*. 2000 Jun;2(6):326–32.
98. Harding HP, Zhang Y, Ron D. Protein translation and folding are coupled by an endoplasmic-reticulum-resident kinase. *Nature*. 1999 Jan 21;397(6716):271–4.
99. Chan C-P, Kok K-H, Tang H-MV, Wong C-M, Jin D-Y. Internal ribosome entry site-mediated translational regulation of ATF4 splice variant in mammalian unfolded protein response. *Biochim Biophys Acta BBA - Mol Cell Res*. 2013 Oct;1833(10):2165–75.
100. McCullough KD, Martindale JL, Klotz L-O, Aw T-Y, Holbrook NJ. Gadd153 Sensitizes Cells to Endoplasmic Reticulum Stress by Down-Regulating Bcl2 and Perturbing the Cellular Redox State. *Mol Cell Biol*. 2001 Feb 15;21(4):1249–59.
101. Novoa I, Zeng H, Harding HP, Ron D. Feedback Inhibition of the Unfolded Protein Response by GADD34-Mediated Dephosphorylation of eIF2 α . *J Cell Biol*. 2001 May 28;153(5):1011–22.
102. Wu S, Tan M, Hu Y, Wang J-L, Scheuner D, Kaufman RJ. Ultraviolet Light Activates NF κ B through Translational Inhibition of I κ B α Synthesis. *J Biol Chem*. 2004 Aug 13;279(33):34898–902.

103. Cullinan SB, Zhang D, Hannink M, Arvisais E, Kaufman RJ, Diehl JA. Nrf2 Is a Direct PERK Substrate and Effector of PERK-Dependent Cell Survival. *Mol Cell Biol*. 2003 Oct 15;23(20):7198–209.
104. Goodall JC, Wu C, Zhang Y, McNeill L, Ellis L, Saudek V, et al. Endoplasmic reticulum stress-induced transcription factor, CHOP, is crucial for dendritic cell IL-23 expression. *Proc Natl Acad Sci U S A*. 2010 Oct 12;107(41):17698–703.
105. Yoshida H, Okada T, Haze K, Yanagi H, Yura T, Negishi M, et al. ATF6 Activated by Proteolysis Binds in the Presence of NF-Y (CBF) Directly to the cis-Acting Element Responsible for the Mammalian Unfolded Protein Response. *Mol Cell Biol*. 2000 Sep;20(18):6755–67.
106. Yamamoto K, Suzuki N, Wada T, Okada T, Yoshida H, Kaufman RJ, et al. Human HRD1 Promoter Carries a Functional Unfolded Protein Response Element to Which XBP1 but not ATF6 Directly Binds. *J Biochem (Tokyo)*. 2008 Oct;144(4):477–86.
107. Yoshida H, Uemura A, Mori K. pXBP1(U), a negative regulator of the unfolded protein response activator pXBP1(S), targets ATF6 but not ATF4 in proteasome-mediated degradation. *Cell Struct Funct*. 2009;34(1):1–10.
108. Okada T, Yoshida H, Akazawa R, Negishi M, Mori K. Distinct roles of activating transcription factor 6 (ATF6) and double-stranded RNA-activated protein kinase-like endoplasmic reticulum kinase (PERK) in transcription during the mammalian unfolded protein response. *Biochem J*. 2002 Sep 1;366(Pt 2):585–94.
109. Ma Y, Brewer JW, Alan Diehl J, Hendershot LM. Two Distinct Stress Signaling Pathways Converge Upon the CHOP Promoter During the Mammalian Unfolded Protein Response. *J Mol Biol*. 2002 May 17;318(5):1351–65.
110. Yamaguchi Y, Larkin D, Lara-Lemus R, Ramos-Castañeda J, Liu M, Arvan P. Endoplasmic Reticulum (ER) Chaperone Regulation and Survival of Cells Compensating for Deficiency in the ER Stress Response Kinase, PERK. *J Biol Chem*. 2008 Jun 20;283(25):17020–9.
111. Kim YS, Ho SB. Intestinal Goblet Cells and Mucins in Health and Disease: Recent Insights and Progress. *Curr Gastroenterol Rep*. 2010 Oct;12(5):319–30.
112. Niederreiter L, Kaser A. Endoplasmic reticulum stress and inflammatory bowel disease. *Acta Gastro-Enterol Belg*. 2011 Jun;74(2):330–3.
113. Kaser A, Martínez-Naves E, Blumberg RS. Endoplasmic reticulum stress: implications for inflammatory bowel disease pathogenesis. *Curr Opin Gastroenterol*. 2010 Jul;26(4):318–26.
114. Shkoda A, Ruiz PA, Daniel H, Kim SC, Rogler G, Sartor RB, et al. Interleukin-10 blocked endoplasmic reticulum stress in intestinal epithelial cells: impact on chronic inflammation. *Gastroenterology*. 2007 Jan;132(1):190–207.
115. Hu S, Ciancio MJ, Lahav M, Fujiya M, Lichtenstein L, Anant S, et al. Translational Inhibition of Colonic Epithelial Heat Shock Proteins by IFN- γ and TNF- α in Intestinal Inflammation. *Gastroenterology*. 2007 Dec;133(6):1893–904.
116. Urano F, Wang X, Bertolotti A, Zhang Y, Chung P, Harding HP, et al. Coupling of stress in the ER to activation of JNK protein kinases by transmembrane protein kinase IRE1. *Science*. 2000 Jan 28;287(5453):664–6.

117. Blackwell TS, Christman JW. The Role of Nuclear Factor- κ B in Cytokine Gene Regulation. *Am J Respir Cell Mol Biol.* 1997 Jul 1;17(1):3–9.
118. Zheng W, Rosenstiel P, Huse K, Sina C, Valentonyte R, Mah N, et al. Evaluation of AGR2 and AGR3 as candidate genes for inflammatory bowel disease. *Genes Immun.* 2005 Oct 13;7(1):11–8.
119. Wang Z, Hao Y, Lowe AW. The Adenocarcinoma-Associated Antigen, AGR2, Promotes Tumor Growth, Cell Migration, and Cellular Transformation. *Cancer Res.* 2008 Jan 15;68(2):492–7.
120. Vanderlaag KE, Hudak S, Bald L, Fayadat-Dilman L, Sathe M, Grein J, et al. Anterior gradient-2 plays a critical role in breast cancer cell growth and survival by modulating cyclin D1, estrogen receptor- α and survivin. *Breast Cancer Res BCR.* 2010;12(3):R32.
121. Fritzsche FR, Dahl E, Dankof A, Burkhardt M, Pahl S, Petersen I, et al. Expression of AGR2 in non small cell lung cancer. *Histol Histopathol.* 2007 Jul;22(7):703–8.
122. Fritzsche FR, Dahl E, Pahl S, Burkhardt M, Luo J, Mayordomo E, et al. Prognostic relevance of AGR2 expression in breast cancer. *Clin Cancer Res Off J Am Assoc Cancer Res.* 2006 Mar 15;12(6):1728–34.
123. Ho ME, Quek S-I, True LD, Morrissey C, Corey E, Vessella RL, et al. Prostate cancer cell phenotypes based on AGR2 and CD10 expression. *Mod Pathol.* 2013 Jun;26(6):849–59.
124. Zhao F, Edwards R, Dizon D, Afrasiabi K, Mastroianni JR, Geyfman M, et al. Disruption of Paneth and goblet cell homeostasis and increased endoplasmic reticulum stress in *Agr2*^{-/-} mice. *Dev Biol.* 2010 Feb 15;338(2):270–9.
125. Hsu KJ, Turvey SE. Functional analysis of the impact of ORMDL3 expression on inflammation and activation of the unfolded protein response in human airway epithelial cells. *Allergy Asthma Clin Immunol.* 2013 Feb 1;9(1):4.
126. Kaser A, Adolph TE, Blumberg RS. The Unfolded Protein Response and Gastrointestinal Disease. *Semin Immunopathol.* 2013 May;35(3):307–19.
127. Cao SS, Zimmermann EM, Chuang B, Song B, Nwokoye A, Wilkinson JE, et al. The Unfolded Protein Response and Chemical Chaperones Reduce Protein Misfolding and Colitis in Mice. *Gastroenterology.* 2013 May;144(5):989–1000.e6.
128. Rutschmann S, Crozat K, Li X, Du X, Hanselman JC, Shigeoka AA, et al. Hypopigmentation and Maternal-Zygotic Embryonic Lethality Caused by a Hypomorphic *Mbtps1* Mutation in Mice. *G3 GenesGenomesGenetics.* 2012 Apr 1;2(4):499–504.
129. Brandl K, Rutschmann S, Li X, Du X, Xiao N, Schnabl B, et al. Enhanced sensitivity to DSS colitis caused by a hypomorphic *Mbtps1* mutation disrupting the ATF6-driven unfolded protein response. *Proc Natl Acad Sci U S A.* 2009 Mar 3;106(9):3300–5.
130. Cao SS, Wang M, Harrington JC, Chuang B-M, Eckmann L, Kaufman RJ. Phosphorylation of eIF2 α is dispensable for differentiation but required at a posttranscriptional level for paneth cell function and intestinal homeostasis in mice. *Inflamm Bowel Dis.* 2014 Apr;20(4):712–22.

131. Namba T, Tanaka K-I, Ito Y, Ishihara T, Hoshino T, Gotoh T, et al. Positive Role of CCAAT/Enhancer-Binding Protein Homologous Protein, a Transcription Factor Involved in the Endoplasmic Reticulum Stress Response in the Development of Colitis. *Am J Pathol.* 2009 May;174(5):1786–98.
132. Tsuru A, Fujimoto N, Takahashi S, Saito M, Nakamura D, Iwano M, et al. Negative feedback by IRE1 β optimizes mucin production in goblet cells. *Proc Natl Acad Sci.* 2013 Feb 19;110(8):2864–9.
133. Adolph TE, Tomczak MF, Niederreiter L, Ko H-J, Böck J, Martinez-Naves E, et al. Paneth cells as a site of origin for intestinal inflammation. *Nature.* 2013 Nov 14;503(7475):272–6.
134. Klinken BJ-WV, Einerhand AWC, Duits LA, Makkink MK, Tytgat KMAJ, Renes IB, et al. Gastrointestinal expression and partial cDNA cloning of murine Muc2. *Am J Physiol - Gastrointest Liver Physiol.* 1999 Jan 1;276(1):G115–24.
135. Hjelmqvist L, Tuson M, Marfany G, Herrero E, Balcells S, González-Duarte R. ORMDL proteins are a conserved new family of endoplasmic reticulum membrane proteins. *Genome Biol.* 2002;3(6):RESEARCH0027.
136. Moffatt MF, Kabesch M, Liang L, Dixon AL, Strachan D, Heath S, et al. Genetic variants regulating ORMDL3 expression contribute to the risk of childhood asthma. *Nature.* 2007 Apr 7;448(7152):470–3.
137. Barrett JC, Hansoul S, Nicolae DL, Cho JH, Duerr RH, Rioux JD, et al. Genome-wide association defines more than thirty distinct susceptibility loci for Crohn's disease. *Nat Genet.* 2008 Aug;40(8):955–62.
138. McGovern DPB, Gardet A, Törkvist L, Goyette P, Essers J, Taylor KD, et al. Genome-wide association identifies multiple ulcerative colitis susceptibility loci. *Nat Genet.* 2010 Apr;42(4):332–7.
139. Barrett JC, Clayton DG, Concannon P, Akolkar B, Cooper JD, Erlich HA, et al. Genome-wide association study and meta-analysis find that over 40 loci affect risk of type 1 diabetes. *Nat Genet.* 2009 Jun;41(6):703–7.
140. Dobbins SE, Hosking FJ, Shete S, Armstrong G, Swerdlow A, Liu Y, et al. Allergy and glioma risk: test of association by genotype. *Int J Cancer J Int Cancer.* 2011 Apr 1;128(7):1736–40.
141. Hirschfield GM, Liu X, Han Y, Gorlov IP, Lu Y, Xu C, et al. Variants at IRF5-TNPO3, 17q12-21 and MMEL1 are associated with primary biliary cirrhosis. *Nat Genet.* 2010 Aug;42(8):655–7.
142. Kurreeman FAS, Stahl EA, Okada Y, Liao K, Diogo D, Raychaudhuri S, et al. Use of a Multiethnic Approach to Identify Rheumatoid- Arthritis-Susceptibility Loci, 1p36 and 17q12. *Am J Hum Genet.* 2012 Mar 9;90(3):524–32.
143. Laukens D, Georges M, Libioulle C, Sandor C, Mni M, Vander Cruyssen B, et al. Evidence for Significant Overlap between Common Risk Variants for Crohn's Disease and Ankylosing Spondylitis. *PLoS ONE [Internet].* 2010 Nov 2 [cited 2013 Dec 4];5(11). Available from: <http://www.ncbi.nlm.nih.gov/pmc/articles/PMC2970560/>

144. Neurath MF, Finotto S, Glimcher LH. The role of Th1/Th2 polarization in mucosal immunity. *Nat Med*. 2002 Jun;8(6):567–73.
145. Levy D, Ehret GB, Rice K, Verwoert GC, Launer LJ, Dehghan A, et al. Genome-wide association study of blood pressure and hypertension. *Nat Genet*. 2009 Jun;41(6):677–87.
146. Cantero-Recasens G, Fandos C, Rubio-Moscardo F, Valverde MA, Vicente R. The asthma-associated ORMDL3 gene product regulates endoplasmic reticulum-mediated calcium signaling and cellular stress. *Hum Mol Genet*. 2009 Oct 8;19(1):111–21.
147. Han S, Lone MA, Schneiter R, Chang A. Orm1 and Orm2 are conserved endoplasmic reticulum membrane proteins regulating lipid homeostasis and protein quality control. *Proc Natl Acad Sci U S A*. 2010 Mar 30;107(13):5851–6.
148. Liu M, Huang C, Polu SR, Schneiter R, Chang A. Regulation of sphingolipid synthesis through Orm1 and Orm2 in yeast. *J Cell Sci*. 2012 May 15;125(10):2428–35.
149. Miller M, Tam AB, Cho JY, Doherty TA, Pham A, Khorram N, et al. ORMDL3 is an inducible lung epithelial gene regulating metalloproteases, chemokines, OAS, and ATF6. *Proc Natl Acad Sci*. 2012 Sep 24;109(41):16648–53.
150. Mekahli D, Bultynck G, Parys JB, De Smedt H, Missiaen L. Endoplasmic-reticulum calcium depletion and disease. *Cold Spring Harb Perspect Biol*. 2011 Jun;3(6).
151. Missiaen L, Robberecht W, van den Bosch L, Callewaert G, Parys JB, Wuytack F, et al. Abnormal intracellular Ca^{2+} homeostasis and disease. *Cell Calcium*. 2000 Jul;28(1):1–21.
152. Berridge MJ, Lipp P, Bootman MD. The versatility and universality of calcium signalling. *Nat Rev Mol Cell Biol*. 2000 Oct;1(1):11–21.
153. Miller M, Rosenthal P, Beppu A, Mueller JL, Hoffman HM, Tam AB, et al. ORMDL3 transgenic mice have increased airway remodeling and airway responsiveness characteristic of asthma. *J Immunol Baltim Md 1950*. 2014 Apr 15;192(8):3475–87.
154. Carreras-Sureda A, Cantero-Recasens G, Rubio-Moscardo F, Kiefer K, Peinelt C, Niemeyer BA, et al. ORMDL3 modulates store-operated calcium entry and lymphocyte activation. *Hum Mol Genet* [Internet]. 2012 Oct 25 [cited 2012 Oct 29]; Available from: <http://hmg.oxfordjournals.org/content/early/2012/10/25/hmg.dds450>
155. Gururaj C, Federman R, Chang A. Orm Proteins Integrate Multiple Signals to Maintain Sphingolipid Homeostasis. *J Biol Chem*. 2013 Dec 7;288(28):20453–63.
156. Breslow DK, Collins SR, Bodenmiller B, Aebersold R, Simons K, Shevchenko A, et al. Orm family proteins mediate sphingolipid homeostasis. *Nature*. 2010 Feb 25;463(7284):1048–53.
157. Nagiec MM, Baltisberger JA, Wells GB, Lester RL, Dickson RC. The LCB2 gene of *Saccharomyces* and the related LCB1 gene encode subunits of serine palmitoyltransferase, the initial enzyme in sphingolipid synthesis. *Proc Natl Acad Sci U S A*. 1994 Aug 16;91(17):7899–902.

158. Fresques T, Niles B, Aronova S, Mogri H, Rakhshandehroo T, Powers T. Regulation of ceramide synthase by casein kinase 2-dependent phosphorylation in *S. cerevisiae*. *J Biol Chem*. 2014 Nov 26; jbc.M114.621086.
159. Roelants FM, Breslow DK, Muir A, Weissman JS, Thorner J. Protein kinase Ypk1 phosphorylates regulatory proteins Orm1 and Orm2 to control sphingolipid homeostasis in *Saccharomyces cerevisiae*. *Proc Natl Acad Sci*. 2011 Nov 29; 108(48):19222–7.
160. Siow D, Sunkara M, Morris A, Wattenberg B. Regulation of de novo sphingolipid biosynthesis by the ORMDL proteins and sphingosine kinase-1. *Adv Biol Regul*. 2015 Jan; 57:42–54.
161. Chueasiri C, Chunthong K, Pitnjam K, Chakhonkaen S, Sangarwut N, Sangsawang K, et al. Rice ORMDL controls sphingolipid homeostasis affecting fertility resulting from abnormal pollen development. *PLoS One*. 2014; 9(9):e106386.
162. Chen Y, Liu Y, Sullards MC, Merrill AH. An Introduction to Sphingolipid Metabolism and Analysis by New Technologies. *Neuromolecular Med*. 2010 Dec; 12(4):306–19.
163. Siow DL, Wattenberg BW. Mammalian ORMDL proteins mediate the feedback response in ceramide biosynthesis. *J Biol Chem*. 2012 Nov 23; 287(48):40198–204.
164. Iwawaki T, Akai R, Kohno K, Miura M. A transgenic mouse model for monitoring endoplasmic reticulum stress. *Nat Med*. 2003 Dec 14; 10(1):98–102.
165. Bernard P, Couturier M. Cell killing by the F plasmid CcdB protein involves poisoning of DNA-topoisomerase II complexes. *J Mol Biol*. 1992 Aug 5; 226(3):735–45.
166. Sanger F, Coulson AR. A rapid method for determining sequences in DNA by primed synthesis with DNA polymerase. *J Mol Biol*. 1975 May 25; 94(3):441–8.
167. Lowry OH, Rosebrough NJ, Farr AL, Randall RJ. Protein Measurement with the Folin Phenol Reagent. *J Biol Chem*. 1951 Jan 11; 193(1):265–75.
168. Laemmli UK. Cleavage of structural proteins during the assembly of the head of bacteriophage T4. *Nature*. 1970 Aug 15; 227(5259):680–5.
169. Hachmann JP, Amshey JW. Models of protein modification in Tris–glycine and neutral pH Bis–Tris gels during electrophoresis: Effect of gel pH. *Anal Biochem*. 2005 Jul 15; 342(2):237–45.
170. Towbin H, Staehelin T, Gordon J. Electrophoretic transfer of proteins from polyacrylamide gels to nitrocellulose sheets: procedure and some applications. *Proc Natl Acad Sci U S A*. 1979 Sep; 76(9):4350–4.
171. Robine S, Huet C, Moll R, Sahuquillo-Merino C, Coudrier E, Zweibaum A, et al. Can villin be used to identify malignant and undifferentiated normal digestive epithelial cells? *Proc Natl Acad Sci U S A*. 1985 Dec; 82(24):8488–92.
172. Wirtz S, Neufert C, Weigmann B, Neurath MF. Chemically induced mouse models of intestinal inflammation. *Nat Protoc*. 2007 Mar; 2(3):541–6.

173. Laroui H, Ingersoll SA, Liu HC, Baker MT, Ayyadurai S, Charania MA, et al. Dextran sodium sulfate (DSS) induces colitis in mice by forming nano-lipocomplexes with medium-chain-length fatty acids in the colon. *PloS One*. 2012;7(3):e32084.
174. Ubeda M, Habener JF. CHOP gene expression in response to endoplasmic-reticular stress requires NFY interaction with different domains of a conserved DNA-binding element. *Nucleic Acids Res*. 2000 Dec 15;28(24):4987–97.
175. Li M, Baumeister P, Roy B, Phan T, Foti D, Luo S, et al. ATF6 as a transcription activator of the endoplasmic reticulum stress element: thapsigargin stress-induced changes and synergistic interactions with NF-Y and YY1. *Mol Cell Biol*. 2000 Jul;20(14):5096–106.
176. Wang Y, Shen J, Arenzana N, Tirasophon W, Kaufman RJ, Prywes R. Activation of ATF6 and an ATF6 DNA Binding Site by the Endoplasmic Reticulum Stress Response. *J Biol Chem*. 2000 Jan 9;275(35):27013–20.
177. Mao W, Fukuoka S, Iwai C, Liu J, Sharma VK, Sheu S-S, et al. Cardiomyocyte apoptosis in autoimmune cardiomyopathy: mediated via endoplasmic reticulum stress and exaggerated by norepinephrine. *Am J Physiol - Heart Circ Physiol*. 2007 Jan 9;293(3):H1636–45.
178. Therauf DJ, Marcinko M, Belmont PJ, Glembotski CC. Effects of the isoform-specific characteristics of ATF6 alpha and ATF6 beta on endoplasmic reticulum stress response gene expression and cell viability. *J Biol Chem*. 2007 Aug 3;282(31):22865–78.
179. Okada T. A Serine Protease Inhibitor Prevents Endoplasmic Reticulum Stress-induced Cleavage but Not Transport of the Membrane-bound Transcription Factor ATF6. *J Biol Chem*. 2003 Jun 4;278(33):31024–32.
180. Liu J, Mao W, Iwai C, Fukuoka S, Vulapalli R, Huang H, et al. Adoptive passive transfer of rabbit α -adrenoceptor peptide immune cardiomyopathy into the Rag2^{-/-} mouse: participation of the ER stress. *J Mol Cell Cardiol*. 2008 Feb;44(2):304–14.
181. Teske BF, Wek SA, Bunpo P, Cundiff JK, McClintick JN, Anthony TG, et al. The eIF2 kinase PERK and the integrated stress response facilitate activation of ATF6 during endoplasmic reticulum stress. *Mol Biol Cell*. 2011 Nov 15;22(22):4390–405.
182. Hong M, Luo S, Baumeister P, Huang J-M, Gogia RK, Li M, et al. Underglycosylation of ATF6 as a Novel Sensing Mechanism for Activation of the Unfolded Protein Response. *J Biol Chem*. 2004 Mar 19;279(12):11354–63.
183. Maley F, Trimble RB, Tarentino AL, Plummer TH Jr. Characterization of glycoproteins and their associated oligosaccharides through the use of endoglycosidases. *Anal Biochem*. 1989 Aug 1;180(2):195–204.
184. Ron D, Walter P. Signal integration in the endoplasmic reticulum unfolded protein response. *Nat Rev Mol Cell Biol*. 2007 Jan 7;8(7):519–29.
185. Yakar S, Setser J, Zhao H, Stannard B, Haluzik M, Glatt V, et al. Inhibition of growth hormone action improves insulin sensitivity in liver IGF-1-deficient mice. *J Clin Invest*. 2004 Jan 1;113(1):96–105.

186. Guo B, Li Z. Endoplasmic reticulum stress in hepatic steatosis and inflammatory bowel diseases. *Front Genet* [Internet]. 2014 Jul 25 [cited 2015 Mar 4];5. Available from: <http://www.ncbi.nlm.nih.gov/pmc/articles/PMC4110625/>
187. Sanchez-Munoz F, Dominguez-Lopez A, Yamamoto-Furusho JK. Role of cytokines in inflammatory bowel disease. *World J Gastroenterol WJG*. 2008 Jul 21;14(27):4280–8.
188. Oyadomari S, Mori M. Roles of CHOP/GADD153 in endoplasmic reticulum stress. *Cell Death Differ*. 2003 Dec 19;11(4):381–9.
189. Gade P, Ramachandran G, Maachani UB, Rizzo MA, Okada T, Prywes R, et al. An IFN- γ -stimulated ATF6-C/EBP- β -signaling pathway critical for the expression of Death Associated Protein Kinase 1 and induction of autophagy. *Proc Natl Acad Sci U S A*. 2012 Jun 26;109(26):10316–21.
190. Nava P, Koch S, Laukoetter MG, Lee WY, Kolegraff K, Capaldo CT, et al. Interferon-gamma regulates intestinal epithelial homeostasis through converging beta-catenin signaling pathways. *Immunity*. 2010 Mar 26;32(3):392–402.
191. Okayasu I, Hatakeyama S, Yamada M, Ohkusa T, Inagaki Y, Nakaya R. A novel method in the induction of reliable experimental acute and chronic ulcerative colitis in mice. *Gastroenterology*. 1990 Mar;98(3):694–702.
192. Karlsson A, Jägervall Å, Pettersson M, Andersson A-K, Gillberg P-G, Melgar S. Dextran sulphate sodium induces acute colitis and alters hepatic function in hamsters. *Int Immunopharmacol*. 2008 Jan;8(1):20–7.
193. Li L, Liu Z, Yang X, Yan H, Bao S, Fei J. Bioluminescence imaging for IL-1 β expression in experimental colitis. *J Inflamm*. 2013 Apr 11;10(1):16.
194. Perš, E M, Cerar A. Dextran Sodium Sulphate Colitis Mouse Model: Traps and Tricks. *BioMed Res Int* [Internet]. 2012 May 14 [cited 2013 Dec 2];2012. Available from: <http://www.hindawi.com/journals/bmri/2012/718617/abs/>
195. Hetz C, Bernasconi P, Fisher J, Lee A-H, Bassik MC, Antonsson B, et al. Proapoptotic BAX and BAK Modulate the Unfolded Protein Response by a Direct Interaction with IRE1 α . *Science*. 2006 Apr 28;312(5773):572–6.
196. Londos C, Brasaemle DL, Schultz CJ, Segrest JP, Kimmel AR. Perilipins, ADRP, and other proteins that associate with intracellular neutral lipid droplets in animal cells. *Semin Cell Dev Biol*. 1999 Feb;10(1):51–8.
197. Lee J-S, Zheng Z, Mendez R, Ha S-W, Xie Y, Zhang K. Pharmacologic ER stress induces non-alcoholic steatohepatitis in an animal model. *Toxicol Lett*. 2012 May 20;211(1):29–38.
198. Röhrl C, Eigner K, Winter K, Korbilius M, Obrowsky S, Kratky D, et al. Endoplasmic reticulum stress impairs cholesterol efflux and synthesis in hepatic cells. *J Lipid Res*. 2014 Jan 1;55(1):94–103.
199. Melgar S, Karlsson A, Michaëlsson E. Acute colitis induced by dextran sulfate sodium progresses to chronicity in C57BL/6 but not in BALB/c mice: correlation between symptoms and inflammation. *Am J Physiol - Gastrointest Liver Physiol*. 2005 Jan 6;288(6):G1328–38.

200. Alex P, Zachos NC, Nguyen T, Gonzales L, Chen T-E, Conklin LS, et al. Distinct cytokine patterns identified from multiplex profiles of murine DSS and TNBS-induced colitis. *Inflamm Bowel Dis*. 2009 Mar;15(3):341–52.
201. Whitehead A, Crawford DL. Variation in tissue-specific gene expression among natural populations. *Genome Biol*. 2005 Jan 26;6(2):R13.
202. Wang M, Wey S, Zhang Y, Ye R, Lee AS. Role of the Unfolded Protein Response Regulator GRP78/BiP in Development, Cancer, and Neurological Disorders. *Antioxid Redox Signal*. 2009 Sep;11(9):2307–16.
203. Joubert A, Simoneau P, Campion C, Bataillé-Simoneau N, Iacomi-Vasilescu B, Poupard P, et al. Impact of the unfolded protein response on the pathogenicity of the necrotrophic fungus *Alternaria brassicicola*. *Mol Microbiol*. 2011 Mar;79(5):1305–24.
204. Kondo S, Murakami T, Tatsumi K, Ogata M, Kanemoto S, Otori K, et al. OASIS, a CREB/ATF-family member, modulates UPR signalling in astrocytes. *Nat Cell Biol*. 2005 Feb;7(2):186–94.
205. Zhang K, Shen X, Wu J, Sakaki K, Saunders T, Rutkowski DT, et al. Endoplasmic reticulum stress activates cleavage of CREBH to induce a systemic inflammatory response. *Cell*. 2006 Feb 10;124(3):587–99.
206. Kumashiro N, Erion DM, Zhang D, Kahn M, Beddow SA, Chu X, et al. Cellular mechanism of insulin resistance in nonalcoholic fatty liver disease. *Proc Natl Acad Sci*. 2011 Sep 27;108(39):16381–5.
207. Lee AS. Coordinated regulation of a set of genes by glucose and calcium ionophores in mammalian cells. *Trends Biochem Sci*. 1987;12:20–3.
208. Badiola N, Penas C, Miñano-Molina A, Barneda-Zahonero B, Fadó R, Sánchez-Opazo G, et al. Induction of ER stress in response to oxygen-glucose deprivation of cortical cultures involves the activation of the PERK and IRE-1 pathways and of caspase-12. *Cell Death Dis*. 2011 Apr 28;2(4):e149.
209. Schröder K, Martoglio B, Hofmann M, Hölscher C, Hartmann E, Prehn S, et al. Control of glycosylation of MHC class II-associated invariant chain by translocon-associated RAMP4. *EMBO J*. 1999 Sep 1;18(17):4804–15.
210. Yamaguchi A, Hori O, Stern DM, Hartmann E, Ogawa S, Tohyama M. Stress-associated endoplasmic reticulum protein 1 (SERP1)/Ribosome-associated membrane protein 4 (RAMP4) stabilizes membrane proteins during stress and facilitates subsequent glycosylation. *J Cell Biol*. 1999 Dec 13;147(6):1195–204.
211. Dersh D, Jones SM, Eletto D, Christianson JC, Argon Y. OS-9 facilitates turnover of nonnative GRP94 marked by hyperglycosylation. *Mol Biol Cell*. 2014 Aug 1;25(15):2220–34.
212. Bogaert S, De Vos M, Olievier K, Peeters H, Elewaut D, Lambrecht B, et al. Involvement of Endoplasmic Reticulum Stress in Inflammatory Bowel Disease: A Different Implication for Colonic and Ileal Disease? *PLoS ONE*. 2011 Oct 18;6(10):e25589.
213. Park S-H, Choi HJ, Yang H, Do KH, Kim J, Lee DW, et al. Endoplasmic Reticulum Stress-activated C/EBP Homologous Protein Enhances Nuclear Factor- κ B Signals

- via Repression of Peroxisome Proliferator-activated Receptor γ . *J Biol Chem*. 2010 Dec 11;285(46):35330–9.
214. Ahmed QL, Manzoor S, Tariq M, Khalid M, Ashraf W, Parvaiz F, et al. Hepatitis C virus infection in vitro triggers endoplasmic reticulum stress and downregulates insulin receptor substrates 1 and 2 through upregulation of cytokine signaling suppressor 3. *Acta Virol*. 2014;58(3):238–44.
215. Tardif KD, Mori K, Kaufman RJ, Siddiqui A. Hepatitis C virus suppresses the IRE1-XBP1 pathway of the unfolded protein response. *J Biol Chem*. 2004 Apr 23;279(17):17158–64.
216. Fawcett TW, Martindale JL, Guyton KZ, Hai T, Holbrook NJ. Complexes containing activating transcription factor (ATF)/cAMP-responsive-element-binding protein (CREB) interact with the CCAAT/enhancer-binding protein (C/EBP)-ATF composite site to regulate Gadd153 expression during the stress response. *Biochem J*. 1999 Apr 1;339(Pt 1):135–41.
217. Zhang K, Wong HN, Song B, Miller CN, Scheuner D, Kaufman RJ. The unfolded protein response sensor IRE1 γ is required at 2 distinct steps in B cell lymphopoiesis. *J Clin Invest*. 2005 Feb 1;115(2):268–81.
218. Reimold AM, Etkin A, Clauss I, Perkins A, Friend DS, Zhang J, et al. An essential role in liver development for transcription factor XBP-1. *Genes Dev*. 2000 Jan 15;14(2):152–7.
219. Luo S, Mao C, Lee B, Lee AS. GRP78/BiP Is Required for Cell Proliferation and Protecting the Inner Cell Mass from Apoptosis during Early Mouse Embryonic Development. *Mol Cell Biol*. 2006 Aug;26(15):5688–97.
220. Wanderling S, Simen BB, Ostrovsky O, Ahmed NT, Vogen SM, Gidalevitz T, et al. GRP94 Is Essential for Mesoderm Induction and Muscle Development Because It Regulates Insulin-like Growth Factor Secretion. *Mol Biol Cell*. 2007 Oct;18(10):3764–75.
221. Ishikawa T, Okada T, Ishikawa-Fujiwara T, Todo T, Kamei Y, Shigenobu S, et al. ATF6 α/β -mediated adjustment of ER chaperone levels is essential for development of the notochord in medaka fish. *Mol Biol Cell*. 2013 May 1;24(9):1387–95.
222. Harding HP, Zeng H, Zhang Y, Jungries R, Chung P, Plesken H, et al. Diabetes Mellitus and Exocrine Pancreatic Dysfunction in *PerK*^{-/-} Mice Reveals a Role for Translational Control in Secretory Cell Survival. *Mol Cell*. 2001 Jun;7(6):1153–63.
223. Zinszner H, Kuroda M, Wang X, Batchvarova N, Lightfoot RT, Remotti H, et al. CHOP is implicated in programmed cell death in response to impaired function of the endoplasmic reticulum. *Genes Dev*. 1998 Jan 4;12(7):982–95.
224. Kojima E, Takeuchi A, Haneda M, Yagi A, Hasegawa T, Yamaki K, et al. The function of GADD34 is a recovery from a shutoff of protein synthesis induced by ER stress: elucidation by GADD34-deficient mice. *FASEB J Off Publ Fed Am Soc Exp Biol*. 2003 Aug;17(11):1573–5.
225. Tanaka T, Tsujimura T, Takeda K, Sugihara A, Maekawa A, Terada N, et al. Targeted disruption of ATF4 discloses its essential role in the formation of eye lens fibres. *Genes Cells*. 1998 Dec 1;3(12):801–10.

226. Hettmann T, Barton K, Leiden JM. Microphthalmia due to p53-mediated apoptosis of anterior lens epithelial cells in mice lacking the CREB-2 transcription factor. *Dev Biol.* 2000 Jun 1;222(1):110–23.
227. Efstratiadis A. Genetics of mouse growth. *Int J Dev Biol.* 1998;42(7):955–76.
228. Lupu F, Terwilliger JD, Lee K, Segre GV, Efstratiadis A. Roles of Growth Hormone and Insulin-like Growth Factor 1 in Mouse Postnatal Growth. *Dev Biol.* 2001 Jan 1;229(1):141–62.
229. Liu JL, LeRoith D. Insulin-like growth factor I is essential for postnatal growth in response to growth hormone. *Endocrinology.* 1999 Nov;140(11):5178–84.
230. Baker J, Liu J-P, Robertson EJ, Efstratiadis A. Role of insulin-like growth factors in embryonic and postnatal growth. *Cell.* 1993 Oct 8;75(1):73–82.
231. Zhou Y, Xu BC, Maheshwari HG, He L, Reed M, Lozykowski M, et al. A mammalian model for Laron syndrome produced by targeted disruption of the mouse growth hormone receptor/binding protein gene (the Laron mouse). *Proc Natl Acad Sci U S A.* 1997 Nov 25;94(24):13215–20.
232. Barton ER, Park S, James JK, Makarewich CA, Philippou A, Eletto D, et al. Deletion of muscle GRP94 impairs both muscle and body growth by inhibiting local IGF production. *FASEB J.* 2012 Jan 9;26(9):3691–702.
233. Ostrovsky O, Eletto D, Makarewich C, Barton ER, Argon Y. GLUCOSE REGULATED PROTEIN 94 IS REQUIRED FOR MUSCLE DIFFERENTIATION THROUGH ITS CONTROL OF THE AUTOCRINE PRODUCTION OF INSULIN-LIKE GROWTH FACTORS*. *Biochim Biophys Acta.* 2010 Feb;1803(2):333–41.
234. Li Y, Iida K, O'Neil J, Zhang P, Li S, Frank A, et al. PERK eIF2alpha kinase regulates neonatal growth by controlling the expression of circulating insulin-like growth factor-I derived from the liver. *Endocrinology.* 2003 Aug;144(8):3505–13.
235. Zhang P, McGrath B, Li S, Frank A, Zambito F, Reinert J, et al. The PERK eukaryotic initiation factor 2 alpha kinase is required for the development of the skeletal system, postnatal growth, and the function and viability of the pancreas. *Mol Cell Biol.* 2002 Jun;22(11):3864–74.
236. Kayama H, Takeda K. Regulation of intestinal homeostasis by innate and adaptive immunity. *Int Immunol.* 2012 Sep 7;dxx094.
237. Bouma G, Strober W. The immunological and genetic basis of inflammatory bowel disease. *Nat Rev Immunol.* 2003 Jul;3(7):521–33.
238. Niessner M, Volk BA. Altered Th1/Th2 cytokine profiles in the intestinal mucosa of patients with inflammatory bowel disease as assessed by quantitative reversed transcribed polymerase chain reaction (RT-PCR). *Clin Exp Immunol.* 1995 Sep;101(3):428–35.
239. Fuss IJ, Neurath M, Boirivant M, Klein JS, de la Motte C, Strong SA, et al. Disparate CD4+ lamina propria (LP) lymphokine secretion profiles in inflammatory bowel disease. Crohn's disease LP cells manifest increased secretion of IFN-gamma, whereas ulcerative colitis LP cells manifest increased secretion of IL-5. *J Immunol Baltim Md 1950.* 1996 Aug 1;157(3):1261–70.

240. Ito R, Shin-Ya M, Kishida T, Urano A, Takada R, Sakagami J, et al. Interferon-gamma is causatively involved in experimental inflammatory bowel disease in mice. *Clin Exp Immunol*. 2006 Nov;146(2):330–8.
241. Noguchi M, Hiwatashi N, Liu Z, Toyota T. Enhanced interferon-gamma production and B7-2 expression in isolated intestinal mononuclear cells from patients with Crohn's disease. *J Gastroenterol*. 1995 Nov;30 Suppl 8:52–5.
242. Charles A Janeway J, Travers P, Walport M, Shlomchik MJ. The major histocompatibility complex and its functions [Internet]. 2001 [cited 2014 Aug 5]. Available from: <http://www.ncbi.nlm.nih.gov/books/NBK27156/>
243. Bär F, Sina C, Hundorfean G, Pagel R, Lehnert H, Fellermann K, et al. Inflammatory bowel diseases influence major histocompatibility complex class I (MHC I) and II compartments in intestinal epithelial cells. *Clin Exp Immunol*. 2013 May;172(2):280–9.
244. Cuvelier C, Mielants H, De Vos M, Veys E, Roels H. Major histocompatibility complex class II antigen (HLA-DR) expression by ileal epithelial cells in patients with seronegative spondylarthropathy. *Gut*. 1990 May;31(5):545–9.
245. Fransen K, Visschedijk MC, van Sommeren S, Fu JY, Franke L, Festen EAM, et al. Analysis of SNPs with an effect on gene expression identifies UBE2L3 and BCL3 as potential new risk genes for Crohn's disease. *Hum Mol Genet*. 2010 Sep 1;19(17):3482–8.
246. Robinson DS, Hamid Q, Ying S, Tsicopoulos A, Barkans J, Bentley AM, et al. Predominant TH2-like Bronchoalveolar T-Lymphocyte Population in Atopic Asthma. *N Engl J Med*. 1992 Jan 30;326(5):298–304.
247. Webb DC, McKenzie AN, Koskinen AM, Yang M, Mattes J, Foster PS. Integrated signals between IL-13, IL-4, and IL-5 regulate airways hyperreactivity. *J Immunol Baltim Md 1950*. 2000 Jul 1;165(1):108–13.
248. Teixeira LK, Fonseca BP, Barboza BA, Viola JP. The role of interferon-gamma on immune and allergic responses. *Mem Inst Oswaldo Cruz*. 2005 Mar;100:137–44.
249. Lee YC, Lee KH, Lee HB, Rhee YK. Serum levels of interleukins (IL)-4, IL-5, IL-13, and interferon-gamma in acute asthma. *J Asthma Off J Assoc Care Asthma*. 2001 Dec;38(8):665–71.
250. Kim Y-S, Choi S-J, Choi J-P, Jeon SG, Oh S-Y, Lee B-J, et al. IL-12-STAT4-IFN- γ axis is a key downstream pathway in the development of IL-13-mediated asthma phenotypes in a Th2 type asthma model. *Exp Mol Med*. 2010 Aug 31;42(8):533–46.
251. Kiefer K, Carreras-Sureda A, García-López R, Rubio-Moscardó F, Casas J, Fabriàs G, et al. Coordinated Regulation of the Orosomucoid-Like Gene Family Expression Controls de Novo Ceramide Synthesis in Mammalian Cells. *J Biol Chem*. 2014 Dec 17;289(51):34511–21.
252. Ramachandran S, Engel A, Barton G, Thorner J. Sphingolipid biosynthesis and inflammatory signaling in asthma (605.21). *FASEB J*. 2014 Jan 4;28(1 Supplement):605.21.
253. Li B, Alli R, Vogel P, Geiger TL. IL-10 modulates DSS-induced colitis through a macrophage–ROS–NO axis. *Mucosal Immunol*. 2014 Jul;7(4):869–78.

254. Ren K, Torres R. Role of interleukin-1 β during pain and inflammation. *Brain Res Rev.* 2009 Apr;60(1):57–64.
255. Biesiada G, Czepiel J, Ptak-Belowska A, Targosz A, Krzysiek-Maczka G, Strzalka M, et al. Expression and release of leptin and proinflammatory cytokines in patients with ulcerative colitis and infectious diarrhea. *J Physiol Pharmacol Off J Pol Physiol Soc.* 2012 Oct;63(5):471–81.
256. Uko V, Thangada S, Radhakrishnan K. Liver Disorders in Inflammatory Bowel Disease. *Gastroenterol Res Pract.* 2012 Feb 15;2012:e642923.
257. Kaser A, Blumberg RS. Endoplasmic reticulum stress and intestinal inflammation. *Mucosal Immunol.* 2009 Oct 28;3(1):11–6.
258. Cader MZ, Kaser A. Recent advances in inflammatory bowel disease: mucosal immune cells in intestinal inflammation. *Gut.* 2013 Jan 11;62(11):1653–64.
259. Yamamoto K, Takahara K, Oyadomari S, Okada T, Sato T, Harada A, et al. Induction of Liver Steatosis and Lipid Droplet Formation in ATF6 -Knockout Mice Burdened with Pharmacological Endoplasmic Reticulum Stress. *Mol Biol Cell.* 2010 Jul 14;21(17):2975–86.
260. Rutkowski DT, Wu J, Back S-H, Callaghan MU, Ferris SP, Iqbal J, et al. UPR pathways combine to prevent hepatic steatosis caused by ER stress-mediated suppression of transcriptional master regulators. *Dev Cell.* 2008 Dec;15(6):829–40.
261. Zhang K, Wang S, Malhotra J, Hassler JR, Back SH, Wang G, et al. The unfolded protein response transducer IRE1 α prevents ER stress-induced hepatic steatosis. *EMBO J.* 2011 Apr 6;30(7):1357–75.
262. Basseri S, Austin RC. Endoplasmic Reticulum Stress and Lipid Metabolism: Mechanisms and Therapeutic Potential. *Biochem Res Int.* 2012;2012:1–13.
263. Kerbiriou M, Le Drévo M-A, Férec C, Trouvé P. Coupling cystic fibrosis to endoplasmic reticulum stress: Differential role of Grp78 and ATF6. *Biochim Biophys Acta BBA - Mol Basis Dis.* 2007 Dec;1772(11–12):1236–49.
264. Chan C-P, Mak T-Y, Chin K-T, Ng IO-L, Jin D-Y. N-linked glycosylation is required for optimal proteolytic activation of membrane-bound transcription factor CREB-H. *J Cell Sci.* 2010 May 1;123(Pt 9):1438–48.

8 Supplements

8.1 List of abbreviations

ADRP	adipose differentiation related protein
AGR2	encoding the anterior gradient protein-2
APS	ammonium persulfate
ATCC	American Type Culture Collection
ATF4	activating transcription factor 4
ATF6	activating transcription factor 6
ATF6 α (N)	N-terminal fragment of ATF6 α
ATG16L1	autophagy-related protein 16-1
BMDM	bone marrow-derived macrophages
BSA	bovine serum albumin
BW	body weight
Ca ²⁺	calcium
CD	Crohn's disease
cDNA	complimentary DNA
CHOP	CCAAT-enhancer-binding homologous protein
CHX	cycloheximide
CO-IP	Co-immunoprecipitations
CREBH	cAMP responsive element-binding protein
CXCL1	chemokine (C-X-C motif) ligand 1
DAI	disease activity index
DBD	DNA-binding domain
DMSO	dimethylsulfoxid
DNA	deoxyribonucleic acid
DSS	dextran sulfate sodium
DTT	ditriothreitol
ECL	enhanced chemiluminescence
EDTA	ethylenediaminetetraacetic acid
eIF2 α	eukaryotic translation initiation factor 2 α
eIF2 α ^{AVA_IEC}	nonphosphorylatable Ser51A1a mutant of eIF2 α in IECs
ELISA	Enzyme-linked immunosorbent assays
EndoH	endoglycosidase H
eQTL	expression quantitative trait loci
ER	endoplasmic reticulum
ERAD	ER-associated protein degradation
ERN	endoplasmic reticulum to nucleus signaling
ERSE	ER stress response element
FACS	fluorescence-activated cell sorting
FCS	fetal calf serum
FL	full length
FRT	flippase recognition target
FSC	forward scatter

GADD34	growth-arrest DNA damage gene 34
GH	growth hormone
GRP78	78-kDa glucose-regulated protein
GRP94	94-kDa glucose-regulated protein
GWAS	genome-wide association studies
HDL	high-density lipoprotein
HE	hematoxylin and eosin
HERC2	probable E3 ubiquitin-protein ligase
HRP	horseradish peroxidase
IBD	inflammatory bowel disease
IEC	intestinal epithelial cell
IFN γ	interferon gamma
IGF1	insulin-like growth factor 1
IHC	immunohistochemistry
IL	interleukin
IRE1	inositol-requiring kinase 1
IRES	internal ribosome entry site
JNK	c-Jun-N-terminal kinase
kDA	kilodalton
KO	knockout
L	DNA SmartLadder
LCB	long-chain base
Lgr5	leucine-rich repeat-containing G-protein coupled receptor 5
Lyz1	lysozyme 1
<i>Mbtps1</i>	membrane-bound transcription factor S1P-encoding gene
MEF	mouse embryonic fibroblasts
MHC	major histocompatibility complex
MOPS	4-Morpholinepropanesulfonic acid
mRNA	messenger ribonucleic acids
Muc2	mucin 2
NeoR	neomycin resistance
NFY	nuclear transcription factor
NF- κ B	nuclear factor kappa-light-chain-enhancer of activated B cells
NOD2	nucleotide-binding oligomerization domain-containing protein 2
NRF2	nuclear factor erythroid 2-related factor
OASIS	old astrocyte specifically induced substance
ORMDL	orosomuoid 1 (<i>Saccharomyces cerevisiae</i>)-like protein
<i>Ormdl1</i> ^{-/-}	<i>Ormdl1</i> -deficient mice
<i>Ormdl3</i> ^{-/-}	<i>Ormdl3</i> -deficient mice
<i>Ormdl3</i> ^{ΔIEC}	IEC-specific <i>Ormdl3</i> deficiency
OS-9	lectin osteosarcoma amplified 9
p36ATF6 α	36 kDA fragment of ATF6 α
p50ATF6 α	50 kDA fragment of ATF6 α
p58 ^{IPK}	protein kinase inhibitor of 58 kDa
PBA	4-phenylbutyrate
PBS	phosphate-buffered saline

PCR	polymerase chain reactions
p-eIF2 α	phosphorylated form of eIF2 α
PERK	double-stranded RNA-activated protein kinase (PKR)-like ER kinase
PP1	protein phosphatase 1
PTPN2	tyrosine-protein phosphatase non-receptor type 2
PuroR	puromycin resistance
PVDF	polyvinylidene difluoride
qPCR	quantitative real-time PCR
RAMP4	ribosome-associated membrane protein 4
RIDD	regulated IRE1-dependent decay of mRNA
RLU	relative light units
RT	reverse transcriptase
S1P	site 1 protease
S2P	site 2 protease
SDS-PAGE	sodium dodecyl sulfate polyacrylamide gel electrophoresis
SEM	standard error of the mean
SERCA2b	sarcoplasmic/endoplasmic reticulum calcium ATPase 2
siRNA	small interfering RNA
SNP	single nucleotide polymorphisms
SPT	serine palmitoyltransferase
SPTLC1	serine palmitoyltransferase, long chain base subunit 1
SSC	side scatter
STAT3	signal transducer and activator of transcription 3
TEMED	tetramethylethylenediamine
TG	thapsigargin
Th1	T helper 1
Th2	T helper 2
TLR	Toll-like receptor
TM	tunicamycin
TNBS	trinitrobenzene sulfonic acid
TNF α	tumor necrosis factor alpha
TRAF2	tumor necrosis factor receptor-associated factor 2
TRAP α	translocon-associated protein alpha
TUDCA	tauroursode-oxycholate
UC	ulcerative colitis
UG	unglycosylated
untr	untreated
UPR	unfolded protein response
UPRE	unfolded protein response element
WT	wild-type
XBP1	X-box binding protein 1
XBP1s	spliced XBP1
<i>Xbp1</i> ^{ΔIEC}	IEC-specific <i>Xbp1</i> deficiency
YY1	Ying Yang 1

8.2 Applied buffers and solutions

Table 8.1: List of applied buffers or solutions

Buffer or solution	Composition or company
10x TAE buffer	Carl Roth, Karlsruhe, Germany, cat. nr. T845.2
10x TBS	200 mM Tris (pH 7.6), 1.37 M sodium chloride
10x TGS buffer	25 mM Tris (pH 8.3), 192 mM glycine, 0.1 % (w/v) SDS
5x SDS loading dye	250 mM Tris (pH 6.8), 10 % (w/v) SDS, 50 % (v/v) glycerol, 500 mM DTT
Anode buffer 1	30 mM Tris, 20 % (v/v) methanol
Anode buffer 2	300 mM Tris, 20 % (v/v) methanol
Blocking solution	5 % (w/v) non-fat dry milk in TTBS
Cathode buffer	25 mM Tris, 20 % (v/v) methanol, 40 mM 6-amino-n-caproic acid
Cell fractionation 1	10 mM HEPES (pH 7.9), 10 mM potassium chloride, 1.5 mM magnesium chloride, 10 mM sodium fluoride
Cell fractionation 2	20 mM HEPES (pH 7.9), 420 mM sodium chloride, 1.5 mM magnesium chloride, 0.2 mM EDTA, 25 % (v/v) glycerol, 10 mM sodium fluoride
CO-IP binding and washing buffer	PBS, 0.02 % (v/v) Tween20
CO-IP elution buffer	50 mM Glycin (pH 2.8)
DNA loading dye	50 % (v/v) glycerol, 0.1 % (w/v) bromophenol blue, 0.1 % (w/v) xylene cyanol
ECL substrate	GE Healthcare, Freiburg, Germany, cat. nr. RPN2109
FCS	PAA Laboratories/ GE Healthcare, Freiburg, Germany, cat. nr. PAA A15-151
FWB	0.5 % (w/v) BSA in PBS
Ketanest S 25mg/ml, 10ml	Pfizer, New York, USA
Loading gel	0.5 M Tris (pH 6.8), 0.4 % (w/v) SDS
MOPS SDS Running Buffer (20X)	Novex/Life Technologies, Darmstadt, Germany, cat. nr. NP001
OPTI-MEM	Gibco/Life Technologies, Darmstadt, Germany, cat. nr. 31985-047
PBS	8 g/l sodium chloride, 0.2 g/l potassium chloride, 1.56 g/l disodium phosphate, 0.24 g/l monopotassium phosphate, pH 7.4
RIPA	150 mM sodium chloride, 1 % (v/v) NP40, 0.5 % (w/v) deoxycholic acid, 0.1 % (w/v) SDS, 50 mM Tris (pH 8.0)
Rompun	Bayer, Leverkusen, Germany
Separation buffer	1.5 M Tris (pH 8.8), 0.4 % (w/v) SDS
SmartLadder	Eurogentec, Cologne, Germany, cat. nr. MW-1700-10
Stacking buffer	0.5 M Tris (pH 8.8), 0.4 % (w/v) SDS
Stripping buffer	62.5 mM Tris (pH 6.8), 2 % (w/v) SDS
SYBR Safe DNA gel stain	Life Technologies, Darmstadt, Germany cat. nr. S33102
TE	10 mM Tris, 1 mM EDTA
TTBS	1x TBS, 0.1 % (v/v) Tween20

8.3 Media

Table 8.2: List of applied media

Media	Composition or company
BMDM medium	50 % (v/v) Mouse Macrophage medium, 50 % (v/v) DMEM, 250 µg/ml Amphotericin, 1x Penicillin/Streptomycin
DMEM	Gibco/Life Technologies, Darmstadt, Germany cat. nr. 41966-029
LB Agar	10 g/l tryptone, 5 g/l yeast extract, 5 g/l sodium chloride, 15 g/l agar agar
LB Medium	10 g/l tryptone, 5 g/l yeast extract, 5 g/l sodium chloride
Mouse Macrophage medium	Life Technologies, Darmstadt, Germany, cat. nr. 12065-074
RPMI	Gibco/Life Technologies, Darmstadt, Germany, cat. nr. 52480-025
S.O.C medium	Life Technologies, Darmstadt, Germany, cat. nr. C4040-10

8.4 Chemicals

Table 8.3: List of applied chemicals

Chemical	Company
2-Mercaptoethanol	Sigma-Aldrich, Munich, Germany
6-amino-n-caproic acid	Sigma-Aldrich, Munich, Germany
Acrylamide Bis Sol.30%	Bio-Rad, Munich, Germany
Ammonium persulfate (APS)	Sigma-Aldrich, Munich, Germany
Amphotericin	PAA Laboratories/ GE Healthcare, Freiburg, Germany
Ampicillin	Sigma-Aldrich, Munich, Germany
Bovine serum albumin (BSA)	Carl Roth, Karlsruhe, Germany
Bromophenol blue	Sigma-Aldrich, Munich, Germany
Deoxycholic acid	Sigma-Aldrich, Munich, Germany
Dimethylsulfoxid (DMSO)	Sigma-Aldrich, Munich, Germany
Dithiothreitol (DTT)	Th. Geyer, Renningen, Germany
DSS reagent grade, molecular weight 36000-50000	MP Biomedicals, Illkirch Cedex, France
Dynabeads Protein G	Life Technologies, Darmstadt, Germany
EDTA	Sigma-Aldrich, Munich, Germany
Ethanol	Merck, Darmstadt, Germany
Glycerol	Carl Roth, Karlsruhe, Germany
Glycine	Carl Roth, Karlsruhe, Germany
HEPES	Sigma-Aldrich, Munich, Germany
Isopropanol	Merck, Darmstadt, Germany
Kanamycin	Merck, Darmstadt, Germany
LE Agarose	Biozyme, Hessisch Oldendorf, Germany
Magnesium chloride	Merck, Darmstadt, Germany
Methanol	Merck, Darmstadt, Germany
Monopotassium phosphate	Sigma-Aldrich, Munich, Germany

Chemical	Company
Non-fat dry milk (NFDM)	Bio-Rad, Munich, Germany
Nonidet p 40 substitute	Sigma-Aldrich, Munich, Germany
Penicilin/Streptomycin	Life Technologies, Darmstadt, Germany
Potassium chloride	Sigma-Aldrich, Munich, Germany
Potassium dihydrogen phosphate	Merck, Darmstadt, Germany
RNase-free water	Qiagen, Hilden, Germany
Sodium chloride	Merck, Darmstadt, Germany
Sodium dodecyl sulfate (SDS)	Carl Roth, Karlsruhe, Germany
Sodium fluoride	Sigma-Aldrich, Munich, Germany
Sodium phosphate dibasic	Sigma-Aldrich, Munich, Germany
SYBR safe	Life Technologies
Tetramethylethylenediamine (TEMED)	Sigma-Aldrich, Munich, Germany
TRIS	Merck, Darmstadt, Germany
Triton-X	Sigma-Aldrich, Munich, Germany
Tween20	Carl Roth, Karlsruhe, Germany
Xylene cyanol	Sigma-Aldrich, Munich, Germany

8.5 Enzymes and inhibitors

Table 8.4: List of applied enzymes

Enzyme	Company
FastDigest BamHI	Thermo Scientific, Bremen, Germany
FastDigest BglII	Thermo Scientific, Bremen, Germany
FastDigest EcoRI	Thermo Scientific, Bremen, Germany
FastDigest KpnI	Thermo Scientific, Bremen, Germany
Gateway [®] BP Clonase [®] II enzyme mix	Life Technologies, Darmstadt, Germany
GoTaq [™] polymerase	Promega, Mannheim, Germany
Proteinase K	Thermo Scientific, Bremen, Germany
RNase-free DNase Set	Qiagen, Hilden, Germany
Trypsin/EDTA	Life Technologies

Table 8.5: List of applied inhibitors

Inhibitor	Company
AEBSF (4-(2-Aminoethyl) benzenesulfonyl fluoride hydrochloride)	Calbiochem, Darmstadt, Germany
Halt [™] combined protease and phosphatase inhibitor	Thermo Scientific, Bremen, Germany
Cycloheximide (CHX)	Sigma-Aldrich, Munich, Germany
Thapsigargin (TG)	Calbiochem, Darmstadt, Germany
Tunicamycin (TM)	Calbiochem, Darmstadt, Germany

8.6 Kits

Table 8.6: Overview of applied kits

Kit	Composition
BigDye Terminator v1.1.Cycle Sequencing Kit	Applied Biosystems, Darmstadt, Germany
BigDye [®] Terminator v1.1 cycle sequencing Kit	Life Technologies, Darmstadt, Germany
Dual-luciferase [®] reporter assay system	Promega, Mannheim, Germany
GeneJET Plasmid Miniprep Kit	Thermo Scientific, Bremen, Germany
Lamina Propria Dissociation Kit	Miltenyi Biotec, Bergisch-Gladbach, Germany
Maxima H Minus First Strand cDNA Synthesis Kit	Thermo Scientific, Bremen, Germany
Mouse/Rat IGF-1 quantikine ELISA kit	R&D systems, Minneapolis, USA
PureLink [®] HiPure Plasmid Filter Midiprep Kit	Life Technologies, Darmstadt, Germany
QIAquick Gel Extration Kit	Qiagen, Hilden, Germany
QIAquick PCR Purification kit	Qiagen, Hilden, Germany
QIAshredder	Qiagen, Hilden, Germany
Rapid DNA Ligation Kit	Roche, Mannheim, Germany
Rat/Mouse Growth hormone ELISA kit	EMD Millipore, Schwalbach, Germany
RNeasy Mini Kit	Qiagen, Hilden, Germany
Roti Histokit	Carl Roth, Karlsruhe, Germany
SYBR [®] Select Master Mix	Life Technologies, Darmstadt, Germany
TOP10 chemically competent E. coli	Life Technologies, Darmstadt, Germany

8.7 Plasmids and oligonucleotides

Table 8.7: Plasmid names and their origin or production method

Plasmid name	Generated by
p3xFLAG-ATF6	Chen <i>et al.</i> , 2002; purchased from Addgene, Cambridge, USA, cat. nr.11975
pCAX-XBP1delDBD	Iwawaki <i>et al.</i> , 2003
pCMV-HA-EGFP	Gateway cloning
pCMV-HA-hORMDL1	Gateway cloning
pCMV-HA-hORMDL3	Gateway cloning
pDEST53	purchased from Life Technologies, Darmstadt, Germany, cat. nr. 12288-015
pDEST53-hORMDL3	Gateway cloning
pDONR221	purchased from Life Technologies, Darmstadt, Germany, cat. nr. 12536-017
pGL3-ATF4	restriction enzyme based cloning using BglII and KpnI
pGL3-Basic	purchased from Promega, Mannheim, Germany, cat. nr. E1751
pGL3-ERSE	restriction enzyme based cloning using BglII and KpnI
pGL3-UPRE	Wu <i>et al.</i> , 2007; purchased from Addgene, Cambridge, USA, cat. nr. 11976
pRL-TK	purchased from Promega, Mannheim, Germany, cat. nr. E2241

All oligonucleotides were generated and desalted by Microsynth AG (Balgach, Switzerland). All sequences are shown from 5' to 3' direction.

Table 8.8: List of applied oligonucleotides with their sequences

Target	Species	Forward sequence	Reverse sequence
Ormdl1 PCR WT	murine	AACGTTAGTGCTGTTTGGACA CACG	AACATGCTTCCCTATACTGTGC CACT
Ormdl1 PCR KO	murine	CCCCAAAAGTGTATGCTCAC GACA	TCCCTATACTGTGCCACTAC CCATTGT
Ormdl3 PCR WT	murine	CTTCATCCGTTGTTGCTTGC	TCCCCTACAGATCTCCTGAGG
Ormdl3 PCR KO	murine	CTTCATCCGTTGTTGCTTGC	TCACAGTGCCAGTAGGAAACC
Ormdl3 PCR cond	murine	CTTCATCCGTTGTTGCTTGC	TCCCCTACAGATCTCCTGAGG
Ormdl3 PCR cre	murine	GTGTGGGACAGAGAACAAC C	ACATCTTCAGGTTCTGCGGG
<i>Ormdl1</i>	murine	ACTCACTGGGAACAGCTGGA	ATTCCAAAGATGCGAACACC
<i>Ormdl2</i>	murine	CTTTTGACACATTGGGAGCA	GGTAGCTTAGGCAGCAGCAC
<i>Ormdl3</i>	murine	GTGGCATCTGGCTCTCCTAC	TGAGCACAGTCATCAAGGACA
<i>Gapdh</i>	murine	CCGGGGCTGGCATTGCTCTC A	CTTGCTCAGTGTCTTGCTGG GG
<i>Xbp1</i>	murine	GAACCAGGAGTTAAGAACAC G	AGGCAACAGTGTCAAGAGTCC
<i>Igf1</i>	murine	ACACCTCTTCTACCTGGCGCT CTGC	CTAGATTCTGTAGGTCTTGTTC CCTG
<i>Il-1β</i>	murine	GGCTGTCCTGATGAGAGCAT	TGTTTCATCTCGGAGCCTGTA
<i>Ifny</i>	murine	ACTGGCAAAGGATGGTGAC A	TCATTGAATGCTTGGCGCTG
<i>Il-6</i>	murine	GACAACCTTTGGCATTGTGG	ATGCAGGGATGATGTTCTG
<i>Il-10</i>	murine	TGCTATGCTGCCTGCTCTTA	TTTTACAGGGGAGAAATCG
<i>Cxcl1</i>	murine	GCTGGGATTCACCTCAAGAA	TGGGGACACCTTTTAGCATC
<i>Tnfa</i>	murine	TCACACTCAGATCATCTTCTC	AGACTCCTCCCAGGTATATG
<i>Atf6α</i>	murine	ATGCCAGTGTCCCAGCAAAA	TCCCCAGTGAAGTCAAGAA
<i>Grp94</i>	murine	TGGGTCAAGCAGAAAGGAGG	TCTCTGTTGCTTCCCGACTTT
<i>Atf4</i>	murine	ATGGCCGGCTATGGATGAT	CGAAGTCAAAGTCTTTCAGATC CATT
<i>Chop</i>	murine	CTGCCTTTTACCTTGGAGA	CGTTTCCTGGGGATGAGATA
<i>Gadd34</i>	murine	CTGCAAGGGGCTGATAAGAG	AGGGGTCAGCCTTGTTCCT
<i>ORMDL1</i>	human	CTGACCAGGGTAAAGCAAGG	TCCAAAGATCCGAACACCAT
<i>ORMDL2</i>	human	CATACGGTGAAGGGACACC	CGGCAGCAGTACACTTAGCA
<i>ORMDL3</i>	human	GTGGCATCTGGCTCTCCTAC	TGAGCACAAAATGGATCTGG
<i>GAPDH</i>	human	GGCATGGCCTTCCGTGTCCC	TGCCAGCCCCAGCGTCAAAG

Table 8.9: Overview of applied TaqMan probes

Target	Species	Company	Catalog number
<i>Vil</i>	murine	Life Technologies, Darmstadt, Germany	00457074
<i>Muc2</i>	murine	Life Technologies, Darmstadt, Germany	00458299
<i>Lgr5</i>	murine	Life Technologies, Darmstadt, Germany	00438905
<i>Gapdh</i>	murine	Life Technologies, Darmstadt, Germany	99999915
<i>Lyz1</i>	murine	Life Technologies, Darmstadt, Germany	00657323

8.8 Antibodies

All antibodies used for western blotting were diluted in TTBS containing either 5 % (w/v) bovine serum albumin (BSA) or 5 % (w/v) non-fat dry milk (NFDM). Table 8.10 shows all employed primary antibodies. All used secondary antibodies are listed in Table 8.11. Secondary antibodies were linked with horseradish peroxidase (HRP) to enable detection using ECL substrate.

Table 8.10: Detailed overview of applied primary antibodies

Antibody	Species, clonal	Dilution	Company	Catalog number
ADRP	rabbit, poly	1:1000 in NFDM	Abcam, Cambridge, United Kingdom	ab52356
ATF4	rabbit, mono	1:500 in BSA	Cell Signaling Technology, Leiden, The Netherlands	11815
ATF6 α	rabbit, poly	1:1000 in NFDM	GenScript, Piscataway, USA	commissioned work
CHOP	rabbit, mono	1:1000 in BSA	Cell Signaling Technology, Leiden, The Netherlands	5554
cl. ATF6 α	mono, mouse	1:500 in NFDM	Acris, Herford, Germany	SM7007P
FLAG	mouse, mono	1:1000 in NFDM	Stratagene, Darmstadt, Germany	200472-21
GRP78	rabbit, poly	1:1000 in NFDM	Abcam, Cambridge, United Kingdom	ab21685
HA	mono, rat	1:1000 in NFDM	Roche, Mannheim, Germany	11 867 423 001
ORMDL1/2/3	goat, poly	1:500 in NFDM	Santa Cruz Biotechnology, Heidelberg, Germany	sc-161143
pelf2 α	rabbit, poly	1:1000 in BSA	Cell Signaling Technology, Leiden, The Netherlands	3398
XBP1s	rabbit, poly	1:500 in BSA	Santa Cruz Biotechnology, Heidelberg, Germany	sc-7160
TRAP α	rabbit, mono	1:1000 in NFDM	Abcam, Cambridge, United Kingdom	Ab126607
β -Actin	mouse, poly	1:10000 in NFDM	Sigma-Aldrich, Munich, Germany	A-5441

Table 8.11: Detailed overview of applied secondary antibodies

Antibody	Dilution	Company	Catalog number
mouse HRP	1:1000	Amersham Biosciences, Glattbrugg, Switzerland	NA931V
rabbit HRP	1:2500	Amersham Biosciences, Glattbrugg, Switzerland	NA934V
goat HRP	1:1000	Sigma-Aldrich, Munich, Germany	A5420
rat HRP	1:1000	Sigma-Aldrich, Munich, Germany	A9037

Table 8.12: List of applied FACS antibodies

Antibody	Fluorophore	Isotype	Dilution	Company	Catalog number
MHCI	APC	mouse IgG2a	1:75	eBioscience, Frankfurt a. Main, Germany	17-5958
CD11b	PE	rat IgG2b	1:100	eBioscience, Frankfurt a. Main, Germany	12-0112
Isotype for MHCI	APC	mouse IgG2a	1:75	eBioscience, Frankfurt a. Main, Germany	17-4724
Isotype for CD11b	PE	rat IgG2b	1:100	eBioscience, Frankfurt a. Main, Germany	12-4031
MHCII	PE	rat IgG2b	1:100	eBioscience, Frankfurt a. Main, Germany	12-5322
CD11b	APC	rat IgG2b	1:100	eBioscience, Frankfurt a. Main, Germany	17-0112
Isotype for MHCII	PE	rat IgG2b	1:100	eBioscience, Frankfurt a. Main, Germany	12-4031
Isotype for CD11b	APC	rat IgG2b	1:100	eBioscience, Frankfurt a. Main, Germany	17-4031
Fc block CD16/32	none	mouse IgG2b	1:100	BD Biosciences, Heidelberg, Germany	553142

8.9 Devices and consumables

Table 8.13: Overview of used devices

Devices	Company
7900 HT Fast Real-Time PCR System	Applied Biosystems/Life Technologies, Darmstadt, Germany
96-well thermocycler	Applied Biosystems/Life Technologies, Darmstadt, Germany
ABI PRISM® 3700 sequencer	Applied Biosystems/Life Technologies, Darmstadt, Germany
Analytic balance 870-15	Kern, Balingen, Germany
Assistent Mini-Centrifuge SPROUT	Heathrow Scientific, Nottingham, United Kingdom
Automated developer machine	Agfa, Mortsel, Belgium
Axio Imager.Z1	Zeiss, Jena, Germany
Cellometer Auto T4 Plus	PeqLab Biotechnologie GmbH, Erlangen, Germany

Devices	Company
Centrifuge for 15/50 ml tubes: Megafuge 16R	Thermo Scientific, Bremen, Germany
Centrifuge for Eppendorf tubes: Fresco 21	Thermo Scientific, Bremen, Germany
Certomat MV, vortex mixer	B. Braun Biotech Internat., Melsungen, Germany
ChemiDoc XRS Imaging System	Bio-Rad, Munich, Germany
Confocal microscope: TCS SP5	Leica Microsystems, Wetzlar, Germany
Electronic pipet filler	Eppendorf, Hamburg, Germany
Eppendorf Research [®] , adjustable-volume pipette	Eppendorf, Hamburg, Germany
FACSCalibur flow cytometer	BD Biosciences, Heidelberg, Germany
GeneAmp PCR System 9700	Applied Biosystems/Life Technologies, Darmstadt, Germany
Gentle-MACS [™] Dissociator	Miltenyi Biotec, Bergisch Gladbach, Germany
Incubator for cell lines	Binder, Tuttlingen, Germany
Incubator for <i>E.coli</i> in media: Orbital Incubator S150	Stuart Equipment, Staffordshire, United Kingdom
Incubator for <i>E.coli</i> on agar plates: Incucell 111	MMM Group, Planegg, Germany
Laminar flow workbench HERASafe KS	Thermo Scientific, Bremen, Germany
Leica RM 2255 microtome	Leica Microsystems, Wetzlar, Germany
Magnetic stirrer C-MAG HS 7 IKAMAG	IKA, Staufen, Germany
Microwave R-239	SHARP, Hamburg, Germany
Mini-Sub Cell GT	Bio-Rad, Munich, Germany
Molecular Imager ChemiDoc XRS Imaging System	Bio-Rad, Munich, Germany
NanoDrop ND-1000 spectrophotometer	PeqLab Biotechnologie GmbH, Erlangen, Germany
Power Pac 300	Bio-Rad, Munich, Germany
Symphony Benchtop Meters	VWR, Darmstadt, Germany
Tecan Infinite F200 pro plate reader	Tecan, Männedorf, Switzerland
Thermomixer compact 5350	Eppendorf, Hamburg, Germany
Trans-Blot [®] Turbo [™] Transfer System	Bio-Rad, Munich, Germany
Tube roller SRT6	Stuart Equipment, Staffordshire, United Kingdom
Vortex-Genie 2 Variable Speed	Sartorius, Göttingen, Germany
Water bath 1003	GFL, Burgwedel, Germany
Water purification system	TKA, Niederelbert, Germany
Wide Mini ReadySub-Cell GT	Bio-Rad, Munich, Germany
XCell SureLock [®] Mini-Cell	Life Technologies, Darmstadt, Germany

Table 8.14: List of applied consumables

Consumable	Company
0.5 ml, 1.5 ml and 2 ml reaction tubes	Sarstedt, Nümbrecht, Germany
1 ml syringes	
100 ml culture flasks	Schott, Mainz, Germany
15 ml and 50 ml tubes	Sarstedt, Nümbrecht, Germany
26G needles	B. Braun, Melsungen, Germany
Blot paper	Bio-Rad, Munich, Germany
Chemiluminescence hyperfilm	Applied Biosystems/Life Technologies, Darmstadt, Germany
Glass beads	Carl Roth, Karlsruhe, Germany
HistoBond	Paul Marienfeld GmbH& Co. KG
MicroAmp Optical 384-Well Reaction Plates	Applied Biosystems
Microvette 500 (Potassium-EDTA)	Sarstedt, Nümbrecht, Germany
NuPAGE [®] Bis-Tris gel	Life Technologies, Darmstadt, Germany
Pipette tips and filter tips	Sarstedt, Nümbrecht, Germany
Pipette tips for electronic pipette	Biohit, Göttingen, Germany
Polyvinylidene difluoride (PVDF) membranes	Bio-Rad, Munich, Germany
Rotilabo 0.22 µm syringe filter	Carl Roth, Karlsruhe, Germany
Serological pipettes	Sarstedt, Nümbrecht, Germany
Surgical disposable scalpels	B. Braun, Melsungen, Germany
Tissue culture dishes 96-, 24- and 6-well	Sarstedt, Nümbrecht, Germany

8.10 List of tables

Table 2.1: Overview of applied cell lines	19
Table 2.2: Overview of applied cell culture dishes for experiments with cell lines.....	19
Table 2.3: Overview of formats and volumes of plasmid DNA transfections.....	20
Table 2.4: Overview of formats and volumes of siRNA transfections	20
Table 2.5: Components and incubation conditions of a reverse transcription reaction mixture	24
Table 2.6: Components and cycling protocol for endpoint PCRs.....	24
Table 2.7: Reaction mixture and cycling protocol for a cloning hot start PCR.....	26
Table 2.8: Gateway cloning: Components for BP and LR Clonase II reactions	27
Table 2.9: Exemplary components of double digest reactions.....	28
Table 2.10: Gel components for SDS-PAGE.....	31
Table 2.11: License numbers for approved animal research	37
Table 2.12: PCR components and profile for genotyping	37
Table 2.13: Overview of expected amplicon lengths after genotyping PCR.....	37
Table 2.14: Overview of cell culture formats for experiments with primary murine cells. ...	39
Table 2.15: Scoring criteria for the determination of the disease activity index.....	40
Table 2.16: Overview of the three histological scoring components	41
Table 8.1: List of applied buffers or solutions	129
Table 8.2: List of applied media	130
Table 8.3: List of applied chemicals	130
Table 8.4: List of applied enzymes.....	131
Table 8.5: List of applied inhibitors.....	131
Table 8.6: Overview of applied kits	132
Table 8.7: Plasmid names and their origin or production method.....	132
Table 8.8: List of applied oligonucleotides with their sequences	133
Table 8.9: Overview of applied TaqMan probes.....	134
Table 8.10: Detailed overview of applied primary antibodies.....	134
Table 8.11: Detailed overview of applied secondary antibodies	135
Table 8.12: List of applied FACS antibodies	135
Table 8.13: Overview of used devices	135
Table 8.14: List of applied consumables	137

8.11 List of figures

Fig. 1.1: Overview of the UPR with its three signaling pathways.	5
Fig. 1.2: Alignment of the human ORMDL amino acid sequences using the CLUSTALW2 program.	13
Fig. 2.1: Functional principle of the life cell XBP1 splicing assay using a XBP1-venus reporter construct.	22
Fig. 2.2: Targeting strategy for the generation of conditional and constitutive <i>Ormdl1</i> knockout alleles.	34
Fig. 2.3: Overview of the targeting strategy for the generation of conditional and constitutive <i>Ormdl3</i> knockout alleles.	35
Fig. 2.4: Representative example of genotyping results obtained from <i>Ormdl1</i> ^{-/-} (A), <i>Ormdl3</i> ^{-/-} (B) and <i>Ormdl3</i> ^{ΔIEC} (C) mice.	38
Fig. 3.1: Analyses of human and murine <i>ORMDL</i> transcripts investigated by endpoint PCR.	42
Fig. 3.2: ER stress-inducing reagents alter ORMDL protein levels <i>in vitro</i>	43
Fig. 3.3: ORMDL proteins reduce <i>XBP1</i> mRNA splicing and UPR promoter activation.	45
Fig. 3.4: ORMDL proteins regulate the p36ATF6α fragment.	46
Fig. 3.5: ORMDL proteins induce translocation of p36ATF6α to the nucleus and activate the ERSE promoter.	47
Fig. 3.6: The effect of ORMDL proteins on the p36ATF6α fragment is modulated by S1P.	48
Fig. 3.7: Effects of all UPR pathway mediators on the ERSE promoter activity.	49
Fig. 3.8: The full length form of ATF6α is affected by ORMDL3.	50
Fig. 3.9: Effect of ORMDL3 on ATF6α functions independently of glycosylation processes.	51
Fig. 3.10: Dose-dependent effect of ORMDL3 on ATF6α UG and ATF6α (N).	52
Fig. 3.11: CHX-treated ORMDL3 overexpressing cells display increased cleavage of ATF6α FL.	52
Fig. 3.12: ORMDL3 co-localizes with ATF6α.	53
Fig. 3.13: Interaction of ORMDL3 and ATF6α shown by co-immunoprecipitation.	54
Fig. 3.14: ORMDL proteins modulate the PERK pathway.	56
Fig. 3.15: ORMDL3 promotes ATF6α-dependent CHOP induction.	57
Fig. 3.16: mRNA expression and protein levels of ORMDL homologues in <i>Ormdl3</i> ^{-/-} mice.	59

Fig. 3.17: <i>Ormdl3</i> ^{-/-} mice exhibit reduced body weight.....	60
Fig. 3.18: Level of growth hormone in the serum of 4 and 10 weeks old wild-type and <i>Ormdl3</i> ^{-/-} mice.	60
Fig. 3.19: Effect of <i>Ormdl3</i> deletion on serum IGF1 levels and liver <i>Igf1</i> mRNA expression.	61
Fig. 3.20: Hematoxylin and eosin staining of lung and liver tissues from wild-type and <i>Ormdl3</i> ^{-/-} mice.	62
Fig. 3.21: Hematoxylin and eosin staining of ileum and colon tissues from wild-type and <i>Ormdl3</i> ^{-/-} mice.	62
Fig. 3.22: <i>Ormdl3</i> deficiency does not affect marker transcripts in ileum and colon tissues.	63
Fig. 3.23: Representative examples of serum cytokines of <i>Ormdl3</i> ^{-/-} and wild-type mice.....	64
Fig. 3.24: Tissue-specific effect of <i>Ormdl3</i> on <i>Ifny</i> mRNA levels.	65
Fig. 3.25: <i>Ormdl3</i> ^{-/-} mice express less MHC I and MHC II on CD11b ⁺ lamina propria cells.	66
Fig. 3.26: <i>Ormdl3</i> deficiency increases susceptibility to DSS-induced colitis.	67
Fig. 3.27: DSS-induced colitis affects colon length and liver weight of <i>Ormdl3</i> ^{-/-} and wild-type mice.	67
Fig. 3.28: Histological scores and HE stainings of <i>Ormdl3</i> ^{-/-} and wild-type mice after DSS treatment.	68
Fig. 3.29: DSS-induced cytokine secretion in <i>Ormdl3</i> ^{-/-} and wild-type mice.	69
Fig. 3.30: DSS-induced colonic mRNA expression of genes involved in the UPR in <i>Ormdl3</i> ^{-/-} and wild-type mice.	70
Fig. 3.31: Short-term DSS treatment induces prolonged upregulation of p-eIF2α in <i>Ormdl3</i> ^{-/-} mice.	70
Fig. 3.32: Effect of tunicamycin injection on body weight of <i>Ormdl3</i> ^{-/-} mice.	71
Fig. 3.33: ORMDL3 regulates ER stress-dependent chaperone expression in the liver upon tunicamycin injection.	73
Fig. 3.34: <i>Ormdl3</i> deficiency prolongs upregulation of ADRP and CHOP in kidney tissues.	74
Fig. 3.35: Tunicamycin administration affects lipid contents in <i>Ormdl3</i> ^{-/-} and wild-type mice.....	75
Fig. 3.36: mRNA expression levels of <i>Ormdl</i> homologues in <i>Ormdl3</i> ^{AIEC} and wild-type mice.....	76
Fig. 3.37: HE stainings of kidney and colon tissues of wild-type and <i>Ormdl3</i> ^{AIEC} mice.....	77

Fig. 3.38: Body weight assessment of <i>Ormdl3</i> ^{ΔIEC} mice during chronic DSS-induced colitis.....	78
Fig. 3.39: Colon length and spleen weight in <i>Ormdl3</i> ^{ΔIEC} and wild-type mice during chronic colitis.	78
Fig. 3.40: Histological scores and HE stainings of <i>Ormdl3</i> ^{ΔIEC} and <i>Ormdl3</i> ^{fl/fl} mice after DSS treatment.	79
Fig. 3.41: DSS-induced cytokine secretion in <i>Ormdl3</i> ^{ΔIEC} and <i>Ormdl3</i> ^{fl/fl} mice.....	80
Fig. 3.42: mRNA expression levels of <i>Ormdl</i> homologues in <i>Ormdl1</i> ^{-/-} mice.....	81
Fig. 3.43: Protein levels of ORMDL1, ORMDL2 and ORMDL3 in <i>Ormdl1</i> ^{-/-} and wild-type mice.	82
Fig. 3.44: HE staining of ileum and colon tissues of wild-type and <i>Ormdl1</i> ^{-/-} mice.	82
Fig. 3.45: Comparable body weight loss in <i>Ormdl1</i> ^{-/-} and wild-type mice during DSS-induced colitis.	83
Fig. 3.46: Colon length and spleen weight of <i>Ormdl1</i> ^{-/-} mice after acute DSS-induced colitis.....	84
Fig. 3.47: Histological scores and HE stainings of <i>Ormdl1</i> ^{-/-} and <i>Ormdl1</i> ^{+/+} mice after DSS treatment.	84
Fig. 4.1: Proposed mechanisms of ORMDL3 on the UPR pathways.	92

8.12 Curriculum vitae

PERSONAL DATA

First and last name: Marlene Jentzsch
 Date of birth: 10th of December 1984
 Place of birth: Schwerin
 Nationality: German
 Contact: marlene.jentzsch@gmail.com

EDUCATION

11/2010 – now **PhD student** at the Christian-Albrechts-University Kiel, Germany
 Institute of Clinical Molecular Biology
 Leading scientist: Prof. Philip Rosenstiel
 Title: “Functional characterization of ORM DL proteins involved in endoplasmic reticulum stress and intestinal inflammation”

04/2008 – 09/2008 **Diploma thesis** at Roche Diagnostics GmbH, Penzberg, Germany
 Leading scientist: Dr. Ulrich Göpfert
 Title: “Characterization of CHO production cell lines”

10/2004 – 09/2008 **Diploma studies** at the University of Applied Sciences Hamburg, Germany
 Course of studies: Biotechnology

08/2002 – 06/2004 **Secondary School** Gymnasium Fridericianum, Schwerin, Germany
 Higher education entrance qualification

International experiences

03/2007 – 08/2007 **Internship** at the Bioprocessing Technology Institute, Singapore
 Leading scientist: Dr. Danny Chee Fung Wong
 “The effects of reactive oxygen species on animal cell culture viability and productivity”

08/2001 – 06/2002 **Exchange year** at the Hesston High School, Kansas, USA

Working experiences

10/2008 – 10/2010 **Engineer** at Roche Diagnostics GmbH, Penzberg, Germany
 Focus: Determination of gene copy numbers and mRNA levels of antibodies produced by CHO cells

Poster presentation

- 02/2015 **International 5th Annual Cluster Symposium** "Inflammation at Interfaces", Kiel, Germany
"Functional characterization of ORMDL3 in ER stress and intestinal inflammation"
- 12/2013 **Studierendentagung** Life Sciences, Kiel, Germany
"ORMDL3 as a new activator and interaction partner of the ER stress-sensor ATF6"
- 11/2012 **Norddeutsche Immunologentagung**, Borstel, Germany
"ORMDL proteins as potential regulators of ER stress-induced intestinal inflammation"

Awards

- 12/2013 **Studierendentagung** Life Sciences, Kiel, Germany
Best poster: "ORMDL3 as a new activator and interaction partner of the ER stress-sensor ATF6"

Paper

- In preparation **Ormdl proteins as key modulators of ER stress responses.**
Marlene Jentzsch, Maren Falk-Paulsen, Anne Luzius, Philip Rosenstiel

8.13 Acknowledgements

Foremost, I would like to sincerely thank my doctorate supervisor Prof. Dr. Philip Rosenstiel, who has provided me with the interesting topic of my thesis and supported me throughout my work with his extensive knowledge. During this time, he enabled me to reward a great graduate student experience by giving me intellectual freedom in my work, supporting my attendance at various conferences and meetings, engaging me in creating new ideas, and demanding high quality of work. Without his guidance and help this dissertation would not have been possible.

My sincere thanks also go to my second academic advisor Dr. Maren Falk-Paulsen, who not only supported me with helpful tips and advice throughout my scientific work, but also contributed to this thesis by giving productive feedback and motivating words. Without her effort my project would have undoubtedly been more difficult. I also want to thank her for the great supporting hand and the proofreading of my scientific documents.

In addition, I want to thank Prof. Dr. Thomas Roeder for his interest in my doctoral thesis and for kindly taking over the co-referat.

I am grateful for having friendly and helpful colleagues and fellow lab-mates in the cell biology group at the IKMB, which provided my daily work with assistance and great working atmosphere. I would like to acknowledge especially Tanja, Katharina, Sabine, Maren, Dorina, Karina, and Tatjana for the technical support in the lab and their great helpfulness. Additionally, I would like to thank Anne, Manja, Helene, Jan, and Lars for scientific exchange on methods and findings, as well as for the nice conversations also outside the lab.

I would like to acknowledge the various members of the animal facilities at the University Medical Center of Schleswig-Holstein in Kiel and at the Kiel University for their effort in breeding the mice, which was of strong importance for a successful work.

My special thanks go to my family who supported me throughout my work and gave me their constant love. Finally, I would like to acknowledge my life partner for his great patience and unyielding support, especially during the time of my doctoral thesis. Thank you for being my energy resource.

8.14 Eidesstattliche Erklärung

Hiermit erkläre ich, Marlene Jentsch, an Eides statt, dass die vorliegende Arbeit nach Inhalt und Form die eigene Arbeit ist und ich keine weitere Hilfe außer der Beratung durch meine Betreuer, Prof. Dr. Philip Rosenstiel und Dr. Maren Falk-Paulsen, in Anspruch genommen wurde.

Weiterhin habe ich keine anderen als die von mir angegebenen Quellen und Hilfsmittel benutzt und die den verwendeten Werken wörtlich oder inhaltlich entnommenen Stellen als solche kenntlich gemacht. Die Arbeit wurde unter Einhaltung der Regeln guter wissenschaftlicher Praxis der Deutschen Forschungsgemeinschaft erstellt. Auszüge der Dissertation wurden bereits in Posterbeiträgen veröffentlicht.

Ich versichere, dass ich weder an der Christian-Albrechts-Universität zu Kiel noch anderweitig versucht habe, eine Dissertation einzureichen oder mich einer Promotionsprüfung zu unterziehen.

Kiel, den _____

Marlene Jentsch